2018

Evaluation of Surface and Groundwater availability under Changing Climate in Abaya-Chamo Lakes Basin, Ethiopia

A Thesis Submitted to the School of Earth Sciences;
Presented in Partial Fulfillment of the Requirements for the Degree of Doctor of Philosophy (Hydrogeology)

Dagnachew Daniel Molla
Addis Ababa University, Addis Ababa, Ethiopia
5/10/2018

Evaluation of Surface and Groundwater availability under Changing Climate in Abaya-Chamo lakes basin, Ethiopia

Dagnachew Daniel Molla

A Thesis Submitted to the School of Earth Sciences

Presented in Partial Fulfillment of the Requirements for the Degree of Doctor of Philosophy (Hydrogeology)

Addis Ababa University

Addis Ababa, Ethiopia

May, 2018

Addis Ababa University

School of Graduate Studies

This is to certify that the thesis prepared by Dagnachew Daniel Molla, entitled:"Evaluation of surface and groundwater availability under changing climate in Abaya-Chamo lakes basin, Ethiopia" and submitted in partial fulfillment of the requirements for the Degree of Doctor of Philosophy (Hydrogeology). It complies with the regulations of the University and meets the accepted standards with respect to originality and quality.

Signed by the Examining Committees:

Principal: (Advisor)	Tenalem Ayenew (Prof)	Signature……	Date……
Examiner : (Internal)	Dessie Nedaw (Asso. Prof)	Signature……	Date……
Examiner: (External)	Dagnachew Legesse (Asso. Prof)	Signature……	Date……

……

Chair of School or Graduate Program Coordinator

ABSTRACT

The study employed steady-state integration approach through a parameter which involves the coupling of climate model outputs (CMIP5); a distributed surface water balance model (WetSpass) and a groundwater flow model (ModFlow). The main focus is to quantify the present and future water resource availability under Changing Climate until 2099, and in a way to understand the hydrologic system in Abaya-Chamo lakes basin, Ethiopia. The lakes basin is part of Main Ethiopia Rift system characterized by complex rift margin, escarpment, and highland.

Though the record of river flow data plays an essential role in water resource management and planning, there is high limitation and irregularity in data and many of hydrologic basins are ungauged. Understanding base flow processes in particular as a groundwater contribution of river flows can be used as an indicative tool to describe hydrologic systems. In this regard, a multivariate analysis using BFI in controlling basin hydrology suggests, morphometric variables such as slope, Elevation, hypsometric integral with associated climate appear to be a dominant factor than land cover and lithological factor.

Spatially distributed water balance simulation at annual time step shows, 74.6% of the precipitation is lost through actual evapotranspiration, 15.7% becomes surface runoff and only 9.7% recharges the groundwater system. Besides, the model indicated the spatial variation of components with different land cover and soil texture combinations. Surface runoff and groundwater recharge are more sensitive to soil textural classes while actual evapotranspiration varies well with land use type.

The future climate (precipitation and temperature) is projected using RCP4.5 and RCP8.5 scenarios of the latest CMIP5 Multi-model outputs (available 24/26 GCMs). The projected annual temperature shows a rise by +0.84, +1.58, and +1.95^{0}C under the rcp4.5 in 2020s, 2050s and 2080s respectively whereas the change increased by +0.94, +2.13 and +3.57^{0}C under rcp8.5 in the study area. Similarly, the projected annual precipitation change is increased by 4%, 5.9%, and 8.9% under the rcp4.5; whereas, 1%, 9%, and 19.54% under rcp8.5 in the respective period. A significant decrease of wet season precipitation is also anticipated in 2050s.

Future water balance components were then simulated using the WetSpass model. The results show that the average recharge continuously increasing for all scenarios; the increases are 5.8%, 19.7% and 43.1% in 2020s, 2050s, and 2080s respectively. The simulated mean actual evapotranspiration increase is about 2.1%, 5.7% to 9.8% respectively with small range uncertainties. The mean annual surface Runoff is increased by 4%, 6% and 9% for corresponding future periods. The changes of groundwater level simulated in main aquifers are correlated with an increase of precipitation and/or recharge, thus average annual groundwater level could rise by 0.15%, 0.4%, and 2.03%. These, in turn may increase in groundwater discharge.

Seasonally, during the dry period, significant increases in all simulated mean water balance components have estimated with relatively smaller ranges of uncertainty as compared to the wet season. But, an increase of seasonal temperature and a decrease of precipitation in 2050s during the wet months could lead to a decrease in surface runoff. A clear linear correlation is observed in between precipitation and surface runoff in all months from the near to the far future under both low-intermediate and high-end scenarios.

The uncertainty range of projected precipitation in 2080s is about -1 to 69.9% as compared to the base period and the simulated corresponding impact as a change would be about (-0.5 to 35.6%) AET, (-1 to 72.2%) ROF and (-4.9 to 329.1%) R.

Generally, there is a remarkable change in the percentage fraction of future water balance particularly in actual evapotranspiration and recharge; while surface runoff will keep constant. The mean projected percentage fraction of actual evapotranspiration is showing a decline by 1.3, 2.1 and 3.5% (is about 73.7%, 72.5% and 71% of annual projected precipitation in 2020s, 2050s, and 2080s respectively). While recharge about 11.8%, 12.4%, and 13.6%, will increase by 2.1, 2.7 and 4.1% respectively as compared to present day water balance. Thus, these average values indicate significant changes in the water balance and groundwater system. It is therefore important for water resource developers to take the changes into account for future sustainable water resource management, planning, and implementation strategies.

Keywords: base flow index, multivariate, water balance, surface and groundwater, RCP, CMIP5, projected, future periods, major-river basin, lakes basin, Abaya-Chamo

ACKNOWLEDGMENT

Thanks be unto God for his unspeakable mercy, blessings and control with unlimited love and great care along all way.

I would like to express my deepest gratitude to Prof. Tenalem Ayenew for the opportunity to proceed in the school under his supervision. I am really thankful and appreciate his constant guidance and constructive comments with great encouragement throughout the research I was privileged to benefit from him through enormous advice, prospective opinions, provided workshops and shared life experiences. Moreover, the hope he has in me has been my strength to many of my engagements. And also, he has allotting much time for shaping the research and reviewing the manuscripts.

I would also like to extend my sincere gratitude to Prof. Christopher Fletcher as a Co-advisor from University of Waterloo, Department of Geography and Environmental Management, Canada, for hosting me as an International Visiting Graduate Student, in providing high cluster computing facilities for climate models, technical support and invaluable advice and also the research team in the department (PhD and post doc. candidates) for teaming up and providing me an excellent working environment during my stay in Canada.

I would also like to thank Dr. Dessie Nedaw, for continuous encouragement, productive thoughts during progress report/seminars evaluation as a chair of Advisory committee. Additionally, thanks for allowing me to participate in his project work and sharing experiences. I would also thank Dr. Seifu Kebede for his initial positive support to proceed in the school as a former School Head, constructive suggestion during proposal evaluation and the field works experiences as well.

I sincerely thank and acknowledge Head of the School (Dr. Balemwal Atnafu), Graduate Program Coordinator (Dr. Mulugeta Alene), Members of the School graduate and Supervisory committees for their follow-up and management of the progress and accomplishment of the Thesis works and special thanks to Prof. Tilahun Mamo.

I would like to acknowledge the Arba Minch University, Addis Ababa University, Ethiopia, University of Waterloo, Canada and the Sida project for the funding to support my Ph.D. work.

I acknowledge Prof. O. Batelaan and Dr.ing. Abdollahi Bashir from the Department of Hydrology and Hydraulic engineering, Vrije Universities Brussel, Belgium for providing me the Seasonal WetSpass GRAPHICAL USER INTERFACE Model and professional suggestion during model calibration.

I am thankful to the hydrology section of the Ministry of Water, Irrigation and Electricity, Ethiopia, and National Meteorological Services, for the provision of relevant data.

There are people who should deserve great acknowledgment for their contribution in one way or another during the entire research period: all senior Ph.D. candidates (Dr. Fikadu Teklemariam, Dr. Mersha Alemu, Dr. Behilu Brihanu, Dr. Bisrat Elias Dr. Daniel Alemayehu, Dr. Tadesse Tujuba and Mr. Abraham Asha).

Special acknowledgment to my sister Kuku and her husband Mr, Fiseha Israel, I really appreciate your support for all helpful assistance that you have made for me on a day to day life throughout the research period.

Last but by no least, I would like to convey a heartfelt gratitude to my family and friends for their unfailing support and prayer.

THIS WORK IS DEDICATED TO MY PARENTS

For their endless love, support, and encouragement

Table of Contents:

FIGURES

TABLES

APPENDIX

ACRONYMS

AET	Actual evapotranspiration
BF	Base Flow
BFI	Base flow index
Cat_A	Catchment Area
CI	Climate index (RF/PET)
CMIP5	Fifth phase of the Climate Model Inter-comparison Project
CV	Coefficient of variation
DD	Drainage Density
DEM	Digital Elevation Model
EALLJ	East African Low-Level Jet
ENSO	El Niño-Southern Oscillation
Escarp	Portion of Escarpment
FAO	World Food Organization
GCM	General Climate Model
GHB	General Head Boundary
GIS	Geographic Information System
HI	Hypsometric Integral
I	Interception
IDW	Inverse distance weighting
IPCC	International Panel on Climate Change
ITCZ	Inter Tropical Convergence Zone
JASO	Months from July to October
m/d	meter per day
m/day	meter per day
m/s	meter per second
m2/d	meter square per day
Ma	Million years
MAMJ	Months from March to June
MCM	Million Cubic Meter
MER	Main Ethiopian Rift
mm	millimeter
mm/yr.	millimeter per year
Mm3	million cubic meters
MoWIE	Ministry of Water, Irrigation and Energy
MWR	Ministry of Water Resources
NDJF	Months from November to February
NE–SW	North East to South West
NMS	National Meteorological service

NNE	North Northeastern
NNE-SSW	North North East South South West
P	Precipitation
PET	Potential Evapotranspiration
q	Specific discharge
R	Groundwater recharge
RAP	River analysis package
RF	Rainfall
RoF	Direct Surface Runoff
S	Surface runoff
Slop	Slope
Sp.BF	Specific Base flow
Sp.RoF	Specific Runoff
SSW	South Southwestern
T	Transmissivity
TEJ	Tropical Easterly Jet
TP	Time Plot
T-RoF	Mean total flow
WFB	Wonji Fault Belt
WMO	World Meteorological Organization

CHAPTER ONE

1. BACKGROUND

1.1. Introduction

The Great East African Rift is one of the most extensive rift systems on Earth. It is an impressive geological feature that extends from the Jordan-river in the Middle East southward to Mozambique in South East Africa with a dimensional extent of 6400km and 48 to 64km width. In particular, the Ethiopian rift valley is part of the East African rift system, which extends from the Kenyan border, northwestern to the Red Sea. It provides a unique translational area between continental rifting in Kenya and new seafloor spreading of Afar in the onshore extension of the Red Sea and Gulf of Aden (Mackenzie et al., 2005).

In this area, the northern Main Ethiopian Rift (MER) and Afar rifts are virtually active seismically and volcanically, and existing as the only places worldwide where the transition between continental and oceanic rifting is exposed on land (Keir et al., 2006). The rift valley is the result of spreading or rifting, between tectonic plates, which, if it continues, may ultimately transform the horn of Africa into an island in the Indian Ocean (Maguire et al, 2006).

The complex geological processes of the intra-rift faulting and associated volcanic activities resulted in the formation of volcano-tectonic structural depressions, which became born sites and creation of several of East Africa's largest lakes as well as much of its topography (Maguire et al, 2006).

The lakes of Ethiopian rift valley are extending from the Djibouti and Eritrea border in the north from Afar to Lake Rudolf in the south at the Ethio-Kenyan border. The Main Ethiopian Rift (MER) is mainly structurally controlled and fill NNE trending tectonic depressions that contain lakes of different hydrological and morphometric characteristics, (Le Turdu et al., 1999).

The central part of the MER is occupied by lakes; Ziway, Langano, Abiyata, and Shalla, and the southern section consists of the lake such as Hawassa, Abaya, Chamo and Chew Bahir, which make up different lakes basin in the region.

The lakes basin are thought to be hydrologically separate units surfacially, but they may form a unique system hydrogeologically within the rift due to the underground interconnection by NE–SW aligned regional faults that exhibit different ranges of hydro-climatic features (Alemayehu et al., 2005).

Hydro-climatology deals with the interactions of climate with water resource. It recognizes that climate (local and global) as a driving force for the hydrologic cycle. One of the main focuses of the hydro-climatic study is the interactions among hydrological compartments' such as precipitation, actual evapotranspiration, surface runoff, soil moisture storage and groundwater recharge, (Shelton, 2009).

The study of the water budget at a given location and time period essentially deals with the components of hydro-climatology. Indeed, hydrologic modeling is one of the efficient and valuable approaches for understanding the relationship between climate, and water resources or hydrologic cycle in general.

The interaction between groundwater, stream flow, and prevailing climate has gained increasing attention in hydrology, hydrogeology and land reclamation in solving problems dealing with the management of water resources (e.g. droughts, water supply, irrigation, water pollution) and with the prediction of changes in the water regime arising as a result of human activity. This issue also provides the basis for the study of the ecological consequences of alterations in a natural water regime

In Ethiopia, the current trend and future scenarios of unsustainable water resource utilization demands modeling studies that provide accurate spatiotemporal information on hydrological and climatological variables. The main obstacles to such investigations are lack of sufficiently high-quality geospatial and climate data for distributed hydrologic model input calibration and validation. This work tries to assess the predictability based on the relationship between water resource availability and climatic signals by taking reasonable lag relationship. Modeling of resources, impacts and adaptations to climate

seeks to enhance capabilities in building scientific knowledge, advancing technical competence and congruently links scientific and policy communities in the vulnerable developing world which aimed at coping climate impacts. The term "availability" used in this study stands for the amount of water potential under natural process but not exactly referred to committable, usable upon demand to perform its designated or required function.

1.2. Problem and Justification

The environment has been influenced by human beings for centuries. However, it is only since the beginning of the industrial revolution that the impact of human activities has begun to extend to a global scale**.** Today, the scientific evidences disclosed about the increasing concentration of greenhouse gases in the atmosphere and the changing climate of the Earth. At global scale, the temperature is increasing, and the amount and distribution of rainfall are being altered (Cubasch et al. 2001)**.**

According to the International Panel on Climate Change (IPCC) Scientific Assessment Reports, the global average temperature would rise between 1.4 and 5.8°C by 2100 with the doubling of the CO2 concentration in the atmosphere. Sea level rise, change in precipitation pattern (up to ±20%), and change in other local climate conditions are expected to occur as a consequence of rising global temperature (Cubasch et al. 2001). These are expected to have a potential impact on different socio-economic sectors**.** But the full range of consequences would be more complicated on different sectors that are indirectly interrelated to one another (IPCC 2001)**.**

The evaluation of the quality and usefulness of climate modeling systems is dependent matter upon an assessment of both the limited predictability of the climate system and the uncertainties stemming from the model formulation. Many current and more wide studies relied upon hydrological modeling and prediction approaches, still are founded on the stationary assumptions (Milly et al., 2008), which permits extrapolation to the future using models that explain historical data. In a changing world, however, neither the patterns of physical characteristics: land use and land cover, connectivity between channels and wetland environments, or the extent of man-made structures nor external

driver's (temperature and precipitation) forcing of hydrologic response can be treated as fixed (Sivapalan, M et al., 2011). Instead, changes in structure and drivers create new potential dynamics induced, for example by hydrologic systems crossing unknown thresholds. The potential for the emergence of such new dynamics poses significant challenges to modeling and predictability, especially on decadal or longer timescales (Sivapalan, M et al., 2011).

In this regard, a coupled regional climate model and assessing the predictability would enhance the understanding of the complete water processes, cycle and the embedded feedbacks, which allowing a more integrated approach of water resources management and developmental plans in response to the critical water shortage/excess. In particular as a case, the Ethiopian Main Rift fraction, Abaya-Chamo lakes basin can be considered; which is characterized by a complex rift margin zone with associated spatiotemporal variation in hydrogeological and hydro-climatic features.

Besides, it was noted in previous studies (Bekele S., 2001, Halcrow 2008, JICA 2012 and others) on the available key challenges regarding the water resources systems, which includes; increased population and insufficient developed water resources to support the rapid growth of population, Inadequate agricultural food production due to limited use of water for irrigation, arbitrary use of potential & poor management practice in the existing irrigation schemes, degradation of bed and bank, sediment transportation in rivers and deposition of sediment in the lakes, and also flooding of river surrounding with consequent loss and infrastructure damage. Moreover, the limited scientific awareness of water resource potential and non-existent coordinated water resources research efforts in tackling the problems of the lakes basin can be mentioned.

Furthermore, the impact of different climate change scenarios is predicted at a global scale; however, the exact type and extent of such impact at a small watershed scale remain untouched in most parts of the world. Hence, identifying the local impact of climate change at a basin level is quite important. This gives an opportunity to define the degree of vulnerability of local water resources and able to plan appropriate adaptation measures that must be taken ahead of time. Above and beyond, this will provide

sufficient space to deliberate possible future risks in all stages of water resource development activities and projects.

With this background, this research in general is intended to address and investigate how climatic forcing contributes into the local water resource management related policies and planning so that social and economic resources could be utilized optimally amongst the grass-root levels. The scientific results from such study are therefore aimed at creating awareness among the stakeholders of climate-water related service managers, providers and produce user-tailored information that enables the society to mitigate either the possible water scarcity or flooding related burden and minimize the likelihood risks.

1.3. Rationale and Research significance

As per the current increasing population size and water demand, only a few hydrological/ hydrogeological studies were carried out in the Abaya-Chamo lakes basin, (Bekele S., 2001, Halcrow 2008, JICA 2012 and others). Those few studies were aimed to assessing quantity and identify water quality of both surface and sub-surface compartments as a separate and independent system, and sometimes in part at river basin level, however, these studies provides preliminary overview of the climate, hydrology and hydrogeology of the region. Though, none of these studies adequately address important groundwater integration and interaction with surface water and climate change issues as one unit basin system. In this regard, recent water resource modeling efforts at basin level are focusing on the integration and interaction of the hydrologic processes in distributed manner (climate -surface water- groundwater), and also the prediction of the future water budget under changing climate are well recognized. These kinds of studies' approach make use of spatiotemporal distributions of historical hydrogeological, hydrological and meteorological records to calibrate and validate models. The most important result is the elaboration of basin intricate nature of the surface and subsurface hydrology though focused the much greater role of climate change in driving the water availability. Which may in turn enhancing scientific understanding of the hydroclimatic system of the basin as a single unit.

This integration concept signifies the substance of such study with particular reference to the movement and occurrence of groundwater and its interaction with hydraulically interconnected nested surface waters (lakes and rivers) with associated present climate and under projected climate change. In contrast, establishing the future water management plan for the basin without accounting the groundwater fluxes under future stress will certainly lead to erroneous water use practices.

Moreover, it is increasingly recognized that appropriate water resources planning and management at a river basin level is viable only by considering the complete water cycle in the basin, i.e. including subsurface (hydrogeology), land surface (hydrological) and the atmospheric processes. Indeed, steady climatic conditions are no longer considered a valid assumption for sustainable water resources management. The sustainability of water resources, including groundwater, is a significant issue for water planners. Future changes in climate may impact both surface and groundwater resources. This may occur through climate-related alterations in groundwater recharge, as well as from changes from the interactions of groundwater with surface water features. Therefore, despite its significant computational effort water resources studies at basin level are today's increasingly linked to regional climate studies.

1.4. Hypothesis and Research questions

In addition to the population pressure on water consumption and demand, arbitrary water resource use and poor management practice with limited scientific awareness of water resource potential, the projected temperature increase at global scale might reduce the future water availability significantly till the year 2099 in Abaya-Chamo Lake basin. That might affect the main water utilizing sectors like agriculture, water development and supply and the ecosystem.

Thus, the research questions addressed in this study are:

1. How "the platform" as a study area is complex enough with respect to water resource evaluation?
2. What are the most important hydro-climatic features in terms of water resource evaluation in the study area?

3. What are the main dominant controls of the hydrologic system in the lake basin?
4. What are the numbers and characteristics of the available water balance components in the lake basin?
5. How 'possible' to calibrate groundwater flow system over such complex rift margin setting using 500m*500m model grid cell?
6. What are the 21st climate projections of the lake basin and its potential impact on inter annual and long term surface and groundwater resource availability?

1.5. Objectives

1.5.1. General Objective

The current attempt is intended to address & investigate how the long-term regional climatic forcing contributes into the local water resource potential and to understanding the hydrologic system through evaluation of surface and groundwater resource availability and its predictability under projected future climate.

1.5.2. Specific Objectives

The specific objectives are:

1. To analyze and identify the spatiotemporal distribution of hydro-climatic features in the study basin.
2. To undertake multivariate analysis in the characterization of the hydrologic system of the basin.
3. To quantify both surface and dynamic groundwater resource availability in terms of surface runoff, actual evapotranspiration and groundwater recharge using the spatially distributed model,
4. To calibrate groundwater flow system and evaluate alterations in recharge, as well as the interactions with surface water,
5. To analyze the temporal climate change projections till 2099 and its impact on the future water availability
6. To suggest possible strategy and outlooks against resource potential, interactions and impacts for sustainable management and planning.

1.6. Materials and Methods

This particular section is designed to give only the general methodological approach (Figure 1.1(a)-(b)) as guidance for the whole thesis work including main data used; besides the details of methods and material are addressed in each of respective chapters and sub-topics.

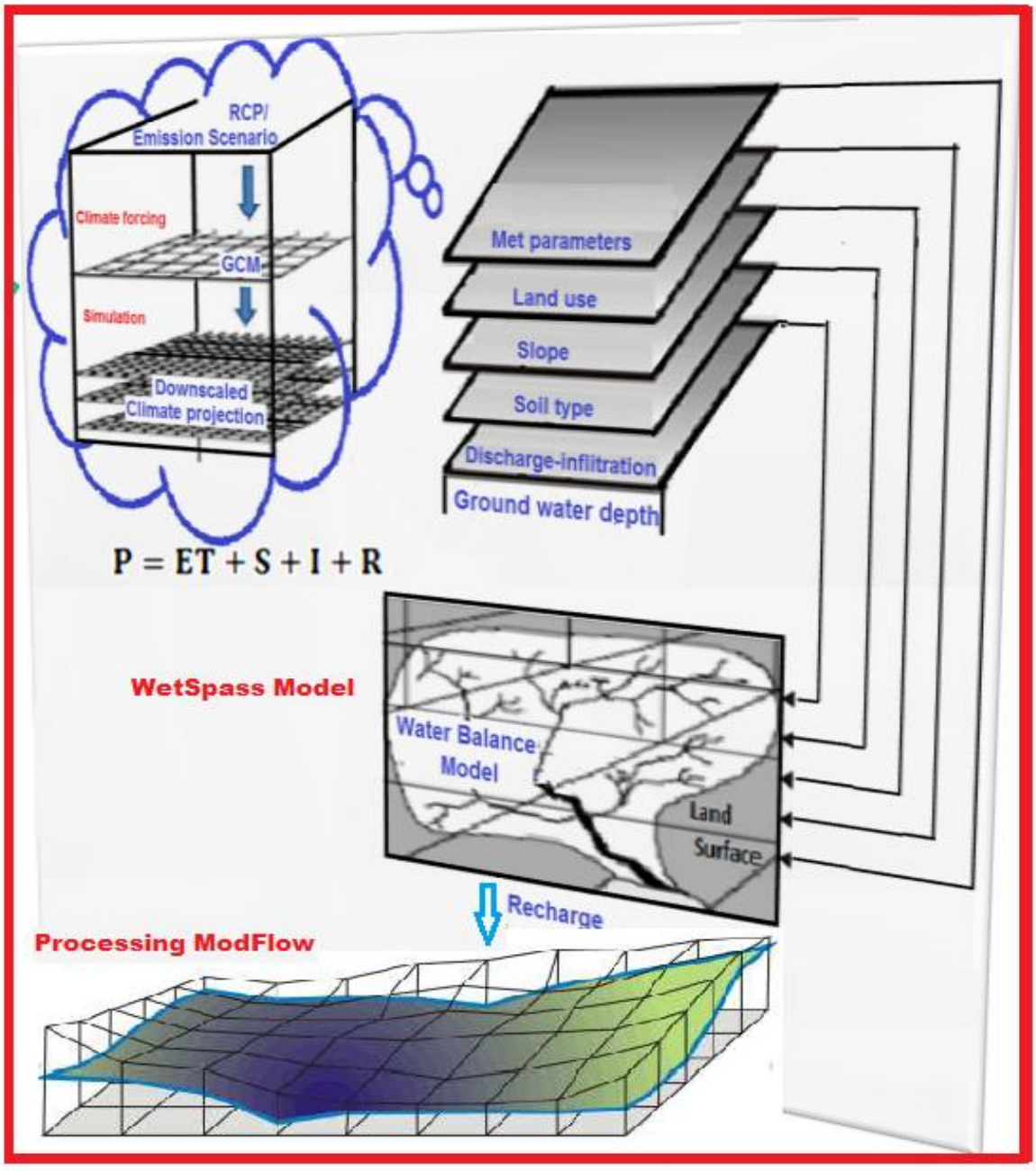

Figure 1.1: (a) Simple schematic conceptual diagram of a methodological approach (Adopted and modified from Batelaan and De Smedt, 2001 and 2007)

An integrated approach was in place spatially at the lakes basin scale with giving emphasis more on the hydrological balance and the hydrodynamics. This effort enabled to understand how the natural and anthropogenic factors affect the water resource availability in Abaya-Chamo lakes basin in a comparative manner.

The lake basin is used for detailed assessment of the recent and future changes due to climatic. The selected basin is located in a hydrogeologically complex rift environment where many natural and anthropogenic factors played important role in changing the water resource. In such a complex rift environment it is prudent to apply a converging evidence and integrated approach. Such studies have used a range of modeling techniques ranging from a point based, empirical, conceptual, soil water balance and lamped to more complex distributed models.

The important parameters that affect the formation of water resources, such as time series meteorological and hydrological, hydrogeological data which cover all available measurement and periods and also geophysical spatial data were collected, reviewed and parameterized from different source including in the field.

As shown in Figure 1.1: (a)-(b), the thesis work generally comprises the following main stages:

1. Identify and characterize the spatial-temporal distribution of important hydro-climatic features and basin multivariate characteristics with respect to both water resource availability and hydrodynamic perspective through various statistical and empirical approaches to the study area under investigation.
2. Surface and groundwater resource availability were handled through quantification of seasonal and annual water balance components such as actual evapotranspiration, surface runoff, groundwater recharge to the aquifer systems using spatially distributed WetSpass model and tested for their fitness to the research area. The model takes into account detailed long-term spatial hydro-meteorological data (available precipitation, temperature, potential evapotranspiration, wind), basin physical data (such as elevation, slope land-use, soil class slope), hydrogeological data (groundwater depth).

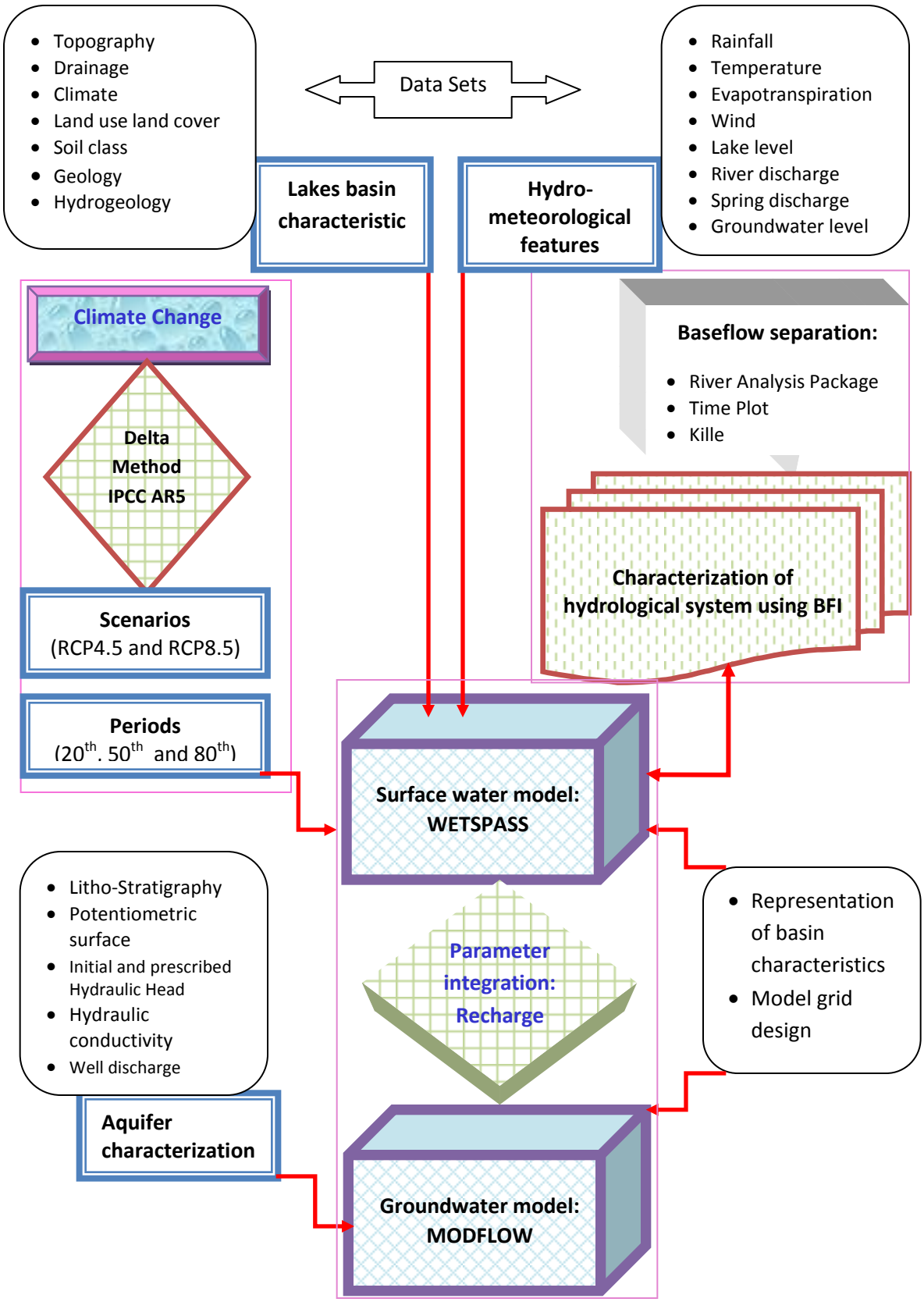

Figure 1.1: (b) Flowchart illustrating the methodology

3. Groundwater flow modeling was undertaken to the whole basin using processing ModFlow to understand flow system and supplement the hydrogeological investigations through reviewing of the conceptual hydrological model (which include identification of aquifer systems, hydro-stratigraphic variations, hydrogeological properties etc.). The groundwater recharge outputs from WetSpass model were used to simulate groundwater system conditions using steady-state MODFLOW model setups. The parameter integration of surface and numerical flow models were conducted to fully characterize the system.
4. Define a methodology to make use of the wide range of climate scenarios and projected climate model outputs (GCM) to basin level using available practical technique and then build the projected climate change with selected scenarios for average temperature and precipitation.
5. Simulation of future water resource availability using the projected climate change under different scenarios as an impact of climate change which was done by assigning a percentage or value changes of seasonal and/or annual time step relative to reference historical or present period. Possible scientific implications were identified against the water resource potential, interaction and impact for sustainable management based on the research result.

1.7. Limitation

Lack of time series data such as evaporation, groundwater level and scarcity of drilled boreholes in parts of the area, scarcity of borehole depth and pumping test data, and lack of a sufficient number of deep boreholes penetrating the whole depth of the stratified multi-layers volcanic aquifer systems are the major limitations.

1.8. Structure of the Thesis

This section describes the structure of the thesis. The thesis is structured into 9 chapters.

Chapter-One deals with a general background about the study area under investigation as well as the thesis work as a whole. It includes a general overview of the study, main problems or research rationale, and relevance, hypothesis, research questions and objectives, general approaches, and materials.

Chapter-Two consists of detail description of the study area, in which location and description of the physical features such as topography, drainage, climate, land use and land cover, soil type are given. Also regional geologic setting and Stratigraphy, the geology of the area including, lithology and geological structures and hydrogeology of the area are treated.

Chapter-Three consists of the basic important hydro-meteorological analysis with respect to water resource occurrence including assessment of meteorological stations data and its relevance. Here spatiotemporal distribution variation of rainfall, temperature, and evaporation are analyzed and also spatial variations, long-term trend changes and relationship with topography were included. Furthermore, areal rainfall depth calculation, clustering of homogeneous climate zones, duration of the hydrologic cycle, and frequency of rainfall event were incorporated.

Chapter-Four is all about the hydrology of the area considering available time series lake level, river, and spring discharges. The properties, annual and intra-annual variability and the relationship among them together with climate were discussed in detail.

Chapter-Five, mainly focused on the groundwater contribution where discharge conditions of aquifers systems are described in detail and the importance of base flow index in characterization of a hydrological system on which different base flow separation techniques were presented and moreover, base flow index was related to other multivariate basin characteristics such as various geomorphometric, hydro-Climatic, land use and aquifer variables which provided important implications for hydrologic system.

Chapter-Six presents, the quantification of water balance components such as actual evapotranspiration, surface runoff and groundwater recharge and calibration of the spatially distributed model on which digital data preparation and validation of the model result included.

Chapter-Seven provides the numerical groundwater flow modeling, that includes a description of the conceptual hydrological model based on the available thoughts and converging data information. Here, details of the model process such as model grid discretization, identification of Aquifer system, the specification of boundary conditions

and hydrogeological properties, model stresses, simulation of steady-state simulation and calibration processes and other related were presented.

Chapter-Eight presents methodological approach related to the climate model, the projected climate of the study based on the ensemble mean of CMIP5 model outputs using low-intermediate (rcp4.5) and high-end emission scenario (rcp8.5) for precipitation and average temperature. And also the projected impact of climate change on the future water availability with respect to historical period as reference including interaction against the impact was described.

Chapter-Nine is all about conclusions on only important results and recommendations and outlooks for further investigations

CHAPTER TWO

2. DESCRIPTION OF THE STUDY AREA

2.1. Location

The study area, Abaya-Chamo lakes basin is located in the southern Main Ethiopian Rift valley as given in Figure 2.1. Geographically the region is bounded within 37° 15' 36" E to 38° 42' 58" E in the Eastern longitude and 5° 25' 5" N to 8° 07' 4" N in the northern latitude. The total basin area is 18905.5 km^2.

2.2. Topography and Drainage

Ethiopia has big geographic and topographical diversity. The Great Rift Valley has dissected the country into western and eastern parts. The western highlands, which lies at an altitude between 2400-3700m with the highest altitude of 4620m above sea level at Mount Ras-Dashen; the eastern highlands in the eastern part of the country; whereas the Rift Valley gorges down to 120m below sea level at its lowest altitude.

The Rift Valley is topographically fault-bounded with broad flat valley bottom bounded by volcanic mountains and hills defining the Lakes basin boundaries in the eastern and western highland areas. The rift margins are not clearly defined everywhere and the highest elevations of the flanking plateau surfaces is 3,430m in the western side (Chencha towards Fonko and North tip highlands), whereas, in the eastern side (Hager Mariam towards Hager Selam) of the rift, the large up high thrust mountains is around 2,500m which are steeply dipping towards the lake. Generally, the altitude of the region varies between 1107 – 3430m above mean sea level. The basin can be divided into three physiographic regions: the rift floor (1107 – 1404m); a transitional escarpment (1404 - 1833m) and the highland plateau (1833 – 3430m) (Figure 2.1).

The drainage basin comprises the two low-lying lakes: Abaya and Chamo with a surface area of 1109.9 km^2 and 316 km^2 respectively. These lakes occupy much of the rift floor. All rivers drain towards the two lakes. Major rivers converge towards these lakes from both the western and eastern highlands and northern as well. The study focuses on the

whole lakes basin, major rivers dominantly that terminate in Lake Abaya. Lake Abaya outflow to Lake Chamo seasonally through local grabens.

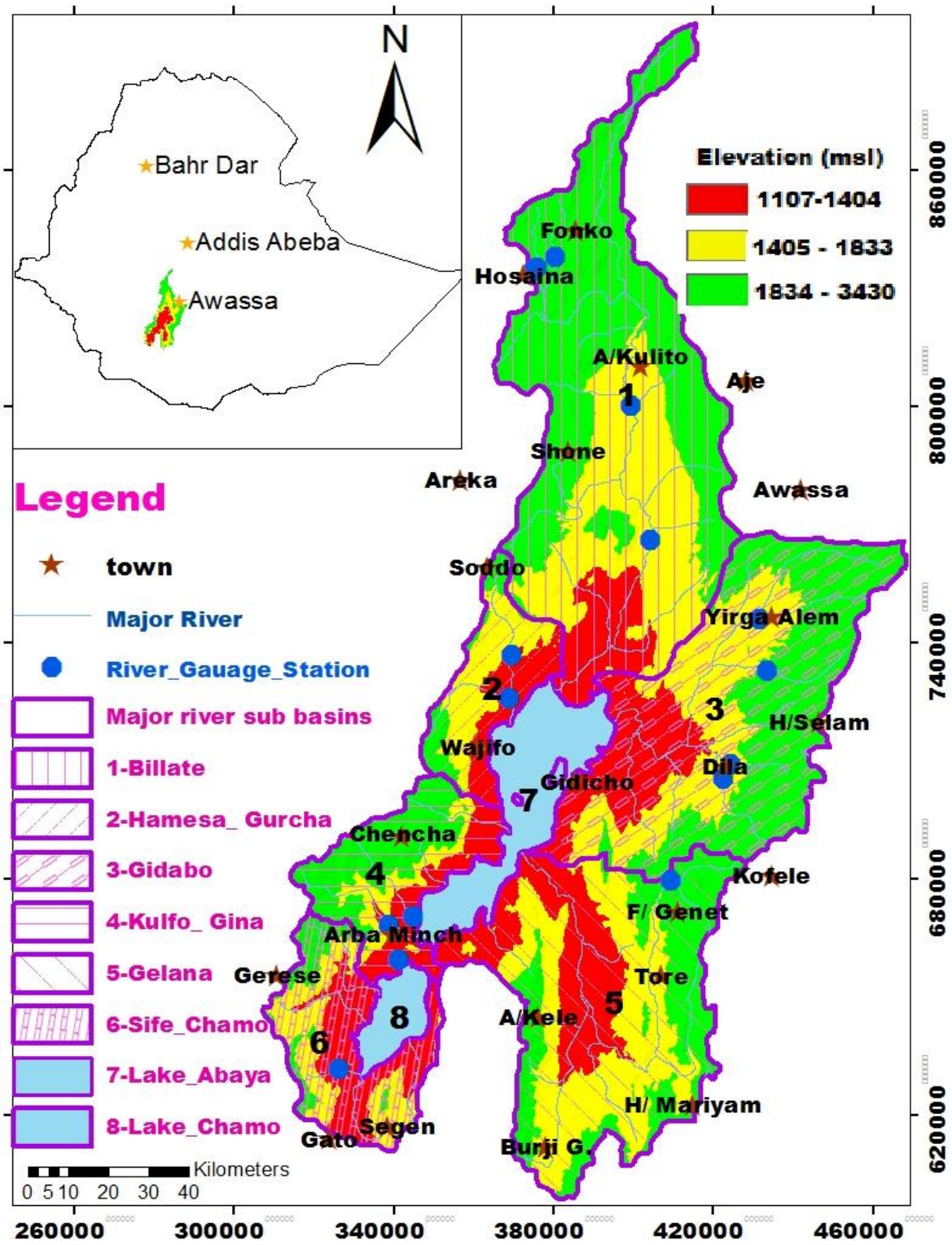

Figure 2.1: Location, elevation, and major river basin of the study area

There are six major rivers that flow into the two lakes. These rivers with corresponding catchment areas include Billate (5659.5km^2), Gidabo (4199.1km^2), Gelana (3865.6km^2); Hamessa-Guracha (1006.7km^2), Kulfo-Gina (1368.7km^2) and Sife-Chamo (1379.4km^2) (JICA, 2012; Halcrow et al. 2008). The study focuses on these major river sub-basins.

2.3. Climate

The differential heating of land and ocean surfaces due to the seasonally changing position of the sun causes latitudinal pressure gradients. The consequent large-scale pressure gradient distribution and asymmetry with movements of pressure systems causing a north-south propagating global tropical rain belt (ITCZ), together with associated wind system such as Tropical Easterly Jet (TEJ), East African Low Level Jet (EALLJ), El Niño-Southern Oscillation (ENSO) (Endalew, 2007) and the development of the Indian monsoon both as part of the seasonal migration, control the climate system and the circulation around tropics (including Ethiopia),(Gadgil et al. 2007).

Thus, the climate pattern and distribution of Ethiopia is mainly determined by the alternations of ITCZ (global pressure systems with the allied wind system, i.e. the wet southeasterly winds meet the dry northeasterly winds and the moist air is forced upward and condenses (Block and Rajagopslsn, 2007) together with the strongly varying topography leads to distinct climate zones and seasons (wet and dry) across the country (Camberlin, 2009). But the movement of the ITCZ is influenced by the variation of the Indian Ocean surface temperatures which, in turn, respond to the variability of the El Niño Southern Oscillation. The significant correlation between ENSO and rainfall has been documented by (Haile, 1990, Beltrando & Camberlin, 1993, Seleshi & Zanke 2004, Gissila et al., 2004, Segele & Lamb 2005 and Korecha & Barnston 2007).

As part of Main Ethiopia rift, the climate of the study area is also mainly controlled by the seasonal migration of the ITCZ, which is conditioned by the convergence of trade winds of the northern and southern hemispheres and the associated atmospheric circulation. The rainy season in the area extends from March to May and from June to September; indicating bimodal rainfall pattern (Otterbach L., 1995). Mean annual rainfall varies across the river basins from 951mm to 1653mm. The Abaya- Chamo lakes

basin climate is further characterized by high rate of potential evaporation (about 2300 mm per year on average from pan-evaporation measurement). The mean annual temperature is about 20.2°C in the rift floor with slightly lower values in the adjacent highlands.

2.4. Land Use and Land Cover

The land cover of the basin is summarized in Figure 2.2. The information has been obtained from FAO (1998).

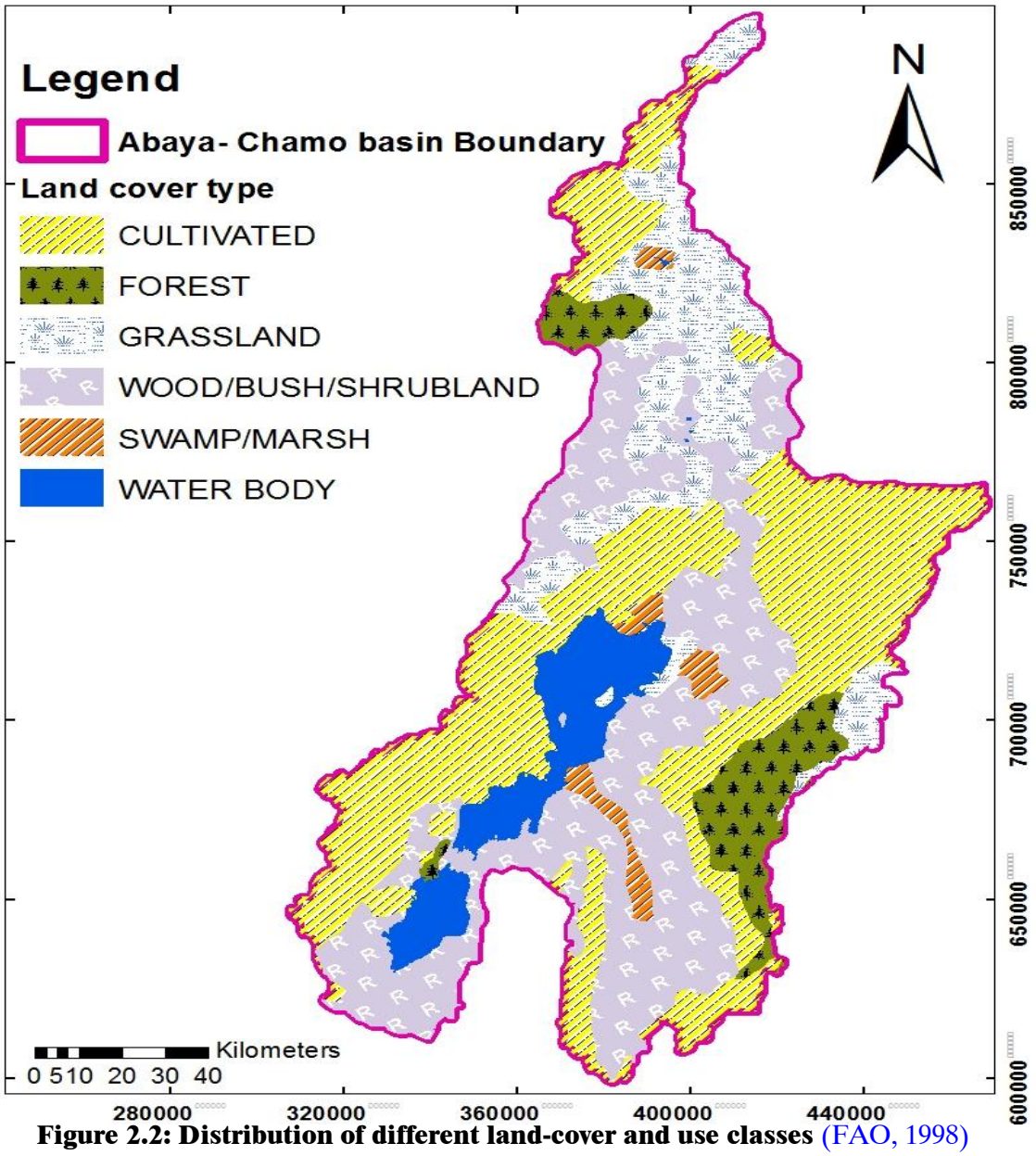

Figure 2.2: Distribution of different land-cover and use classes (FAO, 1998)

Six land-use classes were identified and the land cover and use map of the basin shows, cultivated (49.1%), wood/bush/Shrubland (33.9%), forest (5.4%), grassland (10.5%), swamp/marsh (0.8%) and water body (7.4%). The rift floor and the highlands are mostly farm plots with intervening grazing land. The transitional escarpments are mostly woodland and bushes. There are riparian vegetation and irrigated farms along the course of some of the rivers.

2.5. Soil type

Soils existing in Abaya-Chamo lakes basin have been classified by FAO (1998).

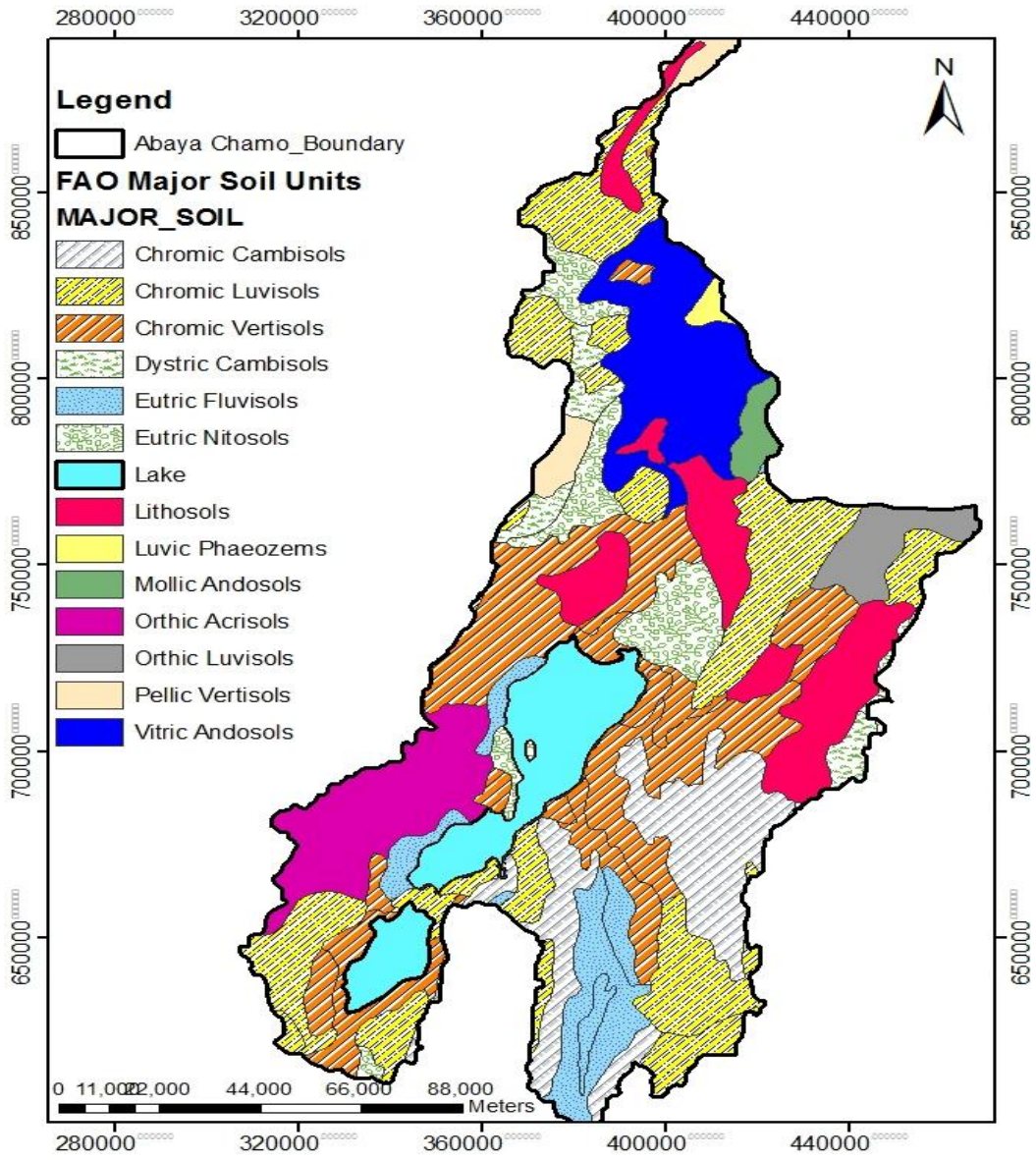

Figure 2.3: The soil map of the study area (FAO, 1998)

Further. it has been described in detail by BCEOM (1999) and SMEC (2007) as a function of color, cation exchange capacity, base saturation percentage, soil horizons developed, landform/slope and chemistry, which are summarized. The soil types of the lake basin can be identified as given in Figure 2.3.

2.6. Geology

2.6.1. Regional Geological Setting

As a part of East African rift system, the regional geological setting of Ethiopian main rift system has been studied and explained by Merla et al. (1973); Kazmin, (1973) Mengesha et al. (1996) and WoldeGabriel et al, (1990). The region has evolved over a span from late Precambrian to the Quaternary period during which there are significant volcanic activities are documented in Oligocene, middle Miocene, late Miocene, early-middle Pleistocene, and Holocene.

In this particular region of southern Ethiopia, the oldest highly metamorphosed and deformed gneissic formation existence as a part of the Mozambique belt (Gilboy, 1970; Chater, 1971; Kazmin, 1978a) is apparently believed of the Middle Proterozoic age. These Precambrian metamorphic basement grades belong to the middle to upper amphibolite facies, up to granulite facies rock outcrop is exposed in around toward south-east of Lake Abaya and Chamo (Davidson, 1983).

The oldest volcanic activities representing the pre-rift volcanic succession provided volcanic formation (Alaji groups such as are basalt and rhyolite flows) and created lava plateau in between Oligocene–Miocene, which exposed in and around the rift margins (Kazmin et al., 1978).

The uplifting doming and subsequent rupture, dissection and spreading of the Afro-Arabian continent resulted in the formation of the East African Rift system oriented in NE–SW and NNW–SSW directions. The initial opening of the Main Ethiopian Rift began around 15 to 14 million years (Ma) ago to the development of rift around 10 Ma ago; (Davidson, 1983, Coulie et al., 2003; Abebe et al., 2005) with faulting of the pre-rift volcanic succession. In this period (around 9.5–4 Ma), a huge pyroclastic flow called

Nazareth group consists of a thick succession of steroid silicic, ignimbrites, unwelded tuffs, ash flows, rhyolite and trachyte flows and domes covered the rift escarpments and margins of the plateau. This group is currently observed through geothermal well in the basin rift floor at the depth around 2100m overlain by a sequence of flood basalts of Pliocene age (WoldeGabriel et al. 1990).

In Pleistocene, tectonic movements related to the main spreading axis of MER produced step-like structures at the rift floor so called Wonji Fault Belt (WFB), with associated volcanic activity which represented by Wonji group such as rhyolite, trachyte lava flows, pumice, unwedded tuffs, obsidians and pitch stones (Kazmin et al., 1980). These volcanic activities mainly characterized by per-alkaline fissure basaltic and rhyolite eruptions created calderas and many lakes appeared and disappeared by obstruction of volcanic deposit.

In quaternary, the extensional fractures in the WFB produced another type of volcanic eruption of basalt lava flows from fissures and these are mostly found on the rift floor, to the north of Lake Abaya. Thus, the post-rift volcanic activity very often took place in the lacustrine environment and produced rocks with volcano-lacustrine facies (pyroclastic, rhyolite, and ignimbrite, diatomite, pumice, tuffs, clays, etc.).

Recent fractures began during the Holocene and are still considered as present day; they run NNE-SSW and have shared all the earlier formations of the rift floor (Mohr, 1967).

2.6.2. Stratigraphy

The summarized Stratigraphy scheme of the region with the age and common lithological units of the formations is shown in Table 2.1. Precambrian metamorphic, quaternary volcano-clastic and lacustrine-volcanic rock deposits and various volcanic rocks of Tertiary to Quaternary age cover the Rift Valley floor, tectonic escarpment and adjacent plateau (JICA, 2012).

Table 2.1: Regional Stratigraphy of main Ethiopian rift; (source: JICA, 2012)

Era	Period	Age (Ma)	Formation	Lithology	Thickness (m)
Quaternary	**Pleistocene – Holocene**	<0.8	Volcano sedimentary complex	Polygenetic infill and sedimentary (lacustrine, eluvia and alluvial) and volcano-sedimentary rocks	200
			Central volcanic complexes	Rhyolite and trachyte lava flows	750
				Obsidian and pitch stone	350
				Pumice and unwelded tuff	450
				Ignimbrites	350
				Rhyolite and ignimbrite	850
			Quaternary basaltic volcanism	Basaltic flows and cones	100
				Basaltic phreatomagmatic tuffs	150
				Pleistocene basalts	250
	Pleistocene	1.5–0.8	Dino formation	Dino Ignimbrites, tuffs	30
				Pumiceous pyroclastic	250
Tertiary	**Pleistocene - Pliocene**	4.5–1.5	Shield volcano	Basalt, trachyte, rhyolites ignimbrites	700
				Arba Guba basalt and shield volcanoes	850
	Upper Miocene – Pliocene	9.2	Nazareth formation	Rhyolite dome and ignimbrite flows	1630
				Nazareth formation undifferentiated	
				Trachyte minor tuffs and basalts	
				Basal, trachyte, tuff	
	Oligocene - Miocene	30–15	Pre-rift volcanic	Lower basalt, rhyolite trachyte, Transitional basalt and rhyolite	1600
Precambrian	**Middle Precambrian**	3400-3000	Intrusive	Granite	
			Low grade	Mica and chlorite schist	
			High grade	Gneiss, amphibolite, mafic and ultramafic rocks	

2.6.3. Lithological units and Geological structure

The study area, Abaya-Chamo lakes basin is highly variable as a result of repeated volcanic and tectonic events with the associated erosion of volcanic rocks and deposition

processes. Grabens, a block fault geological structure in which the valley floor has become vertically displaced with respect to the valley sides is one of the prominent features of the Lakes basin and also prevailing tectonic activity and lithological variation control partly the drainage density and drainage pattern. Most of the river channels follow the young lineaments in the rift (Kefale et al., 2013, Thomas et al., 2015).

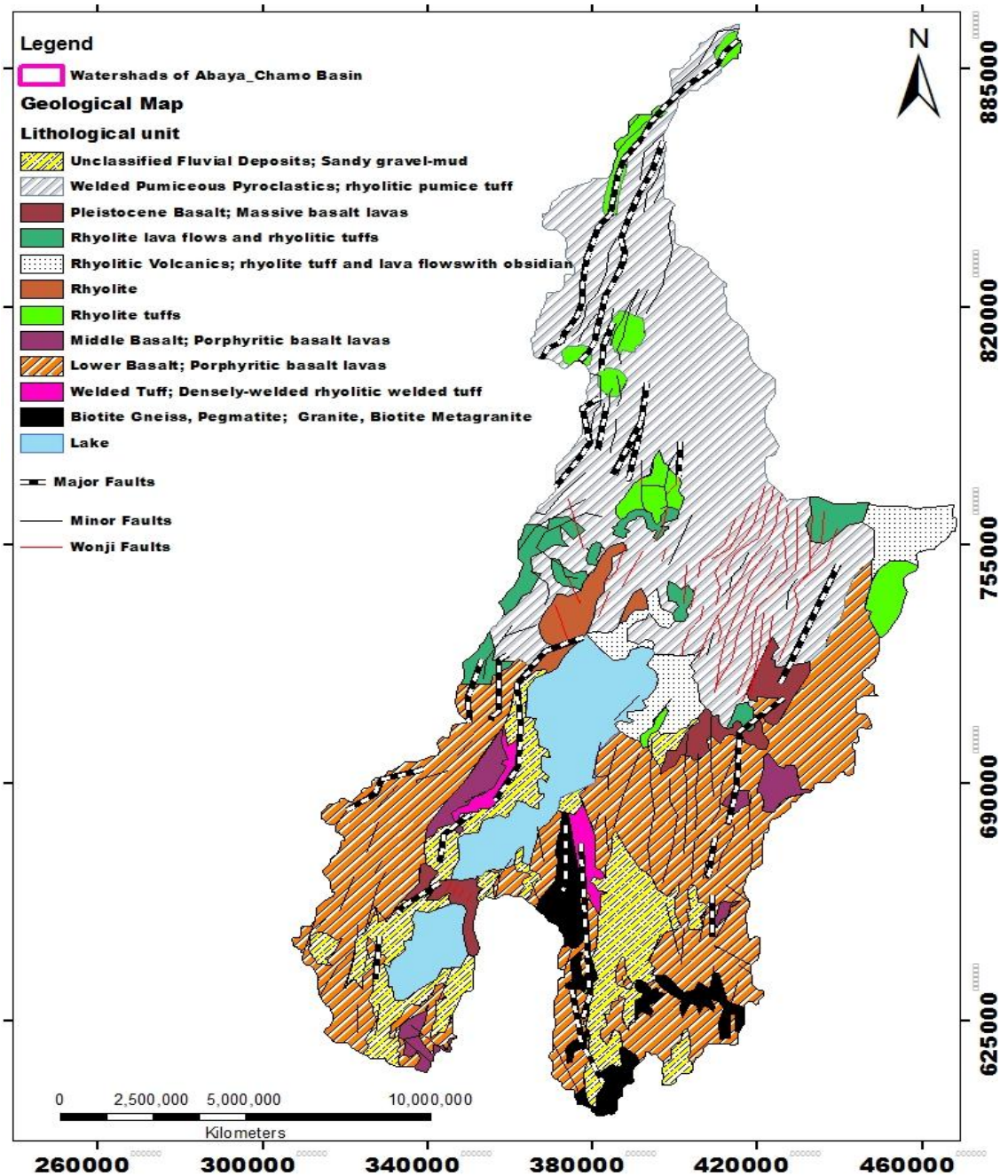

Figure 2.4: Simplified geological map of the Abaya-Chamo Lakes basin (source: JICA, 2012, Kefale et al., 2013, Thomas et al., 2015)

The study area as a part of the southern main Ethiopian rift, characterized by active extensional tectonics with an E–W oriented the direction of extension. Two main fault systems have been identified as shown in Figure 2.4 and Figure 2.5. (1) The rift margins: N30E–N40E trending faults system and (2) the rift floor: N–S to N20E trending fault system along the active Wonji Fault Belt (WFB).

The former, rift margins fault system are characterized by a few widely spaced faults with very large vertical displacements in the rift floor, which is well developed and defined by a more or less continuous system in the eastern margin whereas the western margin is marked by a few major faults, particularly in the Arba Minch and Fonko area.

The second one, WFB, which shows a number of sigmoidal, overlapping, right stepping en-echelon fault arrangement zones obliquely cutting the rift floor have steep scarps and was formed around 1.6 million years (Ma) ago (Mohr, 1968; Kazmin et al., 1980).

The geology of the basin as given in Figure 2.5 above is highly complicated and extremely faulted, as described by; (Kazmin, et al 1980; Harclow, 2008; Woldegebriel et al., 1990, JICA, 2012). The region is characterized by volcanic rocks within tectonically active rift system.

The southern part of the study area is covered by high and low-grade metamorphic rocks of the Mozambican belt, which consist of Biotite Gneiss amphibolite, Mafic and ultramafic Granite Mica and chlorite rocks (JICA, 2012). Older pre-rift Tertiary volcanic succession consisting of basaltic and silicic lava plateaus outcrop on the rift escarpment or margin and the recent volcanic cover the entire rift floor (Kazmin, et al 1980, Harclow, 2008).

With the formation of the WF Belt, Tertiary to Quaternary volcano-tectonic and sedimentation processes result in present-day geologic and geomorphic features in the area and mainly characterized by volcanic rocks of Tertiary period (such as; trap series alkali basalt, trachyte, ignimbrites inter-bedded with acidic tuff, pumice, rhyolite, lava flows, pyroclastic, obsidians and pitch stones) is distributed throughout the entire study area/chiefly in the rift floor area.

Also, the dominant parts of the rift floor, especially the surroundings of lakes Abaya, are covered by volcano-sedimentary/alluvium deposits (Aden series basaltic flows and related spatter cones) materials of the Pleistocene–Holocene age (Woldegebriel et al., 1990). Generally, the age of the rocks becomes older as one goes from the north through the rift toward the south of Lake Chamo.

2.7. Hydrogeology

The hydrogeology of the study area is based on the assessment from existing reports and maps of previous hydrogeological work at different scale (Astatke Kiflu, Jiri Sima, 2012, Kefale Tilahun, Jiri Sima, 2013, JICA, 2012, Woldegebriel et al., 1990).

2.7.1. Aquifer type and Aquifer potential

The rocks with different ages representing various lithological unit and forming alternating permeability and impermeable components affected by different sets of faults and degree of weathering resulted in differences in hydrogeological features.

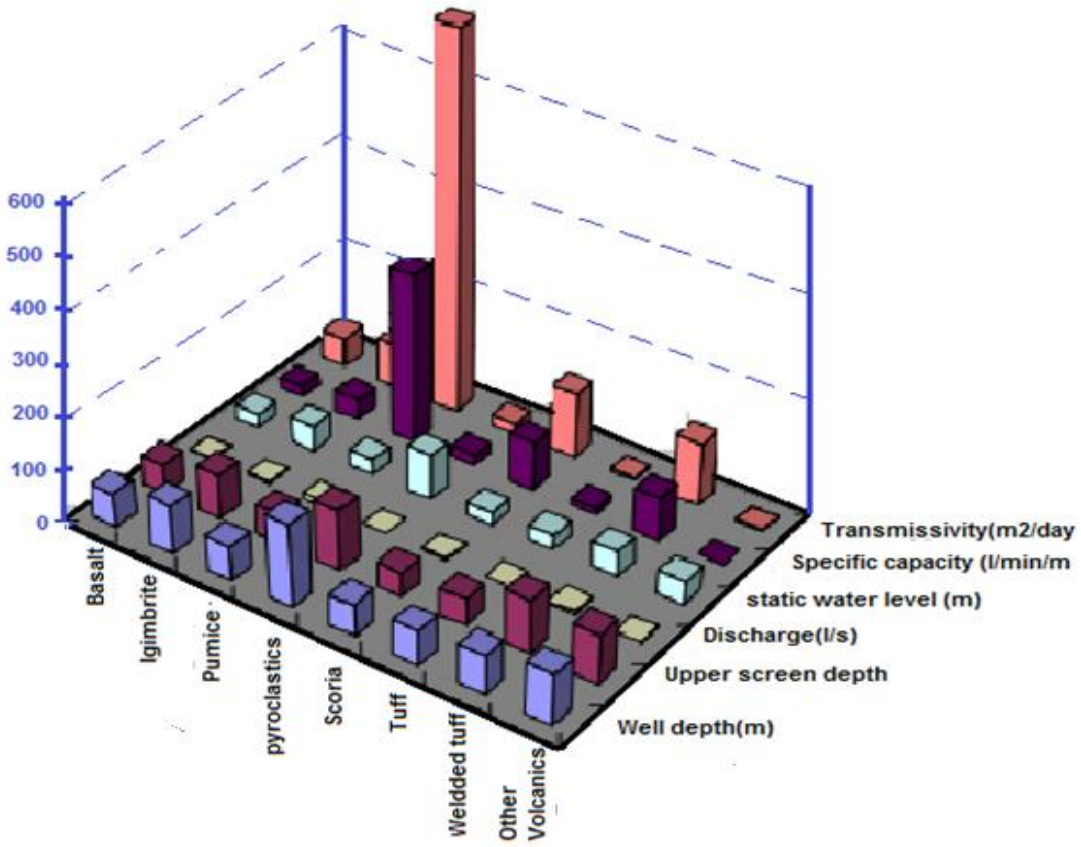

Figure 2.5: Average hydrogeological features of different major volcanic aquifers (JICA, 2012)

The weathered and fractured volcanic rocks with minor sediments deposited (Alluvium, clay, sand, Gravel, sand, and gravel between different series of lava flows accounts for the major part of the aquifer. With regard to the degree of weathering and fracturing and position of volcanic aquifers, hydrogeological studies in the area identified the major aquifers such as basalt, and pyroclastic, ignimbrite, tuff, welded tuff, scoria and pumice, ash deposited and other volcanic (trachyte, Rhyolite, volcanic sediments) during different ages.

About 70% of aquifers in the area composed of volcanic rocks with a large degree of variation in hydrogeological aquifer properties, even the same aquifer would have a very large range of values of transmissivity, for example, lacustrine sediment aquifer has transmissivity varies from 81.8 to 2,080 m2/day. The diversified variation is increased among different aquifer units as given in Figure 2.5.

Among aquifers in the area such as above, gravel, pumice, welded tuff and scoria are found to be potentially good aquifers that exist with an average well depth is about 50m below surface level. Halcrow (2008) estimated representative aquifer parameters in the rift valley, for instance, Transmissivity of Alluvium, ranges between 40–345 m/day, Lacustrine 10–2,800 m/day, Basalt, 39–130 m/day and Ignimbrite 1–1,300 m/day.

During past volcanic events, the rocks have been weathered and/or eroded with subsequent deposition of alluvial materials giving rise to layers of inter-volcanic alluvial deposits and soils. Accordingly, the distribution is laterally and vertically complex and the layers have defined the geometry.

In the lakes basin, in summary, the aquifer types are categorized as the range of confined to semi-confined aquifers, however, shallowest aquifers are unconfined. The complexity of the aquifers resulting from above-mentioned intercalation of volcano-sedimentary distribution and along with persisting tectonic activity affected evenness in the formations and thus a single aquifer system doesn't exist. A combination of the above aquifer types could occur at a single locality.

This is also pointed out by JICA (2012) as It is difficult to review the aquifer potential by the stratigraphic classification, however, major aquifer unit can be classified better

based on the discharge & major lithology. The classification of major aquifers is given in Table 2.2 below.

Quaternary Sediments & Lacustrine aquifer is a good aquifer due to its nature of formation (sand, gravel) most of which is shallow and unconfined. It is assumed to be easily affected by surface pollution and could show seasonal variation in the water table.

Pleistocene tuff, welded tuff and basalt is classified as extensive aquifer with fracture permeability with highest hydrogeological properties than others (about mean of 6.3 l/s, 134 l/min/m, and 242 m2/day discharges, specific capacity, and transmissivity respectively).

Tertiary tuff and basalt aquifer is distributed in the entire area particularly continuously in the south of Dila and also found in a fissure in the volcanic rock. It is relatively poor aquifer and considered as good aquifer in remote areas.

Table 2.2: Aquifer classification in the basin (source: JICA, 2012)

Aquifer	Lithology	Q [l/s]			Sp.cap [l/min/m]			T (m2/day]		
		Ave	Max	Min	Ave	Max	Min	Ave	Max	Min
Quaternary Sediments & Lacustrine	Alluvium	2.8	6.5	0.2	0.5	1.2	0.1	75.3	92.6	43
	Gravel, sand mud	4.6	7.3	1.5	0.3	0.7	0.01	69	137	1
Pleistocene tuff, welded tuff and basalt	Tuffs and pumice	5.5	47	0.2	0.7	1.8	0.02	42.5	84.8	0.2
	Rhyolite welded tuff	4.6	18.5	0.2	0.5	1.5	0.01	65.3	173.9	0
	Basaltic tuff	6.3	22	0.1	2.2	6.9	0.04	242	914.4	12.5
	Basalt	2.9	7.7	0.2	0.3	0.9	0.05	77.7	211.7	2.7
Tertiary tuff and basalt	Rhyolite lava and tuff	4.9	19.6	0.6	0.2	0.4	0.1	9.3	24.8	0.1
	Rhyolite tuff and basalt	3.9	6	2	0.2	0.2	0.2	12.6	12.6	12.6

In comparison, aquifers in the plateaus due to the lower density of fracturing its productivity (lower than 10 m^2/day) is low as compared to the escarpment area. In the escarpment area, its transmissivity value ranges 50 to 200m^2/day. Thus the extensional rift tectonics strongly controls the movement and occurrence of the deep groundwater system (Gizaw, 2002).

In general, based on the conclusions of the JICA (2012) study, highly productive water sources can be found in the area between the slope along the rift ridge and the flat lowlands with high groundwater gradient can be expected on the escarpment. Thus High discharge cannot be expected on the escarpment on the eastern and western ridges.

2.7.2. Hydrogeological Map

Quantitative classifications of various geological units as aquifers are given in Table 2.2.

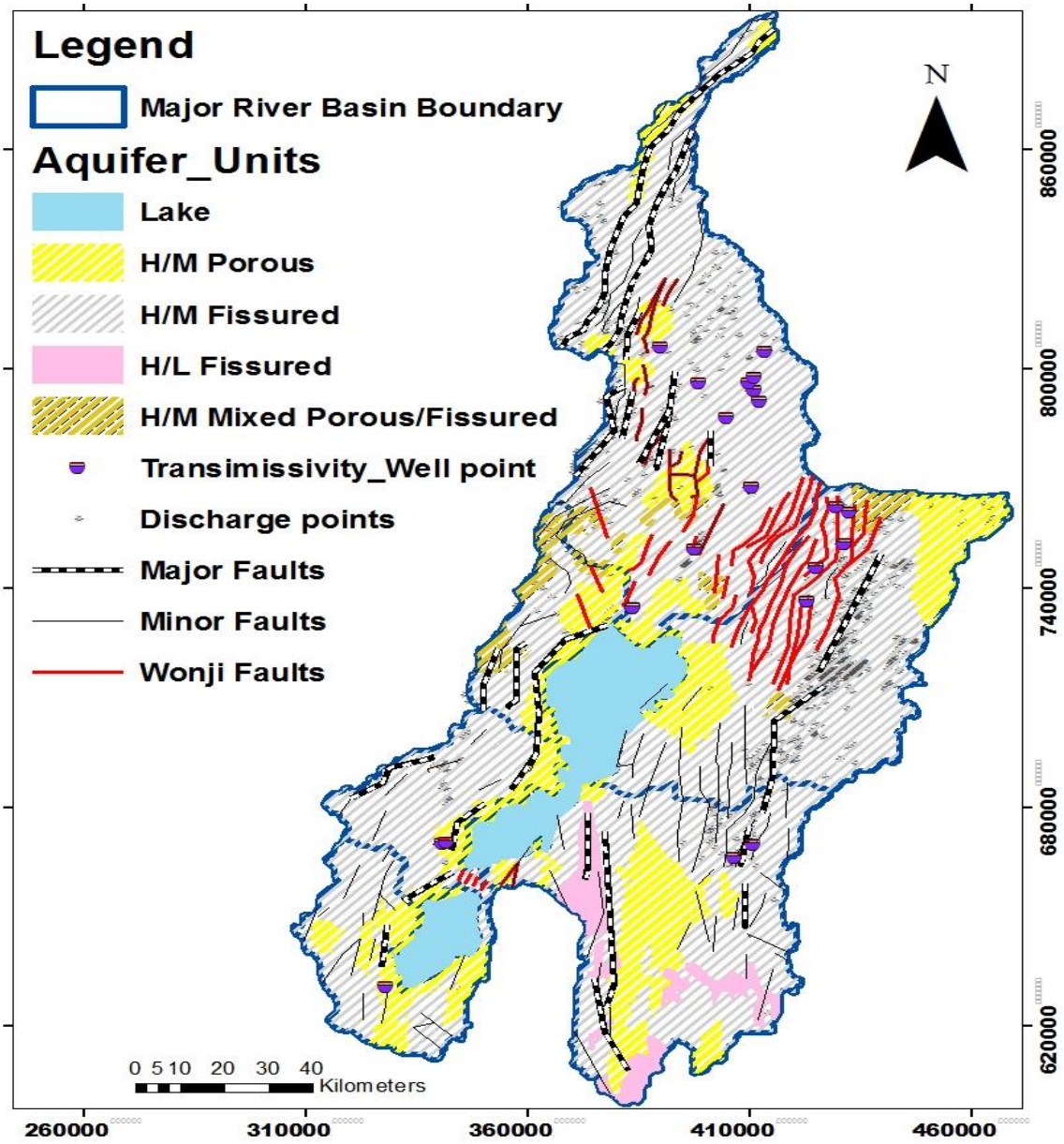

Figure 2.6: Simplified hydrogeological map of the study area.
(in the figure, H/M & H/L stands for aquifer productivity from High to Moderate and High to Low respectively) (Source: JICA, 2012, Kefale et al., 2013, Thomas et al., 2015)

Table 2.2 can be described qualitatively (refer Figure 2.6) with their topographical position within the area, which leads to a definition of elements of the hydrogeological system and its conceptual hydrogeological model.

Kefale et al., (2013) and Thomas et al., (2015*)* tried to classify the hydro-stratigraphic units of the basin (as shown in Figure 3). Accordingly, three classes have been identified. (1) Porous media aquifer (formed in lacustrine and alluvial and colluvial sediments and volcano-sedimentary type of rocks of Quaternary age along the rivers, lakes and as an infill of depressions on the rift floor; (2) Fractured aquifers (formed in Tertiary and Quaternary basalts, trachyte, ignimbrite, and rhyolite in the highlands, escarpment and rift floor areas; and (3) Fractured and porous media mixed aquifers (formed in volcanic rocks intercalated with sedimentary and pumiceous pyroclastic rocks).

CHAPTER THREE

3. HYDROMETEOROLOGY

3.1. Meteorological stations and data

All-important meteorological and hydrological stations used in sections (Chapter-3 and Chapter-4) for the study area are operated under National Meteorological Service (NMS) and Ministry of Water, Irrigation and Energy (MOWIE), Ethiopia. Particularly, meteorological series data sets such as rainfall, temperature, etc. are available for the period from early 1980's to present for stations but the range of record history differs among available station. Whereas the hydrological data has relatively lower record history in comparison, the majority of station record has started measurement on time series from 1980's onward.

A set of daily available meteorological data were collected for 46-stations from National Meteorological Agency (NMA) and its branch offices (Hawassa branch). The observation, measurements and data collection procedures have been conducted according to world meteorological organization (WMO) guidelines since; Ethiopia is one of the members of WMO. Observation stations in the area are classified as class-1 or synoptic, where around 12 met parameters are recorded, class-3 (rainfall, minimum and maximum temperature) and class-4 (only rainfall amount is measured).

The collected meteorological data were supposed to cover all available stations for the record period in the study area. The measurrnents of stations were identified as relevant as per their data quality and missing records within the study area and nearby bordering stations as given in Appendix 1.

From water balance assessment point of view, a given river or lake basin is considered as a basic spatial unit in hydrology to account the complex interaction among hydrologic processes, Accordingly, the basin of Abaya and Chamo lakes is assumed to be hydrologically single closed basin where there is no surface inflow/outflow of water from/to the other basins due to its geo-topographic characteristics (JICA 2012). Thus,

assessment of the cause for surface water formation and accumulation in the underground reservoirs throughout the geological period is critical issue for resource management and development plan.

Under the natural circumstances for a given hydrological basins, the surface and sub-surface water resources over the basin area are created by rainfall rate and pattern. The amount and distribution of the rainfall is then responsible in determining the respective amount and distribution of surface and groundwater resource availability together with other geomorphometric characteristics in the basin.

In general, the formation of water resources and its demand can be seriously affected by the meteorological conditions of a given wide and independent area more than any other factors. In relation to this especially the amount and distribution of hydro-meteorological elements such as rainfall, temperature, and evapotranspiration play the major role in affecting the occurrence of both surface and groundwater resources among other climatic parameters.

Therefore, upon the objective of this study, attention is given for the mentioned parameters above in order to grasp the hydro-meteorological characteristics of the Abaya-Chamo lakes basin along with other significant sets of data and which is a base to analyze water balance of the lakes basin. So that, the data was collected, organized and analyzed in such manner.

3.2. Rainfall analysis

3.2.1. Relevant station data

All data used for rainfall analysis were checked for data quality using double mass curve at early stage, and all the obviously error period in the time series data and stations were erased and rejected with respect to consistency against the climatological history of the remaining period and also adjacent stations. The collected data was verified before analysis and the apparent errors found were all corrected and then 46 stations were used. The locations of the stations from which rainfall data was collected and period of record are shown in Figure 3.1 and Appendix 1.

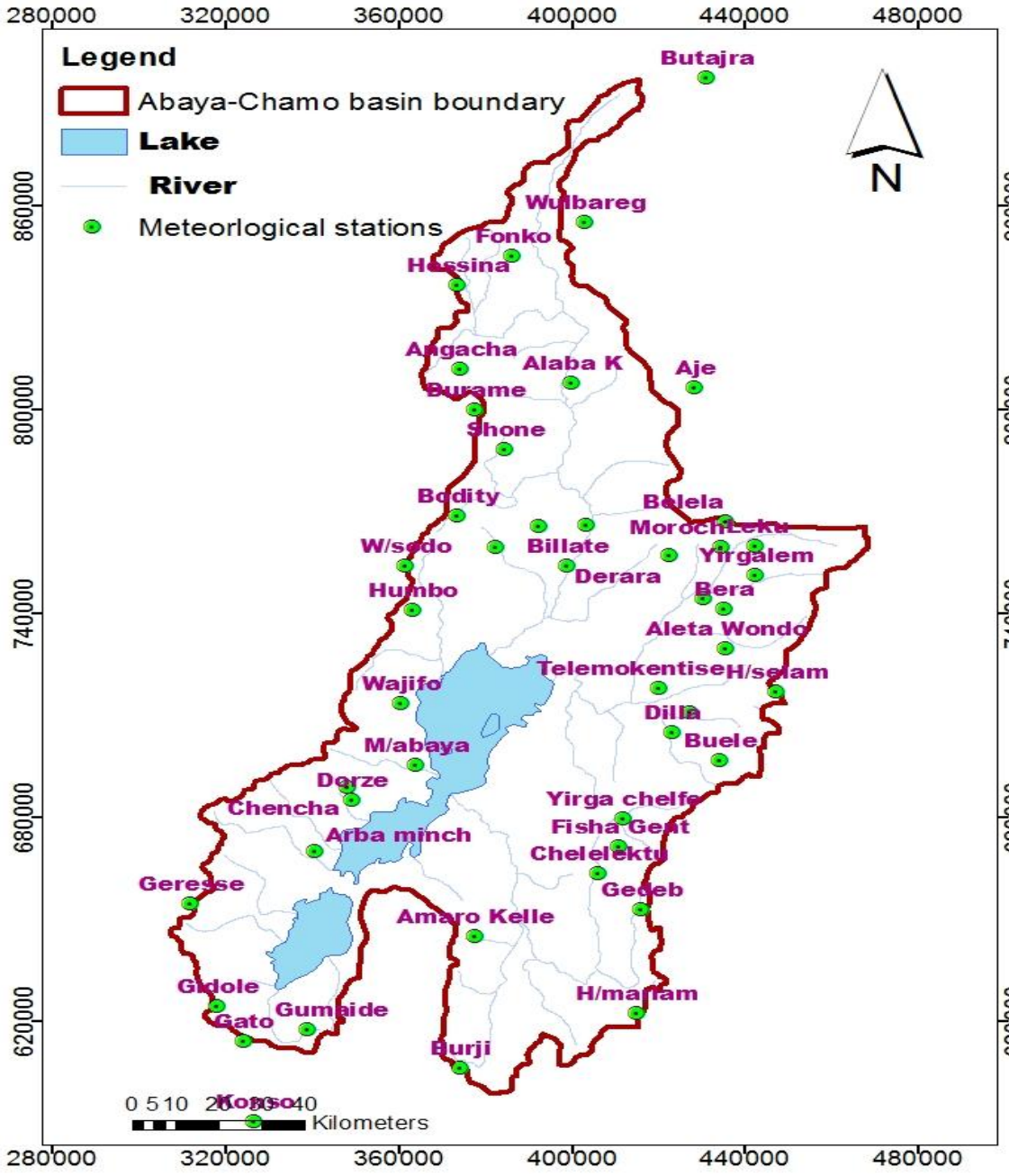

Figure 3.1: Shows the geographical distribution of rainfall

3.2.2. Distribution of mean Rainfall

Due to erratic characteristics of rainfall over space and time, where the amount of rainfall changes every year or season in a given region (i.e. the same area might have got possibly either above or below as compared to the climatological mean rainfall rate as a deviation over some course of a year/season). Consequently, it has been also an issue and sometimes even a problem in studies aimed to understand the general characteristics of

water resources amount in a given area since the hydrological conditions of a given region is fundamentally depend more on rainfall rate and pattern. Despite its critical importance of annual/seasonal rainfall rate and distribution particularly extreme cases in wet and dry conditions, this can be seen through water resources evaluation to prevent and control excessive flood and, drawdown of groundwater etc.

In this view, the spatiotemporal insight was appeared to be an important aspect to look at the climatological history of the total annual rainfall for each observation stations in the Abaya-Chamo lakes basin. The data were then analyzed and compiled based on the available reliable data as given in Appendix 1.

The analysis result of the average annual rainfall amount for the lake basin shows the rate range in between 704mm and 2582mm at Gidole and Gerese station respectively, indicating considerably large difference.

Taking into account the difference in length of stations data measurement, the maximum and minimum rainfall rates were appeared naturally in different years over the area. But nearly about 6 stations (such as Arba Minch, Bedessa, Chencha, Fonko, Shone and Teltele) recorded the maximum annual rainfall in 1997and whereas, other 4 groups of station measured high record in another period of year, (For example, Aje, Gato, Hager selam & Hossaina in 1982: Billate Tena, Humbo, Kebado & Yirgachefe in 1996: Angacha, Bera, Chelelektu & Konso in 2001).

While, the minimum annual rainfall occurs over pairs of station in 1999 at Burji, Billate, Aposto/yekatit 25 & Telemokentise, in 2000 occurs at Bodity, Gumaide, Derara, Konso and also in 1984/2009 at Ymbadubanch, M/abaya, Butajra, Belela Leku station as long as the collected data can reveal.

Based on these extreme records of annual rainfall cases in the lakes basin, particularly in the period from 1999 to 200l, the study area was much subjected to high annual variation even if the stations are distributed in different part over the area.

Overall, for all available stations in the lakes basin, the mean largest and smallest annual rainfalls recorded were l983mm and 745mm respectively, showing a difference of about 1238mm.

Another very important feature of rainfall distribution is the spatial variations of annual rainfall over space. These spatial variations of rainfall over the study area are shown in Figure 3.2 based on reliable data, which are regionalized using commonly known interpolation such as Inverse distance weighted (IDW) and Kriging geospatial techniques.

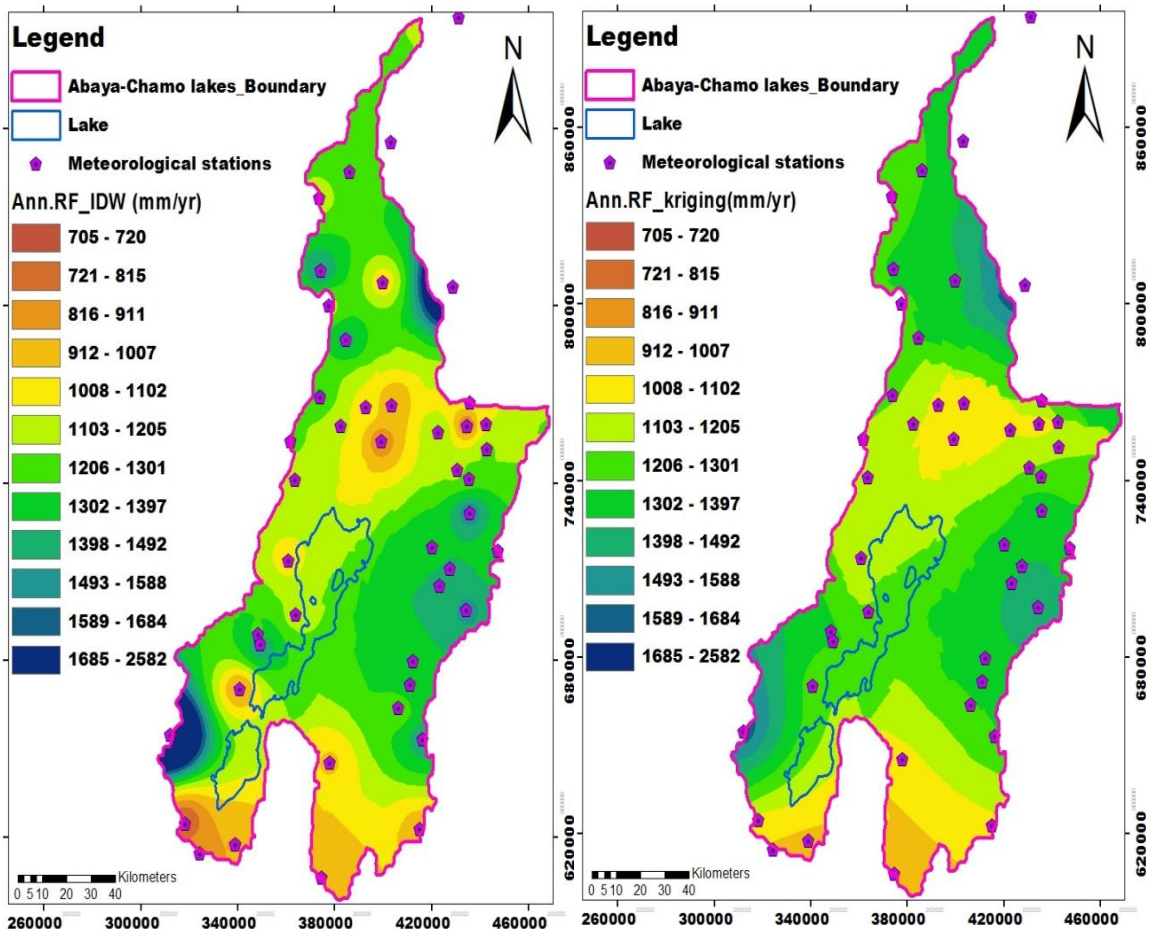

Figure 3.2: The spatial distribution of annual total rainfall (using kriging (left in the figure) and IDW (right one))

The spatial annual rainfall plots in Figure 3.2 shows a significant variation over the study area usig both techniques with toleration of some amount difference due to interpolation errors as comparison. Thus, the ridges of the study area have generally highest annual rainfall rate particularly the northern tip, the mid-eastern highland, and the southwestern highland to mention. While, toward the rift floor around the lakes (Abaya and Chamo) has relatively lower amount (<1200mm/yr) over the climatological history. Moreover, it

became important to check whether the rainfall across the study area compliments with the topographic variation in a way to clear out errors introduced during spatial estimation.

3.2.3. Rainfall – Altitude Relation

The important characteristic of spatial variation of the lakes basin as discussed in above section (Section 3.2.2), the surface topography is a well-known factor in many studies as a factor in affecting rainfall amount in a given area. Hence, further analysis was made to look for the relationship between rainfall and altitude as shown in Figure 3.3.

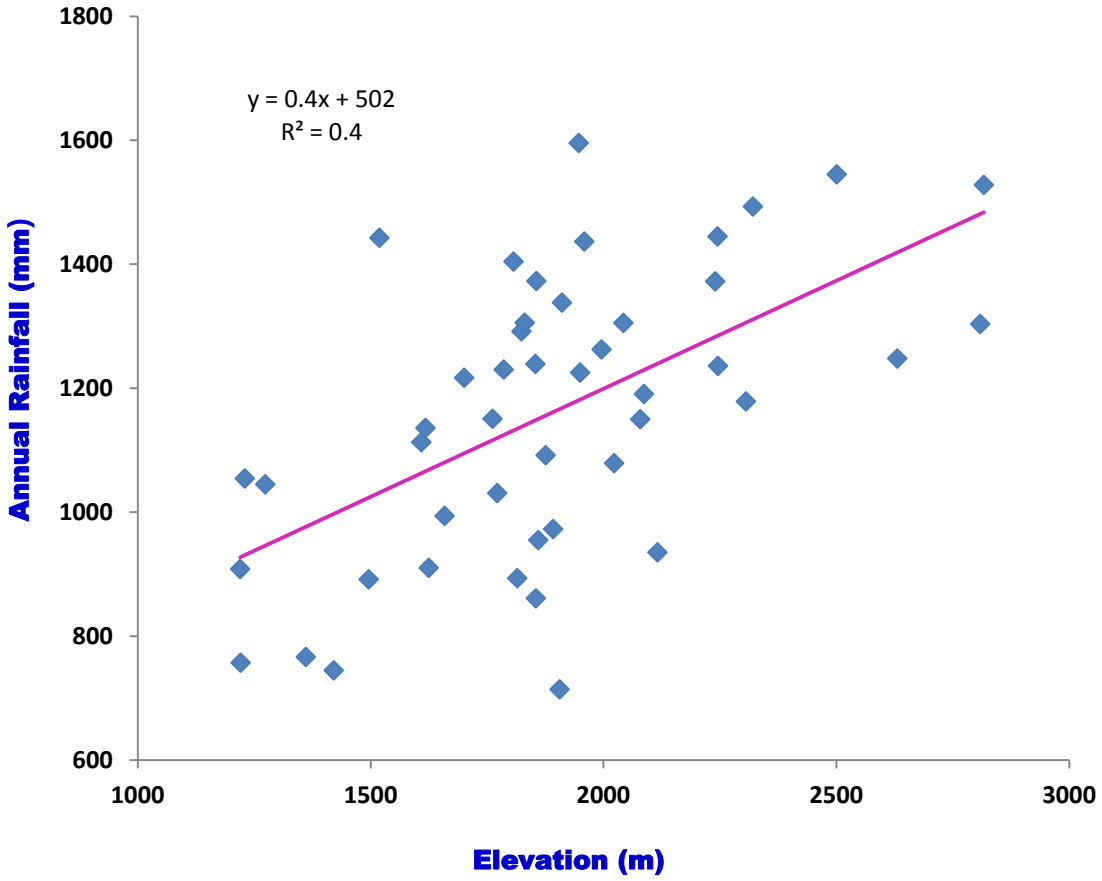

Figure 3.3: shows the correlation result between Rainfall and Altitude

The annual mean rainfall amounts of stations together with corresponding station's altitude were used by assuming the existing distribution were capable in producing at least information on the relationship even though the distribution of the station doesn't seem fairly even across the study area.

The rainfall-altitude graph (in Figure 3.3): shows the slight tendency of an increasing rainfall amount with altitude. Which means the amount of rainfall is moderately related to altitude and affected somehow by topography. This supports the former spatial distribution result in the above Section 3.2.2 that the rainfall relatively occurs at the mountainous edge than in the flat plain along the central axis of study area but still, it doesn't reveal a clear relation to recognize topography as the only factor that controls rainfall amount. So, the determination of areal rainfall depth using altitude relation does not possible in turn. Therefore, it should better to account areal rainfall depth through in placing other technique for resource potential over the sub-basins in the study area.

3.2.4. Areal Rainfall depth

Due to the extent of the study area (over 18,000km^2) and topographical spatial variation, the determination of areal rainfall based on simple annual mean rainfall amount would have a high risk in introducing a large error in local rainfall amount for the basin. Arithmetic method gives reliable result only when there is even distribution of point measurements in the area and more or less flat topography. Besides, if it were a definitely clear correlation between the rainfall and topography, a contour map of rainfall in consideration of the topography had been created to find out the total amount of rainfall with a high level of accuracy. In our case, as discussed earlier, the relation was not explicitly recognized as a strong enough to represent and use it. So that, Thiessen polygon method (Equation 3.1) was used as conventional approach to calculate the annual average rainfall depth for each sub-basin which produces more reliable result in comparison to arithmetic mean.

$$P_t = \frac{P_1A_1 + P_2A_2 + P_3A_3 + \ldots\ldots\ldots\ldots + P_nA_n}{A_1 + A_2 + A_3 + \cdots\ldots A_n} \quad \ldots\ldots\ldots\ldots\ldots\ldots\ldots\ldots \quad (3.1)$$

Where, P_t is the areal mean total annual rainfall, P_1, P_2, P_3,….., P_n: the rainfall at each station and, A_1, A_2, A_3, ……A_i: the area of influence by the individual station (i) determined based on Thiessen polygon method.

This method gives the areas to which the rainfall values of each observation station represent as given in Figure 3.4**.**

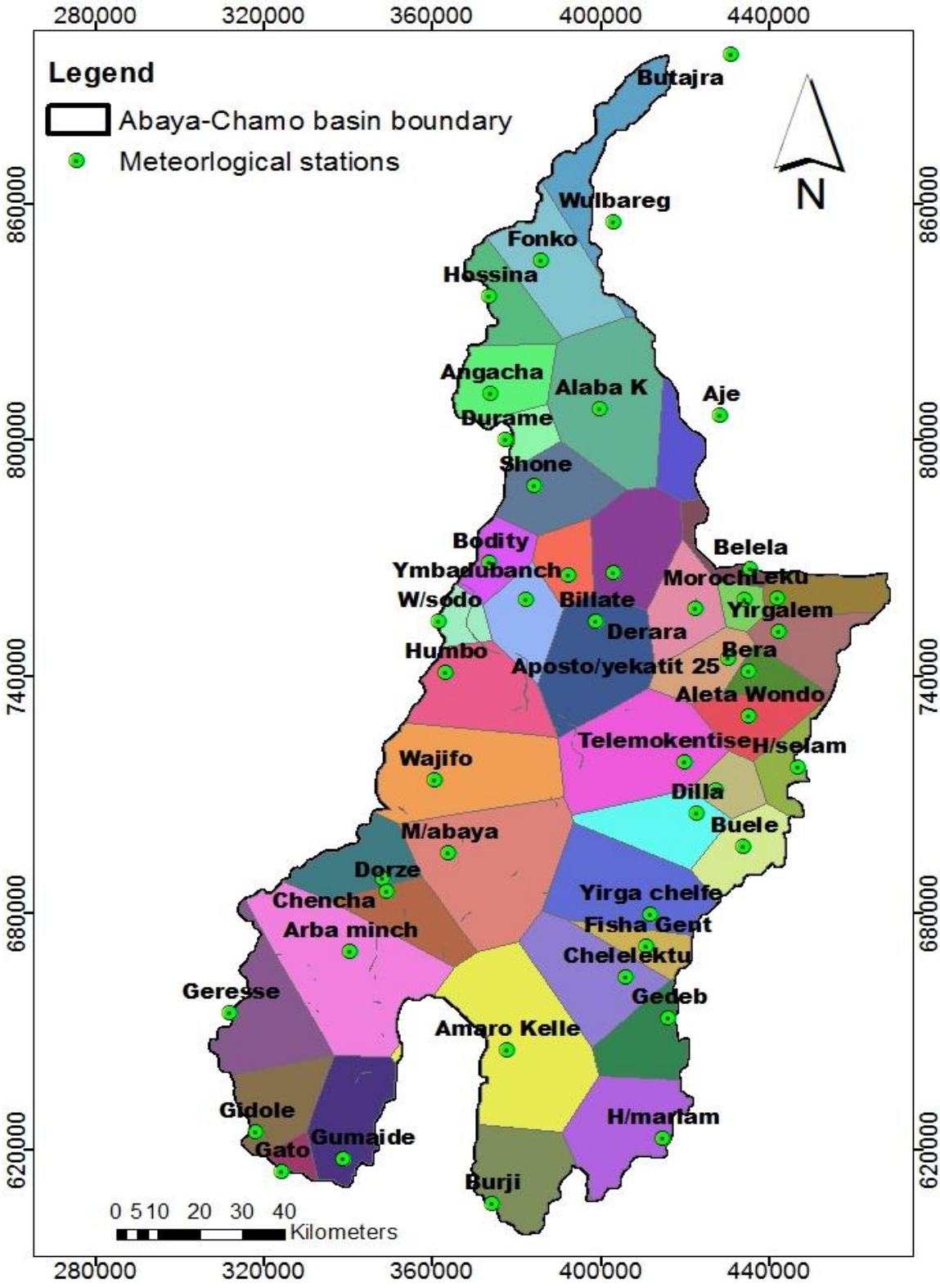

Figure 3.4: shows Thiessen polygon of stations in the study area.

Based on the analysis result, the areal rainfall was calculated per each polygon as given in Figure 3.4 which is used to calculate the total mean rainfall depth for the study area from a water resource availability point of view.

Therefore, the mean annual total rainfall for the study area is about 1164mm/year. Meanwhile, it was found better to organize the areal rainfall amount given in Figure3.4 and Appendix 2 in terms of hydrological basin since it is a basic unit of hydrology. Thus, the whole study area for this particular purpose is treated into six major river sub-basins as identified in subbasin delineation in an earlier section Figure 2.1.

Table 3.1: Summary of annual mean rainfall and potentials over the river sub-basin

Major river basin	**Area** (km2)	**mean RF** (mm/yr.)	**RF*Area** (mm *km2)	**Vol. of RF amount** (Million m3/yr.)	**Vol. of RF amount (**Billion lit/yr.**)**
Bilate	5659.5	1119.4	6335244.3	6335.3	6.3
Gidabo	4199.1	1302.4	5468907.8	5469.0	5.5
Gelana	3865.6	1088.4	4207319	4207.3	4.2
Hamessa-Guracha	1006.7	1095.9	1103242.5	1103.3	1.1
Kulfo-Gina	1368.7	1072.9	1468478.2	1468.5	1.5
Chamo-Sife	1379.4	1429.4	1971714.4	1971.7	2.0
Lake-Abaya	1110.4	1029.3	1142934.7	1142.9	1.1
Lake- Chamo	316.7	964.0	305298.8	305.3	0.3
Sum	18906.1	9101.7	22003140	22003.2	22.0

Arial rainfall depth: $\Sigma (RF_i*A_i)/A$ = 1164mm/year

Accordingly, the station within a given subbasin was considered based on the Thiessen division and the mean total annual rainfall amount was calculated by multiplying the area of the sub-basin by polygon mean rainfall. The total available rainfall potential over the study area was summarized and shown in Table 3.1.

The mean annual rainfall over sub-major basin including the lakes area varies in between 964.0 and 1302.4mm/year, showing the rift over the lakes relatively has low rate. In summary, based on the analysis using rainfall areal depth approach, the total available rainfall for Abaya-Chamo lakes basin, is about 22 billion liters per year.

3.2.5. Seasonal variation in Rainfall

Similar to annual variations, numbers were calculated in monthly bases which are intended to have an insight into inter-annual climate variability for the study area as given in Appendix 3.

In defining climatic regions and seasons, the observations typically are considered just as set of stations or grid points. The monthly rainfall data spread over 46 stations for the available period could suppose to provide an average inter-annual variability. However, a simple averaging and regionalization of rainfall season over such large area has disadvantages of increasing meteorological noise in the delineation of seasons. Moreover, application with a minimized number of variables using single parameter (only rainfall) also amplifies the noise too.

In this regard, traditionally some hydrological studies have not received any attention to the usefulness of the clustering of homogenous climate zones in reducing estimation errors and understanding spatiotemporal rainfall variability, especially over a large area in the past. For instance, Gissila et al. (2004) have pointed out the high spatiotemporal variability of Ethiopian rainfall and suggested the importance of clustering approach rather than using large area as a uniform spatial unit in order to reduce errors.

Another study by Diro et al. (2008) also in similar manner reported a considerable rainfall variability within Ethiopia, over which the rainfall amounts in different rainfall climatic zones are not well correlated with each other, additionally the study indicated the little practical validity of rainfall predictions for the whole of Ethiopia area as a unit, even if the predictions have apparently good skill.

Reduction of regional data and delineation of homogeneous regions is therefore necessary for a given wide region. Due to these and other, clustering approach are quite common in meteorological data analysis, thus the present investigation was motivated by the possibility that the identification of homogeneous climatic zone might contain valuable information as an aid in gaining insight into temporal patterns regarding the intra-seasonal and annual rainfall variability.

3.2.6. Clustering of homogeneous climate zones

Upon its importance, as discussed in above Section 3.2.5, this study was performed clustering using an agglomerative hierarchical approach and Ward's minimum variance method through SYSTAT 8.0 software. The approach considers variables such as the annual and monthly rainfall totals, geographic proximity (longitude, latitude) and altitude of each station. The Euclidean distances between stations with low mean and variance were clustered together to one group, that indicates simply the differences in rainfall are small in absolute terms. As criteria, the maximum Euclidean distance or similarity to classify as one group was 105km. Finally, all available stations in the study area were grouped into eight homogeneous rainfall zones as shown in the cluster tree Figure 3.5.

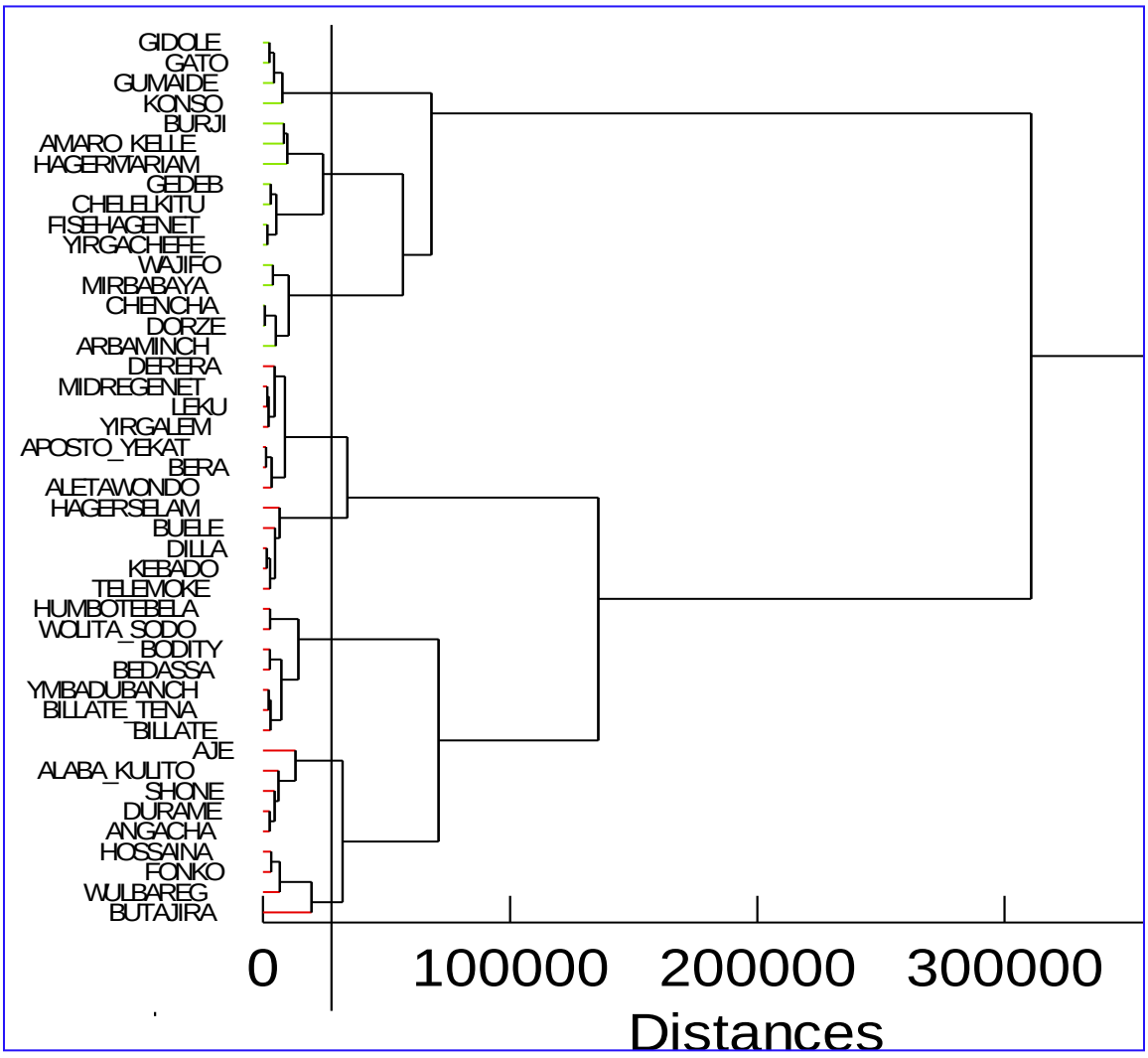

Figure 3.5: Cluster tree using the agglomerative hierarchical method

The cluster tree in Figure 3.5 shows homogeneous rainfall station using the agglomerative hierarchical method in the study area. In order to understand the seasonal variability of the study area, a representative rainfall stations' were selected from each identified homogenous climatic zones, stations with relatively long time series and complete meteorological data among the neighboring stations. So that Hossaina, Alaba Kulito, Bilate Tena, Midre Genent, Arba Minch, Dila, Gato and Chelelektu stations were then analyzed to show the general condition of annual and inter-annual variability rainfall is given in Figure 3.6.

3.2.7. The trend of rainfall

In this section, further analyses were made to examine how the rainfall amount tends to change over a long period of time. These trend analyses based on long-term annual rainfall data have importance in addressing the spatial variation within identified rainfall homogenous zones in the above section. This could have important implication in an identification of hydrologic cycle for a given region which in turn plays a role in long-term water resources management. Indeed, the longer the data period, the more accurate the result of the analysis becomes. So that, the longest data period among the obtained data sets were used to look for rainfall trend through comparison analysis (selected station of each homogeneous zone given in Figure 3.6.

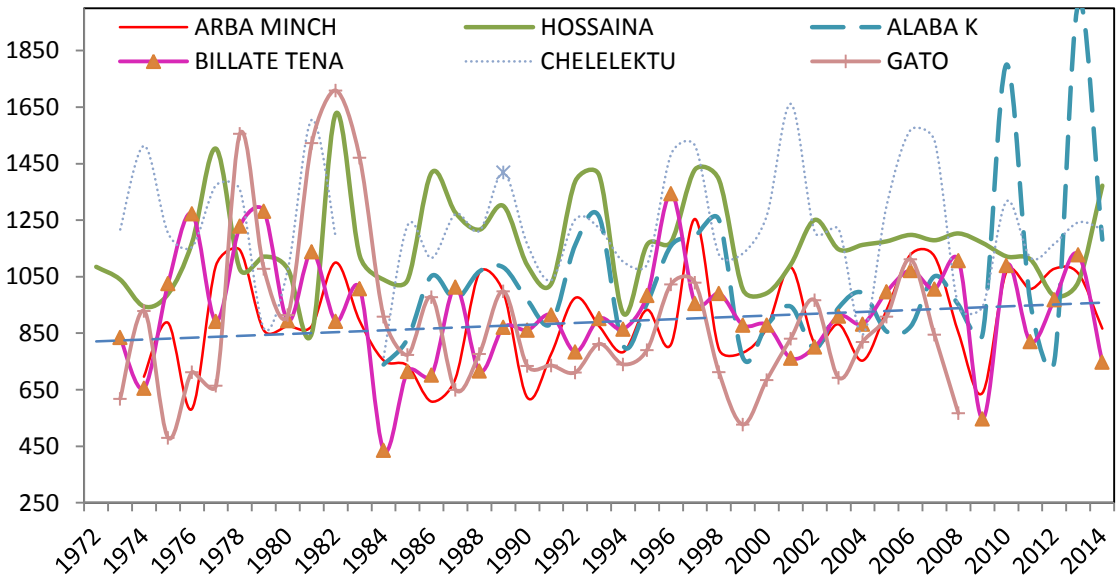

Figure 3.6: The long-term rainfall trend of the selected station from homogenous zones

The spatial correlation analysis among the rainfall homogenous zones (Figure 3.7.) reveals weak relationship with general increase of rainfall trend over time for most of stations (with a correlation coefficient ranges from 0.06 to 0.27).

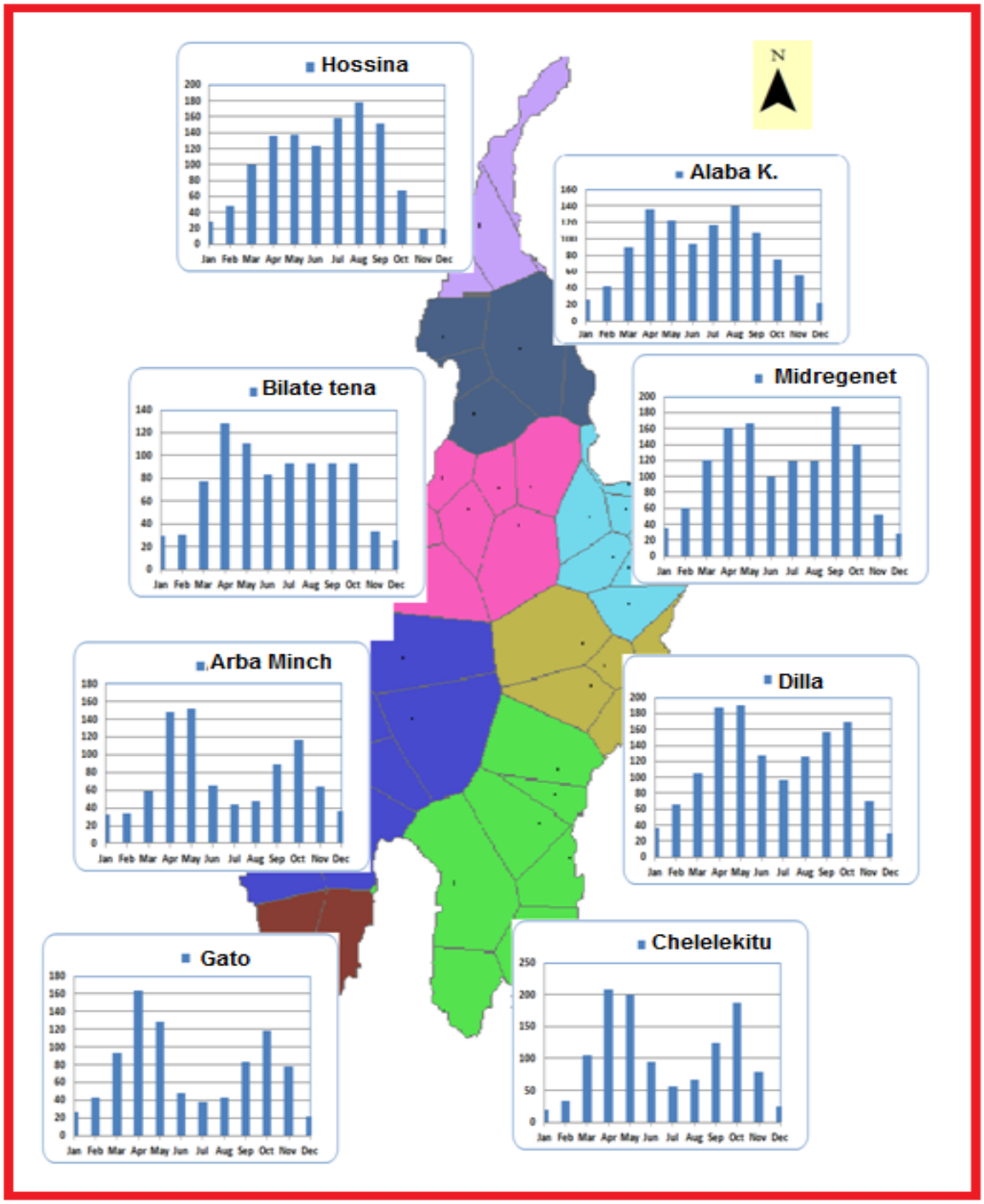

Figure 3.7: Spatial distribution of eight homogenized rainfall zones
(Colored in the figure and illustrates the change of spatial rainfall distribution pattern of each zone)

The coefficient could at least indicate the existence of spatial variation in rainfall across the study area and hence, eight homogeneous zones of rainfall were identified. Which is then used for identification of rainfall season as depicted in Figure 3.7.

The spatial plot of monthly rainfall distribution pattern based on homogeneous rainfall zones clearly shows the systematic changes of seasonal rainfall cycle occurring mechanism.

This pattern is related to the migration of intertropical convergence zone (ITCZ) belt: i.e. during the early March the belt is in the south (south of Arba Minch) and gives rainfall as it moves toward the north tip of the study area. The corresponding raifall peaks are changing from one homogenous rainfall zone to next to noth by a month lag. The final retreat for second rainfall peak southward is happening on September from the north inorder to complete the cycle.

So, the rainfall pattern in the northern tip of the study area (only Hossaina cluster in Figure 3.7 is monomodal pattern which account only small portion as compared to the rest area, however, almost all other portion shows bi-modal rainfall pattern with some variation in intensity. In general to sum up rainfall pattern, the area has got rainfall in the month from March to October with rainfall peak in April and October.

Therefore, the main rainy seasons are identified from March to June with peak rainfall in April and the second season starts from July to October with peaks in September/October. Thus, the study area is generally characterized by two wet/rainy seasons (MAMJ and JASO) and one dry season (NDJF). Locally, MAMJ, JASO and NDJF seasons are referred as "Belg", "Kiremt" and "Bega" respectively

3.2.8. Period of Hydrological cycle

There is a standard method for analyzing the characteristics of rainfall cycle in terms of the periodical appearance of the wet and dry year. The method uses the coefficient of variation (CV) that is calculated from the ratio between the total rainfall amount from each year, and the mean annual rainfall from all years in the data period as given in Equation 3.2.

A single hydrologic cycle is identified based on the cumulative value of the coefficient of variation (CV) when the value becomes 1 or nearly 1. The series of the coefficient of variation (CV) values of the study area are shown up in Figure 3.8.

The cycle is delineated using the cumulative value of CV that is calculated as follows:

$$C_v = \sum \left(\frac{RF_i}{RF_m} - 1 \right) \quad \text{..... (3.2)}$$

Where, RF_i: rainfall in the year; I, RF_m: mean annual rainfall over the entire period

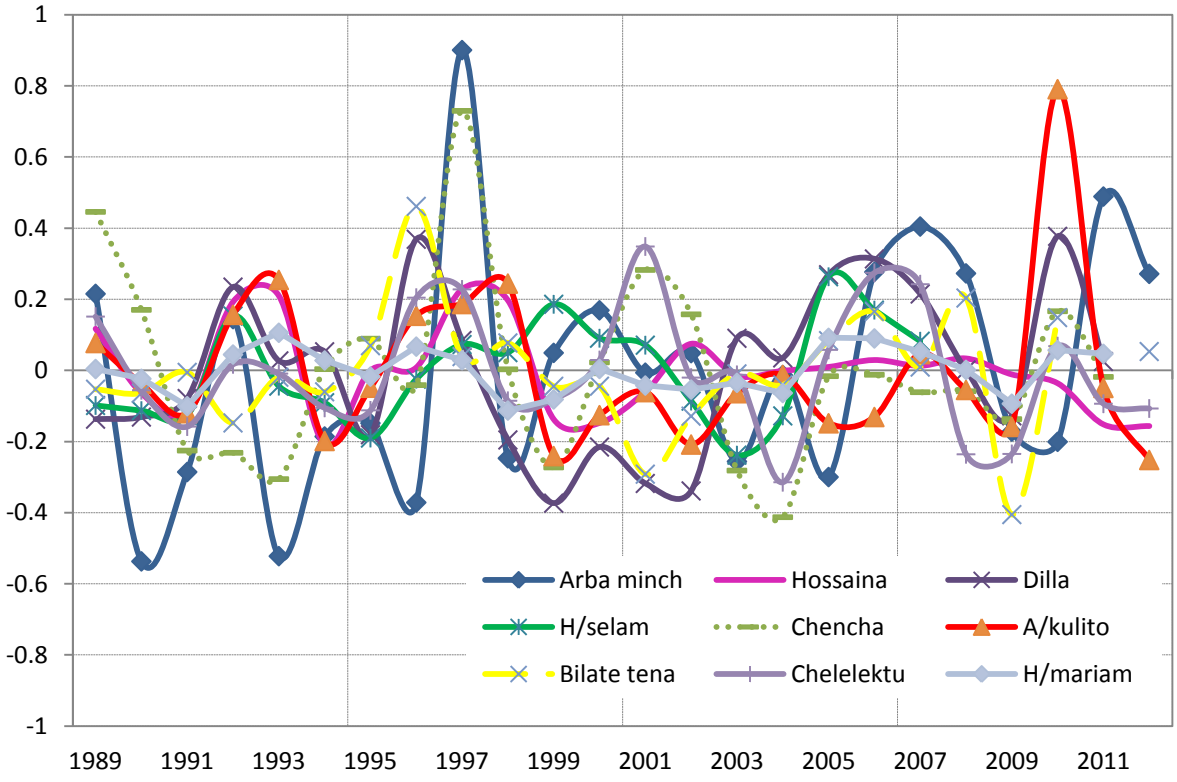

Figure 3.8: shows the coefficient of variation for selected stations in the study area

Equation 3.2 is used to deduce coefficient of variation as it can be seen in Figure 3.8 and the summarized Table 3.2 Several cycles that are made up of series of wet years and dry years can be recognized in the available long year annual rainfall stations. Table 3.2 shows the duration and number of complete hydrologic cycles in a record period of stations.

Table 3.2: Represent duration and number of complete hydrologic cycles.

stations	cycle period	number of complete cycles	Duration of Avg. hydrological cycle
Hossania	1978-2009	5	5
Alaba Kulito	1987-2010	5	5
Billate-Tena	1977-2013	8	5
Midre-Genet	1984-2006	4	6
Dilla	1979-2011	5	5
Arba Minch	1979-2013	8	4
Chelelekitu	1976-2010	9	4
Gato	1975-2006	5	5
Average	**-**	**6**	**5**

As shown in the summarized Table 3.2, which could represent eight homogeneous climate zones in Abaya-Chamo lakes basin as discussed earlier and the spatial variation to some extent explained in terms of the hydrologic cycle. Based on the available length of stations data from late 70's in general, in the study area, there have been about 4 to 9 complete hydrologic cycle (6 in average), which didn't consider the incomplete cycles at the start of the data record and also recently incomplete periods.

To sum up the analysis, the duration of these complete cycles based on the cumulative coefficient of variation across the study area is about 5 years on average. Which means it would be expected a series of consecutive one wet year and one dry year within 5 years to complete the hydrologic cycle under normal condition.

3.2.9. The frequency of Rainfall event

In much hydraulic engineering application and water resource development plan perspective probability of occurrence of a particular extreme rainfall event are important. This information for the study area is calculated through frequency analysis using selected rainfall station over the homogeneous zone. The result of depth–duration-frequency curve is given in Figure 3.9 and Figure 3.10.

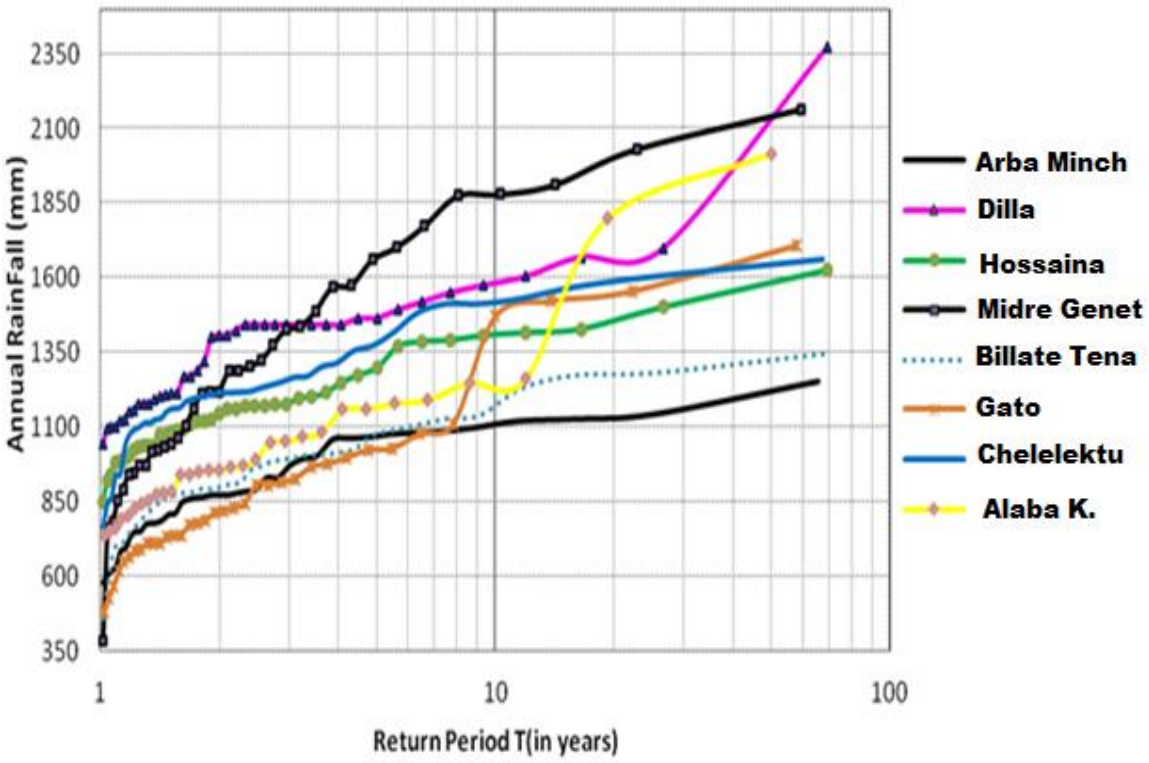

Figure 3.9: Annual rainfall intensity- frequency curve for the study area

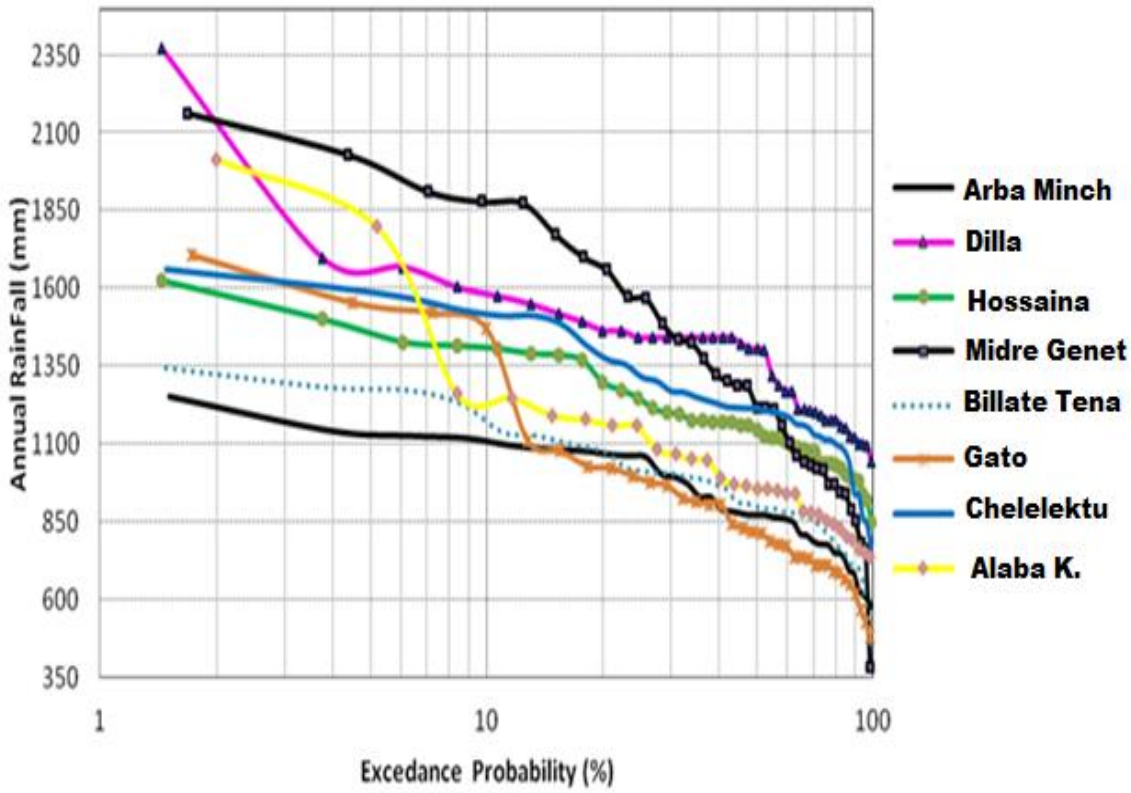

Figure 3.10: Annual rainfall intensity-duration curve for the study area

In the study area, the probability of occurrence of annual rainfall event whose magnitude is more than or in excess of 1100mm is about 10% in ten years whereas the frequency of annual rainfall less than 1100m is high within a few years. But there is no probability of occurrence more than 2400mm mean rainfall over 100 years.

3.3. Temperature

From a water resource management point of view in most cases, it is believed that the influence of temperature is not as great as that of rainfall, however, still, temperature can affect a given water resource through increasing evaporation amount (Warburton et al., 2005) and hence, it is common to analyze its tendency of change.

In regard to temperature measurements, out of all 46 collected meteorological stations shown in Figure 3.1, only 23 of them have given reliable temperature data. The time series data was checked against its climatology and nearby stations. Based on the extent of data period and topographic position of the station, the error/missing data were corrected/filled using arithmetic mean and mean ratio to neighbors station before use. The basic characteristics of the change in temperature at each station were analyzed using the corrected data and presented in Table 3.3.

Table 3.3: present stations available for temperature data in the study area

Station	Duration	Average	Max	Min
Aje	1978-2014	19.1	39.5	1
Alaba kulito	1989-2014	19.7	36.7	1
Amarokele	1983-2014	21.5	37	6
Angacha	1988-2014	19.1	28.7	10
Arbaminch	1987-2014	23.9	38	8
Beleala	2008-2014	21.3	33	10.8
Billate	1988-2014	23.1	38	3.5
Bodity	1981-2014	18.3	32.5	1.1
Burji	1976-2014	25.4	40	1.1
Butajira	1972-2014	18.5	32.9	0.3
Dilla	1988-2014	20.4	39.6	3.2
Gato	1975-2014	24.2	39.9	10
Geresse	1985-2014	16.3	32.3	0.4
Hageremariam	1987-2014	18.2	32	1

Station	Duration	Average	Max	Min
Hagereselam	1965-2014	13	26.2	0.1
Hossana	1981-2014	16.8	32	-0.5
Konso	2004-2014	22.5	34.7	10
Mirababaya	1982-2014	24	39.6	0
Wajifo	1979-2014	22.8	38.3	5.3
Wolaitasodo	1981-2014	19.7	33.3	1
Wulberg	1978-2014	18.4	34.8	0.4
Yirgachefe	1986-2014	18.1	35	-0.2

The presented average annual temperature data in Table 3.3 over the study area shows, the range of values are between 13^0C and 24.2^0C at Hager Selam and Gato station respectively. Over history, it was observed about 11^0C difference in average among station record and the simple average annual temperature of all 23 available stations is 20.2^0C in the Abaya- Chamo Lakes basin.

3.3.1. Spatial distribution of average temperature

The spatial pattern of average annual temperature is depicted in Figure 3.11.

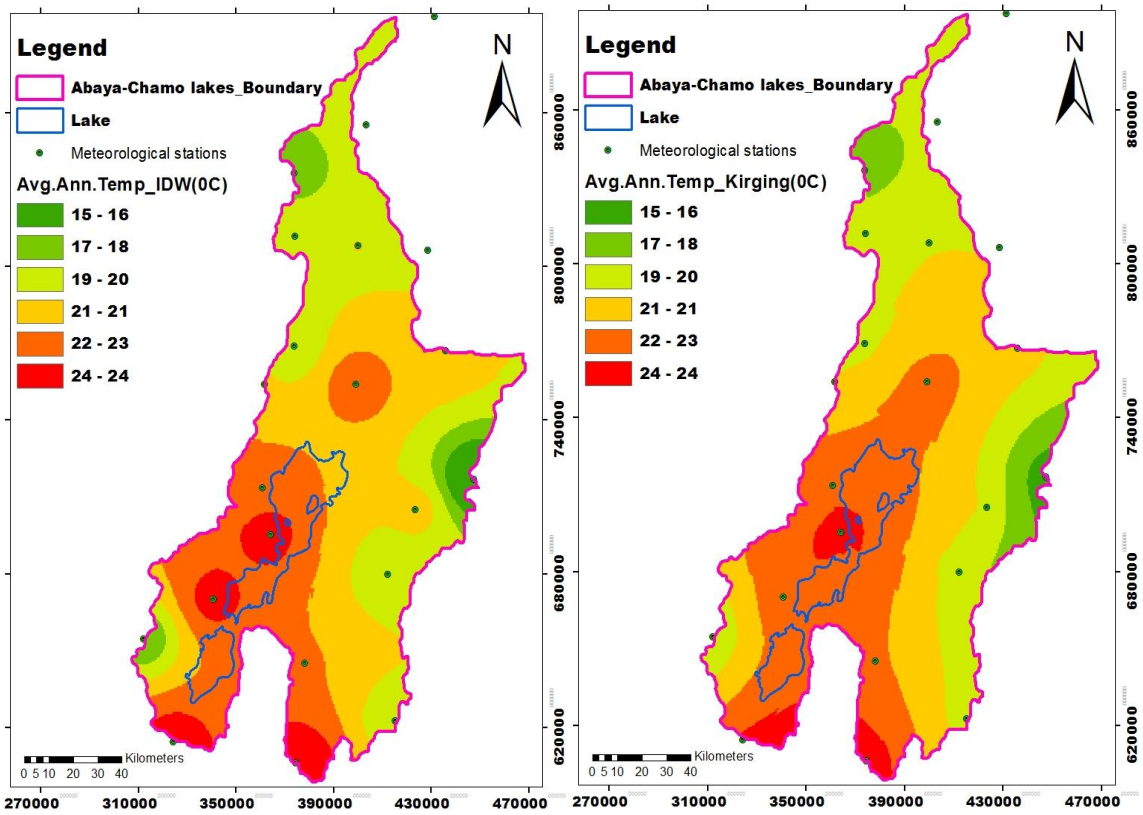

Figure 3.11: Average annual temperature over Abaya-Chamo lakes basin

The pattern is generally unlike the rainfall, where the rift floor is characterized by low altitude and which have high average temperature while the mountains experience low in comparison.

3.3.2. Temperature – Altitude Relation

The temperature–altitude analyses were done using stations record of the annual base given in Figure 3.12. It explains the existence of a close inverse linear relationship between temperature and altitude unlike rainfall. In this case, the relation is clearer which reveals the temperature increase happens as altitude decreases.

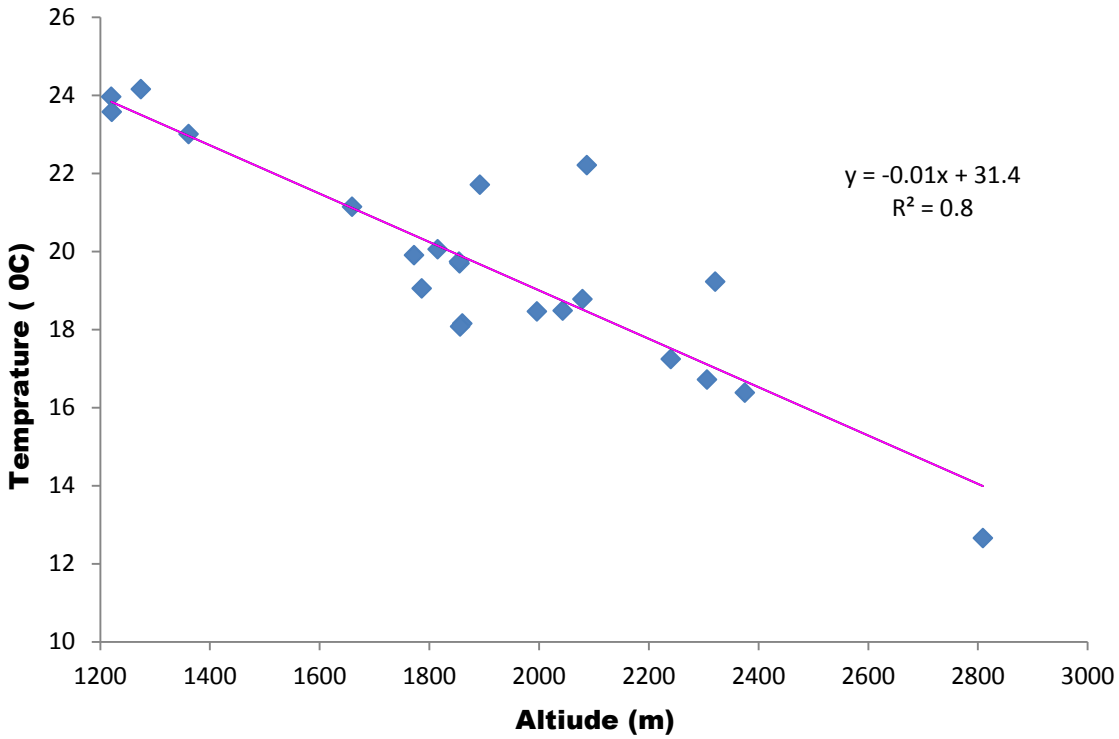

Figure 3.12: Temperature – Altitude Relation

3.3.3. Seasonal Temperature variation

The average monthly temperature analysis of Abaya-Chamo lakes basin is given in Figure 3.13 and Appendix 5. The inter-annual variation in average temperature are not so much throughout the year among the stations, which is even more closer over both dry and wet season in the range of 13 and 24^0C.

The overall monthly variation in average temperature from the stations in Figure 3.13 shows only a slight change about 20^oC throughout a year.

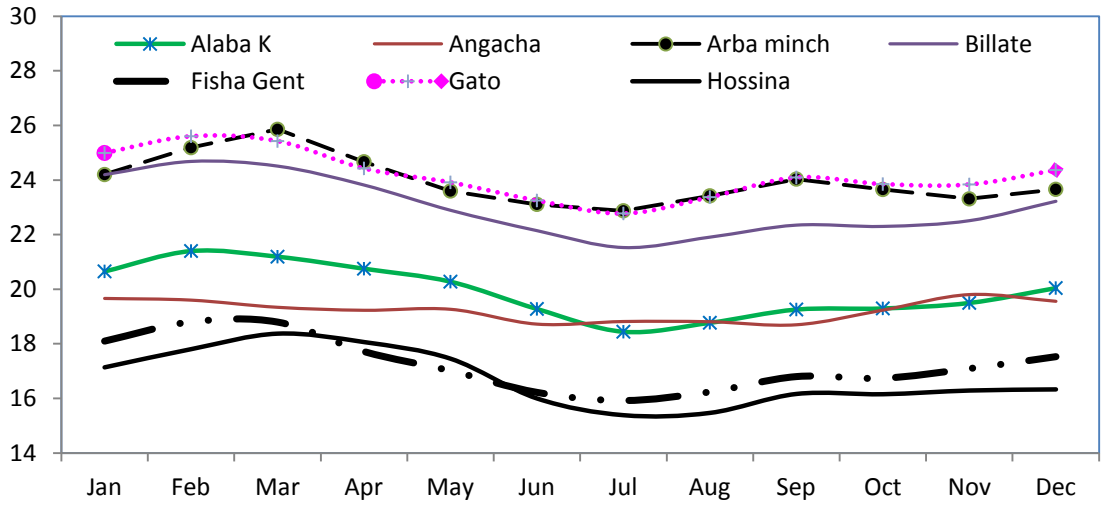

Figure 3.13: monthly average temperature for selected stations

3.4. Evapotranspiration

Evaporation is a very important parameter as rainfall in the water balance of the basin. In the study area, there are only two stations (Arba Minch and Hossaina) that measure evaporation by both Pan and Piche-Evaporimeter. The data record started since 2006-2010 and 2004 -2010, more than 42% and 55% are missing respectively within the study area but there are two stations with relatively longer period outside and nearby the boundary, Jinka (1989-2009) and Hawassa (1985-2010. Lots of missing and limited number of years significantly lowers the reliability of the available data, thus missing data was complemented using the auto-correlation method rather than discarding the important sets of the data periods.

In most cases, evapotranspiration is not usually measured directly, but estimated as a function of other meteorological parameter using different computational methods. For example, for the simplest method, it is necessary to calculate evapotranspiration at least a minimum of daily temperature data. For more complex methods of calculation such as the Penman method, the data from only class one station can be used.

The data, however, is generally incomplete and needs screening before analysis Halcrow, 2008 estimated the potential evapotranspiration for 12 stations using the Penman-Monteith formula (Appendix 6). The calculation was based only on long-term average monthly parameters due to data quality limitations.

3.4.1. Spatial distribution of Evapotranspiration

The amount of evaporation is affected by many physical and meteorological variables such as solar energy, vapor pressure gradient governed by air temperature-humidity-wind speed above the surface, water availability, land cover features such as vegetation, and soil characteristics (Bonan, 2002). As a result, it is one of the most difficult parameter to quantify and the factors are also controlled by the global position and topography.

The spatial annual potential evapotranspiration plots based on the available data in Figure 3.14, shows a small variation over the lakes basin. The spatial interpolation was done using inverse distance weighted (IDW) and kriging geospatial interpolation techniques. Generally, it exhibit silght variation in distribution with high rate south-west of lake Abaya and Chamo while, the northern ridge has relatively low value. In comparesion, the spatial distribution of potential evapotransipiration is somehow linear to temperature distribution.

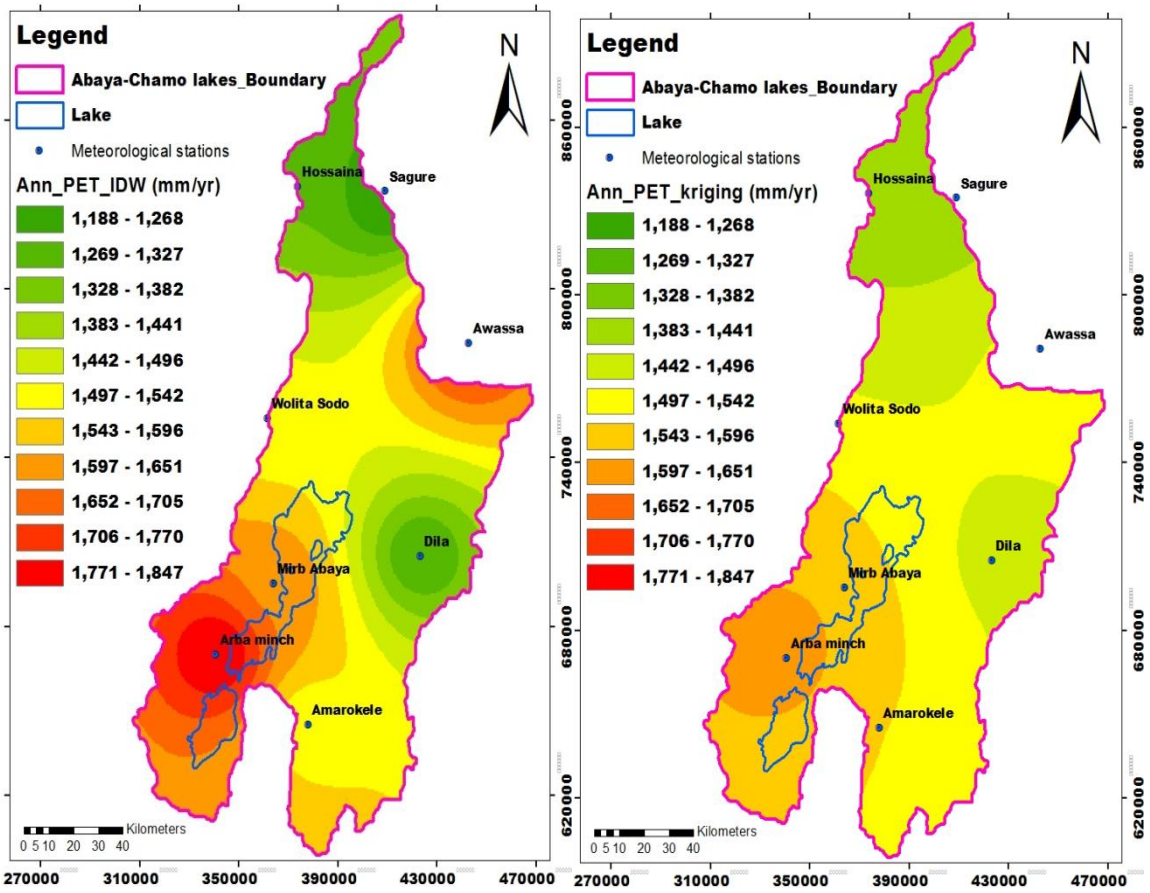

Figure 3.14: Spatial distribution of annual potential evapotranspiration

3.4.2. Evaporation - Altitude Relation

As explained earlier, evaporation is affected by the position on the globe and the topography of the area. Since, the rift valley lakes basins are exist in a relatively similar global position and topographical condition, it is normal to expect small difference in evaporation rate across the area. In line with this, the positions of the stations are nearly at the same valley on a main Ethiopian rift and the analysis was futher conducted to compare and assess the effect of topography on the evaporation rate using observations over the study area and nearby stations (Jinka and Hawassa)as given in Figure 3.15.

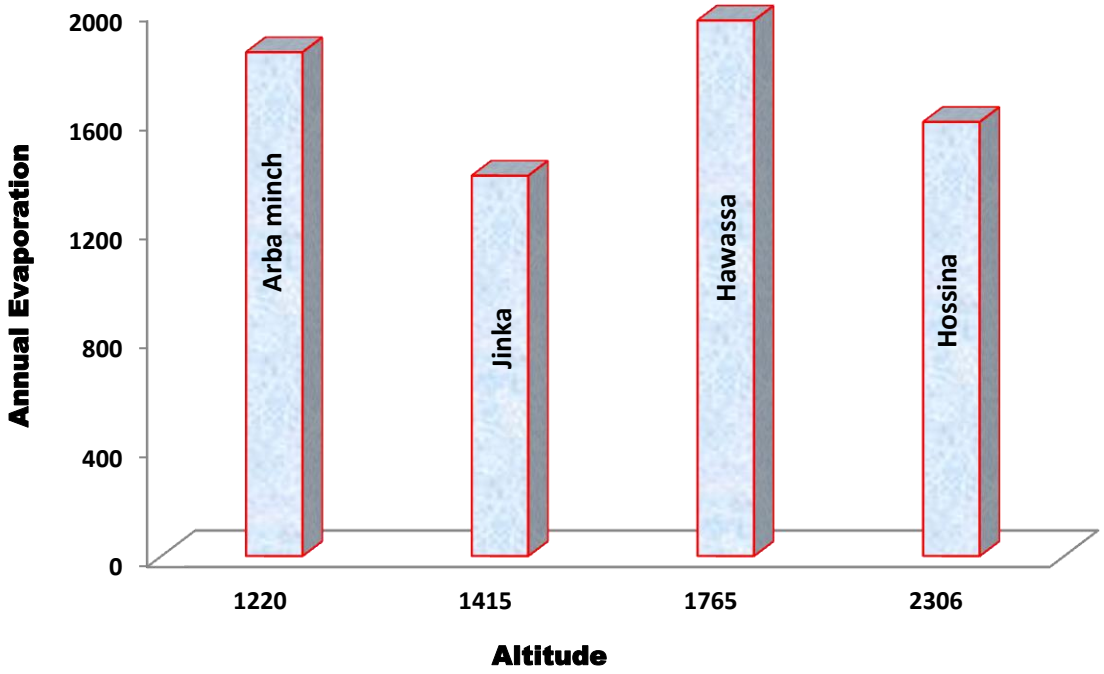

Figure 3.15: Relation between pan-evaporation and elevation

The pan evaporation data plotted in Figure 3.15 from the 4-stations shows, no clear relation between the amount of open water evaporation and its elevation.

3.4.3. Seasonal variation of evaporation

Based on the available pan evaporation data sets over the study area and nearby stations, the monthly average potential evaporation value at stations is presented in Table 3.4 and Figure 3.16.

Table 3.4: Seasonal Average of pan Evaporation in the study area

Month	Jan	Feb	Mar	Apr	May	Jun	Jul	Aug	Sep	Oct	Nov	Dec
A_Minch	188.4	173.1	219.2	147.3	129.1	146.9	126.4	146.6	135.7	143.1	154.8	136.6
Hawassa	191.4	193.3	193.4	161.7	165.2	152.1	132.1	137.1	131.7	151.6	174.5	179.2
Hossana	130.9	147.1	186.5	148.2	118.9	111.4	105.3	89.3	106.6	135.2	166.3	145.6
Jinka	137.5	137.9	139.7	116.7	104.3	95.3	96.1	104	121	112.3	111.6	118.1

The values of monthly average presented in Table 3.4 are all based on the monthly average of each of the stations. The difference in pan-evaporation is much small as 800mm and the average values of the station in the study area and neighboring station are small and almost exhibit similar seasonal trend as shown in Figure 3.16.

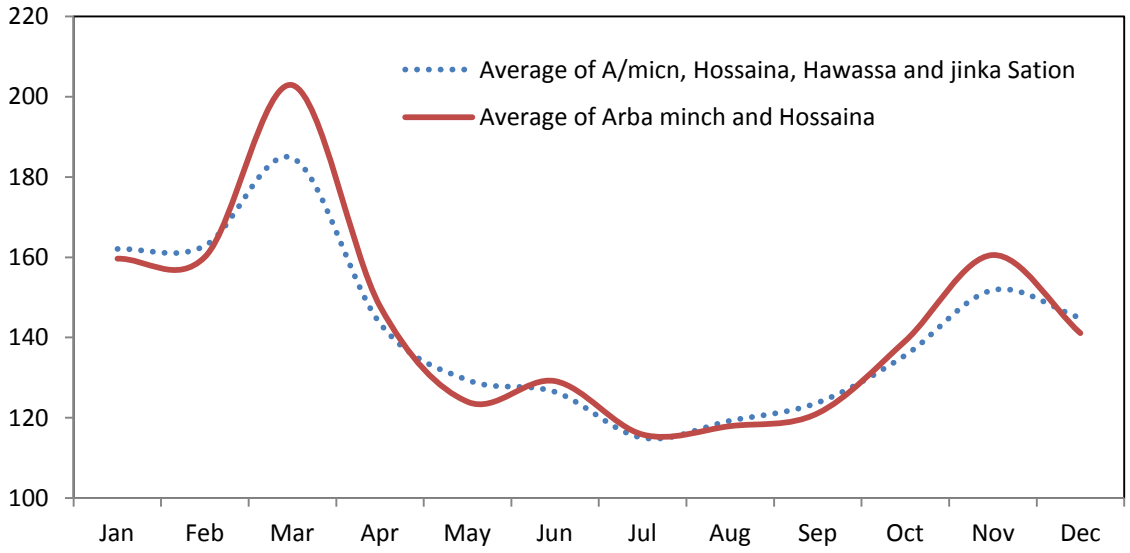

Figure 3.16: Monthly Average potential Evaporation Fluctuation

In fact, the abundance of missing data in the time series may have affected the accuracy of the analysis to some extent as compared to precipitation data. But as per its smaller seasonal and annual variation (PET) over the study area, a relatively longer reliable Hawassa station of an adjoining station can be used by considered its seasonal compliment with stations in the study area and smaller annual variation in the rift valley.

CHAPTER FOUR

4. LAKE LEVEL, RIVER AND SPRING DISCHARGE

4.1. Hydrological Stations and Data

In the study area, about 4-lake level, 16-river and 1-spring discharge gauging stations are measures lake level, river and spring discharges respectively. The measurements at different position have been operating under Ministry of Water, Irrigation and Energy (MOWIE) as given in Figure 4.1.

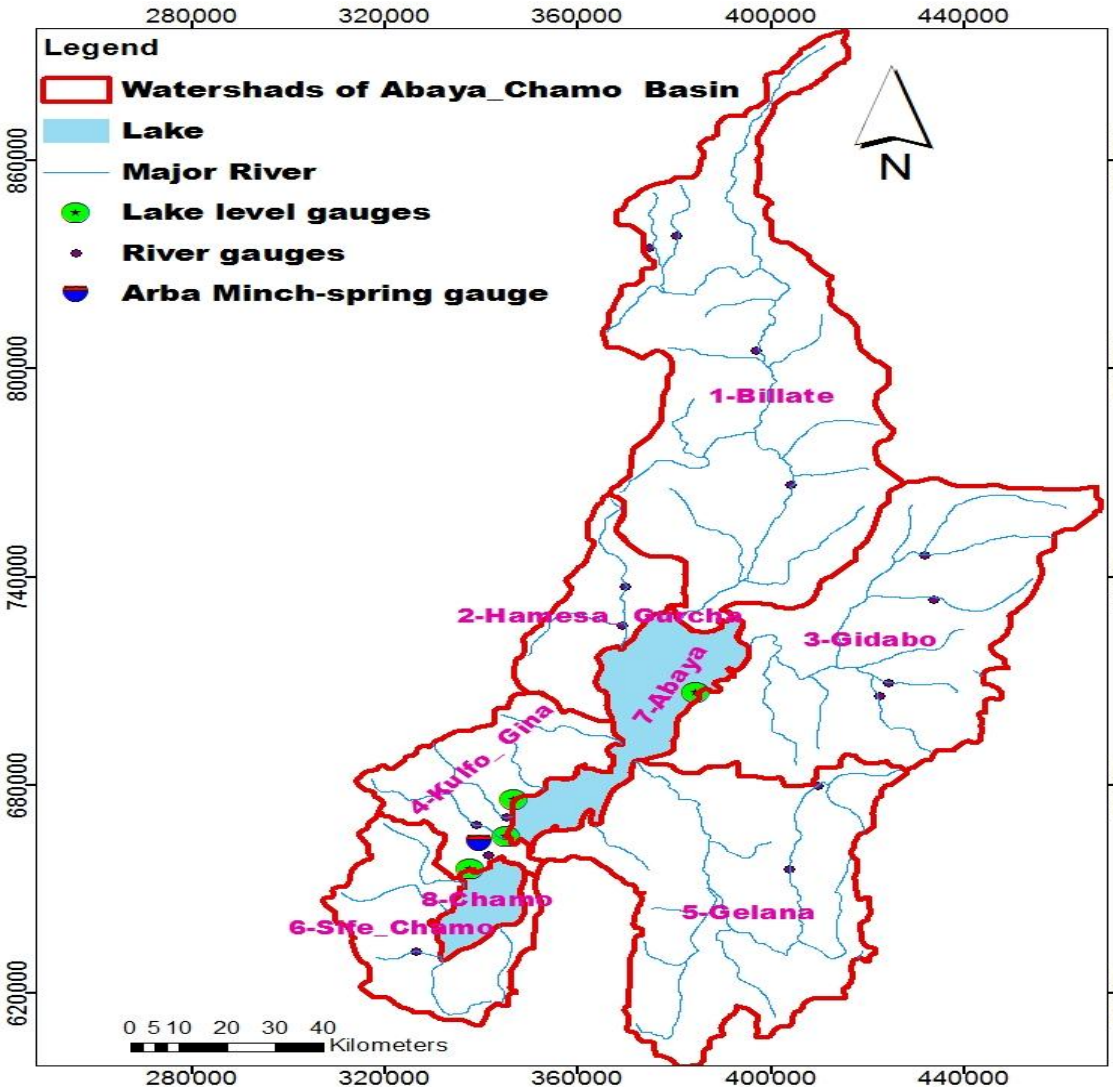

Figure 4.1: Sub-basins distributions, lake level, river, and spring discharge gauging stations

4.1.1. Distribution of Lakes and Rivers

"Abaya" and "Chamo" lakes are dominated the center of the floor as shown in Figure 4.1 which are two laying lakes along the SSW to NNE axis. Lake Abaya is the second largest lake next to Tana in Ethiopia, while Chamo covers only a small part directly next to Abaya in the South. The basic characteristics of the lakes are compiled in Table 4.1.

Table 4.1: Morphometric characteristics of Major Lakes

Lakes	Level Fluctuation Range (m)	Mean Depth(m)	Surface Area (km2)	Volume (mm3)	Surface elevation(m)
Abaya	3.06	7	1140	9818	1176
Chamo	3.28	12	335	4100	1109

(Source: Halcrow 2008)

Regarding sub-basins, as shown in Figure 4.1 in Abaya-Chamo the lakes basin, six major rivers were identified through watershed delineation procedure in Arc-GIS that flow into the two lakes. Relatively the largest sub-basins are the Bilate (with an area of 5,900km2) located to the north of Abaya lake, Gidabo(3,447km2) and Gelana(3,463km2) to the east and Hamessa-Guracha (1006.7km^2) and Kulfo-Gina(1368.7km^2) to the west which drains to Lake Abaya. Whereas Sife-Chamo(1379.4km^2) drains to lake Chamo as a major river (JICA, 2012, Halcrow et al. 2008) and other rivers such as Sego and an ephemeral stream to the south contribute to Chamo.

The two lakes are not physically connected to each other (Ababu, 2005). Which are separated by Pleistocene massive basalt lavas and traditionally it is so-called "ye egizer dildiy" (meaning "Bridge of God" which is approximately 4km wide). However, during intensive wet season when the lake level gets higher, the outflow joins Kulfo-river (the discharge record of Kulfo-river and Abaya outflow is given in Figure 4.2(a)-(b) colored blue, which crossing by keeping western side of lake abaya and end to lake Chamo and become the only way to connect the lakes. Superficially, the inland drainage basin provides the ultimate discharge points for drainage from the hills, escarpments, and valley sides that defines basin boundary.

The total cumulative flow from both the Kulfo-river and Lake-Abaya overflow are measured at Kulfo and Lake-Abaya outflow river gauge. The discharge record is shown in Figure 4.2(a)-(b). The figure shows that the flow is relatively regular with 1.01 coefficient of year to year variation.

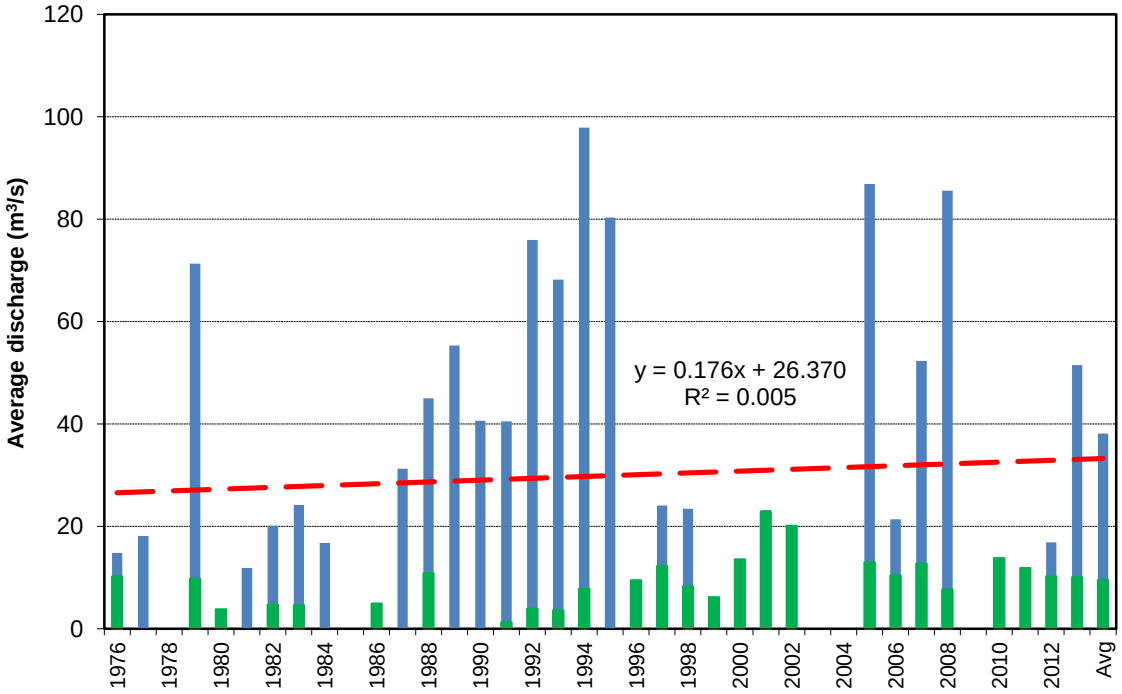

Figure 4.2: (a) Annual variability of Kulfo-river & lake-Abaya outflow

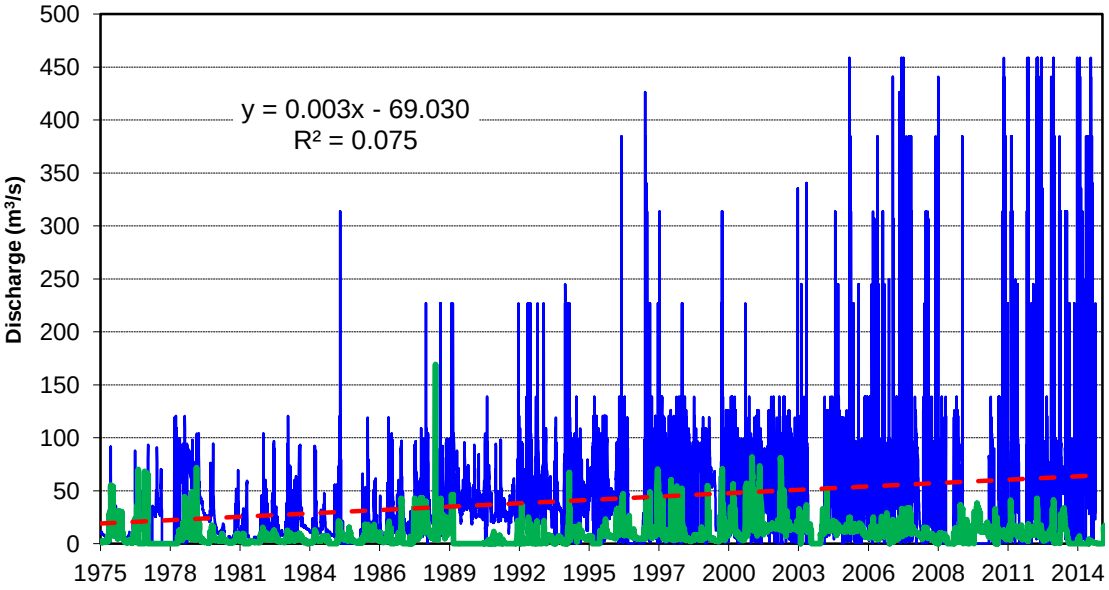

Figure 4.2: (b) Hydrograph of Kulfo-river (green) and Kulfo & lake-Abaya outflow (blue)

The highest daily discharge of 458.6m^3/s was recorded on May 05, 2005 at the river gauge with the calculated mean annual flow of 38.1m^3/s. The mean annual flow at this station is four times greater than that of annual mean flow record at Kulfo-river (green color in Figure 4.2(a)-(b)).

This confirms the existence of overflow from the Abaya Lake to Kulfo-river and ends up at Chamo Lake. Besides, in the hydrograph (Figure 4.2(b), an increase of daily discharge is observed at Kulfo and L-Abaya outlet in the period from 1996-2013 can be taken as an indication of lake level rise in a concurrent period as given lake level plot Figure 4.3 in the western part of Abaya.

4.2. Lake level

The lake level observation station that covers two lakes (Abaya and Chamo) at 4 stations that started in the late 60's or in early 70's. The geographic locations of observation stations are given in Figure 4.1.

4.2.1. The long-term trend of Lake Level

In Abaya-Chamo lakes basin, the long-term trend of the annual lake fluctuation generally increasing over the time based on the available measured data as given in Figure 4.3.

Previous studies in the rift valley lake system have found fluctuations in level attributable to land-use and climate (Servat et al 1998, Awulachew, 2001, 2006, Schutt et al 2002, Ayenew 2002, 2009, Ayenew and Becht 2007) with limited abstraction and manipulation in parallel to an increase of local population which contributing to deforestation and sedimentation (Belete 2009).

The mean annual in-situ records on lake level at various stations are given in Figure 4.3 of the study area. Since, from the start of the record, almost all stations exhibit trends characterized by low and stable values up to 1985; a marked upward trend with increasing spread in between 1997 and 2001, and high and relatively stable values thereafter. Consequently, the progressive increasing trend for lake-Abaya outflow is related to the observed rainfall increase in most of rainfall station in the lake basin.

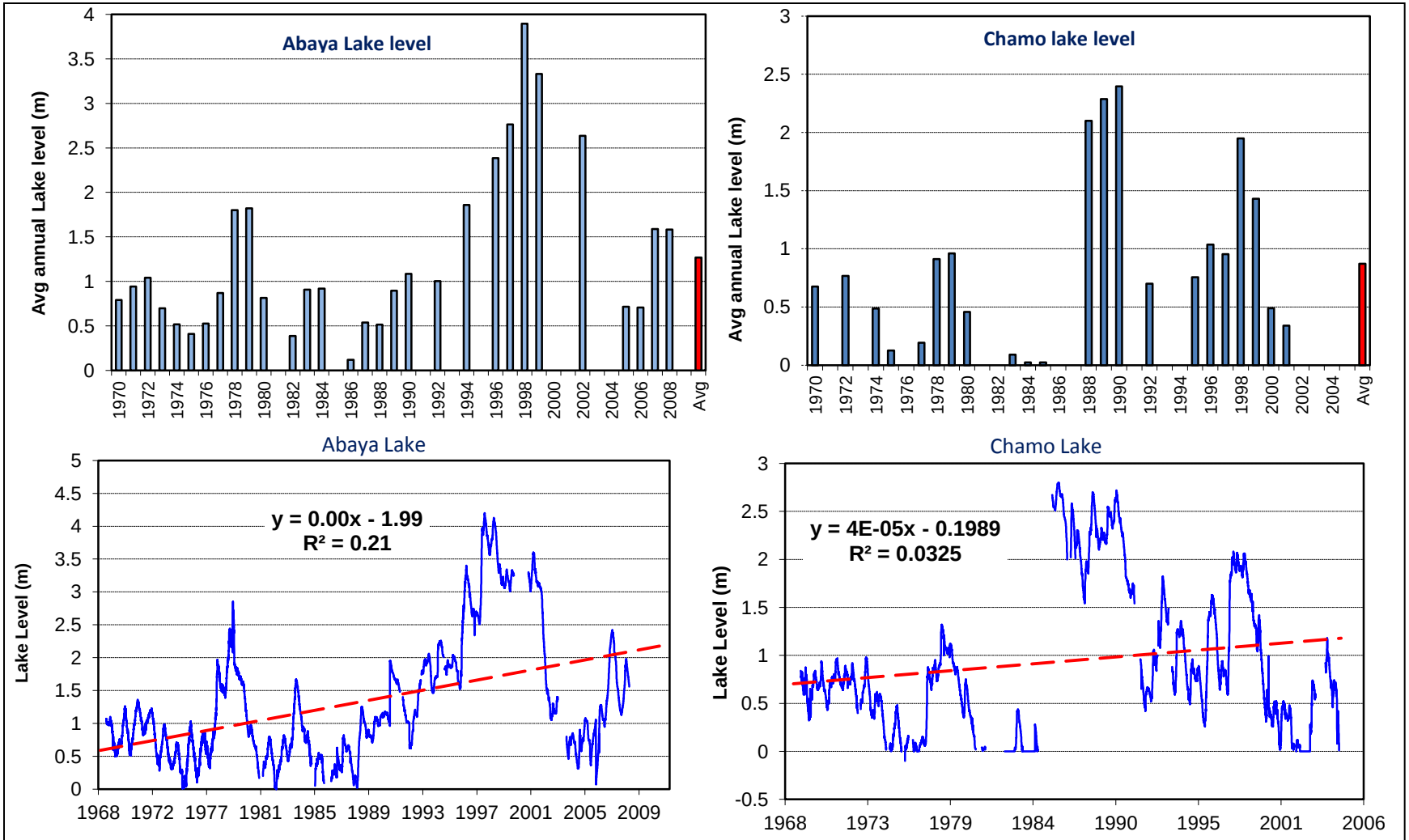

Figure 4.3: Annual variability of the mean annual lake level of the Lakes (upper) and daily hydrograph of lake level :(lower) Abaya near Arba Minch (old) and Chamo near Arba Minch

This signal was explained particularly from 1997 to 2001 as a mirror image in the annual distribution of rainfall in Section 3.2.2 and also shown in the coefficient of variation in Figure 3.8, which is characterized by prevailed an extreme event within short-term in the hydrologic cycle in the study area.

The observed mean long-term increases of lakes at gauging stations are generally, exhibit decadal cyclic pattern (within nearly 15years) as shown in Figure 4.3. The mean annual long-term lake level increase is about, 1.27m at Lake-Abaya near Arba Minch (old) whereas the variability is higher in decadal scale at lake-Chamo and there is about only 0.87m annual mean long-term change which is relatively small in comparison.

4.2.2. Seasonality of Lake level fluctuations

In-situ monthly measurements of lake levels at the stations are given in Figure 4.4(a)-(b) to show the seasonality of lake level fluctuation.

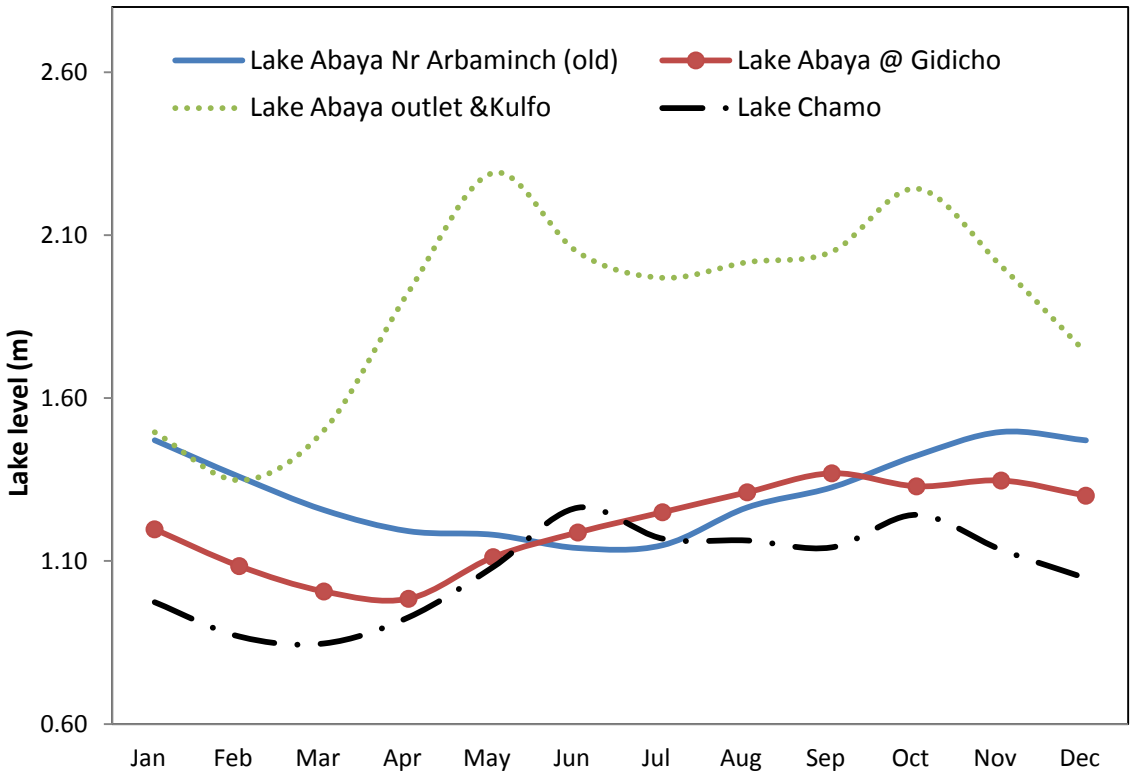

Figure 4.4: (a) monthly Lake level fluctuation of lakes at four stations

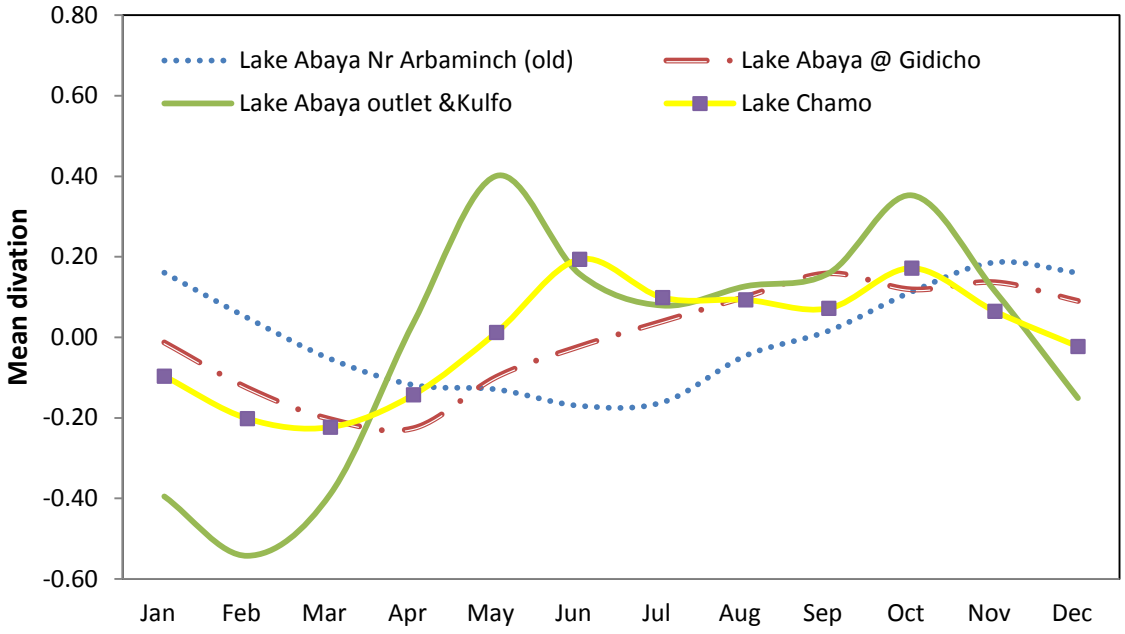

Figure 4.4 (b) Mean deviation of monthly Lake Level fluctuation of lakes at four stations

As given in monthly plot inter-comparisons of lake level and rainfall observation are made for the annual cycle and explains, the seasonal fluctuation of the lakes shows slight seasonality that corresponding to rainfall months with some lags at stations. As indicated in the previous chapter in Figure 3.7, the annual cycle of rainfall shows a major peak in April-May and a minor peak in September-October accordingly the lake level follows in a concurrent and/or by a lag of a month rises gradually to a peak by May and October respectively.

In general, the long-term seasonal fluctuation in the study area persistently reflects an integration of the seasonal climate variation effects of adjacent areas, however, some deviation in seasonal fluctuation in lake level against annual cycle of rainfall may be a sign of short-term extreme events and also related to anthropogenic activities associated to water consumption in rivers flows, land use changes and etc.

4.3. River discharge

Most of the stations in the basin are simple staff-gauged measurement points where benchmarks were established on a stable rock surface with exceptions of only some

major rivers that is equipped by a weather resistant structure and house for automatic recording station on the river bank.

The discharge is calculated often using stage-discharge rating curves at a station. The monthly discharge measurement data obtained from the Hydrology Department of Ministry of Water, Irrigation and Energy (MOWIE) has been compiled to show the range of discharges for major rivers in the study Area. The period of data extends from 1970's to 2015.

The river flows of a reliable 16-gauging stations were collected, as the river discharge data is a most fundamental hydrologic parameter to analyze the characteristics of a given a basin,. The location of the stations is shown in Figure 4.1.

4.3.1. Average total river flow rate

The calculated values based on the complemented data, for average daily flow rate, daily maximum and minimum flow rates for each station are presented in Table 4.2.

As a part of Abaya-Chamo lakes basin, **Bilate-river sub-basin** is the largest per area in which five river recording stations are found. These stations are Batena, Gombora, weira, Bilate-Alaba rivers in the upper stream and Bilate Tena-river at downstream.

The mean annual trends of the measurements are given in Figure 4.5 (a) of the upper stream and downstream in Figure 4.5 (b). In the sub-basin as a whole, the longest measurement started 1970.

The analysis results indicate that there is a large variation in daily average flow rates among the stations the annual mean flow is in the range between 0.04 and 16.9m^3/s with relatively coefficient of variation from 1.23 to 2.17 at Bilate-Tena and Gombora respectively, shows that the flow is relatively regular; however, the total value of annual flow and particularly maximal monthly flow can vary substantially from year to year.

For instance, the measured river discharge at Weira-river gauging station shows regular flow with low annual variation. The highest daily discharge of 210.4m^3/s happened on Oct 4, 1987, with the mean annual flow of 7.4m^3/s.

Table 4.2: Daily average, maximum, minimum flow rates, the coefficient of variation and day of maximum record

Name of River gauge Stations	Area (Km^2)	Duration		Average (m^3/s)	Max (m^3/s)	Min (m^3/s)	CV	Max day
		From	To					
Batena	71	1987	2007	1.10	24.80	0.00	1.62	19-08-1988
Gombora	41	1988	2008	0.40	14.00	0.00	2.17	31-08-1998
Weira_Hossina	522	1987	2007	7.40	210.4	0.31	1.70	10-04-1987
Bilate_Alaba Kulito	2009	1980	2005	10.5	96.6	0.04	1.22	29-04-2005
Bilate_Bilate Tena	5518	1970	2015	16.9	283.5	0.00	1.23	29-07-1986
Hamassa_Humbo	255	1985	2015	0.80	25.70	0.00	1.85	18-10-1989
Hamassa_Wajifo	358	1980	2015	0.50	36.50	0.00	2.12	21-08-2013
Harie	198	1979	2015	1.80	22.40	0.00	0.71	24-07-1985
Kulfo_Arba Minch	374	1976	2015	9.50	79.70	0.00	1.01	10-07-2001
Bedessa	149	1982	2015	2.10	92.30	0.00	1.56	20-09-2013
Kolla_Aletawondo	166	1980	2014	2.90	42.30	0.00	1.03	23-09-2005
Gidabo_Aposto	646	1977	2015	6.50	92.50	0.00	1.00	30-07-1996
Sala_Dilla collage	79	1997	2015	4.70	46.10	0.04	1.06	11-06-2013
U.Gelana_Yirgachefe	95	1981	2007	4.20	69.60	0.00	1.03	26-09-2001
Gelana_tore	376	1990	2015	4.60	18.00	0.07	0.89	20-05-2010
Gato_Gidole	148	1975	2008	0.60	210.4	0.00	3.63	26-07-1981

The highest flow measurement is recorded in the downstream and which is originated from highlands, escarpment part of the rift floor. The highest daily discharge of 283.5m3/s (29th of July, 1986) was recorded at Bilate tena-river gauge whereas for other station in sub-basin the highest record happen from August to September in different years as given in Table 4.2. The annual flow variability is higher at the upstream and compared to the downstream.

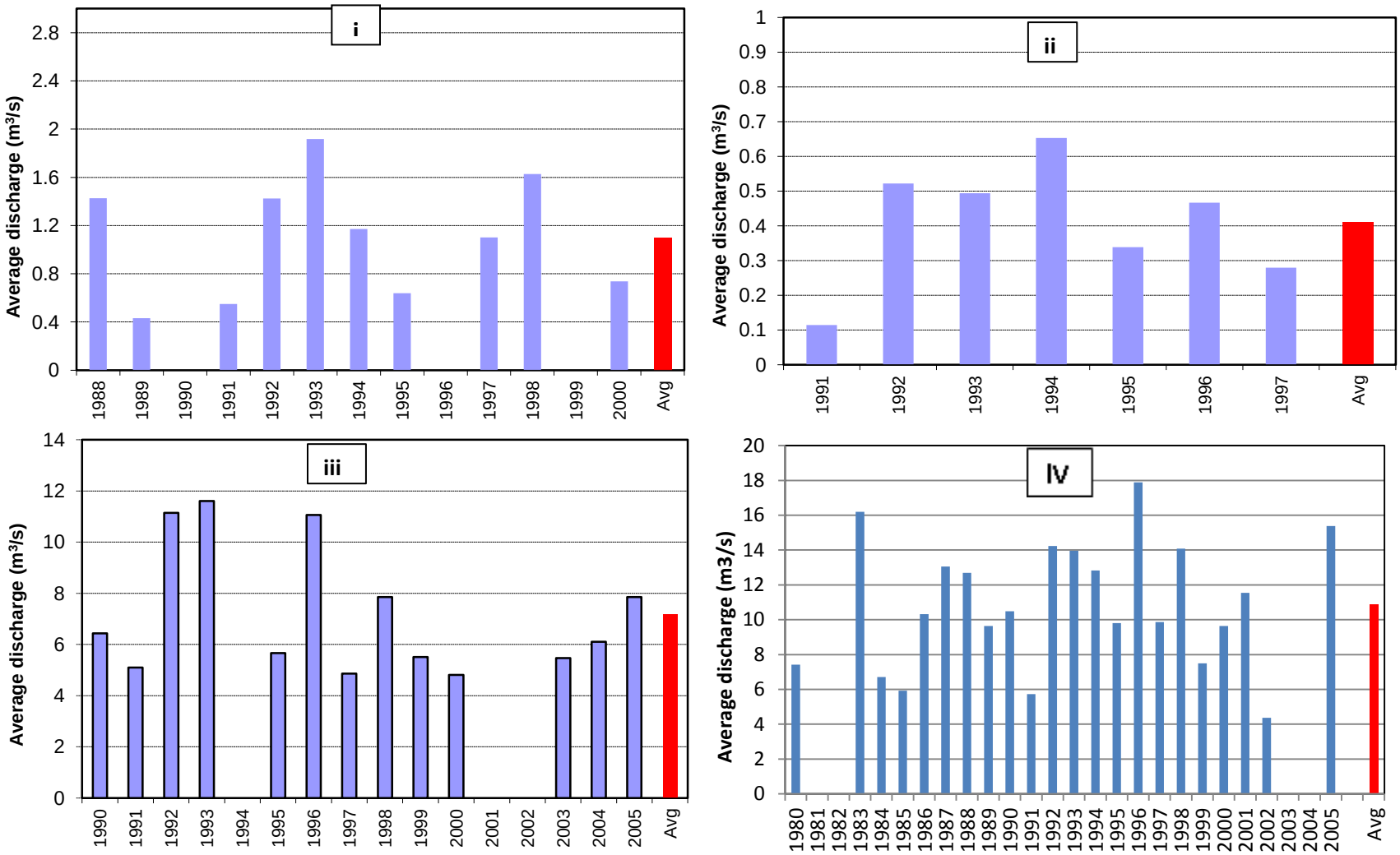

Figure 4.5: (a) Bilate-river sub-basin annual variability of the mean flow of the upstream: Batena (i), Gombora (ii), Weira (iii) and Bilate-kulito (iv)

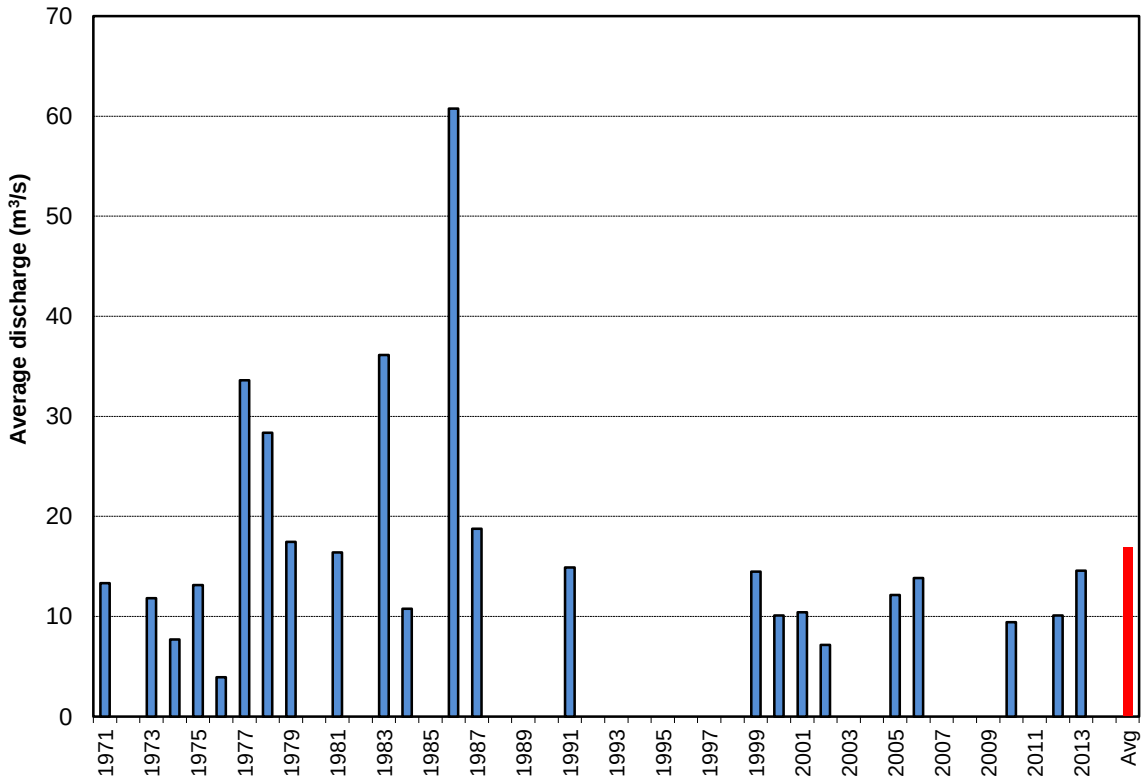

Figure 4.5 (b): The mean annual variability of the downstream flow: Bilate_Tena-river

The second sub-basin represented in the study area is **Hamessa-Guracha-river basin** representing northwest of Abaya lake. Two of which has measuring stations at Humbo and Wajifo gauging stations as shown Figure 4.1.

The annual mean flow is in the range between 0.5 and 0.8m^3/s with a coefficient of variation from 1.85 to 2.12, indicating more stable flow with small catchemeant area than Bilate subbasin.

The measured discharge of Humbo-river in the period from 1985 to 2015 is shown in Figure 4.6. The figure shows that the flow is generally regular with some of the annual flow varies substantially from year to year.

The highest daily discharge of 25.7m^3/s in the month of October 1989. As given in Table 4.2, the calculated mean annual flow of 0.8 m^3/s for the Humbo station represents flow generated mainly in the western escarpment where the Hammesa-river originates and which receives a relatively high volume of precipitation within the area.

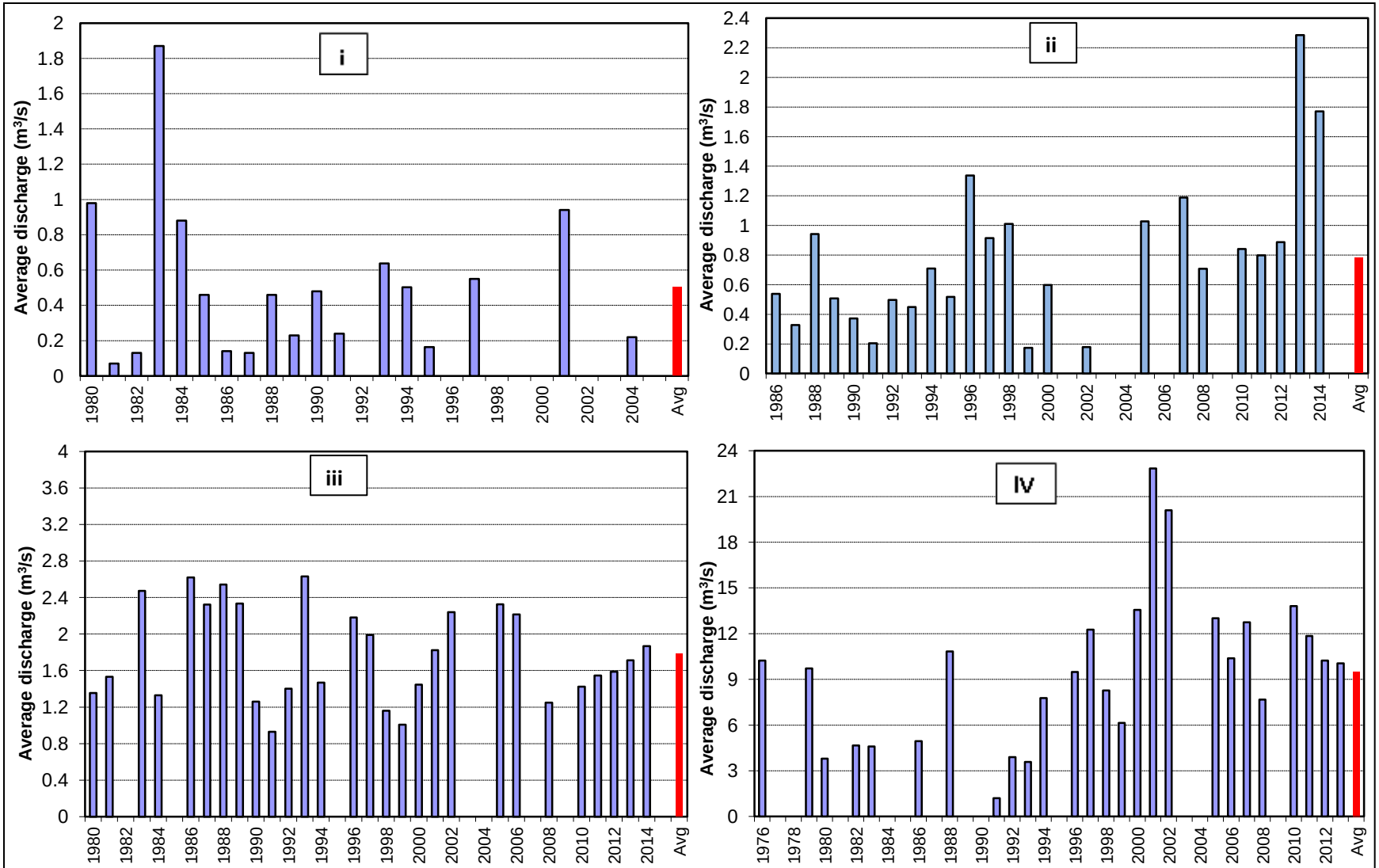

Figure 4.6: Annual variability of the Hamessa-Guracha and Kulfo-Gina sub-basins flows ((i) Humbo; (ii) Wajifo; (iii) Harie and (iv) Kulfo

To the southwest of Hamessa-Guracha-river assigned as "4" in Figure 4.1 in the study area is referred as **Kulifo_Gina-river basin.** Also, two rivers have two measuring stations such as Harie and Kulfo as shown Figure 4.6(lower part). The annual mean flow at these stations ranges in between 1.8 and 9.5m^3/s with a variation of coefficient range from 0.71 to 1.01, indicating more stable flow than Hamessa-Guracha-river basin.

For example, the measured discharge of the Kulfo-river at Arba Minch illustrates relatively regular; yet, the total annual flow and especially the maximal monthly flow can vary substantially from year to year. The highest daily discharge of 79.7m^3/s in the month of October 10, 2001) was recorded at the river gauge.

The flow at Kulfo-river is originated largely in the western escarpment that receives a relatively higher volume of rainfall during the wet season, which is about 9.5m^3/s as an estimated mean annual flow.

The other sub-major sub-basin assigned by "3" in Figure 4.1 representing northeast of Lake Abaya in the study area is **Gidabo-river basin**. This has four measuring stations such as Bedassa, Kolla, Gidabo-Aposto and Sila gauging stations and the annual mean variability is shown Figure 4.7.

The measurement started in 1980's. The annual mean flow is in the range between 2.1 and 6.5m^3/s with a small coefficient of variation from 1.0 to 1.56, indicating more regular and stable flow than all other major-basins. This area also receives a relatively high volume of precipitation within the area.

In the Gidabo-river at the Aposto-river gauge, the measurement the period from 1977 to 2015 is shown in Figure 4.7, which shows that the flow is relatively regular. The highest daily discharge of 92.5m^3/s on the 30th of July, 1996 was recorded at the river gauge.

The flow is contributed from the eastern escarpment where the Gidabo-river initiated and eastern part of the rift floor through which the river is flowing with an estimated mean annual flow value of 6.5 m^3/s

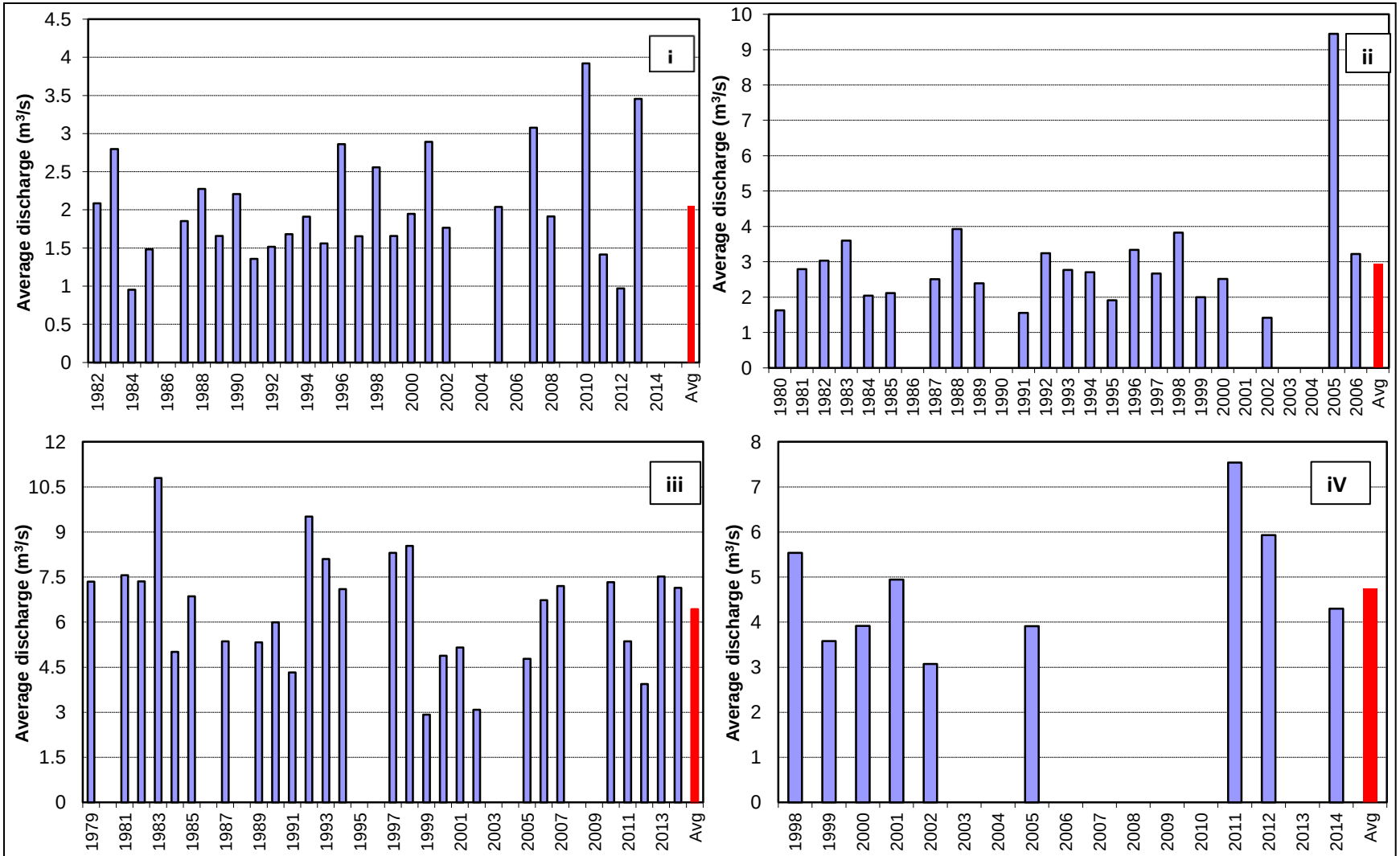

Figure 4.7: The annual mean variability of the Gidabo sub-basin river flows (i) Bedessa (ii) Kolla (iii) Gidabo_ Aposto and (iV) Sala

The next southeast sub-major-basin assigned by '5 representing Southeast of Lake Abaya in the study area is **Gelana-river basin** which has two rivers measuring station such as Upper_Gelana at yirgachefe and Gelana at tore as shown Figure 4.8(a)-(b). The annual mean flow area is 4.2 and 4.6m^3/s with a coefficient of variation from 0.9 to 1, indicating more regular and stable flow to that of Gidabo-river sub-basin.

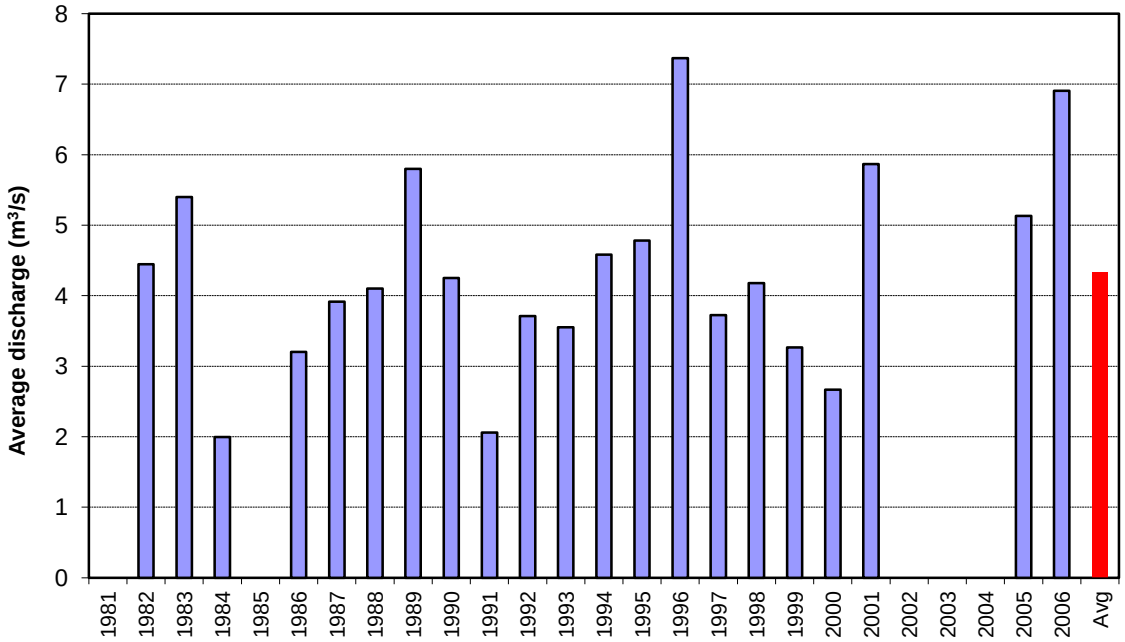

Figure 4.8: (a) Annual mean variability of the Upper-Galana-river flow

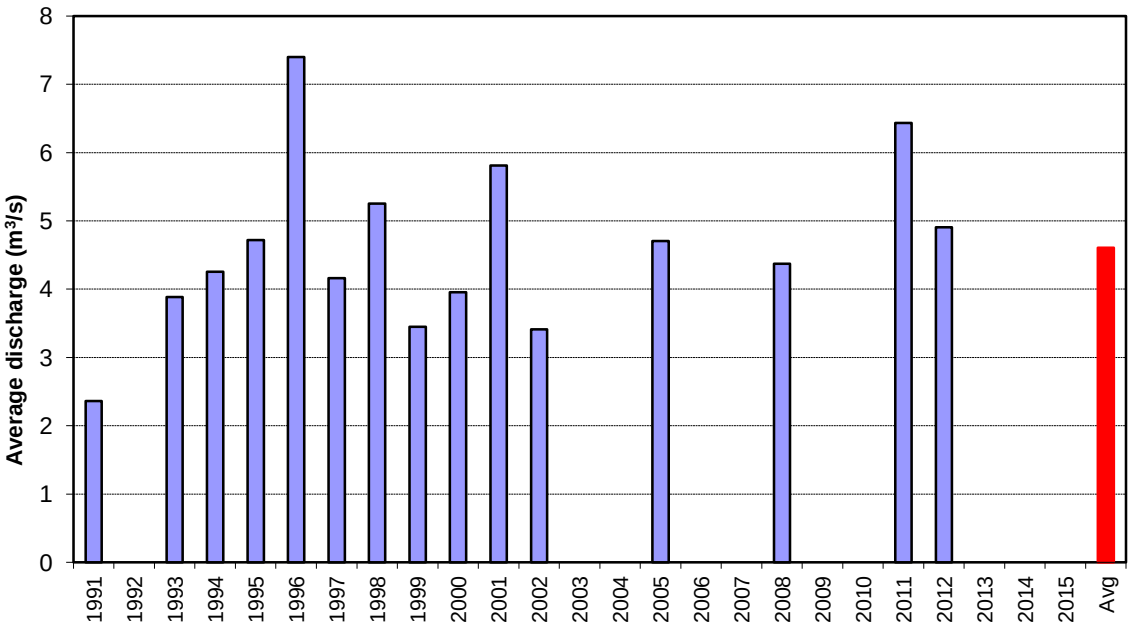

Figure4.8: (b) Annual variability of the mean annual flow of the Gelana-Tora

At Upper-Genale station, in the period from 1981 to 2007 is shown in Figure 4.8(a) indicating stable river flow with a coefficient of variation 1.03. The maximum daily discharge of 69.6 m^3/s recorded on August 26, 2003, with the mean annual flow of 4.20 at the river gauge.

The only river measured that enters into lake Chamo as **Sife-Chamo sub-river basin** at Gato assigned '6' representing the southwestern part of the study area. Measured discharge of the Gato-river in the period from 1977 to 2008 is shown in Figure 4.9.

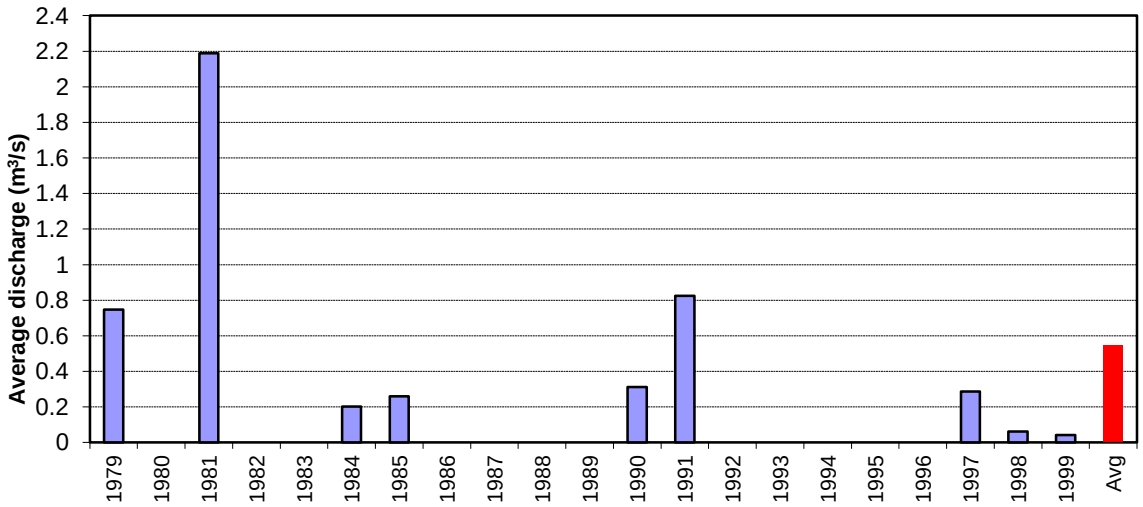

Figure 4.9: Annual variability of the mean annual flow of the Gato-river

The figure shows that the flow is relatively irregular with the highest coefficient of variation about 4.6 as given in Table 4.2. The maximum daily discharge is recorded about 20.4m^3/s on oct 10, 1981, at the river gauge. The calculated mean annual flow of 0.6m^3/s for the station represents flow generated mainly in the western highlands and escarpment where the river originates and flowing.

In summary, the measurement period varies across stations and both measurements exhibit gentle and stable trends up to 1995 on average and it tends to increase significantly to the end of 20^{th} century. Thereafter a rising stable trend has been observed till now. Besides, an increase in overflow from the Lake Abaya to Kulfo-river at gauging station signifies the lake level increase toward the west shoreline. In particular Goerner et al. (2009) associate the increase of lake level trend sedimentation and geological evolution.

4.3.2. Flow Duration curve

The flow Duration curve established from daily discharge records of gauging station of river flows for available data period in the study area is given in Figure 4.10.

The gently sloping curve of Bedessa, Kolla, Weira, Billate-Tena, Billate-Aposto, Upper-Gelana, Sala, Kulfo, Gidabo-Aposto Harie and Gelana-Tore-river flows relatively regular and consistent flows. While steeping slopping curve of river stations such as Gombora and Humbo, Betena-river indicates highly variable quick flow component and high recession rates during low flow. (Figure 4.10, shows duration curve of some of rivers).

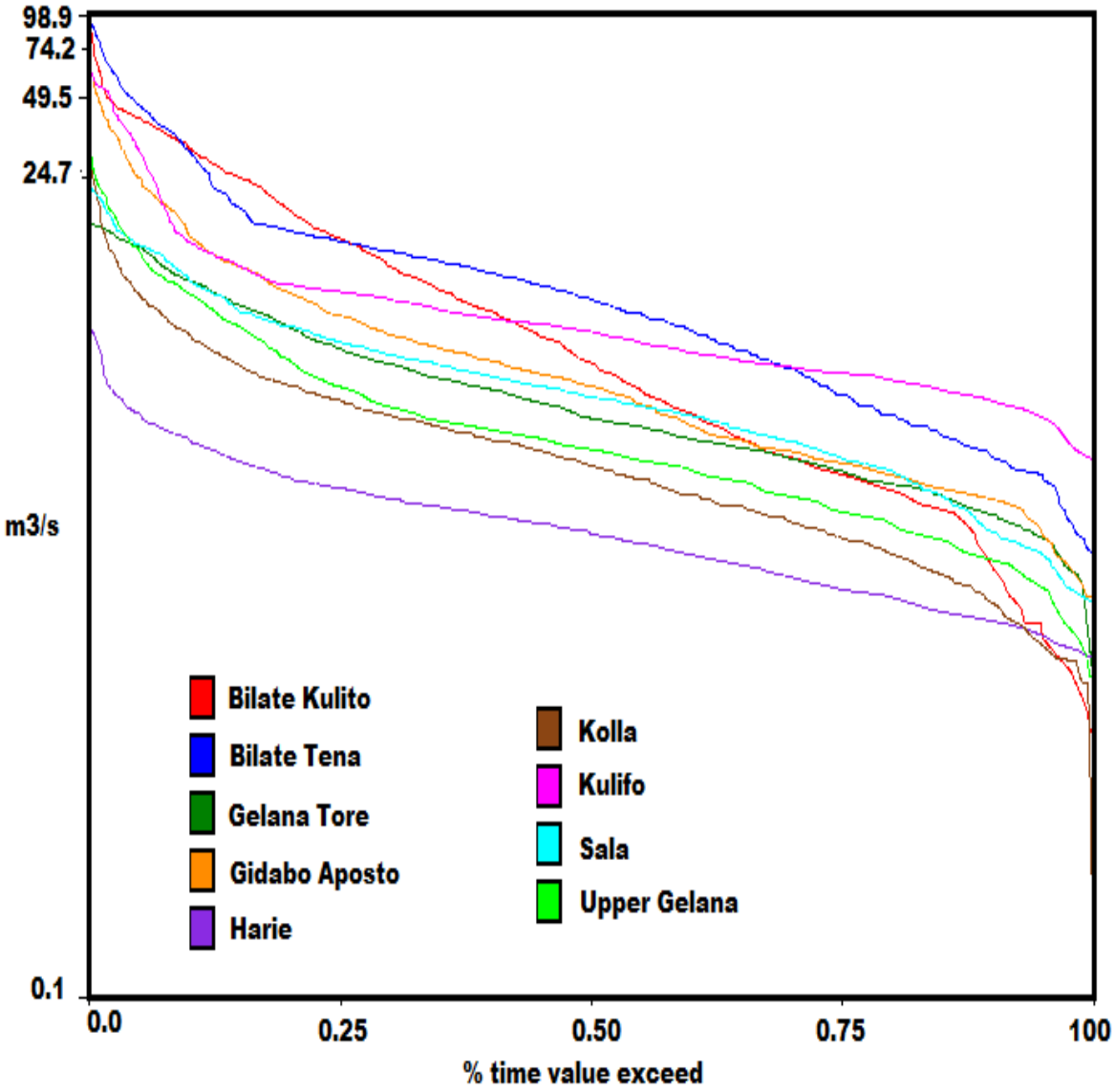

Figure 4.10: Flow duration curves of Gauged Rivers

Generally, in the study area as a whole, the difference in flow rates is explained by the size of the basin and the amount of precipitation over the basin. For example, the Bilate sub river basin is the largest major river basin in the study area with corresponding higher flow 10.5m^3/s and 16.9m^3/s at Alaba-Kulito and Bilate Tena gauging stations. While Gombora gauging station has the lowest mean daily flow of 0.04 with the smallest subbasin area.

4.3.3. Specific total Runoff

The specific runoff (surface and base flow) of a basin can be explained as a total a total flow per area of the basin. This parameter is important to account and comparison of the effect of catchment area in the amount of total flow together with the rainfall amount. The specific runoff and corresponding rainfall amount for the measured river flow in the study area are given in Table 4.3.

Table 4.3: represent the specific runoff in the study area

Major River basin	River gauging station	Mean flow (m^3/s)	Area (km^2)	Annual Rainfall (mm/yr)	Specific Runoff (mm/month)	Specific Runoff (mm/yr)	Specific Runoff (l/s. km^2)
Bilate	Batena	1.1	71	1171	40.16	488.6	15.5
	Gombora	0.4	41	1174	25.29	307.7	9.8
	Weira_Hossaina	7.4	522	1214	36.74	447.1	14.2
	Bilate_Kulito	10.5	2009	1178	13.5	164.8	5.2
	Bilate_Tena	16.9	5518	926	7.94	96.6	3.1
Hamessa	Hamassa_Humbo	0.8	255	1121	8.13	98.9	3.1
	Hamassa_Wajifo	0.5	358	1126	3.62	44.0	1.4
Kulfo-Gina	Harie	1.8	198	978	23.56	286.7	9.1
	Kulfo_Arba Minch	9.5	374	922	65.84	801.0	25.4
Gidabo	Bedessa	2.1	149	1410	36.53	444.5	14.1
	Kolla_Aletawondo	2.9	166	1471	45.28	550.9	17.5
	Gidabo_Aposto	6.5	646	1163	26.08	317.3	10.1
	Sala_Dilla	4.7	79	1403	154.21	1876.2	59.5
Gelana	U.Gelana_Y/ chefe	4.2	95	1372	114.59	1394.2	44.2
	Gelana_tore	4.6	376	1234	31.71	385.8	12.2
Chamo-Sife	Gato_Gidole	0.6	148	958	10.51	127.8	4.1

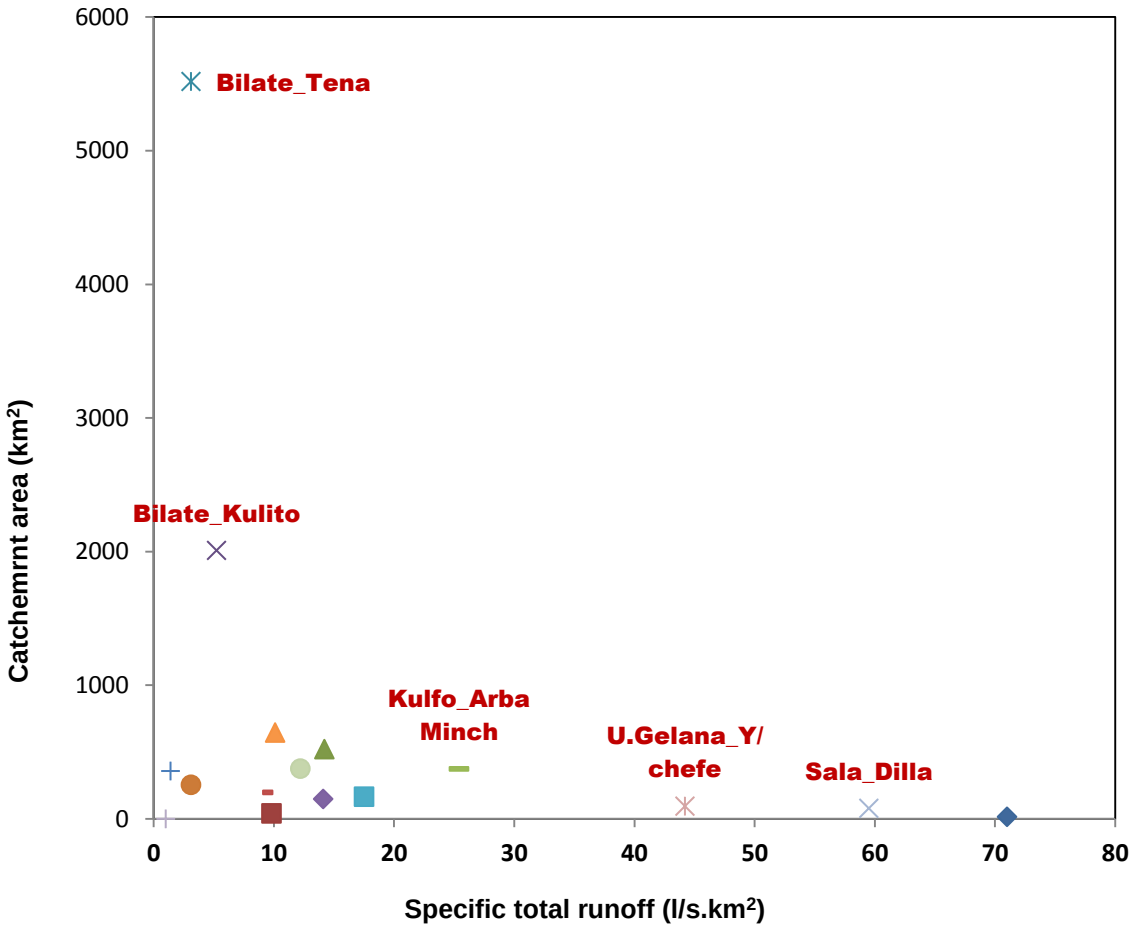

Figure 4.11: The relationship between Specific total runoff and river catchment area

Figure 4.11 shows the river flow characteristics in the study area, on which rivers such as upper-Gelana and Sala-Dilla has relatively highest specific total runoff with small catchment area. The highest specific flow is due to high mean rainfall in the region as indicated Table 4.3, while, rivers such as Bilate-Tena and Bilate-Kulito has the lower specific total runoff and largest catchment area. This mainly related to the size of the river basins connection efficiency of surface runoff and at the same time particularity, the gauging station of Bilate-Tena is placed at the downstream

In particular, the highest specific runoff is estimated in Gelana and Gidabo major-river basins, which are significantly correlated to the land cover futures and the distribution of lithologic formation. As given in Appendix 7 as basin characteristics, the forest cover is estimated in average about 16%, and 8.6%, which accounts the largest coverage as

compared to other land use types (such as grass, cultivations, etc) in the respective river basin. The multivariate correlation analysis given in Appendix 8, for the whole study area shows forest covers has 0.87correlation coefficient with specific runoff. In this regard, previous studies indicated forest cover increases specific flow through decreasing evapotranspiration rates than grassland/cultivation cover (Harr et al., 1982; Keppeler and Ziemer, 1990; Hicks et al., 1991; Smith, 1991). Additionally, the area is relatively characterized by the older geologic formation (late Precambrian to tertiary volcanic and basaltic rocks) with less rock permeability which plays a significant role in the runoff.

Whereas especially the estimated highest specific runoff in Kulfo-Gina major river basin is controlled by morphometric characteristic (elevation, hypsometric integral and slope) in the area. The area has relatively the largest mean elevation in the study area of about 1945. There exist significant correlation coefficients of 0.51 with specific runoff as given in Appendix 8, which facilitate quick flow before the rainwater went to groundwater table as recharge

4.3.4. Seasonality of river flow rates

As it was described in detail in Section 3.2.5, there is a clear distinction between the wet and dry seasons in terms of precipitation, on which northern tip of the study area shows mono-modal rainfall pattern whereas the rest largest area are characterized by bimodal rainfall distribution. In relation to this, since the river flow is formed by direct runoff from precipitation and recharge from groundwater (base flow); analyses were made to identify the seasonal river flow patterns in the study area. If river flow shows some seasonality, the level of variation in river flow is determined by the rainfall occurrence through runoff-rainfall relation. The base flow component generally has assumed to show small seasonal variation in comparison. The monthly average river flow rates for the 16 stations are compiled in Table 4.4.

Table 4.4: The calculated mean monthly flow (m3/s), for 16 river gauging stations

Station	Jan	Feb	Mar	Apr	May	Jun	Jul	Aug	Sep	Oct	Nov	Dec
Batena	0.29	0.44	0.44	0.86	0.9	1.13	1.72	3.29	2.79	1.75	0.55	0.26
Gombora	0.08	0.06	0.07	0.08	0.17	0.34	0.73	1.72	1.16	0.47	0.14	0.06

Station	Jan	Feb	Mar	Apr	May	Jun	Jul	Aug	Sep	Oct	Nov	Dec
Weira	0.86	1.15	2.39	6.3	6.0	5.97	12.9	23.2	16.3	9.43	1.88	0.9
B-Kulito	1.2	1.3	2.7	6.6	8.3	9.1	13.0	25.1	29.6	18.8	6.1	2.4
B-Tena	2.9	3.7	6.8	11	13.6	16.5	23.9	37.4	46.3	31.7	13.2	3.1
Bedessa	0.58	0.36	0.36	1.03	2.78	2.79	1.92	2.18	3.45	4.51	2.27	0.93
Kolla	0.68	0.56	0.59	1.31	2.61	3.12	3.49	5.3	5.26	6.12	3.09	1.72
Gidabo-A.	2.21	2.07	2.54	5.15	8.5	6.93	6.6	9.86	11.53	12.84	5.29	3.1
Sala-Dilla	1.29	0.74	0.91	1.55	5.75	4.7	3.28	5.31	5.96	9.04	4.82	1.81
H-Humbo	0.11	0.11	0.1	0.28	0.73	0.69	1.21	1.72	1.04	0.74	0.48	0.2
H-Wajifo	0.36	0.3	0.63	1.87	2.47	2.11	2.85	3.59	2.12	1.72	0.85	0.39
Harie	1.02	0.99	1.03	1.8	2.71	2.15	2.08	2.31	2.5	2.66	1.7	1.36
Kulfo	5.29	5.1	5.33	9.92	13.29	9.77	11.05	11.41	11.7	14.41	9.86	6.29
U-Gelana	1.31	0.95	0.9	2.71	9.76	6.18	3.21	3.01	5.16	10.22	5.09	2.06
G-tore	1.00	0.98	1.04	1.76	2.71	2.16	2.11	2.33	2.54	2.76	1.79	1.39
Gato	0.4	0.43	0.83	0.84	1.08	0.47	0.82	0.36	0.34	0.65	0.61	0.47

The mean monthly flow given in Table 4.4, were calculated for their anomaly (i.e. the ratio of the mean deviation of monthly flow to the standard deviation) which is standardization of different values aimed to compare values among each other. Accordingly, the Figure 4.12(a)-(d) showing the standardized anomaly of monthly flow rates were estimated based on the data in Table 4.4 in order to visualize the pattern in seasonal fluctuation. As a result, the following four patterns of flow rates variation were recognized in the study area.

The following example of monthly river flow variation is characterized by high level of correlation with the rainfall pattern in the same area. These stations (in the Figure 4.12(a) above) are present in the northern part of Lake Abaya indicating flow area mainly from the northern tip of the study area (gets rainfall in a concurrent month from June to September). The flow rates are high in the rainy season and lower in the dry season.

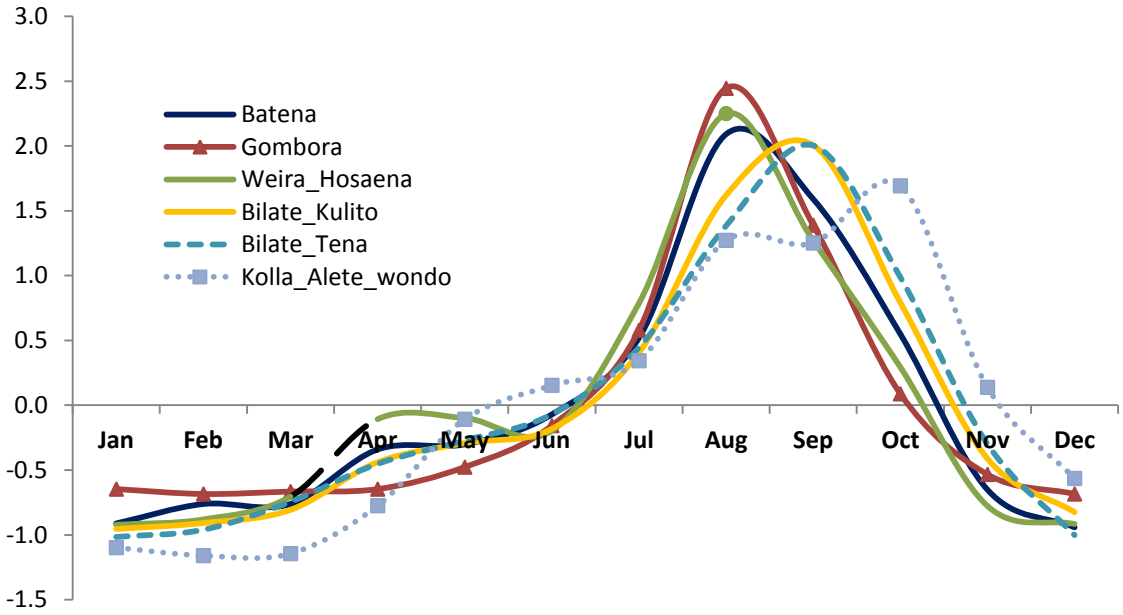

Figure 4.12: (a) shows the standardized anomaly of monthly river flows of stations: With only one peak through the year

Also, the two peaks in flow rates are observed as in the rain pattern for most of the rest of stations shown in the Figure 4.12(b). This indicated a bimodal seasonal pattern of river flow is most common and large coverage in the study area among all collected data sets.

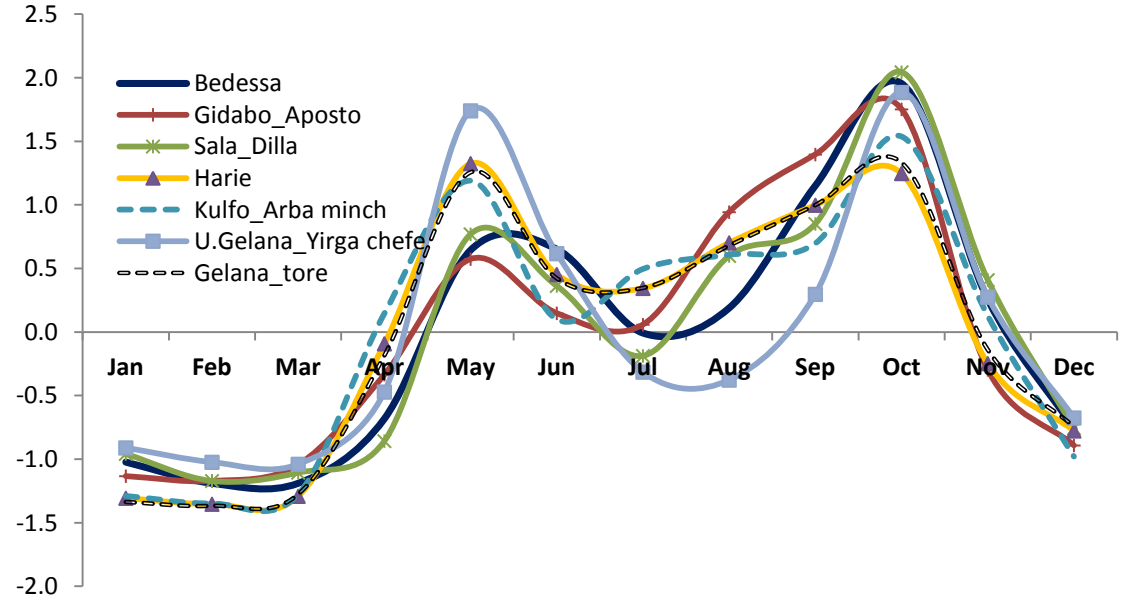

Figure 4.12(b): Shows the standardized anomaly of monthly river flows of stations with two peaks through the year.

The third type given in the Figure 4.12(c) is just in the range between the above two patterns (the monomodal pattern of the northern tip and the bimodal pattern that represent more than 2/3 of gauging rivers in the study area). Accordingly, the geographical position of the station also appeared in the northwestern part next to the northern tip of the study area.

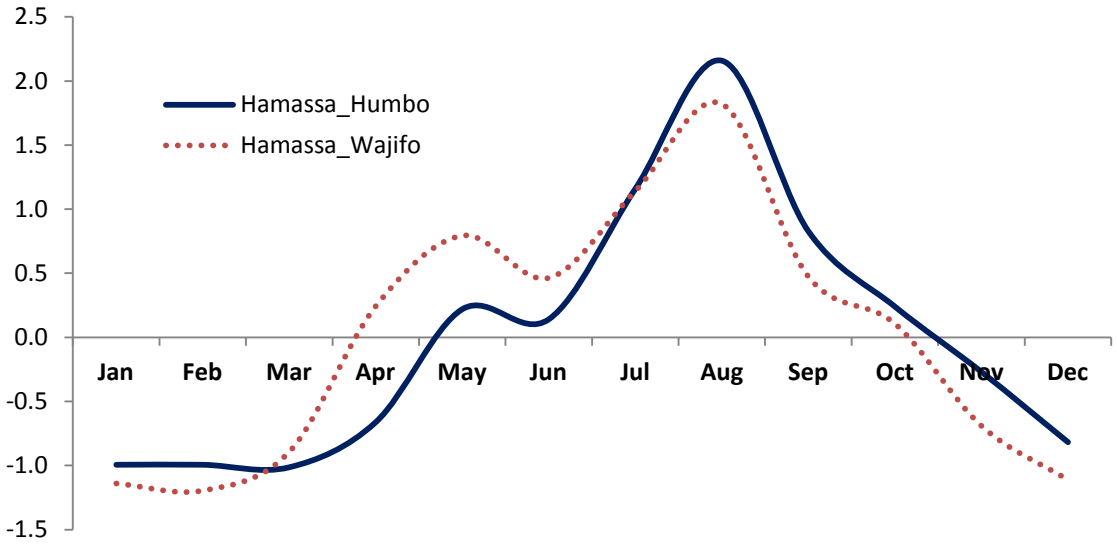

Figure 4.12(c): Shows the standardized anomaly of monthly river flows of stations with one-two peak through the year.

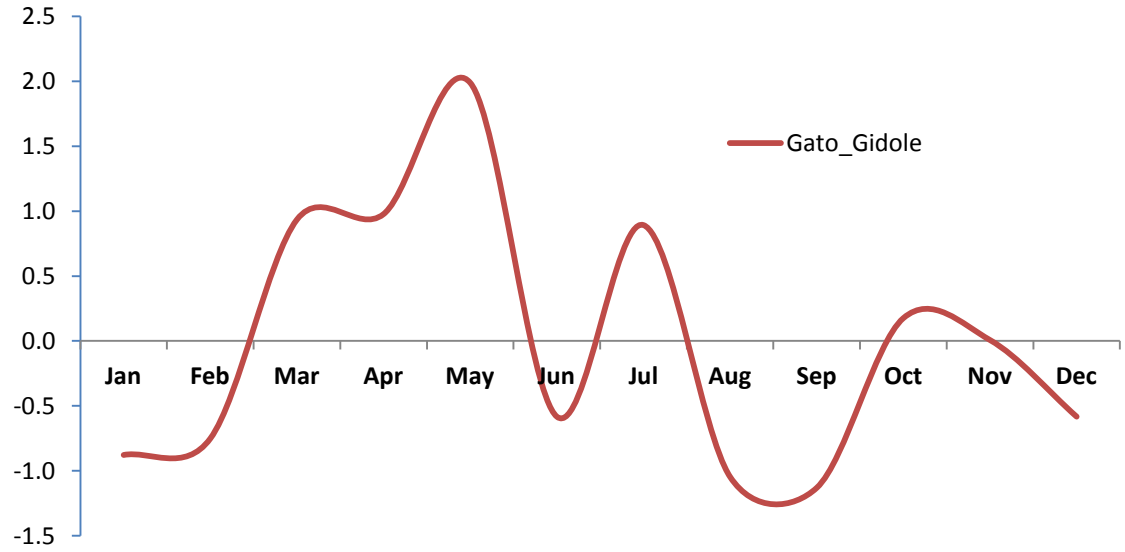

Figure 4.12(d): Shows the standardized anomaly of monthly river flows of the station with relatively no clear seasonality against rainfall through the year.

The last pattern shown in the Figure 4.12(d) is quite different features in seasonal variation of flow rates which was characterized by a high coefficient of variation as compared to other station. The station is found in the southwest of lake-Chamo with the low mean flow (0.4 m3/s). Due to its variability and low mean flow, maybe more of related to groundwater inflow contribution.

Thus, with respect to inter-annual variation as a whole, the river discharge gets peak generally in April and also from rises September-October in most cases. These are also more corresponding to the lake levels. The analysis indicates both the lake levels and river discharges are comparable in the season to the seasonal climate Thus rise in the lake level and river discharge in part related to rainfall event in the region. The annual cycle of rainfall shows a major peak in April-May and a minor peak in September-October.

4.3.5. Runoff- Rainfall Relation

Upon the seasonality characteristics of rivers in the study area, the simple correlation has made between the monthly discharge data and the meteorological rainfall station in the river basin. The result of the correlation coefficient is shown in the Figure 4.13(a).

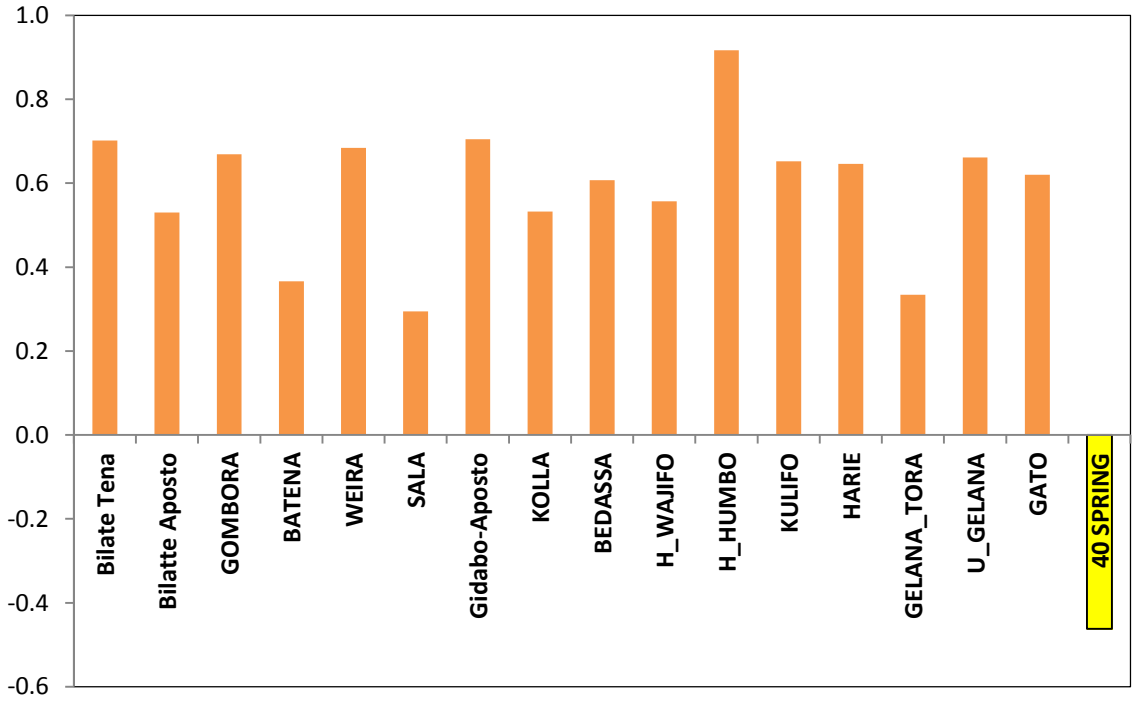

Figure 4.13: (a) correlation coefficient (R2) between discharge and rainfall

The bar graph represents the correlation coefficient (R^2) monthly discharge measuring station with catchment rainfall in that basin, and also the pie diagram (Figure 4.13(b) shows the mean correlation values for a sub-river basin in the study area.

As a given in Figure 4.13(a), almost all river discharge in the study area are significantly correlated to the mean monthly rainfall. The correlation value, r^2 varies from 0.29 (at Sala-river station) to 0.92 (at Humbo) with mean r^2 of 0.6. This implies the most part of the total river flow formed from the rainfall event in the region (nearly about 60%). This particular analysis suggests, the remaining 40% of the total flow contributed from other sources like groundwater discharge.

In the way, the known groundwater contribution as spring (Arba Minch-spring) discharge was also included in the analysis whether to check if there exist direct correlations with rainfall in the vicinity. The result clearly shows a negative relationship with R^2 of -0.46, indicating the spring discharge rate does not respond directly to the local rainfall as a delayed flow. In general, the clear difference in r^2 of river discharge and spring discharge can be used infer the source and mechanism of discharges.

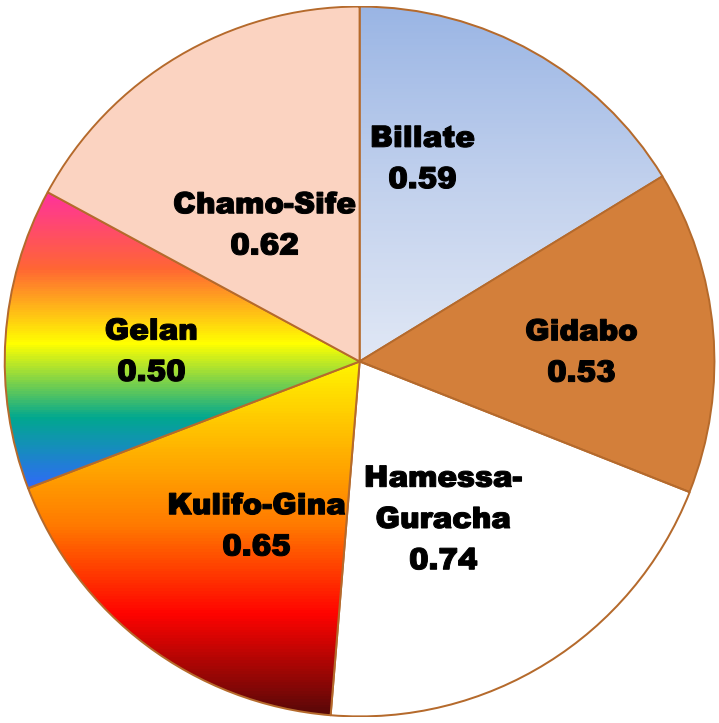

Figure 4.13: (b) the pie diagram represents the relative comparison of mean correlation coefficients between runoff and rainfall for major six-river basins.

The pie diagram (Figure 4.13(b)) shows the summary diagram of the major river basin to get an insight, which part of the study area river discharge is affected more by rainfall event. Indeed, the Bilate, Hamessa-Guracha, Kulifo-Gina, and Chamo-Sife have relatively higher correlation coefficient than Gidabo and Gelana-river basins in the study area. In another word, the rivers that are found in the northern and western part of the lakes in the study area are much sensitive to a seasonal rainfall event.

4.4. Spring discharge

In the study area, the only time series spring discharge measurement have takening at Arba Minch near Abaya lake is called Arba Minch spring (the name source of Arba Minch town is referred from this spring) which is a collected flow from a number of springs (thought to be 40 or more in number) outflow at downstream of kulfo-river basin (Figure 4.1).

4.4.1. Trends of Arba Minch- Spring discharge

Measured discharge of the Arba Minch-spring at Arba Minch gauging station in the period from 1981 to 2015 is shown in Figure 4.14. The figure shows that the flow is very regular and stable with a coefficient of variation 0.32. The annual variability is much smaller than the lake level and river discharges in the basin.

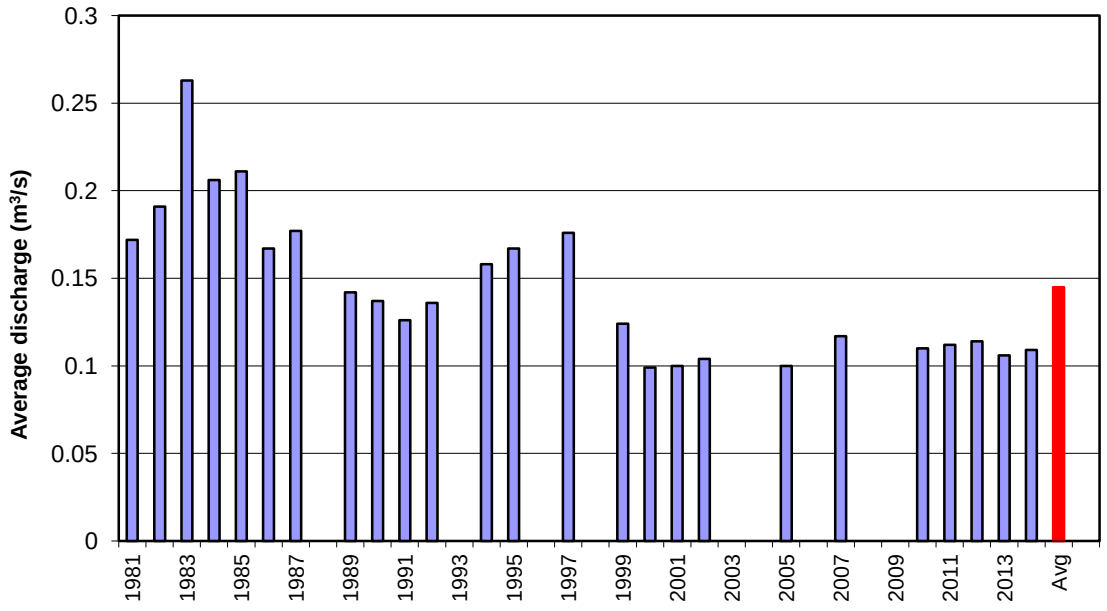

Figure 4.14: Annual variability of the mean annual flow of the Arba Minch spring

The discharge flow during the period from January to December through the year and the the maximum daily discharge was recorded about 0.33m3/s on May 01, 1983 at the spring gauge. While the minimum flow record was 0.059m3/s on January 26, 2005. The calculated mean annual flow of 0.15m3/s for the spring station represents flow generated from groundwater contribution. The annual measurement shows decreasing trend historically as depicted in the Figure 4.15.

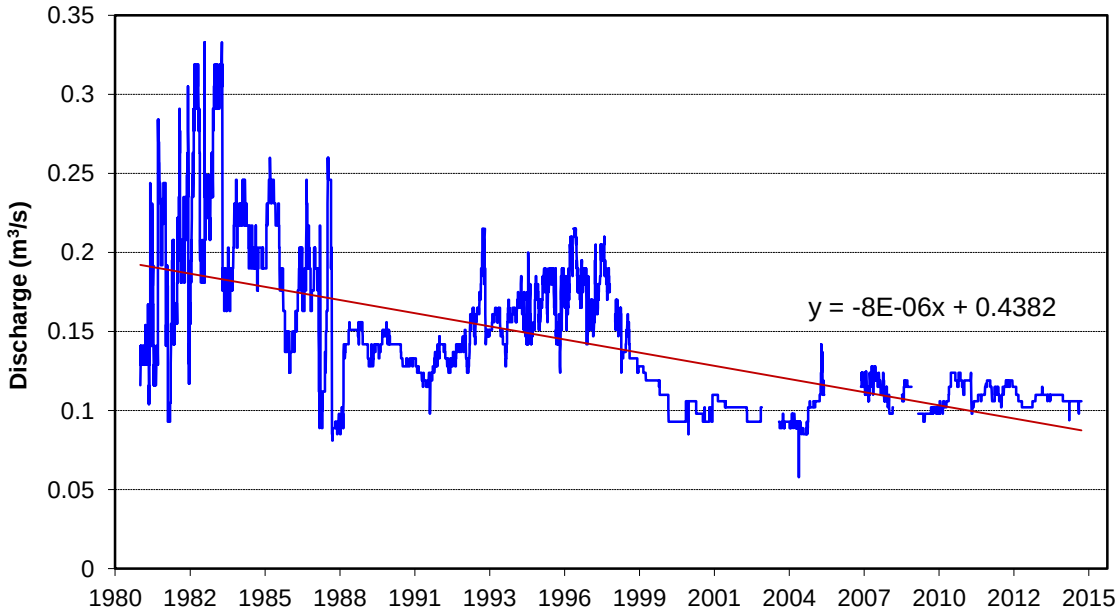

Figure 4.15: Hydrograph of the Arba Minch spring

During field observation, the Arba Minch-spring flow is recognized as fast flow through basaltic fractures at Arba Minch lowland in the floor, the temperature is colder and total dissolved solid of the water is lower than surrounding nearby surface water (lakes and Kulfo River) as a characteristic of the highland water.

Besides, as given in Figure 2.6; the escarpment near to Arba Minch is affected by major faults as a flow control from fractured tertiary basalt and volcanic formations in the western highland area. The long-term mean rainfall in the western highland at Geresse and Chencha gauging stations have been showing decreasing trend as shown in Figure 4.16 which is corresponding to the Arba Minch-spring discharge long mean trend, while the rainfall at Arba Minch shows increasing trend conversely where Arba Minch-spring is located.

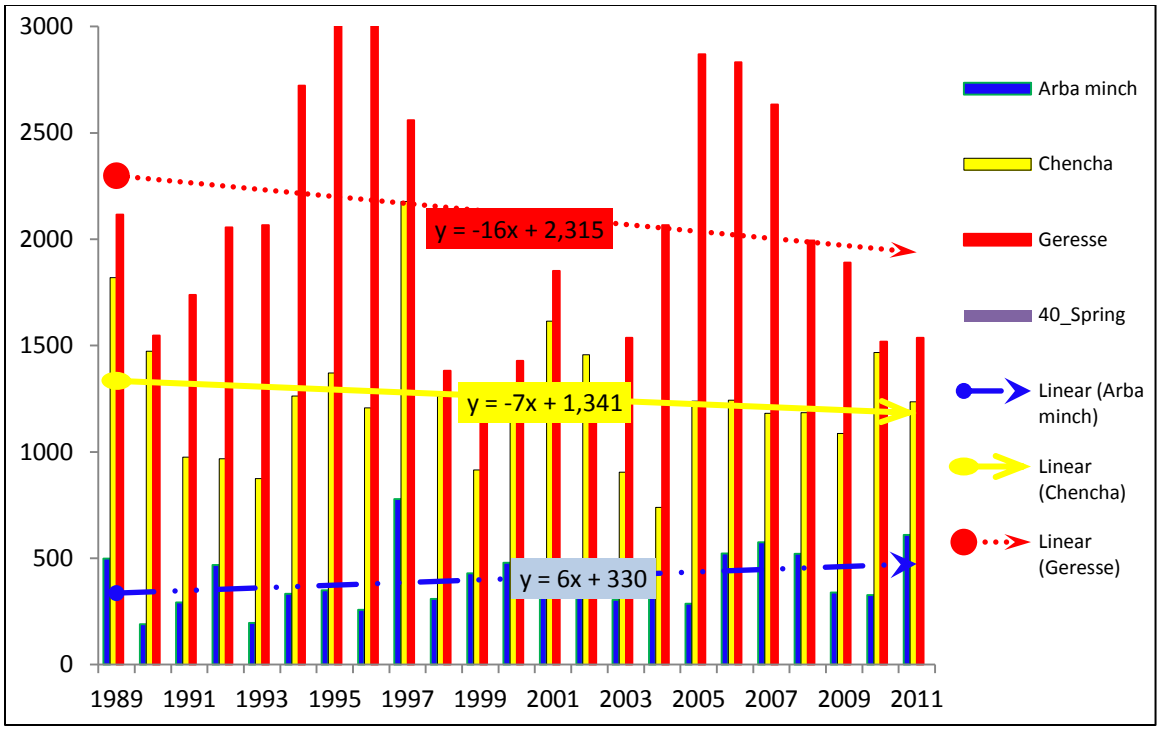

Figure 4.16: Long-term trend of the rainfall in the floor (at Arba Minch station) and the highland (Geresse and Chencha station) near to Arba Minch-spring location.

Thus, these indicate the Arba Minch-spring at Arba Minch results from the recharge of western highland through volcanic and basaltic fracture through local deep flow. Therefore, the decrease of Arba Minch-spring is likely related to the corresponding decrease of recharge at the western highland due to respective rainfall trend and also socioeconomic activities associated with water consumption in the recharge zone.

4.4.2. The residence time of Arba Minch-Spring discharge

As shown in Figure 4.17, the seasonal pattern of Arba Minch-spring discharge shows quite different features in seasonal variation of flow rates as compared with both the lake level fluctuation and river discharge variability in the region.

The monthly variations throughout a year are very small. The reason for this small seasonal variation is associated with the source of discharge at a far distance which is of groundwater outflow. In another word, the inter-annual variability of spring discharge is somehow different from the rainfall seasonal pattern of the area, which is related in time lag with the recharge zone rainfall.

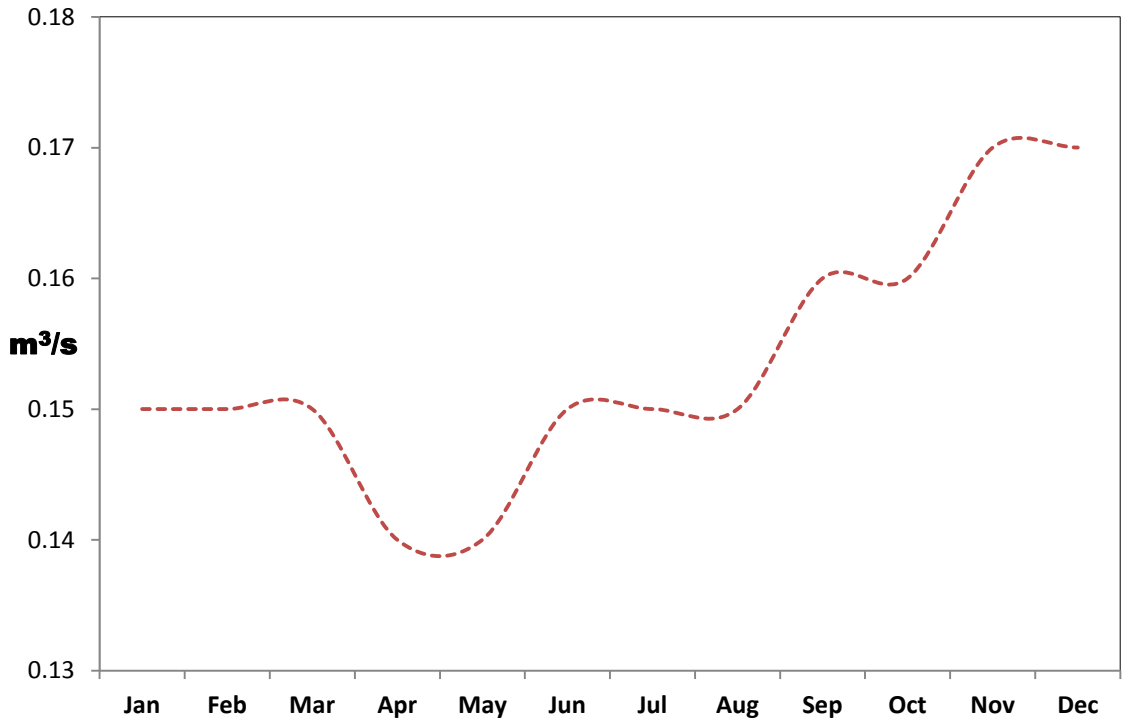

Figure 4.17: the Long-term monthly flow of Arba Minch-spring discharge

As indicated in Figure 4.18 during wet periods where recharge is initiated (in the western highland), the rainfall gets a peak in May and October months accordingly the high flow discharge at Arba Minch-spring gauging station happens after one month in June and November respectively. While in the dry period, the lower rainfall peak is observed in the month of February, this effect correspondingly shown in spring discharge after two month lag in April as low flow throughout the year.

Thus, due to its importance of water age evaluation with respect to recharge source, pathway, storage and outflow in the basin, few previous studies in this regard have been pointed. Of which Nagano K,et. al, (2017) indicated the variation of groundwater's with the season, i.e. the mean residence time of groundwater's in wet season tends to be shorter than in the dry season, and it becomes longer as rainfall and discharge rates decrease.

Accordingly, The analysis result showed seasonal variation in the residence; on which the residence time of the Arba Minch spring flow in the wet season is shorter nearly about 1-month whereas during the dry period it extends up to two months.

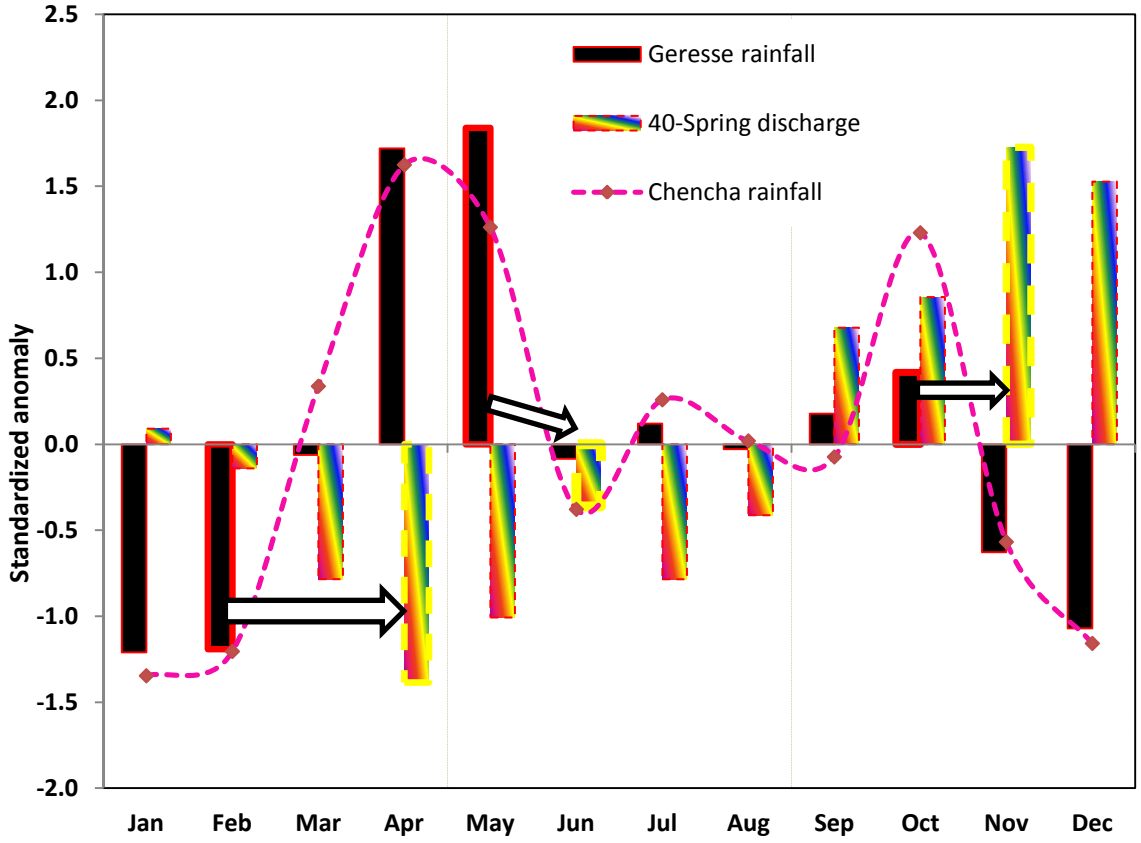

Figure 4.18: the standardized seasonal anomaly of rainfall at Gerese and Chencha station and Arba Minch-Spring discharge at Arba Minch gauging station

CHAPTER FIVE

5. CHARACTERIZATION OF HYDROLOGICAL SYSTEM USING BFI

5.1. Introduction

Understanding and conceptualization of basin hydrologic system provides information needed for effective and efficient management, planning and development of available water resources. Despite the irregular and limited distribution of the hydrological data at the basin scale (Soulsby et al., 2008); a record of total river flow has a vital role in exploring basin hydrology which comprises both direct surface runoff and the sub-surface baseflow. In this regard, baseflow is a desirable entity to know, for water management in general as a part of total discharge that represents the low flow of the river channel (Santhi et al., 2008). Of the most important low flow indices, baseflow index (BFI), is used in many studies as a spatiotemporal descriptor of basin characteristics through its links to physiographic, climatic, geomorphological, land cover, soil type, geological and other related parameters (Nathan et al., 1996; Lacey and Grayson, 1998; Haberlandt et al., 2001; Mwakalila et al., 2002). This index is defined as the long-term ratio of baseflow to total river flow volume (Institute of Hydrology, 1980). and controlled by all catchment characteristics, in turn, affect baseflow timing and quantity Furthermore, this parameter can also be used to calibrate or validate hydrological models as well. (Mazvimavi et al., 2005; Stuckey, 2006; Delin et al., 2007; Gebert et al., 2007; Santhi et al., 2008; Bloomfield et al., 2009).

Baseflow of a given basin cannot be measured directly or exactly, but it can be deduced from measurable total river flow in a systematic manner using appropriate techniques (Eckhardt, 2005). Indeed the results could be numerically reproducible, yet, it is much more difficult to interpret and understand the results. Relevant studies on estimation of baseflow river flow records have been conducted for many years by different authors (Nathan and McMahon, 1990; Arnold et al., 1995; Lim et al., 2005; Lyne and

Hollick, 1979; Szilagyi and Parlange, 1998; Arnold and Allen, 1999). These studies have used graphical, analytical, and digital filtering techniques to separate baseflow from total river flow. The baseflow separation has also been one of the most desperate analysis techniques in use in hydrology'' (Hewelett and Hibbert, 1967). Indeed the procedures available to this purpose are still, to a large extent, arbitrary important for a given river flow in order to provide objective measures of baseflow indices (Chapman and Maxwell, 1996; Chapman, 1999; Eckhardt, 2005). At the same time, the choice of a particular technique may more or less affect the BFI evaluation.

Furthermore, understanding, adopting and transferring hydrologic knowledge from gauged to ungauged basins based on multivariate controlling factor of baseflow characteristics at various spatial scales has become special attention to researchers in different parts of the world (Gebert et al., 2007; Haberlandt et al., 2001; Mazvimavi et al., 2005; Longobardi and Villani, 2008; Santhi et al.,2008). Most studies in this regard have used regression techniques comprising multiple linear regression and stepwise regression to relate baseflow index to basin characteristics such as physiographic, climatic, geomorphological, land cover, soil type, and geological variables. For instance, here in Ethiopia; Abebe (2006) established a relationship between the climatic, morphologic and geologic features of a catchment to baseflow in the Wabi-Shebele river basin. This particular study was found drainage density has a better relationship with BFI than other factors and further suggested the developed equation can be used fairly for estimating the baseflow in ungauged basins as well. Therefore, this study is motivated to explore relationships and the main control of the BFI through the inclusion of more additional multivariate basin characteristics of different six major sub-river basins as a spatial unit in order to assist water balance model calibration in the Abaya-Chamo Lake basin, southern Ethiopia. The result is ultimately useful in providing a conceptualization of the hydrological system of the area and to extrapolate information from ungauged river catchments, which indirectly appreciate how river flow records can be used to characterize hydrologic systems. The parameterizations in the analysis were limited to the sub-river basin, which did not include lakes that are found in the rift floor where these rivers enter.

Therefore, the specific objectives of this section are to: (1) compare and provide reliable result using three different digital filter and graphical baseflow separation algorithms; (2) investigate dominant catchment factors that control baseflow and quantify relationships between aspects of basin-scale geomorphological, hydrogeological, land cover and hydro-climatic attributes in controlling basin hydrology; and (3) establishing regression equation that links multivariate basin characteristics to baseflow index, this potentially opens up the possibility in estimating attributes of flow in similar nearby ungauged catchments.

5.2. Base flow Separation Approaches

As a spatial basic unit, the drainage basin comprises six major sub-river basins and the two low-lying lakes as discussed in Section 4.1(Figure 4.1). (Such as "Abaya" and "Chamo" lakes and rivers sub-basins include Billate, Gidabo, Gelana; Hamessa-Guracha, Kulfo-Gina and Sife-Chamo (JICA, 2012, Halcrow et al. 2008)). This chapter focuses on these major sub-river basins.

In order to analyze the characteristics of the river and their flows, daily river discharge data from 16-stations were used. The location and the basic information of the stations are shown in last section (Figure 4.1 and Table 4.2). The most important criteria used for selecting the gauging stations were the status of availability, the reliability of continuous daily river flow data. Those available river discharge data were then considered to compute the base flow component. The deduced indices were finally used further for hydrologic characterization analysis.

In this study, to account for the influence of different base flow separation estimates three different baseflow separation approaches were used which includes: Filter based River analysis package (RAP), Time Plot baseflow separation program (T_Plot) and The Kille Method.

5.2.1. Filter based River analysis package (RAP)

This package is developed by Monash University Melbourne (Australia) and Lyn-Hollick, (1979). The method of calculating the baseflow component of the hydrograph is

through the digital filter as described in (Grayson et al., 1996). Generally, Lyn and Holick's method is accepted as a suitable approximation on which the Lyn-Hollick filter has an alpha parameter (Grayson et al., 1996). The lyn-Hollick algorithm is given in Equation 5.1:

$$q_t = \alpha * q_{t-1} + (1+\alpha)/2 * (Q_t - Q_{t-1})) \quad (5.1)$$

Where, t – time, q_t - direct runoff at time step t, Q_t - stream flow at time step t, α - filter parameter associated with the catchment.

5.2.2. Time Plot baseflow separation program (T-Plot)

This method uses Gabriel periodic filter algorithm as given in Equation 5.2 is based on a recursive filter commonly used in signal analysis as discussed in Nathan and McMahon, (1990) and Lyne and Hollick, (1979).

$$f_k = \alpha f_{k-1} + \frac{(1+\alpha)}{2} * (y_k - y_{k-1})) \quad (5.2)$$

Where f_k -filtered quick response at the kth sampling instant, y_k- original stream flow, and α- filter parameter; $y_k - f_k$- is filtered baseflow.

The purpose of the filter is to create a relatively smooth transition from a period of baseflow before a storm event to the usually elevated baseflow following the storm event. These filters are calibrated to produce baseflow estimates from total flow data which means that constants in a filter are adjusted until the calculated time series resembles baseflow. To produce an estimate of baseflow, daily mean streamflow data were filtered forward in time and the result was filtered backward in time as Nathen and McMahon, (1990). Grayson et al (1996) recommended a value of 0.975 for α and also by Marsh et al., (2003).

5.2.3. The Kille Method

This graphical method has been used recently in Ethiopia on hydrogeological and hydrochemical mapping (Sima, Jiri et al.2003, 2004, 2009). The method determines the baseflow from series of observed monthly minimum river flow values (Demuth, 1993)

and has advantageous in consolidated rock areas because the minimum river flow values are often affected by interflow leading to a significant overestimation of baseflow, thus a more sophisticated hydrograph separation method based on the Kille method is recommended in these areas as well (Kefaleet al., 2013; and Thomas et al., 2014). The detailed procedure was given in Jiri Sima et al. (2009).

5.3. Multivariate characteristics and parameterization

In deriving the relationship between base flow index and catchment characteristics, multivariate of major river basins referred in Table 5.1 were parameterized with a representative, often mean value. Appendix 8 gives estimated values specifically for each of the six major river basins by averaging from the smaller raster or polygon based sub-units available.

Table 5.1: Major river basin characteristics, description, symbol and their respective unit used in analysis. (Geomorphometric, Hydro-Climatic, Land cover and Aquifer variables)

Variable description	Symbol	Units
Base flow index	BFI	-
Specific Runoff	Sp.RoF	$l/s.km^2$
Specific Baseflow	Sp.BF	$l/s.km^2$
Base Flow	BF	m^3/s
Direct Runoff	RoF	m^3/s
Mean total flow	T_RoF	m^3/s
Rainfall	RF	mm
Potential Evapotranspiration	PET	mm
Climate index(RF/PET)	CI	-
Catchment Area	Cat_A	%
Slope	Slop	%
Elevation	Elv	m
Hypsometric Integral	HI	-
Drainage Density	DD	Km/km^2
Portion of Rift floor	Floor	%
Portion of Escarpment	Escarp	%
Portion of Plateau	Plat	%
Portion of Cultivated	Cult	%
Portion of Forest	For	%
Portion of Grassland	Gras	%
Portion of Wood/Bush/Shrublands	WBS	%
Mean age of Rock	Age	Ma

Variable description	Symbol	Units
Transmissivity	T	m^2/day
Specific discharge	q	l/s

Available climate data sets for the study area were collected from the National Meteorological Agency (NMA). For each major basin, Climatic variables used in the analysis includes: annual Rainfall (RF), Potential evapotranspiration (PET) estimated using Penman-Monteith method and parameterized values are described in (Halcrow et.al. 2008), and also climate index (CI) were deduced from the ratios of rainfall to potential evapotranspiration.

A digital elevation model (DEM) with a resolution of 30m of Abaya-Chamo lakes Basin, produced from USGS was used to derive appropriate major river basins boundaries and basin characteristics such as Mean elevation (Elv), Mean slope (Slop), percentage of basin area with elevation (physiographic regions: Rift Floor, Escarpment, and Plateau), percentage of mean subbasin area with major river basin Area (Cat_A) using Arc GIS Software packages.

For each basin, Drainage densities (DD) and Hypsometric Integral were calculated from DEM. DD, as given in Equation 5.3, was calculated dividing total drainage length by the major river basin area within a basin (Horton, 1945 and Strahler A, 1957). The hypsometric integral of a basin is defined by assigning each Mean elevation (Mean ELV), minimum elevation (Min ELV) and maximum Elevation (Max ELV) values to each sub-basin areas using zonal procedure using Equation 5. 4.

$$DD = \frac{Drainge\ Length\ (Km)}{\text{Drainge area } (km^2)} \quad \ldots\ldots (5.4)$$

$$HI = \frac{\text{Mean ELV} - \text{Min ELV}}{\text{Max ELV} - \text{Min ELV}} \quad \ldots\ldots (5.4)$$

Land use of Abaya-Chamo Lake Basin was extracted and the major land cover class was identified in terms of percentage of the area-weighted average of the assigned individual land cover group in the major river basin area.

Due to relative limitation and reliability of available data on aquifer saturated thickness and hydraulic conductivity, hydrogeological data of aquifer variables such as Transmissivity, Specific discharge and underlying rock age values for the aquifer variables for basins were collected from the Hydrogeology Department of the Ministry of Water, Irrigation and Electricity and also derived from groundwater pumping well, reports and studies in the area (Halcrow et.al. 2008; JICA, 2012; Kefale et al., 2013; Thomas et al., 2014). Transmissivity and Specific discharge Point estimates were used to obtain representative values, whereas the mean age of the rock in each basin used as rock age for a basin.

Pearson correlation coefficients were employed between the variables on a scale of a major river basin as the basic spatial unit of analysis. Finally, a simple empirical approach used as a tool in order to investigate the effects of geomorphometric, hydrogeological, land cover and hydro-climatic features of the basin in controlling baseflow index.

5.4. Comparison of BFI estimates

Comparisons are aimed at finding a correlation between three baseflow separation algorithms to evaluate the most likely representative BFI value for a particular major river basin and to assess the stability of each method in the BFI evaluation.

A stable solution would be desirable when BFI has to be estimated from short river flow records and this would be a frequent case for the studied region. Then the representative BFI values for a major river basin were finally used for further analysis.

The separation of the baseflow component was done by graphical and tuning the filter value in between 0.99 and 0.995 from total flow hydrograph which gave a satisfactory and appropriate result in the recession part of the hydrograph.

Table 5.2, Figure 5.1 and Appendix 7 presents, the results of baseflow yield that deduced from daily river flow time series for 16 gauging stations using baseflow separation techniques within Abaya-Chamo lake basin as discussed in methodology Section 5.2.

Table 5.2: presents the results of base flow obtained from three procedures for gauged rivers

Major River Basin	Gauging Stations	Base flow (m3/s)			Specific Base flow (l/s.km2]			Base flow Index		
		RAP	K	TP	RAP	K	TP	RAP	K	TP
Billate	Batena	0.37	0.28	0.49	5.21	3.9	6.9	0.34	0.25	0.45
	Bilat_Kulito	4.2	4.8	5.6	2.09	2.4	2.8	0.40	0.46	0.53
	Bilate_Tena	8.04	5.58	7.54	1.46	1.0	1.4	0.47	0.33	0.44
	Weira	1.73	1.04	2.71	3.31	2.0	5.2	0.26	0.16	0.41
	Gombora	0.08	0.05	0.13	1.95	1.2	3.2	0.25	0.16	0.41
	Average	**2.88**	**2.35**	**3.29**	**2.80**	**2.11**	**3.88**	**0.33**	**0.26**	**0.42**
Gidabo	Gidabo_Apost	3.1	2.8	3.85	4.8	4.3	6	0.48	0.44	0.6
	Bedassa	0.68	0.63	1.0	4.57	4.2	6.7	0.36	0.33	0.52
	Kolla	1.06	1.0	0.13	6.39	6.0	0.8	0.4	0.38	0.05
	Sala	1.93	1.75	2.91	24.4	22.2	36.9	0.39	0.35	0.59
	Average	**1.69**	**1.55**	**1.97**	**10.0**	**9.18**	**12.6**	**0.41**	**0.38**	**0.44**
Galena	U_Gelana	2.04	1.85	2.18	21.5	19.5	22.9	0.48	0.44	0.52
	Tora	2.06	1.8	2.94	5.48	4.8	7.8	0.45	0.39	0.64
	Average	2.05	1.83	2.56	13.5	12.2	15.4	0.47	0.42	0.58
Kulifo_Gina	Harie	1.12	1.15	1.35	5.66	5.8	6.8	0.62	0.64	0.75
	Kulifo	5.62	4.73	5.86	15.0	12.6	15.7	0.55	0.46	0.57
	Average	**3.37**	**2.94**	**3.61**	**10.3**	**9.20**	**11.3**	**0.59**	**0.55**	**0.66**
Hamessa_ Guracha	Humbo	0.22	0.1	0.38	0.87	0.4	1.5	0.29	0.13	0.51
	Wajifo	0.4	0.2	0.42	1.13	0.6	1.2	0.18	0.09	0.19
	Average	**0.31**	**0.15**	**0.40**	**1.00**	**0.50**	**1.35**	**0.24**	**0.11**	**0.35**
Sife_Chamo	Gato	0.21	0.3	0.26	1.41	2.02	1.7	0.37	0.52	0.46
	Average	**0.21**	**0.30**	**0.25**	**1.41**	**2.02**	**1.70**	**0.37**	**0.52**	**0.46**

Particularly, since Major River basin of Abaya-Chamo lakes Basin is considered to be used as a basic spatial unit in the analysis, so each sub river basin values within it were averaged to represent six major-basins for the study area, So this was important to make compatible scale for comparative analysis with other basin characteristics in the next section. Therefore, average values of the major river basin were shown in Table 5.2 and Appendix 8.

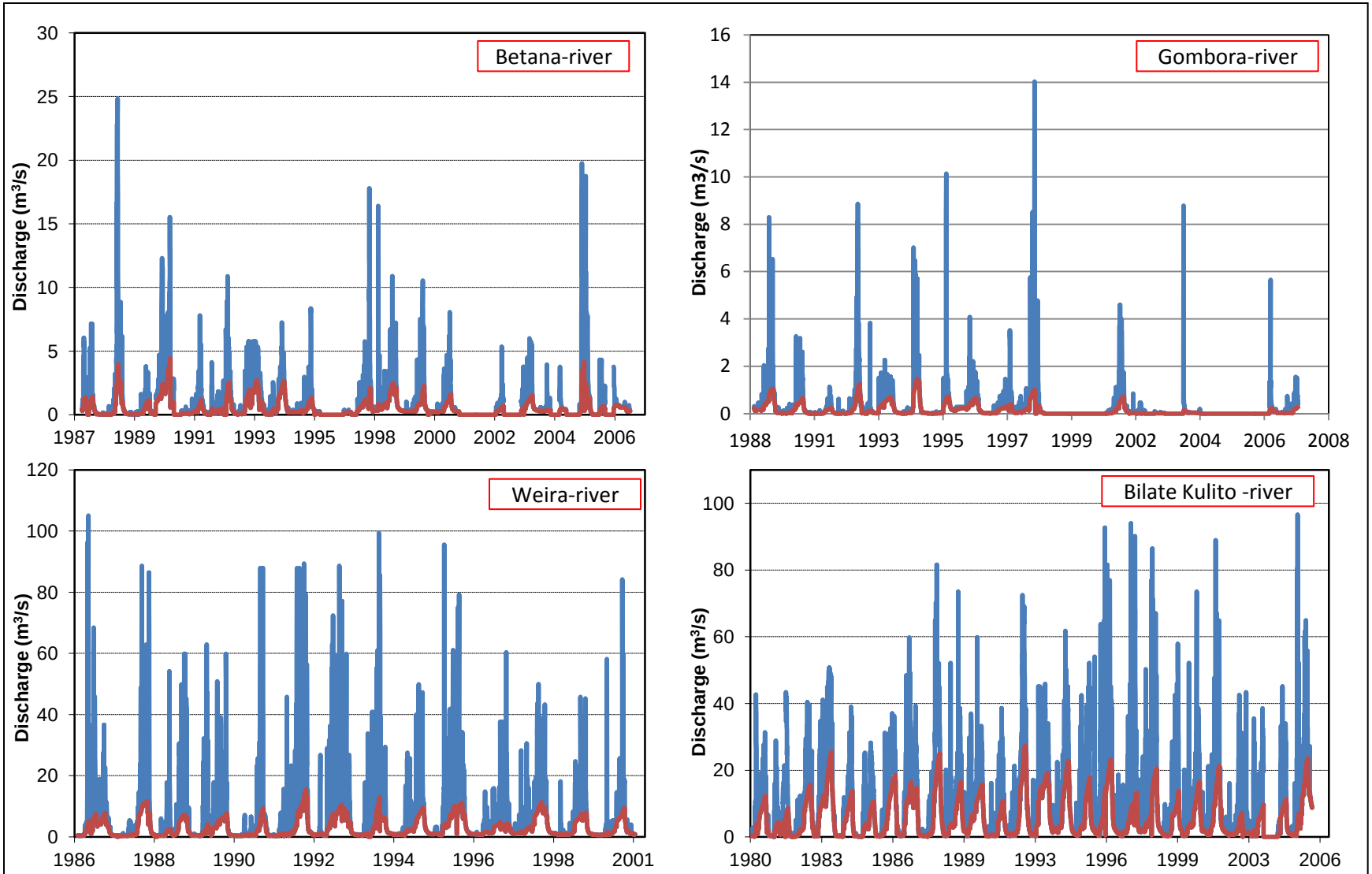

Figure 5.1: (a) Hydrograph of base flow of river

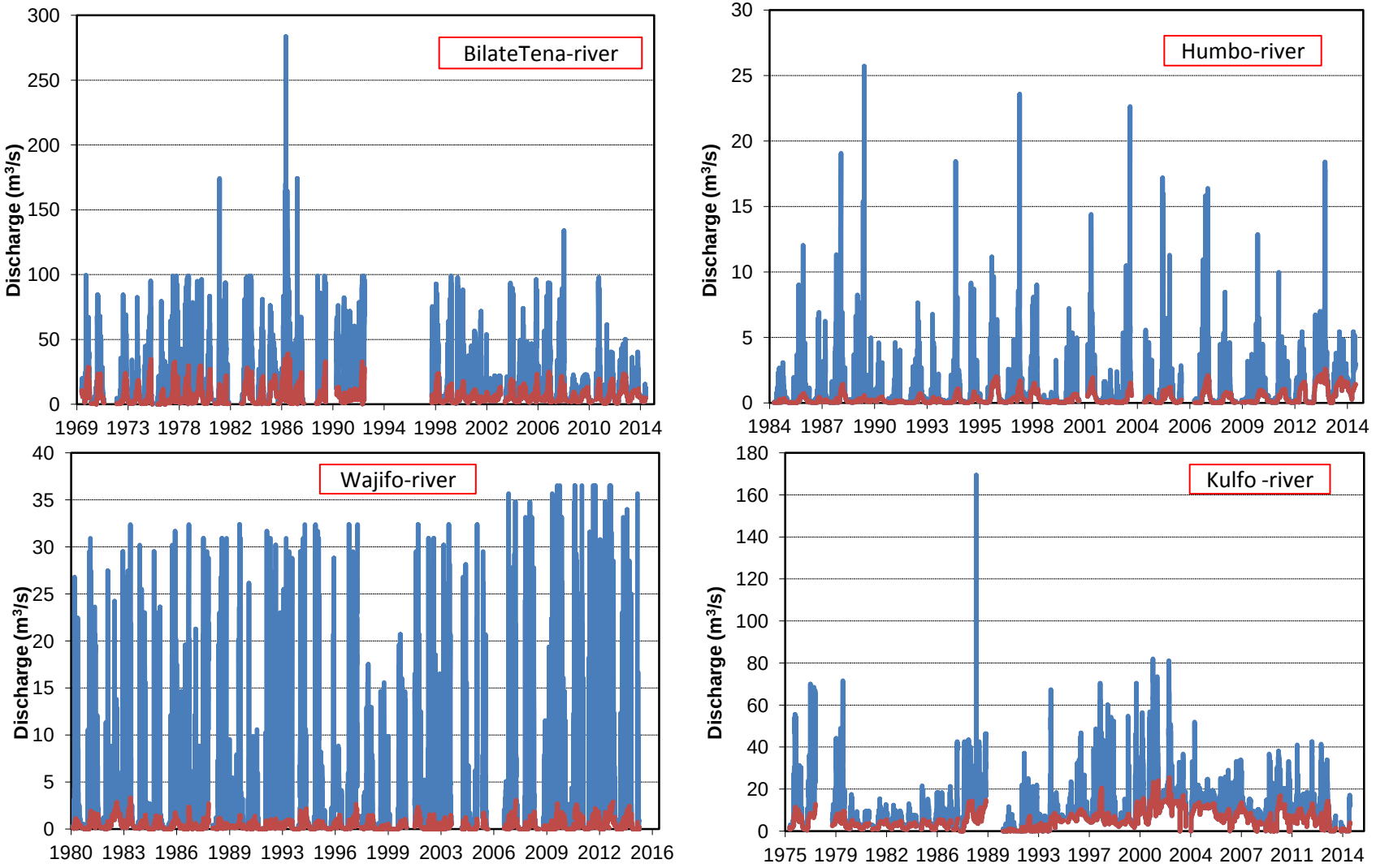

Figure5.1: (b) Hydrograph of base flow of river

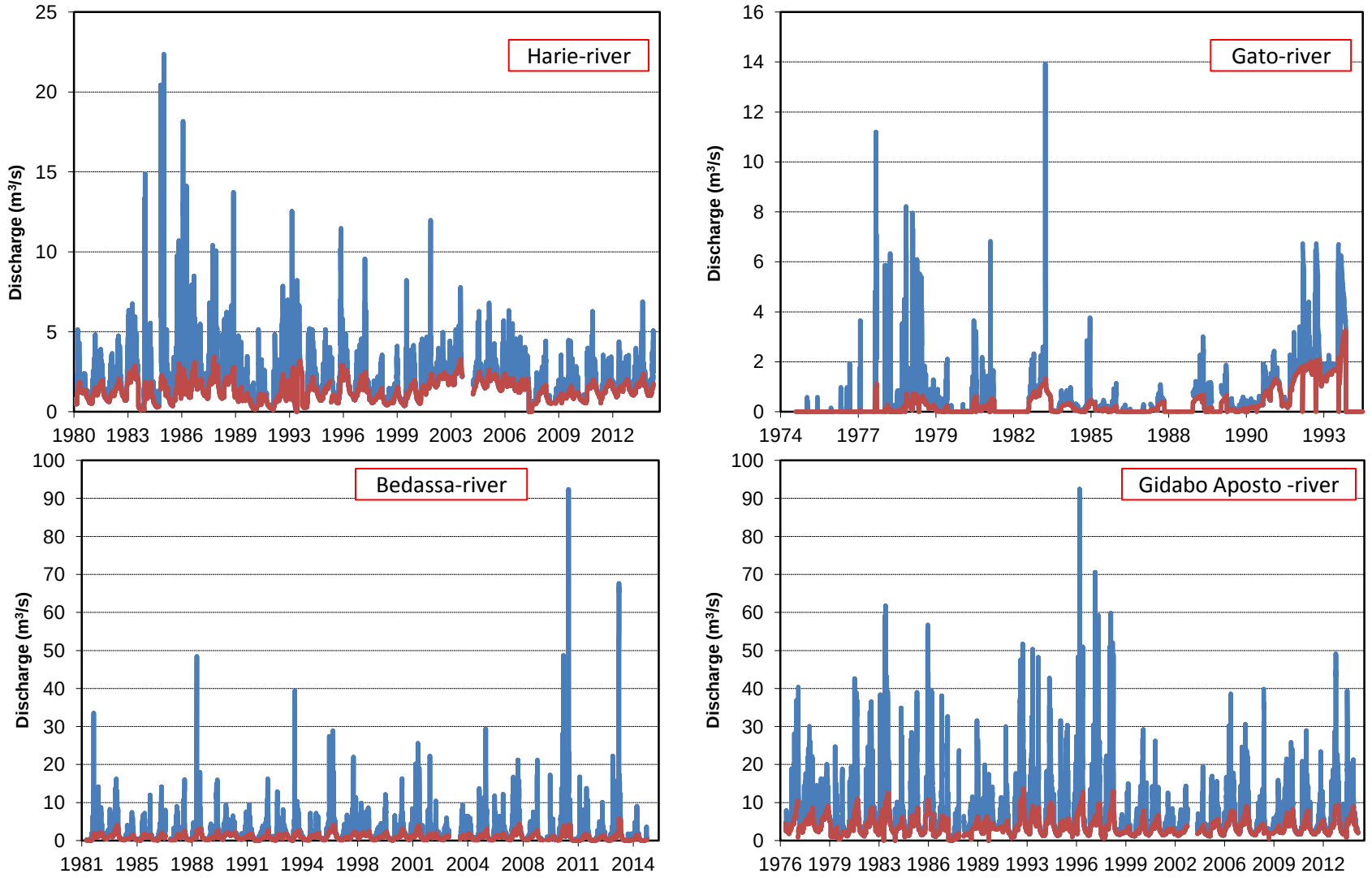

Figure5.1: (c) Hydrograph of base flow of river

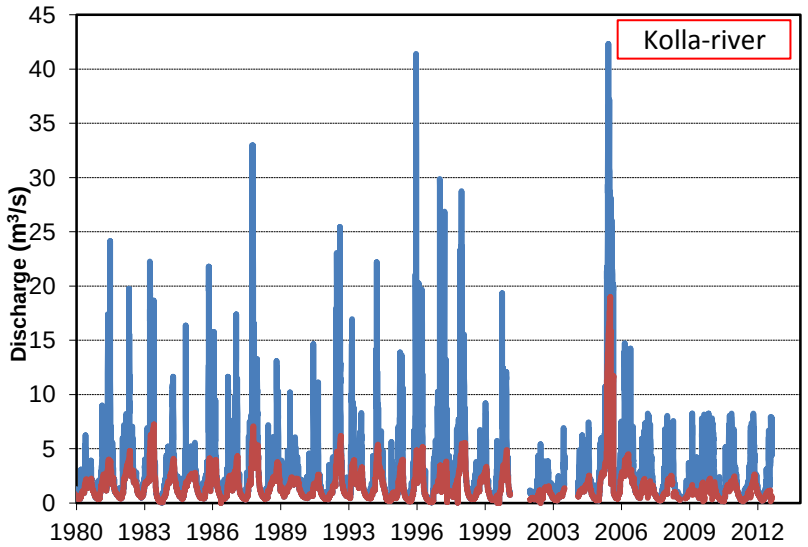

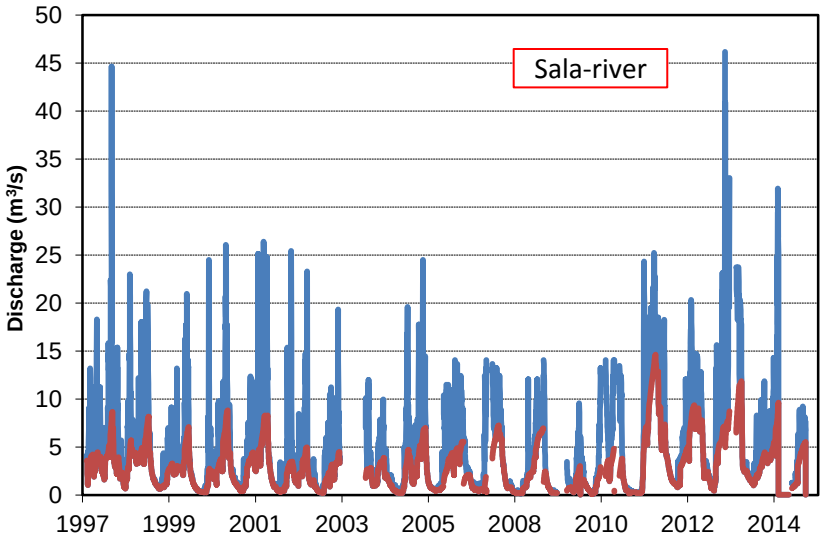

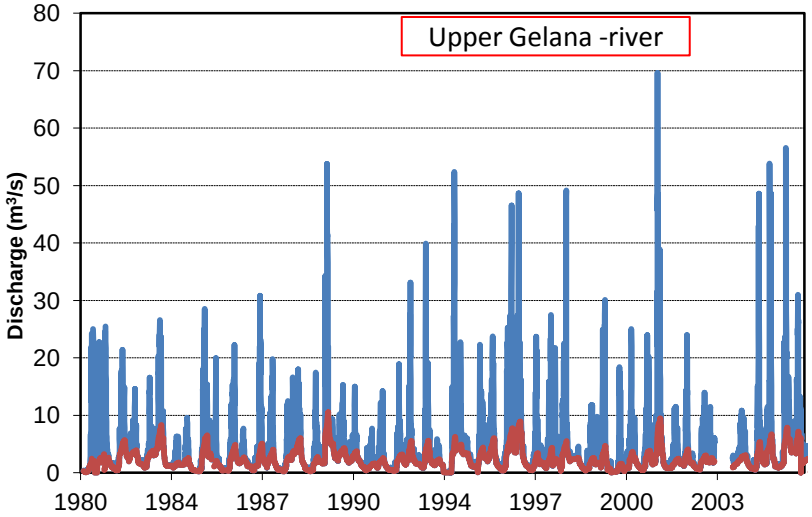

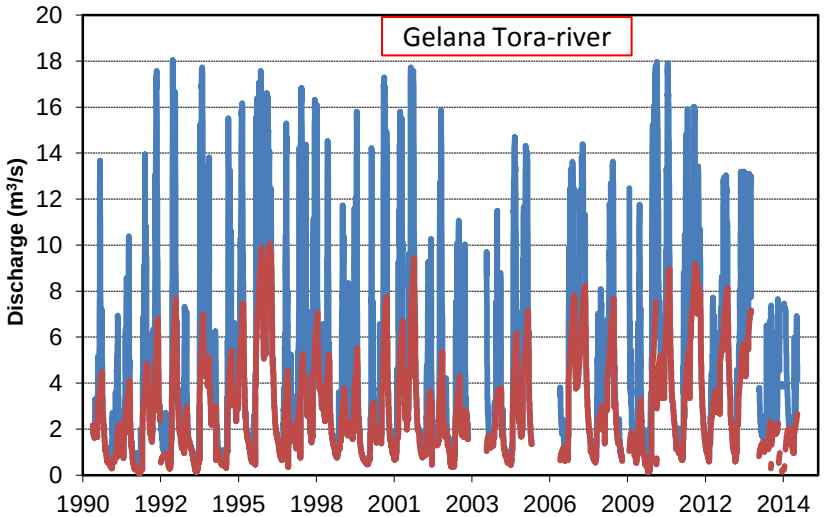

Figure 5.1: (d) Hydrograph of base flow of river

The result provides the most important information about subsurface in/outflow water resources for subsequent utilization in a sustainable manner. The observed average annual total river flows are in the range between 0.40 and 16.9m^3/s over the analysis period. Whereas, the estimated average annual baseflow are in between (0.08 and 8.04)m^3/s, (0.05 and 5.58)m^3/s, (0.13 and 9.25)m^3/s using baseflow separation methods RAP, K, and TP respectively for sixteen river basins, with corresponding catchment size in the range of 41 to 5518km^2. Here, the actual values of the BFI are unknown as a basic problem and are difficult to select which one of the methods approximate the reality at the best. Still, these baseflow results from three methods as shown in Table 5.2 are generally comparable to each other and also to previously published studies by Kefale et al., (2013) and Thomas et al., (2014). In fact, the numerical estimate of the Kille method in most cases underestimate baseflow value over the other two methods and so that, further comparison analysis was employed in order to provide the appropriate representative baseflow index values for the major sub-river basins. Hence, a simple correlation analyses of the baseflow index results of the RAP (BFI_R), Kille (BFI_K), Time plot (BFI_T), together with pairs of their Averages (BFI_RT_{av}, BFI_RK_{av}, BFI_KT_{av}) and averages of three (BFI_Avg) against mean total river flow and Specific runoff (ratio of runoff to its catchment area) were done as given in matrix (Appendix 6).

This comparison assessment of baseflow index among three methods shows, the estimate of average pairs of RAP and TP (BFI_RT) (r^2=0.96), relatively captures the mean flow and specific runoff better than Kille Method and others pair of averages. In other word, which are hydrologically more plausible and accurately producible but the Kille method was underestimated in comparison at gauging stations in Abaya-Chamo lake basin. The underestimation of the Kille method could be possibly related to the fact that the data series are relatively shorter for the method since it is relayed on monthly time series data. While, both separation methods (RAP and TP) are less expensive in term of data and time requirement, and their estimates are comparable to the main hydrologic properties of the corresponding sub-river basin. However, since the baseflow values were resulted by subjective determination and which may introduce some uncertainty due to the filtering parameter; especially for large mesoscale basins, Thus, the estimates using baseflow

separation clearly needs a prove of a more physically based approach for water resource evaluation .

Particularly, hereafter the multivariate analysis considered the average value of the RAP and Time plot index estimate as a representative value for the respective major sub-river basins (Billate = 0.40, Gidabo = 0.43, Galena = 0.53, Kulifo_Gina = 0.63, Hamessa_Guracha = 0.30 and Sife_Chamo = 0.42). Accordingly, the spatial variation baseflow index for the study area based on gauged rivers ranges from 0.19 to 0.69 with a standard deviation of 0.13, which suggests 44% average long-term river channel flow is assumed to be shallow subsurface flow contribution in Abaya-Chamo.

5.5. Multivariate analysis using BFI

As a common practice in previous studies, the Baseflow indices (BFI) estimate were used as dependent variable in investigating the characteristics of the hydrologic system. The BFI characterization analyses are completely based on topographically defined surface catchment as a basic spatial unit (six sub-river basins) regardless of groundwater flux transfer and it require only common technique to delineate six hydrologic unit and parameterization of the corresponding representative value for multivariate characteristics are straightforward computationally.

The multivariate characteristics (such as geomorphometric, lithological, land cover and hydro-climatic features presented in Appendix 8) are used to investigating effects in controlling basin hydrology. Besides, the result is interpreted in line with scientific findings. However, high heterogeneity, uneven data distribution and limitation of variables like hydrogeological parameters (transmissivity, specific discharge, and aquifer age), across the unit may affect the result as a limitation.

Following the multivariate analysis, the result of the correlation matrix in general suggests, baseflow index were correlated to various basin characteristics by scientifically meaningful causal relationship and while the rest of the basin attributes did not reveal a clear pattern. Perhaps some variables in the matrix have shown cross-correlations between them as well; this means some of the variables are statistically related to each other without any meaningful causal relationship. The basin-scale correlations matrix

given in Appendix 9 was used as the basis for interpretations and discussions on the nature of the control and the the the relationships among the multivariate in the following section.

To begin with, physiographic variables such as catchment area, elevation, and slope were found to be one of the most important factors that influence baseflow yield. Particularly in this study, as indicated in Appendix 9; the increase in drainage size, apparently increases the annual baseflow volumes that vary from 0.24m^3/s to 3.79m^3/s, because, the consequence is certainly clear that an increase in surface area has a collection possibility of extra flow to accumulate and this result confirms the direct proportionality of baseflow and drainage areas by Price, (2011). Noticeably in a similar manner, the slope is found to be the strongest predictor or first-order control of baseflow ((r^2=0.75) throughout in the study area. While in the case of elevation, the result clearly showed, the spatially distributed annual baseflow yield estimate, increase downstream with a correlation coefficient of 0.89 (as elevation effect on baseflow yield). These combined effects of elevation and slope steepness could likely relate to the rates and water transmission in determining whether it will be retained and percolate in the soil or reach a channel network

Moreover, systematic baseflow regionalization based on the physiographic region can be a good indicative tool to deduce baseflow occurrence. In this regard, the analysis took into account categorization of the physiographic region into highland (plateau-shaded green), rift margin (escarpment-yellow shade) and lowland (floor-red shade including lakes) as shown in Figure 2.1. The respective regions are partly accounted for about 37%, 34 % and 28% of the study area respectively. Consequently, the strong positive correlation was found on the plateau (with a correlation coefficient of 0.92) with high baseflow yield and which cover the largest physiographic area. Unlike plateau, both the rift floor and escarpment conversely associated with low baseflow yield. In fact, the direct explanation of physiographic regions and baseflow yield seems difficult regardless of linking it with other prevailing climatic factors such as precipitation, potential evaporation. As indicated in Appendix 9 and Figure 5.2 correlation matrix shows the degree of linearity in the correlations between the pairs of variables.

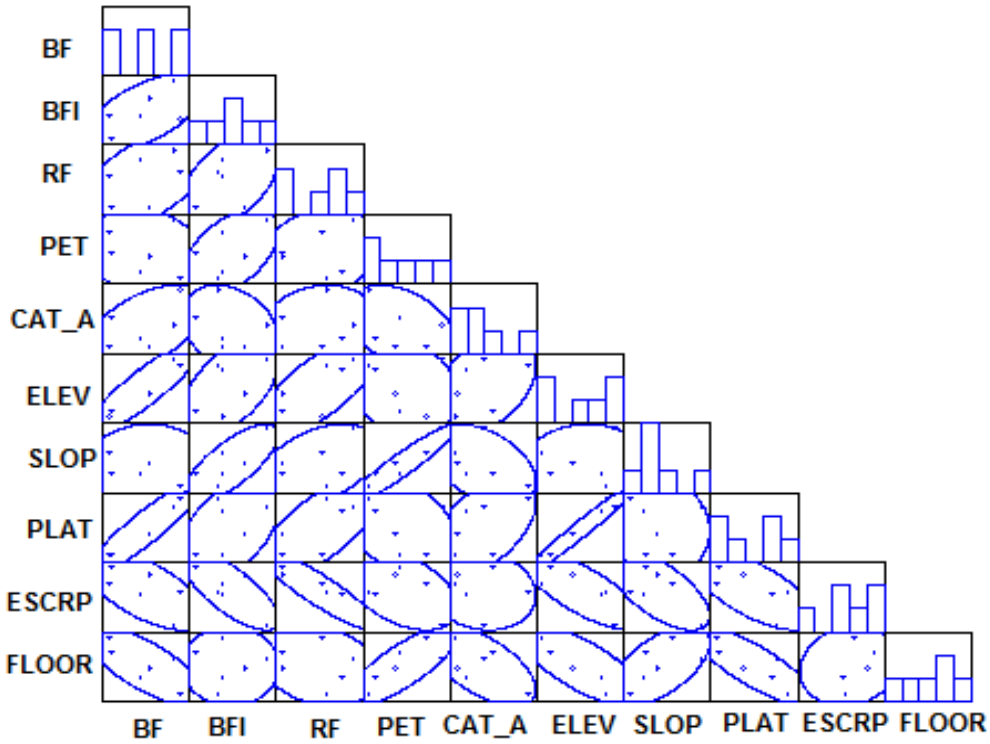

Figure 5.2: scatter plots and associated frequency histogram for pairs of variables (points represent the mean values and degree of spreading; the closer to the diagonal and the narrower curve indicate high liner relation with corresponding variable; foreword/backward orientation shows positive/negative correlation)

Here, the plateau is characterized by high precipitation and low potential evapotranspiration, which means in our case, precipitation goes linearly with elevation in excess of potential evaporation.

While relatively the lower physiographic region of both the escarpment and the rift floor are associated with low precipitation and high potential evapotranspiration. So that these connections could reveal, the occurrence of high baseflow yield on the plateau where the mean precipitation is high and relatively how potential evaporation as well. In particular to this, previous studies explained direct proportionality of precipitation to BFI and it is so clear since precipitation is the major source of subsurface flow to hydrologic systems and also confirmed by a number of studies like Memon,(1995); Santhi et.al.,(2008); Stuckey,(2006), Rumsey,(2015). Conversely, potential evapotranspiration decreases the amount of water available for both baseflow yield or surface runoff as a limiting factor (Memon, 1995), which is also true for Abaya-Chamo lakes basin.

In part, Aridity indices (CI), drainage density (DD) and Hypsometric Integral (HI) analysis were also investigated as other factor and the mean values of the major sub-river basin were given in Appendix 8. The estimated values range from 0.74 to 0.88; 0.17 to 0.26km/km^2 and 0.20 to 0.36 with standard deviation of 0.07, 0.04 and 0.07 respectively.

The spatial distribution of CI shows, the northeast and northern part of Lake Abaya (that includes Bilate and Gidabo river sub-basin) were relatively appeared to be arid (CI=0.88) as compared with southeastern and western part of the basin. Unlike CI, DD was conversely distributed in the study area, which is defined as channel spacing and expressed in terms of climate, topographic index, lithologic age and structure. Further, the distribution of lower DD into northeast and north of Lake Abaya was associated with low relief, highly permeable subsoil and thick vegetation. But, generally, the higher value of DD distribution in the southwestern and eastern basin depicts high relief, impermeable subsurface material and sparse vegetation (Nag et.al., 1998; Strahler A, 1957; Rasool et.al., 2011).

The other morphometric variable in terms of spatial distribution, HI appears somehow heterogeneous pattern across the lake basin. This indicates the variations of erosional stage and level of tectonic activities across major sub-river basins as given in Appendix 8. A low hypsometric integral value to the south of Lake-Abaya indicates the old and more eroded areas and evenly dissected drainage basins. While High HI values (Gidabo and Bilate sub-river basin) indicate that most of the topography is high relative to the mean, such as a smooth upland surface cut by deeply incised streams indicating young and less eroded areas. In this regard many studies in different part of the world, for example: Abebe, (2006); Moglen and Bras, (1995); Willgoose and Hancock, (1998); Huang and Niemann, (2006), Marani et al., (2001), and Vivoniet et al., (2008), Bloomfield et al., (2011), have proved that as HI values provide further valuable information on the tectonic, climatic and lithological factors controlling basin hydrology. In this view, the association among HI, CI and DD, are implied as important factors to explain systematically the hydrologic system in relation to baseflow index and appears to be essential in understanding the hydrodynamics of the study area.

Hence, from visual inspection of Figure 5.3 and Appendix 9, in general, the BFI has a relatively good correlation with HI with correlation coefficient 0.4 than CI and DD.

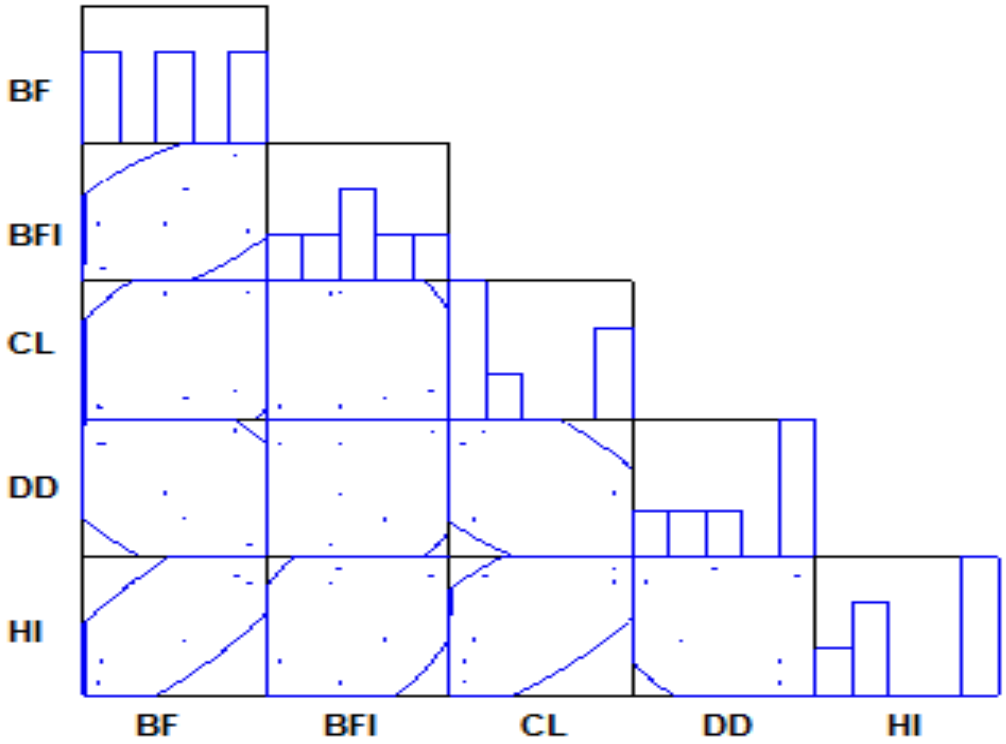

Figure 5.3: scatter plots and associated frequency histogram for pairs of variables (points represent the mean values and degree of spreading; the closer to the diagonal and narrower curve indicate high liner relation with corresponding variable: foreword/backward orientation shows positive/negative correlation))

This relation can imply, HI as a greater influence in control among morphometric characteristics and governs baseflow yield (R^2=0.80) in the study area. On another hand, HI has strong linear relation with CI (R^2 =0.75) and negatively with DD (- 0.35). This means, BFI is still somehow influenced linearly positive and negative by Climate index and drainage density respectively, which in turn affect baseflow and this outcome, corresponds to other studies such as Wang and L. Wu, (2013); De Wit and Stankiewicz (2006), and Abrahams and Ponczynski (1984).

As Wang and L. Wu, (2013) demonstrated, during drought periods when baseflow dominates the river flow, drainage density strongly correlated with base flow yield, similarly in this study, the long-term baseflow yield exhibit negative correlation (r^2 = -

0.50) with drainage density. In Summary, Hypsometric integral appear to be an important indicator for baseflow estimation, however, which is still cross-correlated to aridity index and drainage density. Here, the higher HI found at high elevation or physiographic plateau region where precipitation is in excess of potential evapotranspiration with low DD. Similarly, Price, (2011) proved, the drainage density is higher at higher degree slopes in humid regions than that of lower slope in arid regions.

The land use and cover data of the study area characterized according to FAO (1998) is described in Figure 2.2 into six land cover classes. The importance of land cover characteristics for generation baseflow yield was also statistically explained in the correlation matrix, on which significant correlation was found between the percent of Forest and grassland cover with baseflow index (r^2 = 0.36, -0.56 respectively), This confirms, an increase in forest cover significantly enhance baseflow yield. In this regard there is a noticeable conflict in the previous studies concerning the effect of forest on baseflow yield (Johnson, 1998; Brujinzeel, 2004; Brown et al., 2005) since; it is subjected to greater interception and evapotranspiration rates. Out of which studies particularly Harr et al., (1982); Keppeler and Ziemer, (1990); Hicks et al., (1991); Smith, (1991) pointed forest cover increases baseflow yield. Unlike Forest cover, Grasslands cover has relatively high rates of evapotranspiration which in turn affect the baseflow yield negatively. Besides, the other identified land cover classes do not show clear association in the study area

The quantitative measurement of hydrogeological characteristics for a basin is problematic due to a limitation in data points. In the present study, these aquifer variables used were based the basic hydrologic unit in a similar manner which exhibits significant variation in space across a topographically delineated basin. So that, hydrogeological maps and the available boreholes points are used to deduce aquifer properties for sub-river basins. In this regard, it is apparent that hydraulic conductivity, transmissivity, specific discharge and sometimes aquifer age are the basic lithological descriptor when looking for a meaningful connection with other basin-wide variables. In the study area, due to less reliability of available data on aquifer saturated thickness and hydraulic

conductivity, only transmissivity, specific discharge and aquifer age were considered, which varies between 115 to 355 m^2/day; 3.0 to 22.5l/s and 2.1 to 191.8Ma respectively.

Spatially, northeast and north of Lake Abaya (Billate and Gidabo river basin) has higher Transmissivity/specific discharge with younger aquifer age while the other portions such as Galena, Hamessa-Guracha, Kulfo-Gina and Sife_Chamo has relatively lower Transmissivity or specific discharge and older aquifer age which are located east, west and south of Lake Abaya and Chamo.

Likewise as observed on correlation matrix Appendix 9 there exist a strong linear positive relationship between aquifer transmissivity and specific discharge with correlation coefficient 0.88 and while, aquifer Age has a significantly negative correlation with transmissivity (r^2=-0.41). This combination may be explained systematically as older, less permeable aquifer units (such as the oldest late Precambrian rock within intercalated intrusive granite in the south-east and west of Lake Chamo and the tertiary lower basalt and volcanic rocks east and west plateau of Lake Abaya and Chamo tend to contribute low specific discharge, while the younger, and generally high permeable, Quaternary volcano-sedimentary units of rift floor around lakes supply high specific discharge. Accordingly, among these aquifer variables, transmissivity has a significant correlation (r^2 = 0.33) with baseflow yield than mean age and specific discharge (not clear) in Abaya-Chamo lakes basin.

Furthermore, we systematically looked into aquifer variable with other basin characteristics in relation to baseflow, to start with the representative major river basin Transmissivity value of aquifer that has a significant negative correlation (-0.47) with drainage density has been highlighted in Appendix 9. This relationship occurs because; transmissivity is directly proportional to aquifer permeability or hydrologic conductivity while aquifer permeability is inversely related to Drainage density (Zecharias and Brutsaert, 1988). This means for relatively impermeable lithological units, the ratio of total surface run-off to groundwater baseflow is greater than those that have higher transmissivity or permeability. Besides, previous studies have stated that a difference in

lithology across a range of geological settings has significant variations in drainage density (Carlston, 1963; Tandon, 1974; Kelson and Wells, 1989).

Therefore, In order to put a simple causal explanation on the hydrological system of the study area, relatively high precipitation from highland must find a way to reach the higher drainage network; then a given total surface run-off will be greater for groundwater units with lower drainage density, which may result in amplifying erosion of the underlying river. This provides some reason for the presence of unconsolidated superficial sedimentary deposits up to nearly 30-meters thick throughout the basin floor around Abaya and Chamo lakes which may also contribute in supplying sediments to lakes.

Additionally to the earlier discussion, HI is appears significant variable to imply baseflow yield and also can be use to infer aquifers transmissivity where less or no data point exist but it would require more refined calibration, this can be given by:

$$\boldsymbol{T} = 976.7 * \boldsymbol{HI} - 83.6 \quad \text{..... (5.5)}$$

Where, T is Aquifer transmissivity (m^2/day) and HI-hypsometric integral with R^2 of 0.71. This means, the evolution past and present tectonic activity of the area are highly determined the transmissivity value of aquifer unit and also this relationship can be used to parameterize transmissivity values in a basin.

5.6. Regional multiple regression

The regression model was developed under the computational complexity of the variables on which the indicated variables in Appendix 8 have high multicollinearity because of the existence of high correlations among some variables. Multicollinearity in a model will negatively affect model quality and stability (Rawlings et al., 1998). In the model selection procedure, not only statistical significance (high coefficient of determination, low multicollinearity, and parameter parsimony) but also hydrological plausibility and the practical availability of the variables are considered. In order to overcome multicollinearity to best fit a stepwise multiple regression was performed (Jabson 1991) on the descriptive variables with baseflow index.

As the most suitable relationship model with for explanatory variables is suggested in Equation (5.6), with units of the independent variables specified in Appendix 8 from which the model includes Slope (BFI) and Drainage Density (DD) for the area under investigation.

$$\boldsymbol{BFI} = 0.08 * \boldsymbol{Slop} - 2.73 * \boldsymbol{DD} + 0.67 \quad \ldots\ldots\ldots\ldots\ldots\ldots\ldots\ldots\ldots\ldots (\mathbf{5.6})$$

All regression coefficients are significant at 95% confidence level with coefficient of determination (R^2) estimated for Equation (5.6) is 0.96 and the standard error of estimation is 0.026. The significance of the estimated regression coefficients is given in Table 5.3 and this test shows the statistical significance (p-value < 1%) of the regression model which involves slope and drainage density.

Table 5.3: Results of significance test for the stepwise regression analysis of the BFI

Source	Sum-of-Squares	df	Mean-Square	F-ratio	P-value
Regression	0.061	2	0.031	44.3	0.005
Residual	0.002	3	0.001		
Total	0.06				

The following Figure 5.4 demonstrates a regression relationship developed between estimated and modeled BFI and showed good agreement.

The established regression equation in Equation 5.6 provided as a tool with reasonable accuracy for estimating the base flow yield and which can be used as a tool or base to extrapolate in the ungauged section of the basin with great care. This Equation (5.6) is pointing the advantage of regionalization base flow index using appropriate multivariate analysis for physical characterization of the hydrologic system.

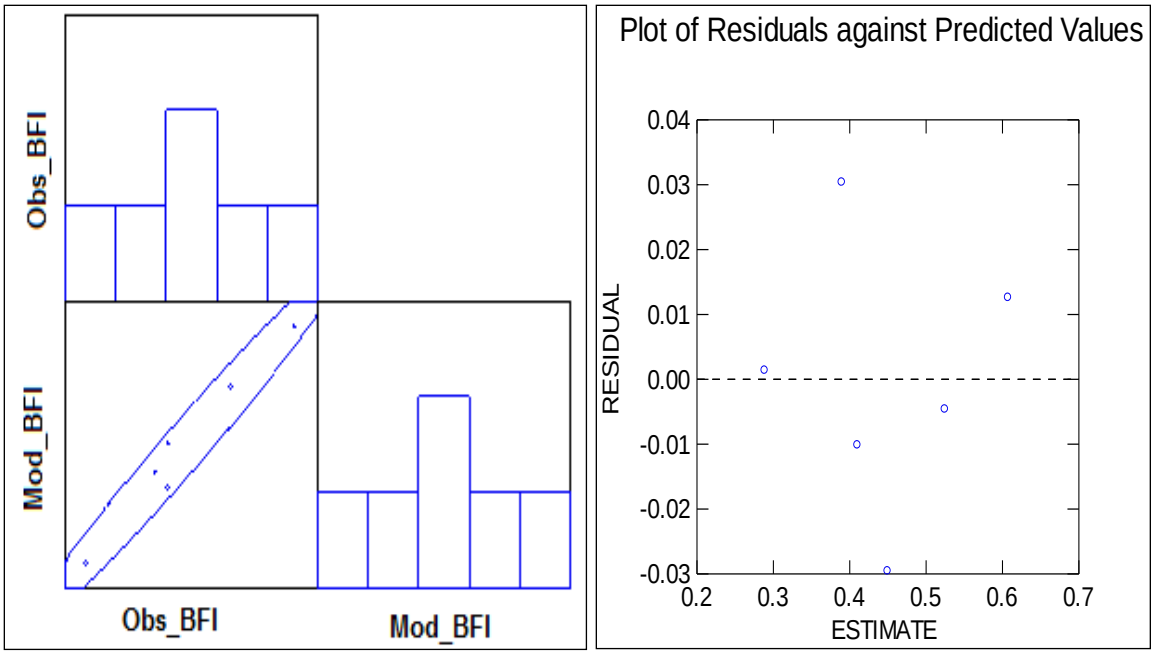

Figure 5.4:: comparisons between the observed and estimated BFI of Abaya-Chamo Lake basin

In summary, the present study in this particular Chapter (5) explored the multivariate attribute that dominantly controls basin hydrology particularity on which the peak baseflow yield is found at highest elevation or physiographic region in the plateau. This highest physiographic region in the study area is characterized and strongly correlated with hypsometric integral (r^2 = 0.96) and low drainage density (r^2 = -0.49) as compared with the escarpment and the rift floor.

In general, since BFI is used to explain the overall hydrologic system of the basin, the study reveals slope, elevation and prevailing climatic conditions appear to be a crucial factor than other multivariate (land cover and lithological variables) in Abaya-Chamo lake basin.

The estimated baseflow values and the physical characterization of the hydrologic system account for only the long-term average for the region. Therefore, this study has important implications for the remote areas where specific data availability is limited to have an insight of hydrologic system. Also, it is better to consider more supplementary potential variables such as soil type, potentiometric water level, hydraulic conductivity...etc. that would help in providing solid knowledge.

CHAPTER SIX

6. SURFACE WATER AND SHALLOW GROUNDWATER RESOURCES AVAILABILITY

6.1. Introduction

The complex geological processes of the intra-rift faulting and associated volcanic activities resulted in the formation of volcano-tectonic structural depressions, which became born sites and creation of several of East Africa's largest lakes as well as much of its topography. Of which, the MER contain tectonic depressions and lakes of different hydrological and morphometric characteristics, that mainly controlled and fill NNE trending structure (Le Turdu et al., 1999). The central part of the MER occupying lakes such as Ziway, Langano, Abiyata, and Shalla, and the southern section consists of the lakes: Hawassa, Abaya, Chamo and Chew Bahir, which make up different lake basins in the region for instance the current study area "Abaya-Chamo lake basin".

The lake basins are thought to be hydrologically separate units with exhibiting different ranges of hydro-climatic features (Alemayehu et al., 2005). Understanding surface and groundwater systems is core issue for sustainable management, planning and development of a given area with strongly growing countries like Ethiopia, particularly in water scarce areas (Rift valley) with arid/semi-arid climate.

In Abaya-Chamo lake basin as a study area, only a few hydrological studies were carried out previously that provides preliminary overview of the hydrology and hydrogeology of region (Bekele S., 2001, Halcrow 2008, JICA 2012 and others), with the main objective of quantity and quality surface water, and groundwater separately and sometimes partly at sub-river level and independently using empirical and simple modeling approach.

Besides, the observed key challenges regarding the water resources systems of Abaya-Chamo Lake basin includes arbitrary use of potential & poor management practice in the existing irrigation schemes, insufficient developed water resources to support the rapid

growth of population, Inadequate agricultural food production due to limited use of water for irrigation, degradation of bed and bank, sediment transportation in rivers and deposition of sediment in the lakes, inadequate clean water supply, improper sanitation and as a result poor health status of inhabitants of the region, flooding of areas surrounding the rivers, loss and damage of infrastructure (Bekele S, 2001).

In general, limited scientific awareness of water resource potential availability and upcoming fate with non-existent coordinated water resources research efforts in tackling the problems of the lakes basin have recognized.

Quantification and visualization of spatiotemporal relations of hydrological processes (such as precipitation, surface runoff, actual evapotranspiration and recharge) occurrence and pattern across basin is significant problem due to their high dynamic and continuous or discontinuous characteristics. Indeed, selection of the appropriate input parameter and physical boundary conditions for estimation of water balance components accounts model creation. The results of such models based on defining variables could provide different estimates as per complexity (Soczynska 1989, Ponce, Shetty 1995, Fiedler, Ramirez 2000, Batelaan, De Smedt 2001, Dobrowski et al. 2011).

In particular, methods for determining groundwater recharge is of a fundamental importance for groundwater resources assessment as surface water resources are typically limited, which have been intensively discussed in related previous works as either point based or lumped areal approaches (Simmers,1988; Lerner et al., 1990; de Vries and Simmers, 2002; Scanlon et al., 2002). From point based estimates of recharge, for example, Cherkauer and Ansari (2005) study used regression relationships between recharge and catchment average topography, hydrogeology and land cover characteristics as lumped areal recharge estimation approach; Fazal et al. (2005) used a conceptual rainfall–runoff model to estimate recharge. Flint et al., (2002) present Chloride mass-balance approach, isotopes approach by (Guimera and Candela, 1999; Scanlon et al., 2002), Meiresonne et al., (2003) and Ladekarl et al., (2005) used soil water balance modelling approach and also groundwater level fluctuations-based approach by Sophocleous (1991); Healy and Cook (2002); Dickinson et al., (2004). These point

estimates were used as a base extrapolation or regionalization over large area, however, the outputs are not such evident as described in Batelaan and De Smedt (2007), Sophocleous, (1992) and (Jackson, (2002) and they suggested that physically distributed approaches are more viable method to improve spatial estimates. Despite this fact, physical-based hydrologic modeling has become important in modern water science for evaluation of available water resource at basin scale. However, most available physically distributed models require high temporal resolution data such as SWAT (Arnold et al. 2000), DREAM (Manfreda et al. 2005), WetSpa (Wang et al. 1996), HBV (Losjo et al. 1999) and SVAT (Armbruster and Leibundgut 2001) are continuous, data intensive and use more complex water balance calculations which questioning the applicability in areas where data availability at hourly or daily time scales is an issue. Hence, WetSpass model (Stands for water and energy transfer between soil, plants and atmosphere under quasi-steady state) was the one recently developing model that built as a physically based methodology for estimation of the long-term average, spatially varying, water balance components and the model have an advantage of coarser time scale (monthly, seasonal and annual time step) (Batelaan and De Smedt, 2001 and 2007; Xu and Singh 1998) and its compatibility with ModFlow model. Indeed, the importance of baseflow component in validating hydrological models is discussed in Chapter-5. It is also a desirable entity to know and for water management in general as a part of total discharge which origins from delayed storages in a river catchment. Moreover, upon the analysis of multivariate characterization of the hydrologic system in the study area, the result identified the existence of high spatial variation, complex distribution and interaction as well. Thus, under such complex margin zone and the current trend of unsustainable water resource utilization and demands need modeling studies to provide accurate spatiotemporal information on hydrological components

Thus, evaluation of water resource availability further explored using a more sophisticated physically based modeling approach due to these features of the study area. The model was selected which suites all above mentioned issues and the data available with regard to the thesis objective. Therefore, the present research aim to employ newer seasonal version of the WetSpass model in such a complex rift margin zone under limited

data conditions and evaluation of spatially varying surface and shallow groundwater resource. It is also intended in a way for applicability of WetSpass model to understanding spatial hydrologic pattern, which would help in building scientific and technical capacity, advancing scientific knowledge, and linking scientific and policy communities.

6.2. WetSpass model

WetSpass is a quasi steady state spatially fully distributed water balance numerical model to simulate and predict long-term average hydrological processes at seasonal and annual time step on basin scale and the interaction hydrologic behavior (Batelaan and De Smedt, 2001, 2007). This newer seasonal graphical user version of the model has ability to simulate actual evapotranspiration, interception; surface runoff, soil water balance, and groundwater recharge (Batelaan and De Smedt 2007). The WetSpass model has been widely shown to be suitable for explaining the impacts of climate, land use change and soil texture on water balance of long timescales in mid-latitudes (Batelaan et al. 2003, Wang et al. 2012), and more recently in a tropical setting over Geba basin in Ethiopia (Gebreyohannes et al. 2013). By default in a humid climate setting, the WetSpass model calculates water balances over 6-month seasonal averages for winter (wet) and summer (dry). In line with this, previous studies by Gebreyohannes et al. (2013), Abu-Saleem et al. (2010), Wang et al. (2011) highlighted, the importance of the identification of hydrological seasons (length and type) over different climatic regions in order to provide best estimate. Therefore, in this study we the input parameters applied based on the seasonal cycle of study area and it is also appropriate with regard to the temporal resolution of the available necessary input data for model run. In our case, the area is characterized by semi-humid to a semi-arid climate with bimodal rainfall pattern (two wet and one dry season), hence, the seasons were set into three and each contains four months. The wet seasons are from July to October and March to June and which are locally named as “Kiremt” and “Belg” respectively whereas the dry season locally so-called “Bega” ranges in between November to February.

As described in (Batelaan and De Smedt 2007), the model performs the water balance

computation at a raster cell level. The total water balance is thus calculated as the summation of the water balance of each raster cell for independent vegetated, bare soil, open- water, and impervious fraction of a raster cell.

$$AET_{raster} = a_v \mathrm{AET}_v + a_s \mathrm{AET}_s + a_o \mathrm{AET}_o + a_i \mathrm{AET}_i \quad \ldots\ldots\ldots\ldots\ldots\ldots (6.1)$$

$$ROF_{raster} = a_v ROF_v + a_s ROF_s + a_o ROF_o + a_i ROF_i \quad \ldots\ldots\ldots\ldots\ldots\ldots (6.2)$$

$$R_{raster} = a_v \mathrm{R}_v + a_s \mathrm{R}_s + a_o \mathrm{R}_o + a_i \mathrm{R}_i \quad \ldots\ldots\ldots\ldots\ldots\ldots\ldots\ldots (6.3)$$

Where, AET_{raster}, ROF_{raster}, R_{raster} are the total actual evapotranspiration, surface runoff, and groundwater recharge of a raster cell respectively, each having a vegetated, bare-soil, open-water and impervious area component denoted by av, as, ao , and ai, respectively.

The model uses digital data to separate the precipitation into surface runoff, actual evapotranspiration, interception and groundwater recharge. The detail methodology is given in the newer version of Seasonal WetSpass GRAPHICAL USER INTERFACE manual (Batelaan and De Smedt 2012).

Therefore, the water balance components of a basin depends on the average annual/seasonal precipitation (P), interception fraction (I), surface runoff (ROF), actual evapotranspiration (AET), and groundwater recharge (R) all with the unit of $[LT^{-1}]$, which are estimated from physical basin characteristic, groundwater depth, and climatic variables , given by:

$$\mathrm{P} = \mathrm{AET} + \mathrm{ROF} + \mathrm{R} \quad \ldots\ldots\ldots\ldots\ldots\ldots\ldots\ldots\ldots\ldots\ldots\ldots\ldots\ldots\ldots\ldots\ldots\ldots\ldots\ldots\ldots\ldots (6.4)$$

In order to validate the total flow simulation from the WetSpass model (surface runoff and groundwater recharge), observational flow data from gauging stations given in the previous section were used. The observed total flow and baseflow component were then compared to the model output which estimates mean flow and groundwater recharge of the area.

6.3. Input data for WetSpass model

6.3.1. Geospatial physical maps

The model requires two types of input data, i.e. geo-spatially referenced grid maps and parameter tables (Batelaan and De Smedt, 2007). The grid maps with a cell size of 500*500 m^2 were designed to keep the compatibility to the groundwater flow model (ModFlow).The maps consist of slope angle, land-use, soil texture, groundwater depth, and seasonal/ annual meteorological maps of precipitation, potential evapotranspiration, temperature and wind speed are shown in Figure 6.1 and Figure 6.3.

Digital elevation model (DEM) (NASA JPL; 2013) of the study area is used with a cell size of 30 m. The DEM is processed to prepare topographic elevation map, a slope angle map (Figure 6.1a) and river network of the Abaya-Chamo lake basin (Figure 4.1), using standard Arc GIS 10.3 tools, and shows that slope angles range from 0^0 to 27^0 with a mean of 3.6^0. Spatially, the south west part and the eastern highlands have highest degree of slope.

A land-use map of the basin was derived from cloud free Land sat ETM + satellite images of February (path 168, rows 55 and 56) and November/January (path 169, rows 54, 55 and 56), 2000 (NASA JPL; 2013) using the standard ENVI supervised image classification. Seven land-use classes were identified and the land-use map (Figure 6.1b) of the basin shows, Agriculture (43.6%), Wood/Bush land (28.1%), Forest (7.6%), Grass (10.7%), Swamp/Mersh (2.4%) and Open water (7.4%).

A soil map of the Abaya-Chamo lake basin was extracted from harmonized Database of FAO (FAO, 1998). Soil type classes were translated into USGS soil texture classes, using the topsoil percentages of particle size fractions in order to make the data compatible to model requirement by using hydraulic properties calculator of soil water characteristics tool.

The converted soil textural map (Figure 6.1c) shows the soil texture, i.e. clay (29.5%), clay loam (15.8%), sandy clay (6.7%), sandy clay loam (35.7%), and Sandy loam (12.2%) of the Abaya-Chamo lake basin.

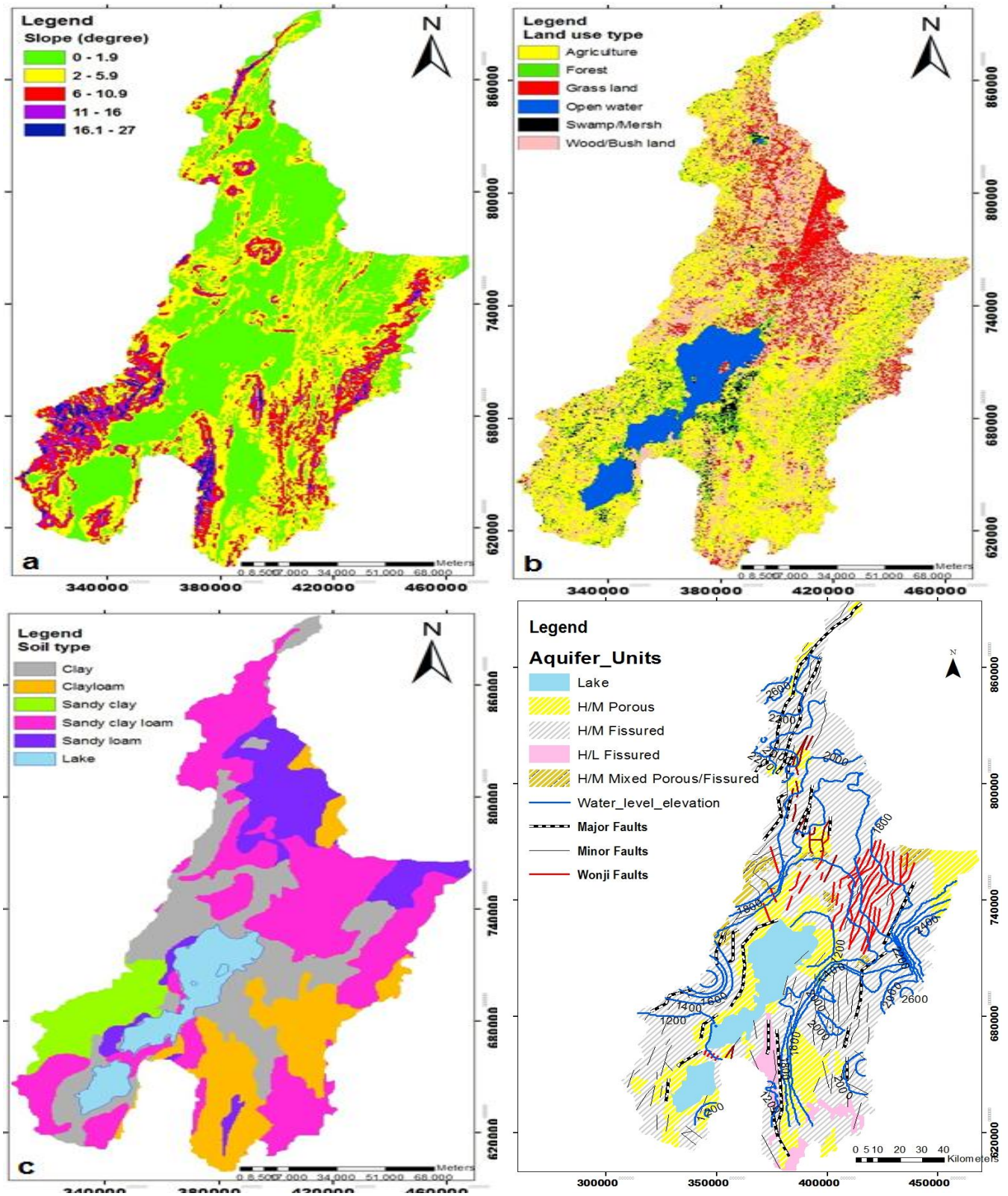

Figure 6.1: Maps used as input for the WetSpass model:

(a) slope angle, (b) land-use, (c) soil type (d) hydrogeological map and water level head elevation contour (in the figure, H/M and H/L stands for aquifer productivity from High to Moderate and High to Low respectively)

Groundwater depth maps used to include seepage fluxes in the water balance calculations in the model. Thus, the groundwater depth of the study area was deduced from spatially available well, lake level and spring point. Figure 6.1(d) shows the groundwater elevation contour above mean sea level.

6.3.2. Hydro-Meteorological Maps

It is known that, meteorological conditions of a given wide and independent area affect the formation of water resources. So that annual and seasonal meteorological parameters given in Figure 6.2 and Figure 6.3(a-d) includes: precipitation, temperature, potential evapotranspiration and wind speed.

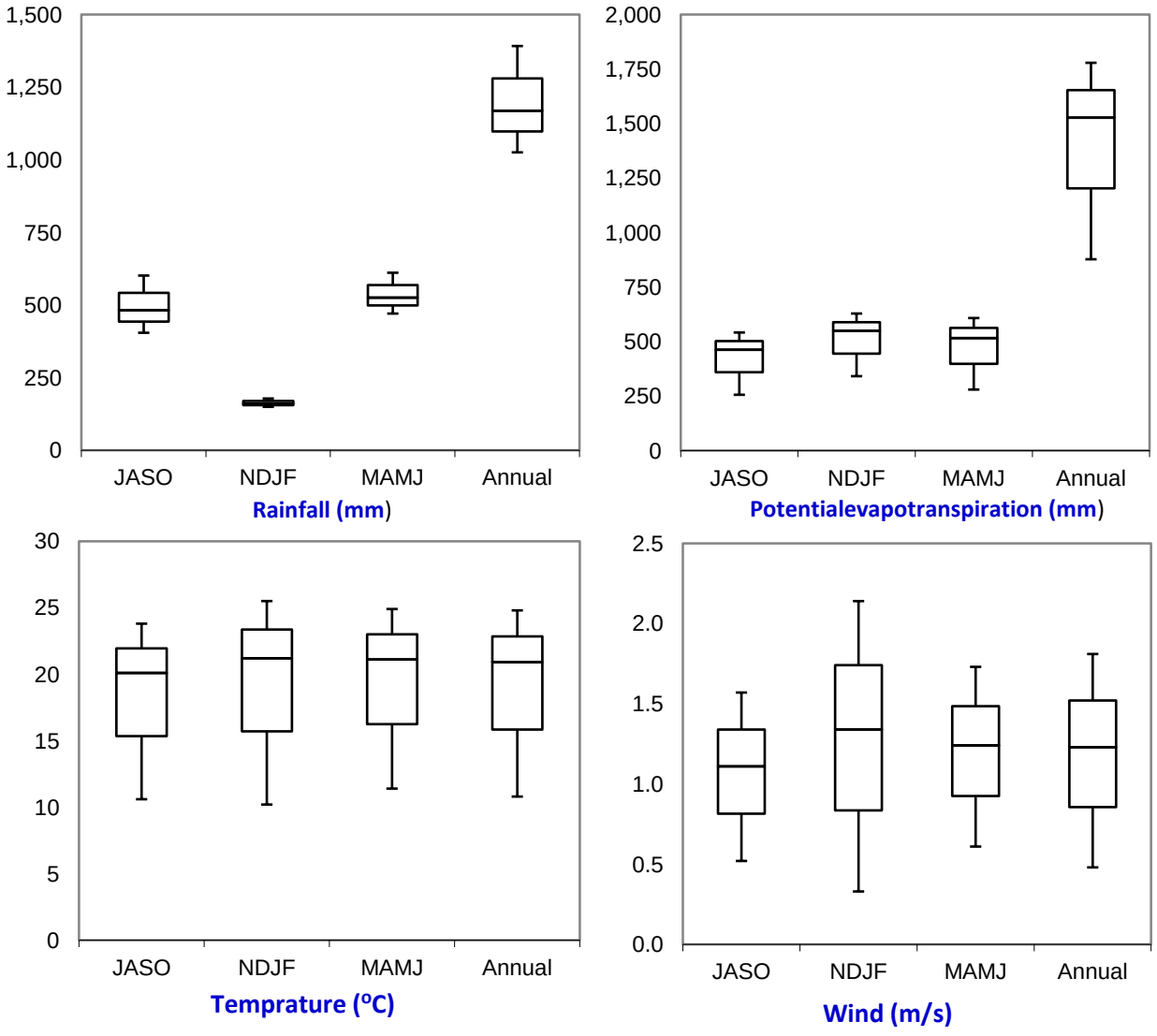

Figure 6.2: Seasonal and Annual variability of Meteorological parameters used as in put

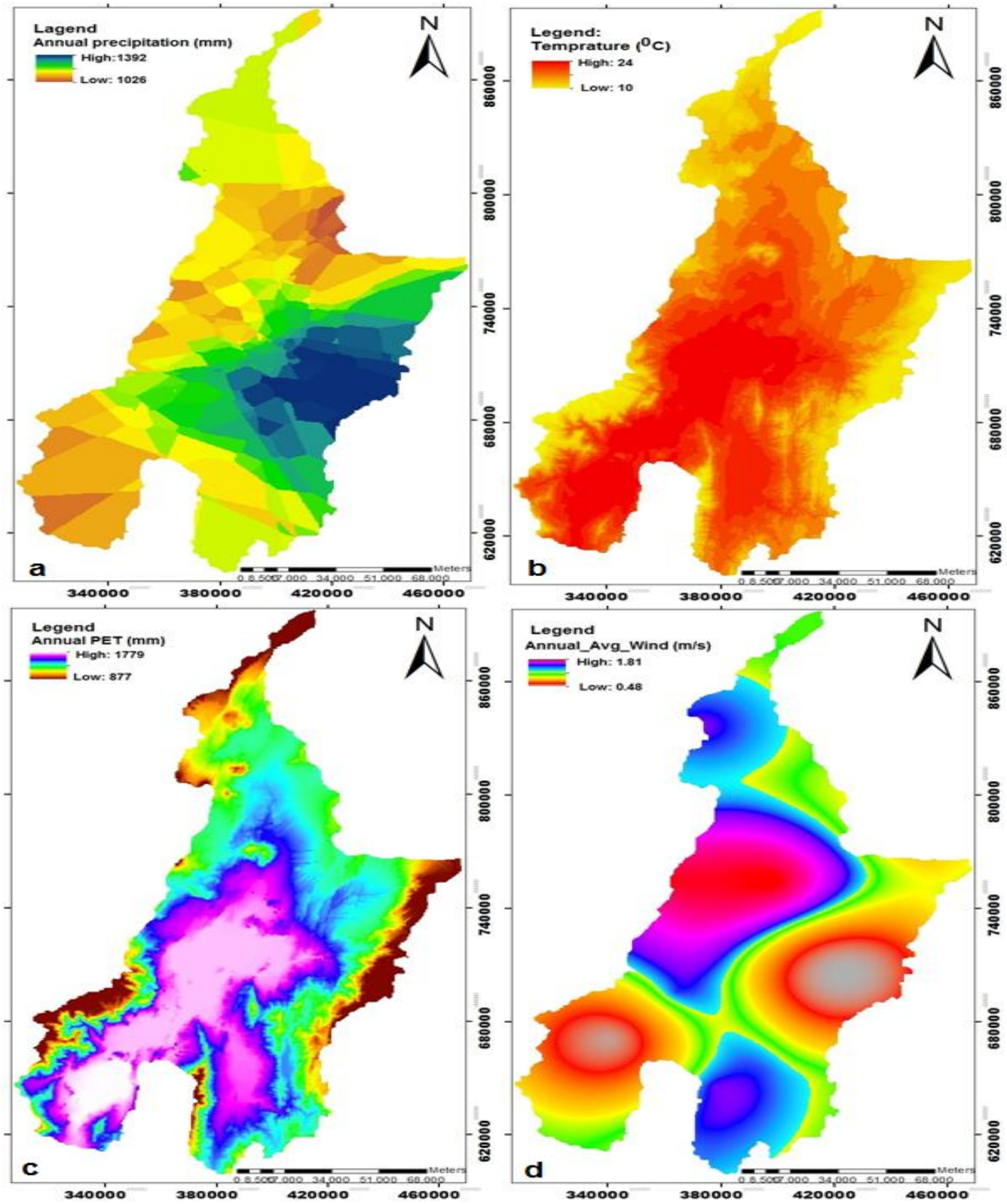

Figure 6.3: Maps used as input for the WetSpass model of meteorological parameters: (a) total annual precipitation (mm), (b) average annual temperature (0C) (c) total annual potential evapotranspiration (mm) and (d) average annual wind (m/s).

The maps were prepared from the available meteorological stations to grasp the hydro-meteorological characteristics of the Abaya-Chamo lakes basin and the data, along with other sets of data, were used to analyze water balance of the basin. All available 46 stations have daily precipitation recordings, but 23 stations has only been recorded temperature, and only 10 stations for wind speed. The spatial information (Figure 6.3) and the temporal variation on meteorological parameters are shown in Figure 6.2.

6.4. WetSpass model Contextualization and Verification

Land-use, soil type and runoff parameters have to be specified in four look-up tables required for running the WetSpass model. The two land-use attribute tables include parameters related to land-use type and soil type. The former contains parameters such as rooting depth, leaf area index and vegetation height (Batelaan and De Smedt, 2007) and which was calibrated for temperate conditions in Belgium (Al Kuisi et al. 2013). While as described in Abu-Saleem et al. (2010), Al Kuisi et al. (2013) application of this model requires more modification of lookup tables in climatologically arid regions. For instance in Ethiopian condition, for Geba basin some parameter adjustments were made by Gebreyohannes et al. (2013) on leaf area index, root depth and bareness). So that in this study, through considering relative difference with Geba basin and the environmental setup, modifications of seasonal land use look up table parameters includes (a) decrease of leaf area index values; (b) substantial decrease of root depth because as described in detail by Jochen et al. (2002), Rooting depths in humid to Arid environments, are likely to be more shallow, because water there tends to be available in the upper soil horizons throughout the growing season, making deeper roots potentially less important and rooting depths will not be strongly related to potential evapotranspiration (PET), because water infiltration depths will be more limiting than evaporative demands and (c) 20% increase of bareness of all land covers proportions from each land-use class.

The WetSpass model simulation results were verified against river flow observations at river gauging stations in the Abaya-Chamo lake basin (Figure 4.1). River measurements account for direct (surface) runoff flow and baseflow (sub-surface) that recharge groundwater reservoir. Model simulation results for mean total flows were compared to

mean annual flows at the gauging stations, and also the simulated groundwater recharge is compared against estimated baseflow as given in Figure 6.4(a)-(b).

The estimated result of baseflow yield deduced from daily river flow time series for river gauging station within Abaya-Chamo basin, using the baseflow separation technique is given in the Table 5.2. This was used only for groundwater recharge simulation of spatially distributed WetSpass.

We compare observed versus simulated total discharge at gauging stations and estimated baseflow versus simulated groundwater recharge respectively in the study area. The scatter plots in Figure6.4 (a)-(b), showed a good agreement with a correlation coefficient of the 'line of goodness of fit' of 0.95 and 0.97 respectively, standard error of 0.12, and 0.20. These figures reflect a degree of accuracy of the WetSpass model application in the study area with strong correlation between the simulated and observed ground truth or estimated values. Tendency of high and low peaks trends are rather well simulated, as well.

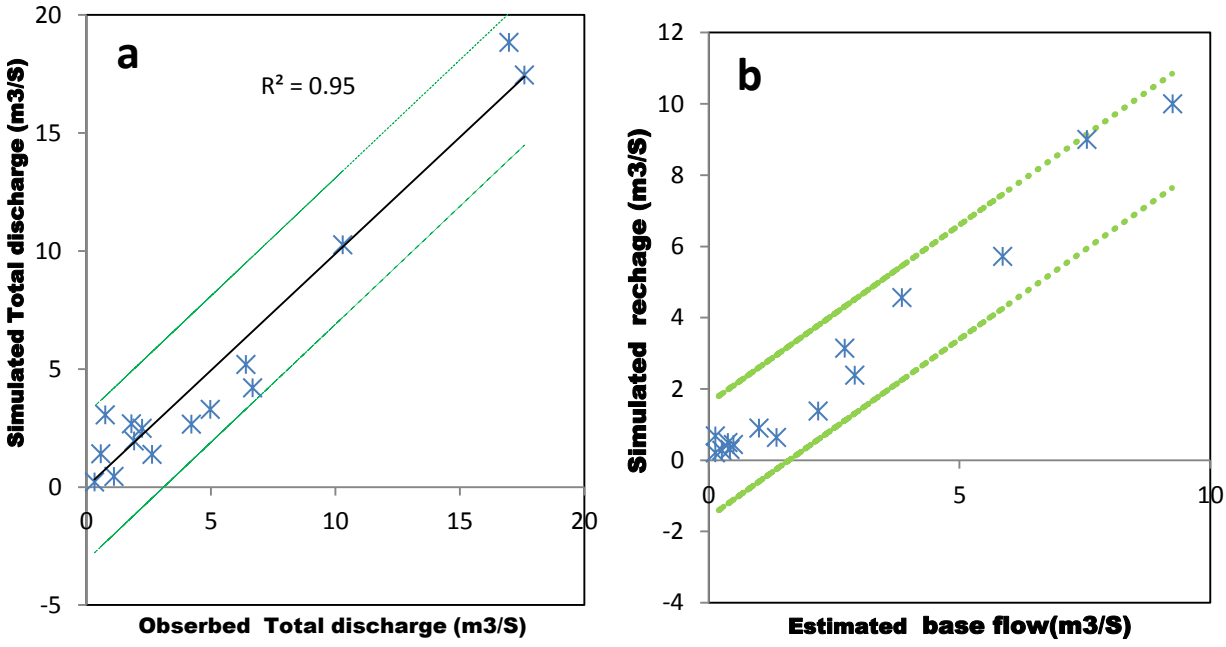

Figure 6.4: Comparison of observed total annual average discharge with WetSpass simulation results (surface runoff plus recharge) and (b) Comparison of estimated baseflow with WetSpass simulated recharge at the gauging stations. The dashed lines (green) shows, 95% confidence interval for the regression fits.

However, the overestimated values are found at the downstream of Billate and Hamessa-Guracha sub river basin just north of lake Abaya (Bilate-Tena and Hamessa-Humbo gauging station) and the underestimated values are observed mainly in the sloppy upper portions of Abaya-Chamo basin (Weira, Kulfo, Sala and U-Gelana gauging station) (refer locations on Figure 4.1, this location are also associated with major geological structures and fissured aquifer which may promote deep groundwater flow. The discrepancy between measured and simulated values becomes smaller for the rest of gauging station. Furthermore, natural variability of hydrologic processes, the complexity of basin characteristics and certainty of the models to represent reality can be also error source.

6.5. Simulated hydrologic Components

We begin by describing the simulated hydrologic cycle averaged over the entire basin, and associated understanding the prior processes such as the spatial pattern and rate of precipitation, actual evapotranspiration and surface runoff. These values are then used to estimate the rate and distribution of groundwater recharge. Figure 6.5 summarizes the variability of each variable by season, and in the annual average and the bar chart shows 25 quartiles (Q_{25}), 50 mean quartile (Q_{50}), 75quartiles (Q_{75}) whereas whisker ends represent maximum and minimum outlier of the simulated hydrological components. Furthermore, the spatial distributions of the long term annual of simulated water balance components are given in Figure 6.6(a)-(d).

6.5.1. Actual Evapotranspiration and Interception

Actual Evapotranspiration is given as a summation of evaporation from bare soil and open water bodies, transpiration by the vegetation, and evaporation of the precipitation intercepted by the vegetation (Batelaan and De Smedt, (2001). The model result in the Figure 6.6(a) shows, the central axis from north east toward south west including Abaya and Chamo lakes has high average actual evapotranspiration, while the northern, eastern, south eastern tip border of the basin have shown lower value. The high values are due to relatively more precipitation, surface water availability and land use and soil type combination is shown in the Table 6.1. From this table it appears that open water, forest land cover with sandy clay loam and sandy loam soils have the highest values of

evapotranspiration. Forests are obvious known by their relatively high evapotranspiration and the courser soil textures are able to conduit more soil water. While agricultural land, Swamp/Mersh with sandy clay, clay or clay loam soils have the lowest values.

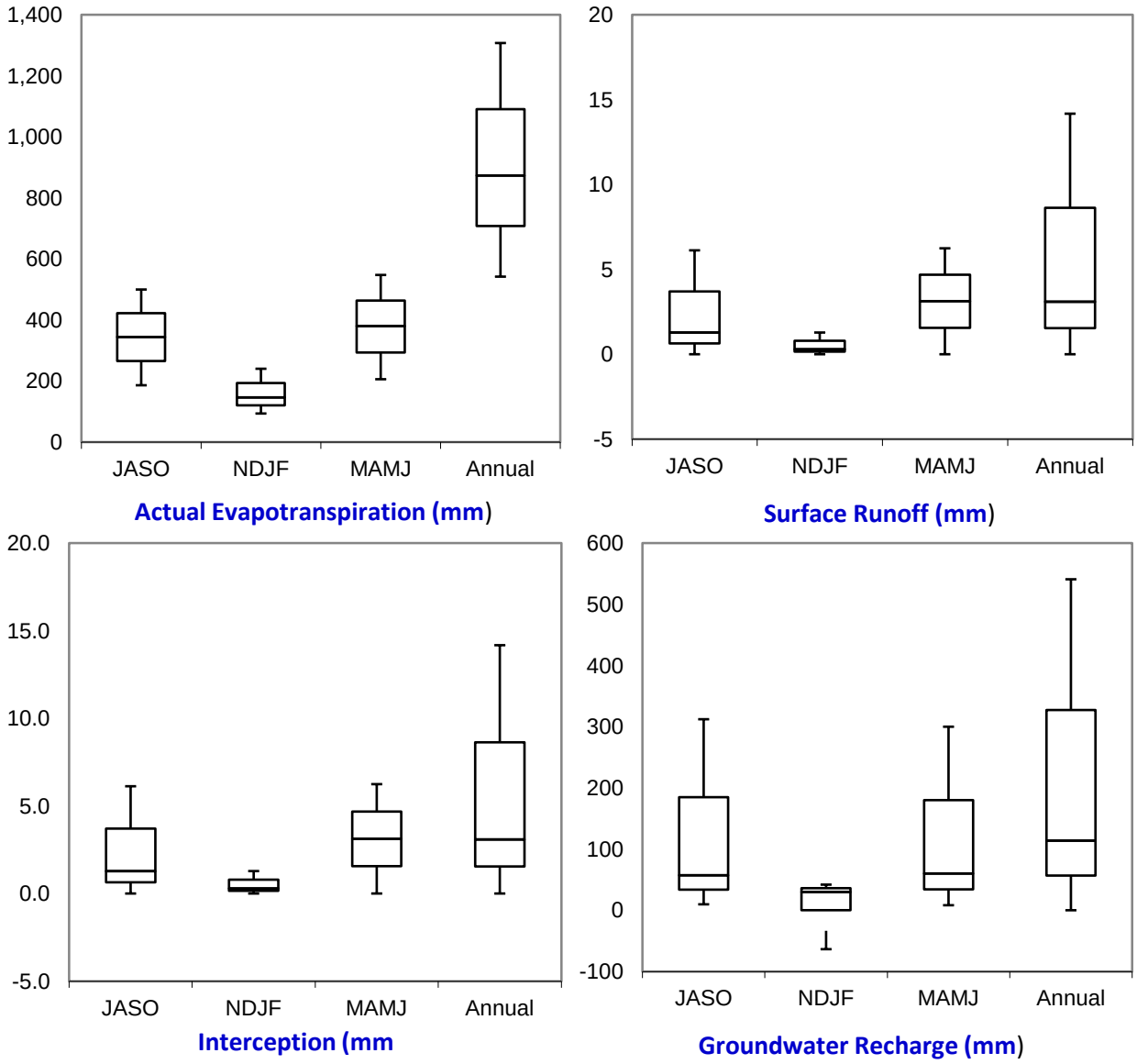

Figure 6.5: Simulated seasonal and annual water balance components

Besides, the average and standard deviation values in Table 6.1 can represent the dominant factor between land cover and soil texture. Which means the factor with smaller standard deviation value could have affect more than the factor with larger value, thus in this case land cover type can amplify evapotranspiration more than soil textural class in Abaya-Chamo basin, while keeping precipitation rate.

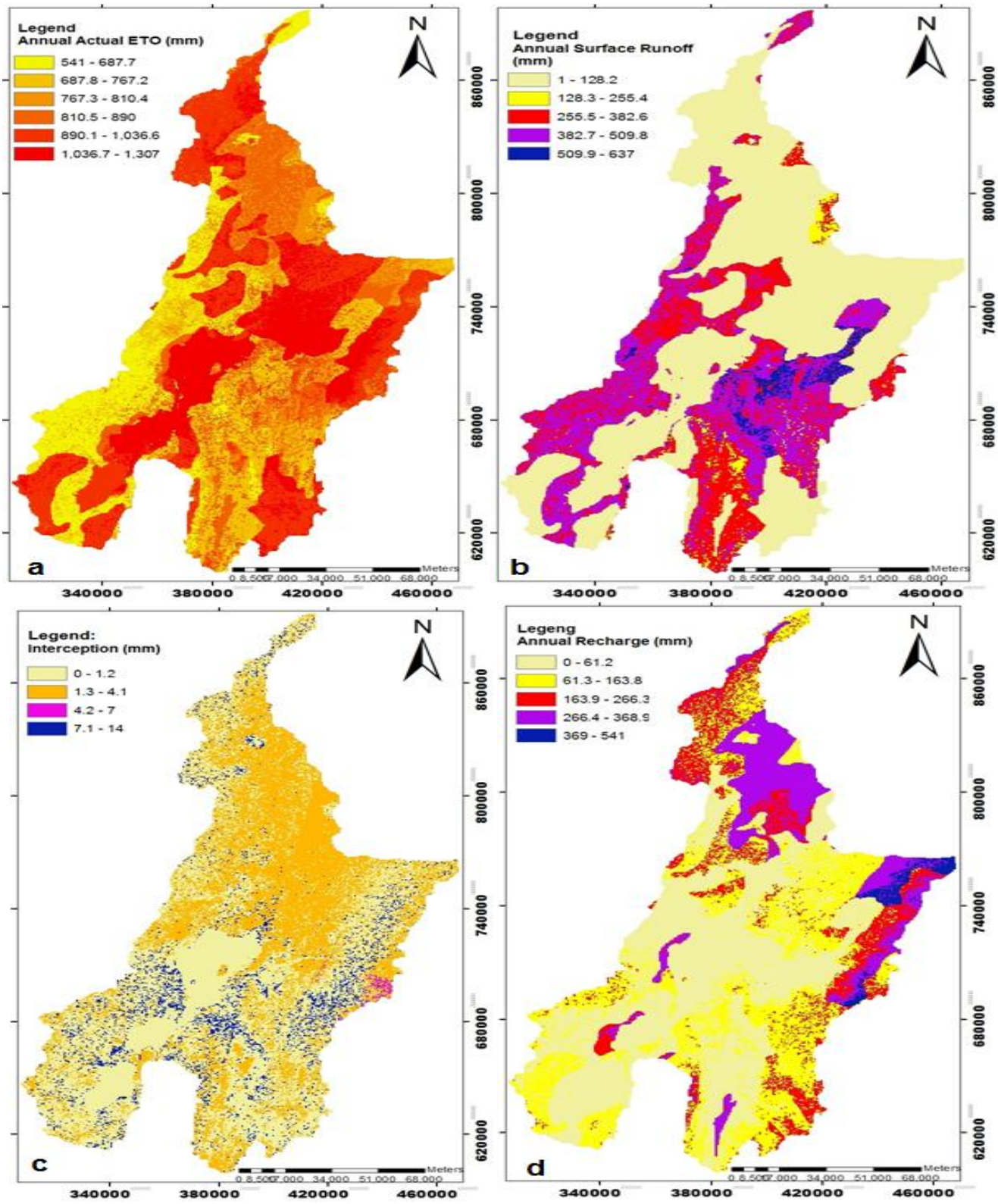

Figure 6.6: Maps of water balance components simulated with the WetSpass model: (a) total annual evapotranspiration (mm), (b) total annual surface runoff (mm), (c) total annual Interception (mm), and (d) total Annual groundwater recharge (mm)

As given in Figure 6.5, the seasonal evapotranspiration value shows significant temporal differences in the basins. The Annual value ranges from 541.9 to 1307.3mm/yr; with a mean of 873.26mm/yr, which constituting 74.7% of the precipitation and appear the largest component of the water balance in the Abaya-Chamo Lake basin. About 29.5% and 32.5% of the evapotranspiration takes place during the wet season (Kiremt and Belg) season, while the remaining 12.5% takes place during the dry (Bega) season.

The seasonal variation is resulted due to uneven seasonal precipitation distribution amount and change in vegetation cover during dry period, for example during the dry period, the energy required for evaporation is not the limiting factor, but rather the water availability. This explains why actual evaporation rate is lower during dry season than wet season.

Table 6.1: Mean annual evapotranspiration amount for different land use and soil class combinations

AET	Clay	Clay loam	Sandy clay	Sandy clay loam	Sandy loam	Mean	STD
Agriculture	670.9	752.4	633.9	989.3	800.7	769.4	139.4
Forest	800.3	818.0	737.0	961.8	836.9	830.8	82.3
Grass land	824.6	876.2	782.6	1087.0	809.7	876.0	122.8
Open water	1094.5	1094.5	1094.5	1094.5	1094.5	1094.5	0.00
Swamp/Mersh	671.6	706.6	623.7	974.6	830.2	761.3	141.6
Wood/Bush land	763.4	826.1	699.4	1058.2	832.7	836.0	135.5
Mean	830.9	864.3	787.4	1035.2	880.8	879.7	96.4
STD	158.4	142.8	181.3	62.8	119.9	127.0	

The interception is given as a fraction of precipitation value and which depend on the vegetation type and distribution (Roberts, 1983), (Calder 1979), (Nonhebel, 1987). The fraction decreases with an increase in an annual total rainfall amount since, vegetation cover is assumed to be constant throughout the simulation period (Batelaan and De Smedt 2007). Annual total interception in the basin ranges from 0 to 14.2mm/yr; with a mean value of 3.09mm/y and account 0.3% of precipitation. Seasonal interception ranges in between 0 to 6.12%; 0 to 1.28% and 0 to 6.24 for Kiremt, Bega and Belg respectively (Figure 6.5). The relatively highest interceptions on the basin occur in the northward of Lake Abaya (Figure 6.6(c)).

6.5.2. Surface Runoff

High spatial surface runoff found in the East and west of Lake Abaya and Chamo than those in the north and south of Lake Abaya and Chamo (Figure 6.6(b)). The Spatial and temporal variation of surface runoff generation can be explained mainly through distribution of precipitation rate, land cover and soil texture combination over physiographic arrangement as given in the Table 6.2.

Table 6.2: Mean annual surface runoff amount for different combinations of land-use and soil class

Sur. Runoff	Clay	Clay loam	Sandy clay	Sandy clay loam	Sandy loam	Mean	STD
Agriculture	473.9	392.5	447.7	4.5	4.0	264.5	239.4
Forest	322.0	265.4	305.6	2.8	2.1	179.6	163.0
Grass land	308.7	236.7	297.7	2.4	2.0	169.5	155.2
Swamp/Marsh	392.3	338	360.9	5.6	4.0	220.2	197.5
Wood/Bush land	374.6	302.7	358.5	3.3	2.8	208.4	189.3
Mean	374.3	307.1	354.1	3.7	3.0	208.4	188.9
STD	65.7	61.2	59.9	1.3	1.0	37.8	

In addition to morphometric factors identified in chapter-5 such as slope, the largest surface runoff occurs on clay soils with agricultural land, Swamp/Marsh or Wood/Bush land use type. In contrast, the lowest values are for sandy loam and sandy clay loam soils with Grassland and forest. The smaller standard deviation values of the runoff for different soil types (Table 6.2) indicate that surface runoff is more influenced by soil type than land-use.

Figure 6.5 and Figure 6.6(b) gives the mean temporal variation of surface runoff values. The annual surface runoff values ranges from 1.01 to 637.8mm/yr with a mean of 183.4mm/y. This value accounts about 15.7% of the annual precipitation in the Abaya-Chamo basin. About 6.8% and 7.4% of the surface runoff occurs during the wet season (Kiremt and Belg respectively) while the remaining 1.6% occurs during the dry (Bega) season. There is considerably small seasonal variation in the runoff, even though the wet season runoff amount is slightly higher due to vegetated surfaces than in dry season.

6.5.3. Groundwater Recharge

It is known that estimation of groundwater recharge is the most challenging parameter in hydrogeology, because it is not only related to specific factors such as land cover and/or soil. Although, the groundwater recharge is estimated in WetSpass as a residual term of the water balance and the simulation result, the eastern highland and northern part of the basin have generally higher groundwater recharge than the central basin floor and the western part of the basin, likely due to a combination of favorable conditions such as high precipitation, permeable soils, gentle topography and land use cover Figure 6.6(d).

As indicated in Table 6.3, the mean annual groundwater recharge values for different land use and soil classes combinations reveals the largest groundwater recharge is observed for Sandy loam and Sandy clay loam soil textural classes with Agricultural and Forest land use type. This is basically because of the high permeability of these soils, but could partly also be due to lower evaporation rates and less runoff on the relatively gentler slopes of agricultural lands. On the other hand, Grass land and Wood/Bush land on any type of soil are found to yield less groundwater recharge due to their high potential of transpiration and interception processes specially clay textural types. This is evidently associated with high transpiration rate, particularly for Wood/Bush land, which was confirmed by the results of research conducted by Sophocleous, Perkins (2000), Batelaan (2006) as well as Okonski and Miller (2006).

As indicated in Table6.3, the highest spatial variation of recharge is found by the soil textural classes which have small standard deviation than land use type. Additionally recharge increases distinctly with course soil texture regardless of the land cover classes.

Annual groundwater recharge in the Abaya-Chamo lake basin ranges from 0 to 540.8mm/yr, with a mean value of 113.74 mm/y (Figure 6.5 and Figure 6.6(d)). This makes up only 9.7% of the total annual precipitation in the Abaya-Chamo lake basin. This result confirmed by previous studies, for example, in north of study area in the Central Ethiopian rift Valley by Zenaw (2003) assessed recharge for the Hawassa basin to be about 5% of the rainfall. WABCO (1990) in Water Resources Development Master Plan for Ethiopia refers greater than 5% of rainfall in the RVLB. Recharge calculated

from mean values of baseflow shows the possibility of recharge variability in Dila Sheet as part of Abaya Chamo basin assessed in between as being 7% to 20% of the precipitation depth by Thomas et al, (2014).

Table 6.3: Mean annual groundwater recharge amount for different land-use and soil class combination

Recharge	Clay	Clay loam	Sandy clay	Sandy clay loam	Sandy loam	Mean	STD
Agriculture	37.2	68.6	45	173.4	337.3	132.3	126.9
Forest	69.5	155.3	93.9	227.2	316.9	172.5	101.2
Grass land	27.6	56.9	33.7	62.4	302.6	96.7	116.1
Swamp/Marsh	145.7	155.2	143.2	198.5	315	191.5	72.5
Wood/Bush land	32.2	68	57.3	103.4	291.6	110.5	104.4
Mean	62.4	100.8	74.6	153.0	312.7	140.7	104.2
STD	49.4	49.6	44.5	68.3	17.1	40.3	

About 4.97% and 5.1% of the recharge occurs during the rainy seasons (Kiremt and Belg respectively), But during the dry (Bega) season, negative recharge values are observed because discharge from groundwater contribute in the range between 0 to -63.6mm/yr to surface water. Thus, in these areas vegetation is able to keep a higher ET through osmosis of groundwater.

6.6. Surface Water Balance

The overall areal water balance (is given in Table 6. 4) and hydrologic behavior of the Abaya-Chamo lake basin is simulated using physical-based distributed WetSpass hydrological model. The comparisons of corresponding observed and simulated river flows at gauging stations are reasonably well realistic and a good agreement was achieved between simulated recharge and estimated baseflow. The small discrepancies in comparisons result are likely from the parameterization of input parameters, river gauge measurements, base flow estimation and error from the numerical model. Generally, the model is proved its applicability on such complex setting to determine the influence of changes in land use or soil cover on the hydrological behavior.

Results indicate that 74.6% of the total annual precipitation is lost to evapotranspiration, which is influenced more by rate of precipitation, and land use type than soil texture. A further 15.7% of the annual total precipitation is partitioned as surface runoff (mainly during the wet season), with an annual mean of 183.4mm and a range from 1.01 to 637.8mm over the study area. The result shows that small changes in soil texture can influence surface runoff more than land cover type. The remaining 9.7% of total annual precipitation is lost to groundwater recharge, with a mean value of 113.74mm and a range from 0 to 540.8mm. The highest rates of groundwater recharge are coarser soil textural classes regardless of land use types.

The water resource potential or availability summary is presented in Table 6.4. The lakes basin as a whole has a total of 22.1billion lit/year rainfall with a mean value of 1169.5mm. Out of which around 16.5billion lit/yr account for the actual evapotranspiration as the largest part and the rest are accounts for surface runoff and groundwater recharge about 3.5 billion lit/yr and 2.1 billion lit/yr respectively.

Table 6.4: The long-term mean annual water balance values of hydrologic components simulated with the WetSpass model.

Water balance component	Min	Max	Annual values (mm/yr.)	Std. dev.	Fractions of mean RF (%)	Volume (MCM/yr)	Volume (Billion lit/yr.)
Precipitation(P)	1026.1	1392	1169.5	75.2	100.0	22109.9	22.1
Actual Evapotranspiration(AET)	541.8	1307.4	873.1	152.9	74.6	16506.4	16.5
Surface runoff (ROF)	1.0	637.7	183.3	188.5	15.7	3467.3	3.5
Recharge (R)	0.0	541.1	113.9	99.3	9.7	2153.3	2.1
Input – Output: P – (AET + ROF + R) = - 0.8							

The mean ratio of groundwater recharge to the total flow (surface runoff plus groundwater recharge) is about 0.38 based on the model output. This means the groundwater recharge is about 38.3% of the total flow and this value is comparable with the base flow index (BFI) estimate in Chapter 5, using base flow separation techniques (BFI = 0.44; (44%)). This confirms the importance of both techniques (base flow separation and modeling approach) in the study area. Hence the multivariate analysis based on the baseflow index in characterizing the hydrologic system of the basin is also given equivalent result. Following these, the physical interpretations about the interaction in the hydrologic system among variables in this section (Chapter-6) does not contradicting to Chapter-5.

In summary, the simulated spatial surface runoff map in Figure6.6 (b) shows that eastern and western part of lake-Abaya in the basin shows high distribution as a surface water resource potential than those in the north and south of lake-Abaya. Here, the western part of the lakes are characterized by relatively high degree of slope and which is much subjected to flashflood and may play a major role sediment transport to the lakes.

While particularly the eastern plateaus especially the Gidabo and Gelana-river basin were identified as recharge zone in the basin with their productive intercalated volcano sedimentary aquifers. Thus, these two major-river basins have appeared to be the largest groundwater contributor to the Lake Abaya.

CHAPTER SEVEN

7. MODELING OF GROUNDWATER FLOW SYSTEM

7.1. Numerical simulation of groundwater flow

Development of a numerical groundwater flow model for Abaya-Chamo lakes basin as part of central Ethiopian rift appeared important, where ongoing socioeconomic developments have been pressurizing the groundwater resource availability. Thus, calibration of the flow system is the way out to better understand the aquifer systems of the lakes basin as a whole.

This helps in determining the long-term groundwater availability and inter basin fluxes by simulating groundwater condition at present and to predict the future condition under projected climate change using low-intermediate and high-end emission scenarios for best sustainable resource management and planning in order to contribute for development alternatives.

The model development was employed assumptions and approximations to simplify the actual aquifer system. The simplification is based upon the data availability to idealize and represent the complex hydrogeological features in relations to the actual system, and the assumptions used to develop it.

The major goals of the numerical groundwater flow model simulation of the Abaya-Chamo lakes basin under steady-state condition are:

(1) to simulate the groundwater gradient and flow direction, (2) to calculate the groundwater balances and flux of the sub-major river basins under water budget code of the MODFLOW, and (3) to predict the future groundwater levels of the lakes basin under projected changing climate using different representative concentration pathway scenarios and then, recommend groundwater potential regime for pumping wells distribution and developmental activities as well for proper management and planning the groundwater resources of the lakes basin.

7.2. Hydrogeological Conceptual Model

A hydrogeological conceptual model is a pictorial representation of the groundwater flow system, usually in the form of a simplified hydrogeological diagram or cross-section.

The conceptualization of the source and mechanism of water influx into the groundwater system and outflux from the flow system is a critical and first step to the development of an appropriate numerical model. The extent of the flow domain is expanded horizontally and vertically to coincide with physical features of the groundwater system which can be represented as flow boundaries.

The first phase of producing a hydrogeological conceptual model is defining the geological framework of the area for which the data is obtained from different geological maps, borehole logs, and additional field works.

Establishing the geological framework permits the hydrological framework to be defined, it includes identification of flow boundary and hydro-stratigraphic units, defining the groundwater flow direction and etc. Indeed, boundary conditions include surface water features (lakes and major rivers), groundwater divide and impermeable units based on the type of model. Hydro-stratigraphic units including a number of layers control the flow. The hydraulic properties of the water also determine the type of aquifer (Winkler et al., 2003).

Hence, numerical groundwater flow modeling depends on an understanding of hydrostratigraphic system, conceptualization and the development. Such conceptual representation of flow and aquifer sytem involves synchronizing number of different data obtained from various sources in suppliment with field observatiotion, measurments, geophysical investigations, water chemistry, isotope hydrology and etc.

Based on converging evidence from exploratory inventories of previous studies in the Abaya- Chamo lakes basin, the occurrence of groundwater and flow consist the relevant parts of the lakes basin such as highlands, escarpments and rift floor. This can be described by dividing into Eastern and Western compartments from the center of the lake in the rift floor.

7.2.1. Conceptual hydrogeological model of the Eastern compartment

The eastern highland ridge chain ranging from 2000msl to over 3000msl associated with high rainfall distribution. The outcrop in the northeastern area is covered mainly with various volcanic rocks intercalated by volcano-clastic and sedimentary rocks.

Outcrops form a gently undulating plain that receives adequate rainfall and has moderate runoff resulting in good infiltration and formation of moderate to extensive high productive fissured and mixed aquifers. While the southeastern part consists of basement rocks (see Figure 2.4). In this region, the recharge is only relatively good in areas where the highland is covered by thick alluvial sediments.

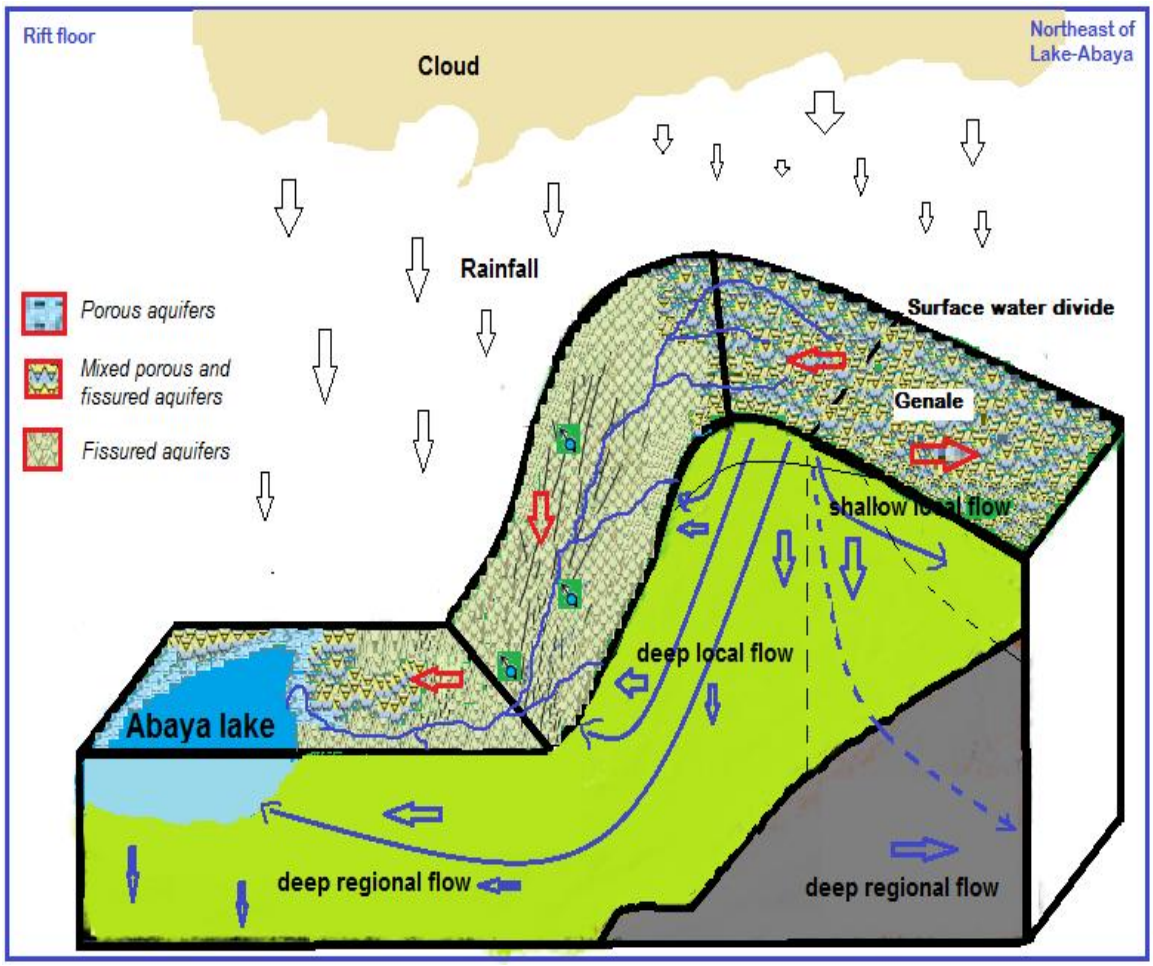

Figure 7.1: (a) Schematic diagram for the eastern compartment along Line A-B of Figure 7.2

As shown up in Figure 7.1(a), the outcrop aquifers in the highland recharge further down the underlying deeper volcanic aquifers vertically and also in some part of the escarpment area is affected by significant geological structures, the local grabens in this region provide a good prospect for water to penetrate underground and recharge the aquifers even if it is relatively steep for infiltration.

The groundwater flow system and direction in the escarpment area were described by Demis (2009) and Halcrow (2008) on which the flow is mainly controlled by faults. Though, some of the faults may act as flow barriers where there are cross fault rays and flow through which accordingly change direction locally.

In this Eastern region, the groundwater contributions through springs are relatively small in mountain areas. This may indicate the existence of shallow local groundwater flow, but the spring discharges at the foot of the escarpment are high in comparison which includes hot springs at Yirgalem as a representation of deep local groundwater flow.

The topography in part plays a role in controlling the observed springs emerging out from the tertiary volcanic hills and basement rocks. The other springs along structures at the escarpment indicating that both topography and geological structure factors are responsible for determining the groundwater flow. Furthermore, eastern highland aquifers can also be recharge partly volcano-sedimentary rocks of the rift bottom through deep regional groundwater flow.

Groundwater from the escarpment area recharges the aquifers on the rift floor in addition to the direct recharge from precipitation. The flow continues by recharging lacustrine sediments and finally discharges into lakes. Conversely, when the lakes water level is higher than the surrounding aquifer's groundwater level, there is also likely recharge flux from lakes to adjacent lacustrine sediments.

7.2.2. Conceptual hydrogeological model of the Western compartment

The western highland is built by faulted basalts and ignimbrite intercalated by volcano-clastic and sedimentary rocks. In similar fashion to the Eastern region, the outcrops form

a gently undulating plain that receives adequate rainfall and has resulted in a moderate runoff with good infiltration and form moderate to high productive fissured and mixed aquifers. Precipitation undergoes through the rock and infiltrations are particularly good in plateau areas where there is substantial coverage of thick alluvial sediments. Aquifers outcropping in the area also recharge deeper fissured aquifers developed in underlying volcanic rocks.

Springs are relatively small in mountain areas, which explain the presence shallow local groundwater flow. Springs at the foot of the escarpment are largely representing deep local groundwater flow. A typical example of these features is a group of Arba Minch-springs at the foot of the escarpment in Arba Minch. The existence of deep regional groundwater flow is also confirmed by the existence a group of hot springs and hot water along the Bilate-river in the Abaya geothermal area.

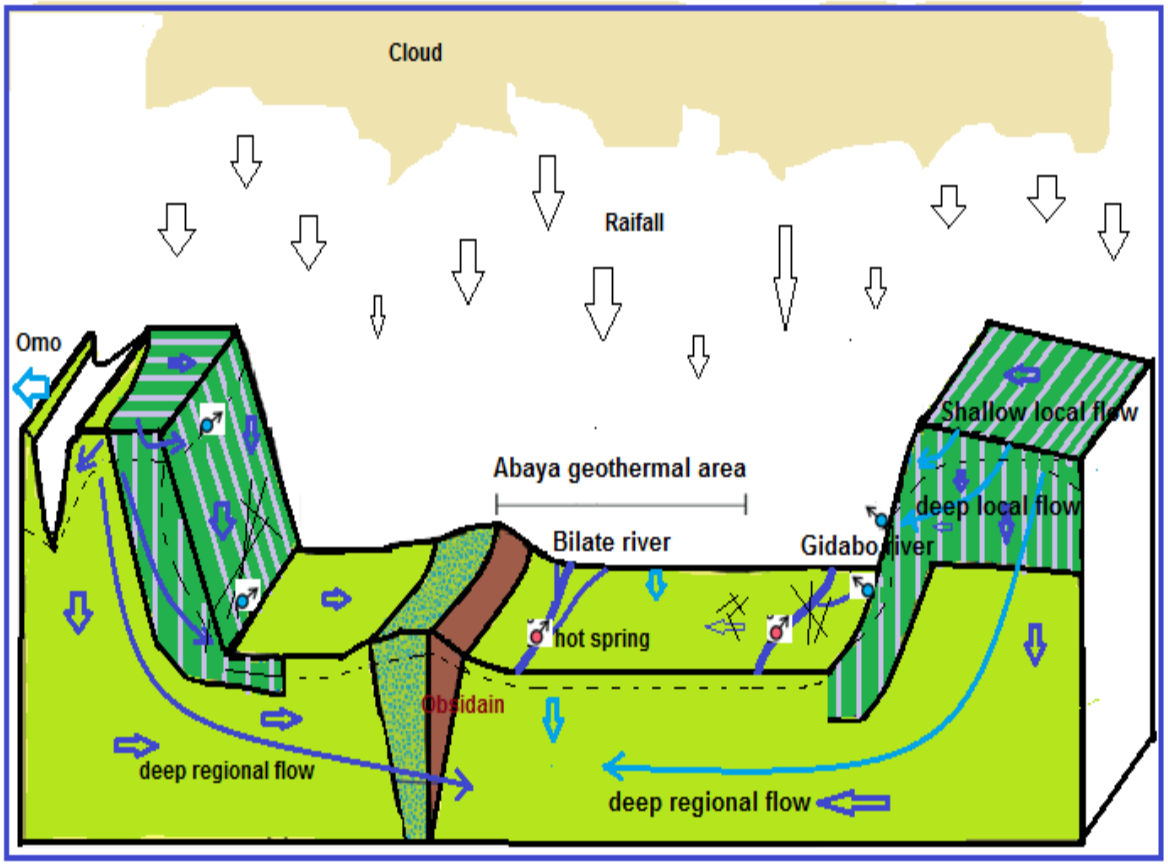

Figure 7.1 (b): Schematic diagram for the Western in addition to the eastern compartment along Line A-B of Figure 7.2

Groundwater from the escarpment area recharges the volcanic and sedimentary aquifers of the rift floor in addition to the direct recharge by precipitation. The groundwater from the western escarpment and western part of the rift floor is drained by the Bilate-river. A simple conceptual hydrogeological model of the western region and also eastern region is shown in Figure: 7.1(b). as well

Here, shallow local groundwater flow on the rift floor is generated by existing local ridges. Both the shallow local and the deep groundwater flow, recharge the lacustrine sediments of lakes in the rift floor which creates regional flow. Accordingly, there is possible recharge flow from lakes to adjacent lacustrine sediments when the water level in the lakes is higher than the surrounding groundwater level in the aquifers. Large alluvial fans on the western bank of Lake Abaya are aquifers transferring groundwater directly into the lake. These fans are also a source of large amounts of sediment transported by local rivers that foul the lake.

To summarize, the general conceptual model principles of Abaya-Chamo lakes basin can be explained by main mechanisms of recharge as well as discharge. These are (a) direct recharge to outcropping aquifers, (b) vertical recharge from overlying aquifers into underlying aquifers (c) horizontal recharge from neighboring aquifers and lakes (c) direct discharge by springs from outcropping aquifers (cold and hot springs at the foot of the escarpment and the rift floor) (d) direct discharge to rivers and lakes (e) indirect discharge from one aquifer to another (vertical as well as horizontal)

In previous hydrogeological studies Halcrow (2008), has reported the existence of Shallow circulation and recharge from river to aquifer in the rift valley with high conductivity of river waters over 500mS. Whereas the deep circulation is demonstrated by hot springs emerging along the Gidabo and Bilate-rivers with high discharge. This deep local or regional groundwater flow passes through recent volcanic centers and emerges within sediments and basalts. Spring water is hot with high TDS and represents water with a longer residence time in aquifers than shallow water emerging as cold springs in the highlands and escarpments.

Therefore, generally, the groundwater flow is parallel to the surface water flow system that is initiated from the highlands through the escarpment to the rift floor. On the rift floor itself, the groundwater flow direction is governed by the relative elevations of static water levels between the individual sub-basin lakes.

7.3. Modeling Approach

The numerical groundwater flow of the Abaya-Chamo lakes basin aquifer system is simulated using the USGS three-dimensional finite-difference groundwater flow model **MODFLOW-20005** with Block centered flow packages (BCF). The latest version of MODFLOW was released in 2005, called MODFLOW-2005(Harbaugh, 2005).

MODFLOW-2005 versions that incorporate the use of parameters to define model input, the calculation of parameter sensitivities and the modification of parameter values to match observed heads, flow or advective transport using the observation, sensitivity, and parameter estimation processes described in detail by Mc Donald and Harbaugh, (2000), Harbaugh (2005).

The Equation used in the computer model to describe groundwater flow is:

$$\frac{\partial}{\partial x}\left(K_{xx}\frac{\partial h}{\partial x}\right)+\frac{\partial}{\partial y}\left(K_{yy}\frac{\partial h}{\partial y}\right)+\frac{\partial}{\partial z}\left(K_{zz}\frac{\partial h}{\partial z}\right)-W=S_s\frac{\partial h}{\partial t} \quad \text{..... (7.1)}$$

where: K_x, K_y, and K_z: are the values of hydraulic conductivity along x, y and z coordinate axes respectively and are assumed to be parallel to the major axes of hydraulic conductivity, in meters per day; h: is potentiometric head, in meters; W: is a volumetric flux per unit volume and represents sources or sinks or both of water, such as well discharge, recharge and water removal from the aquifer by drains, per day; Ss: is the storage coefficient of the porous materials, per meter; t: is time, in days.

The flow Equation (7.1) is solved for heads in each cell by the Preconditioned Conjugate-Gradient with improved nonlinear control (PCGN) package as a method for solving matrix equations using an algebraic multi-grid solver, in the finite-difference grid, through MODFLOW which expressing the relationship between the head at a node (Harbaugh, AW 2005)

The flow system is also defined by, descritizing the aquifer system into finite difference grid and layers, determining the boundary conditions for the aquifers, estimating the rates and distribution of recharge and discharge and estimate the aquifer properties within the model. The accuracy of these input data, in part, determines the accuracy of the model.

The model was calibrated in the steady-state mode with the water levels collected at different times during well-drilling, pumping test and inventories. Hydraulic parameters were iteratively adjusted by trial and error until satisfactory matches to measured variables were achieved in the steady-state simulation with a constant input of spatial recharge estimated by WetSpass model.

7.4. Model Description

7.4.1. Grid Design

The modeled area is 171.5km by 307.5km from UTM 302900m to 474400m and 595700m to 903200m Easting and Northing respectively. The model area covers the entire lakes basin on which five sub-major river basins were included as shown in Figure7.2 (a)-(b). The model uses a grid size of 500m by 500m and contains two layers, 343 columns, 615 rows and 210945 cells in each layer. The aquifer was discretized vertically into two layers (layer-1 and layer-2) (Figure 7.3).

Layer-1 corresponds to entire alluvium and lacustrine deposits which ranges in thickness up to 45m in the floor (near to lakes) and the thickness decrease in the escarpment. The volcanic and weathered bedrock underlying the alluvial sediment of the area is taken as Laye-2 of the model which has an average thickness of 302m which determined based on available lithological well completion reports.

The Floor plain around the lakes, especially north of Abaya geologically is composed of alluvium deposited mainly in deltaic and fluvial environments. Clearly, the tectonic evolution of the region is reflected some recent deposition, because the thickness of the alluvium is small in comparison. The thickness of the alluvial plain is greater on the floor and decrease toward the escarpment and plateau corresponding to the top first layer in the flow model.

Owing to the spatial geologic heterogeneity that is evident from pumping test and the lithologic units, the groundwater aquifers in the area is constituted by more than one aquifer separated by less permeable layers such as clay type as multilayered system (JICA 2012). The lithological layer covering the upper aquifer is not homogenous, but most of part of the aquifer is unconfined in Abaya-Chamo lakes basin.

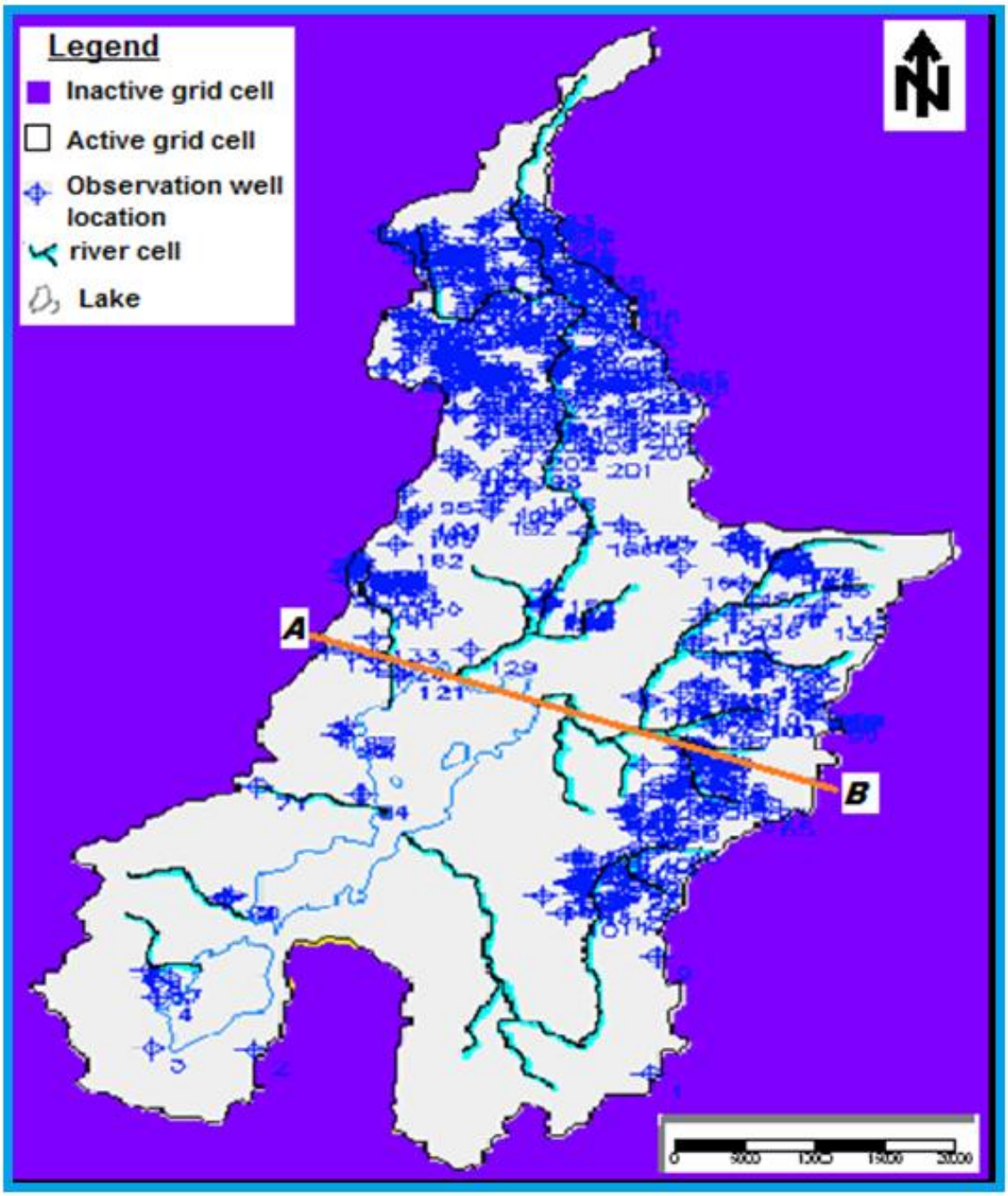

Figure 7.2: (a) 2D-Plan view of the entire model Area, Model grid and Observation well

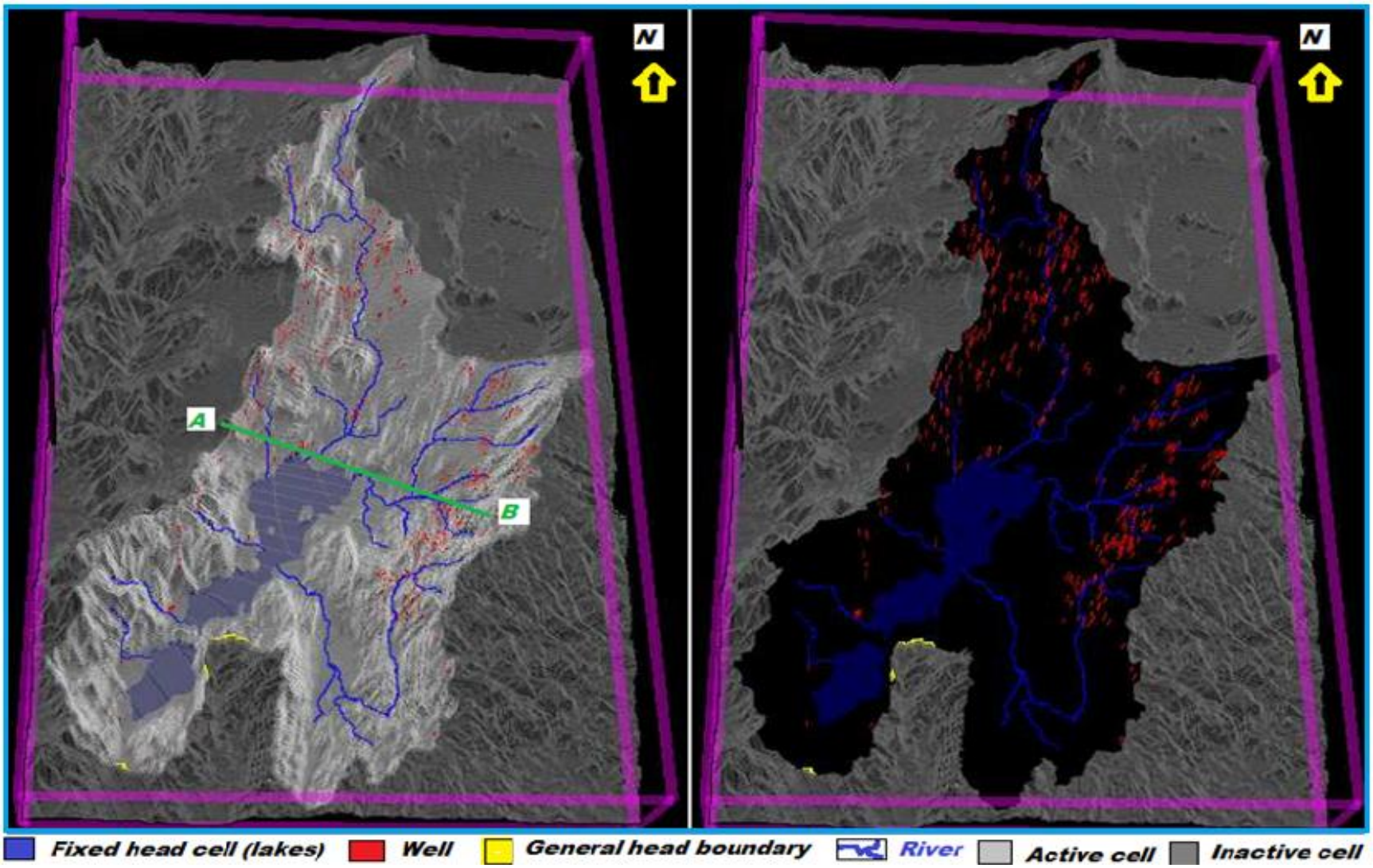

Figure 7.2: (b) 3D-Plan view of the entire model Area

In the representation of ground flow model simulation, the spatial coverage and the thickness of the layer-1 is end enough to account for the anticipated range of water level variation within the aquifer. Layer-1 represents the upper unconsolidated high permeability aquifer and has a thickness ranging from 20-45m and was modeled using unconfined aquifer hydraulic properties (Aquifer type-1). Layer-2 corresponds to the upper weathered and fractured bedrock which underlay the alluvial aquifer. This layer was assumed to be confined aquifer hydraulic properties (Aquifer type-0).

The two layers of the aquifer system of the study area have variable thicknesses depending on the lithological type and permeability differences. The height of each cell in the model was equal to the estimated formation thickness, which was determined based on the USGS 30-meter resolution digital elevation model (DEM) of the land surface and available lithologic wells.

The top altitude of layer-1 represents ground surface elevation above sea level. The bottom altitude of this layer is the bottom of the alluvial sediment that conceptualized from drilling lithology log sample of more than 240 data observed at throughout the study area. These point data were regionalized and gridded using the geospatial techniques by field interpolators. The lower altitude of the Layer-1 bottom is also taken as the top elevation of the Layer-2. The bottom of layer-2 is taken from the average volcanic and weathered bedrock thickness which is estimated from the depth of lithological well log available in the study (Figure7. 3).

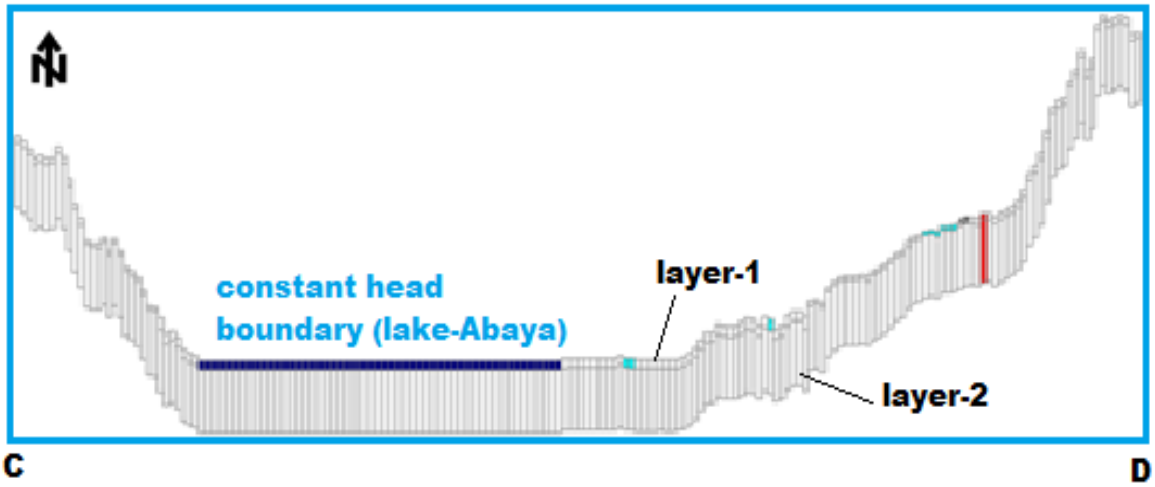

Figure 7.3: Cross-Sectional View of the Model Area along Line A-B of Figure 7.2

7.4.2. Boundary Conditions

Boundary conditions represent quantitative specification of dependable variables such as head and related flux variables at the boundaries of the model domain (Anderson and Woessner, 1992). Due to its effect on the simulation results of the flow model, identification and determination of appropriate model boundary conditions are very critical. In common sense, model boundaries are supposed to be the actual hydrologic boundaries of the problem domain.

In principle, generally, boundary conditions are categorized as: (a) a specified-flux boundary or no flow boundary, (b) a specified-head boundary and (c) a head-dependent flux boundary, for which the boundary flux is the product of a specified factor and the difference between the simulated head at the boundary and specified head of an external source/sink.

One the most important boundary condition in the study area that supposed to affect groundwater system was surface water features such as main rivers and the lakes. Both lakes (Abaya and Chamo) were considered as specified constant head boundary cell and limed to the first model layer for simplification since the depth of the lakes actually does not exceed the model thickness. The specifications of water levels for constant head boundary cells to lakes were specified to its mean water level elevation, which is about 1176m and 1109 for Abaya and Chamo Lake respectively. Whereas, the major rivers were simulated by river package where the water heads in the river-cells was assumed nearly greater by 0.5 to 2m toward downstream from the average elevation in each cell.

The lateral basin boundaries of the model area are bounded by volcanic mountains which are related to less permeable that coincide with surface water divides into all sides. Thus, lakes basin boundary is assigned to be no-flow boundaries at these surface water divides. So that at this condition, there is no groundwater flux enter into the modeled area was assumed from the ridges of surrounding basins of Abaya-Chamo lakes basin. In relation to these, there is no significant evidence shown that water enters into the model area from the surrounding mountainous areas at the contact. Topographically, the lower area, particularly in the south part, studies the area along which surface water and groundwater

outflow are also considered as the head dependent flux boundary. At these localities in Figure 7.2(b) (yellow shades), the model is simulated with the General-Head-Boundary (GHB) module for both layers of the model.

The model top boundary or layer-1 or the upper boundary was considered as a free surface boundary, which includes head-dependent flux and specified-flux at boundary cells. Here, spatially distributed groundwater recharge estimated by WetSpass model was given as the specified-flux boundary and the head-dependent boundary represents springs and groundwater seeps from major river beds. Recharge was specified and simulated with the recharge (RCH) module. The bottom boundary of the model is a specified no-flow boundary. This no-flow boundary is located where the aquifer comes in to contact with massive bedrock.

7.5. Model Input Parameters

Specification of aquifer properties and stresses are a very important step in the simulation, which are considerably varies both horizontally and vertically and thus, these properties are subjected to a range of values since the basin characterized by high topographic, geologic and hydrogeological variation as a complex rift margin zone. Therefore, the properties cannot be precisely parameterized in a flow numerical model.

The aquifer properties and fluxes specified for each active cell in the model are estimates of the average conditions in the area represented by the cell. The initial aquifer properties were estimated from analysis of pumping test and different previous hydrologic and hydrogeological studies conducted in the area. Indeed, the aquifer properties were modified in the possible range during groundwater flow calibration.

7.5.1. Initial and Prescribed Hydraulic Heads

MODFLOW requires initial hydraulic heads in order to solve the numerical solution for the grid cell. In principle, the initial hydraulic heads at constant head cells are used as specified head values and remain constant throughout the flow simulation. Since the simulation is steady-state flow, the initial heads are used only to solve the iterative equation using block centered finite difference and thus, initial heads at the constant head cells were assigned to the actual values while all other values were set at an arbitrary

level with in the layers thickness. Therefore, for both assigned unconfined and confined aquifer layer types, the initial hydraulic head of a constant head cell was prescribed in between the top and bottom layer elevation. The elevation difference below 15m was assumed as the initial and prescribed hydraulic heads for corresponding layers. This helps in filling the incapability of MODFLOW in converting a dry fixed-head cell.

7.5.2. Horizontal/Vertical hydraulic conductivity and Transmissivity

In the development of groundwater flow simulation specification of horizontal and vertical hydraulic conductivity values of the aquifer system is essential because groundwater flow within the flow system across the model layers was theoretically assumed to be horizontal. Which means a combining effect this aquifer property with hydraulic head gradient determines the groundwater flow direction.

Hydraulic conductivity can be expressed as a function of the effective permeability of aquifer material that measures water-transmitting properties. The coarser high permeable materials (weather and fractured) are corresponding to have a higher hydraulic conductivity than the finer and poorly sorted materials (massive less affected).

The horizontal hydraulic conductivity for the aquifer system of the study area was obtained from previous studies. Though, due to a very few data distributions on this parameter per different aquifer types made difficult to fully summarize aquifer parameter based on existing reliable information for each layer. So that transmissivity was considered to be better as an interchangeable parameter for generalization as a whole, on which the study area has relatively more information than hydraulic conductivity.

Transmissivity is defined as a product of hydraulic conductivity and saturated thickness (in our case corresponds to the thickness of aquifer layer) to represents the water transmitting properties of the saturated section of the aquifer.

Therefore, the information retrieved from the most relatively available transmissivity data are shown in Figure 7.4, which was then used to specify the hydraulic conductivity by considering

the litho-hydro-stratigraphic distribution in the model domain. Finally, the conductivity was grouped into different zones and each of these was assigned to the active cells of model layers

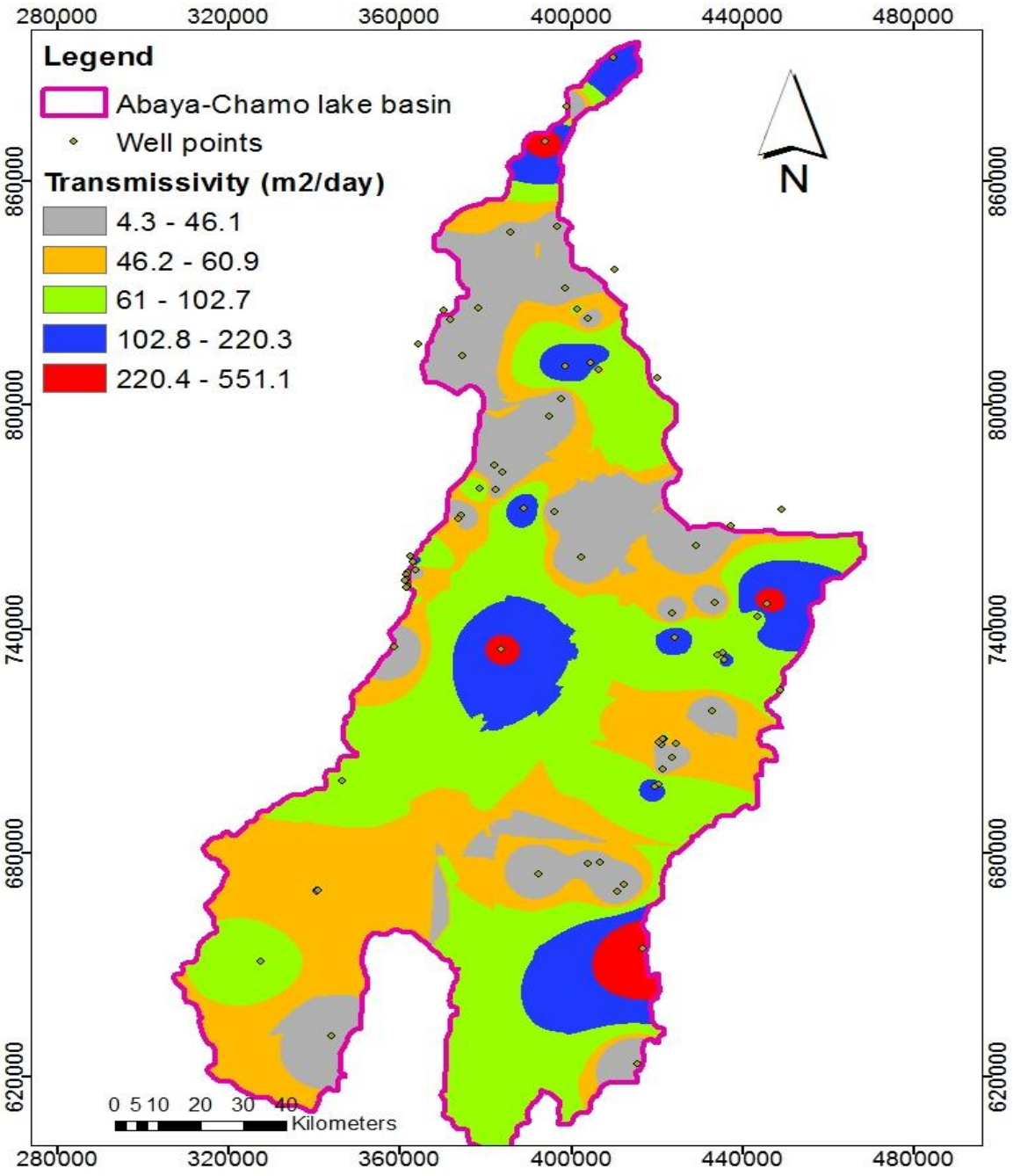

Figure 7.4: Regionalized transmissivity map from available pumping test data

The complication of hydraulic conductivity specification increases with variation in the aquifer types, saturated thickness, and range of various values of transmissibility in

different locations for the same aquifer. Such variation generally makes the model simulation hard to converge. Thus, this parameter was much subjected to modification during calibration and it took more effort and time to conduct this very intensive calibration.

In addition to the specific data in the study area, previous hydrogeological studies (Halcrow ,2008;, JICA ,2012 and Kefale et.al ,2013) summarized transmissivity values for the major aquifers as converging information based on all available well in main Ethiopian rift valley which includes the study area (given in Table7.1).

Table 7.1: Range of aquifer transmissivity values of some major aquifer types.

Aquifer types	Transmissibility （m2/day）		
	Minimum	Maximum	Average
Fine sand (unclassified fluvial deposits)	90.2	388.0	239.1
Lacustrine sediment	10.0	2080.0	1045.0
Rhyolite	2.5	376.5	189.5
Volcanic (trachyte, tuff, volcanic sediments)	1980 .0	3801.0	3801.0
Volcanic & sedimentary rocks	2.0	3801.0	1901.5
Scoria	158.7	158.7	158.7
Basalt	64.0	79.0	71.5
Welded tuff	12.5	914.0	463.3

While, the Vertical hydraulic conductivities were calculated by assuming ratios between horizontal and vertical hydraulic conductivities, which accounts for the ability of vertical flow that the aquifer is subjected to transmit water at expense of hydraulic head gradient between layers. Upon the converging literature evidence, the vertical hydraulic conductivity to horizontal hydraulic conductivity ratio is in a range of 0.01 and 0.1(Anderson and Woessiner, 1992).

Therefore, the initial vertical hydraulic conductivity of the aquifer units for the study area was estimated about 10% of the horizontal hydraulic conductivity for calibration purpose and these values are assigned to the active cells of the model layers.

7.6. Model Stresses

Potentiometric heads distribution in the groundwater flow system respond to the external flux stressed on the aquifer system. The major water fluxes can be related to the amount and distribution of recharge to the groundwater system of the study area is from the infiltration of precipitation and sub-surface inflow to the model area at the head dependent flux boundaries and river beds. While discharge from the system is through pumping well, groundwater outflow at the river beds, springs and subsurface outflow from the modeled area at the general head boundary.

7.6.1. Recharge

Groundwater recharge to the ground system results through infiltration of precipitation which left from actual evapotranspiration, interception and surface runoff. The spatial distribution of recharge rate in the study area was determined by spatially distributed surface water balance model (WetSpass) as given Figure 6.6(d) by considering different basin features. The calibrated surface model output estimated about 113.7mm/yr as an average groundwater recharge for the study area as discussed in Chapter-6. This spatially distributed recharge was then applied to the top active cell of the model as a spatially varying specified flux to the uppermost active layer.

7.6.2. Withdrawals

The steady-state simulation of Abaya-Chamo lakes basin considers outflow flux from groundwater system. These outflows include abstraction from pumping wells of the aquifer system for water supply and irrigation in the area, spring discharges from the system. Available measured outflow was collected as given in Figure 7.5: which shows general spatial distribution and relative amount all outflows in the basin. This water pumping from groundwater system through wells were represented by the well-package in the processing ModFlow.

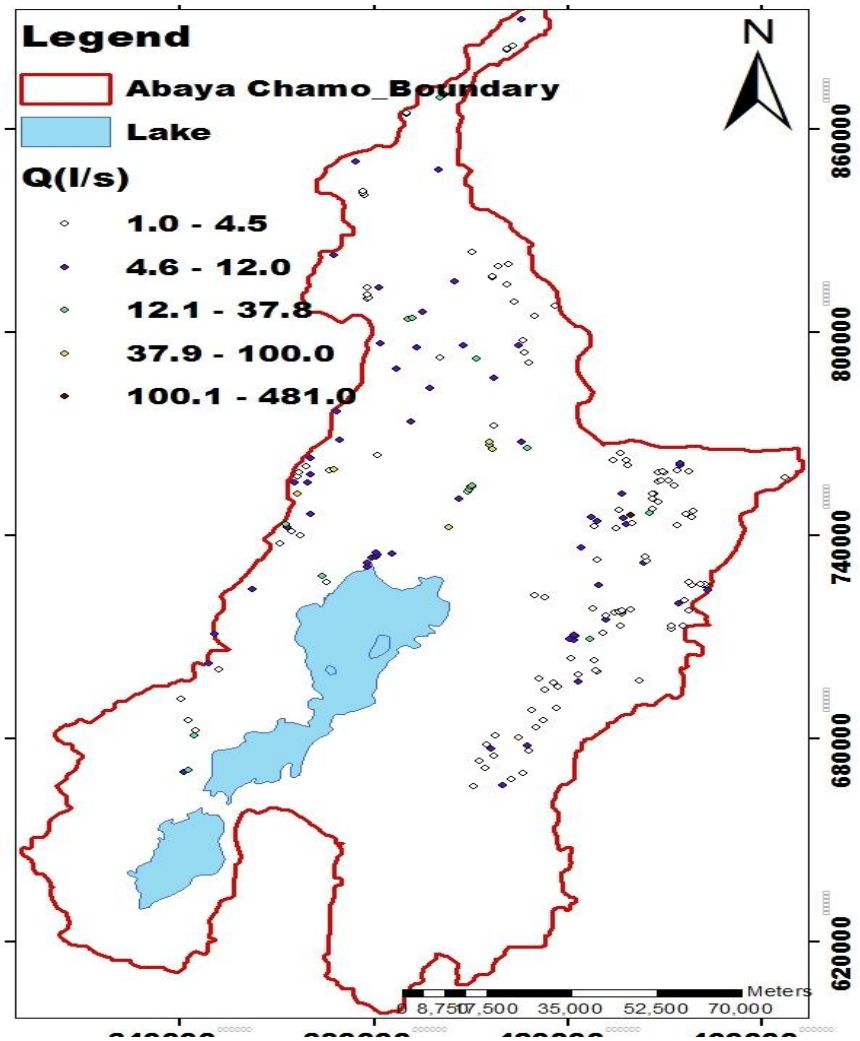

Figure 7.5: observed spring and pumping well distribution discharge, Q (l/s)

The river leakage systems were also simulated using river package for flow into/out from the groundwater system and the lateral subsurface inflow/outflow into/out from the model area in the southeast of Lake-Chamo was stimulated by the general head boundary condition.

Furthermore, losses from groundwater system through groundwater evaporation were also assumed around the northeast of Lake Abaya in the rift floor, since the floor around the lakes is covered mainly by highly permeable alluvium deposition with groundwater level very close to the surface and subjected to evaporation due to high radiation and also availability of significant forest vegetation in the capillary zone whose root can abstract

some amount of groundwater. This parameter was represented by the evaporation module in ModFlow as the outflow from the aquifer system

The study doesn't consider the addition of water flux by the agricultural drain and artificial recharge since there is no known recharging well in the study area.

7.7. Groundwater flow model calibration

The model simulation includes the entry of organized input data and interpretation of the model results. Calibration of the model is achieved when simulated results were compared with the observation in an acceptable range with a minimum error. The level of error is acceptable when the input parameter values are adjusted within reasonable ranges through an interactive and iterative method.

Here, the calibration target was adjusted to match the hydraulic heads simulated by the model with the observed hydraulic heads. The observed hydraulic heads as calibration values represent the static groundwater level obtained from records measured during drilling and field observation and the lake level as well.

The water level measurements are representing an average value of layers crossing both the unconfined and confined aquifer types. Though, the absence of monitoring well, uneven well distribution and measurement time of some observed head (have taken once during drilling or later) affects model calibration process. Thus, it should be noted to some extent that errors in the model result and simulation in addition uncertainties related to parameterizations and representations of properties for the model estimation.

All these mentioned prospective uncertainties, data limitation and distribution of necessary hydrogeological data across the study area together with a complex hydro-litho-stratigraphic setting made the calibration process very challenging and tough task in some part of the model.

Indeed, trial and error calibration were applied (Anderson and Woessner, 1992). It is the process of manual adjustment of input parameters until the model simulates the measured heads within range of the error criteria. The calibration was conducted through keeping out recharge constant with varying aquifer hydraulic conductivity, well discharge

and riverbed material conductance values as given in Figure 7.4, Figure 7.5 and Table 7.2. So that, the parameter values per cells/zones were modified manually within acceptable range and trial runs were then carried out until the simulated heads distribution are close to the observation heads. In order to overcome over/under paramerization to some extent due to the limitation of hydrogeological data in part of remotes areas, hydraulic conductivity zones were systematically extrapolated following converging information and hydrogeological map to achieve the best fit results.

7.7.1. Steady-State Simulation

The steady-state of groundwater flow model provides the quantified groundwater balance, fluxes and a flow direction of the system as well as the water flux between surface and groundwater. Indeed, the hydrogeological properties and stress parameters were adjusted during calibration through an iterative procedure based on the conceptual model as discussed above. The balance between the inflow and outflow can be used to expressing the steady-state flow conditions with null aquifer storage (in Equation 7.1 the term: $S_s \frac{\partial h}{\partial t} = 0$).

The groundwater flow modeling of Abaya-Chamo lakes basin using steady-state simulation was based on the water level measurement of 376 observation wells. The results of the calibration were also evaluated both qualitatively and quantitatively (Anderson and Woessner, 1992). The mean difference of the observed and simulated heads was used to quantify the average error in the calibration process. A closer simulated water level result against observed water level should establish as a criterion to a quantitative statistical error description In qualitative manner , the simulated head distribution result was supposed to comparable to the conceptual model in terms of groundwater gradient and flow direction.

Basically, as, the water table is known be to generally follow the topography with gentler fluctuation. The simulated of the steady-state calibration result in 2D/3D-diagram as given in Figure 7.6(a)-b) illustrate the highest groundwater level will be found along the basin boundary (chain of mountain ridges), flows toward low altitude into the lakes from all direction.

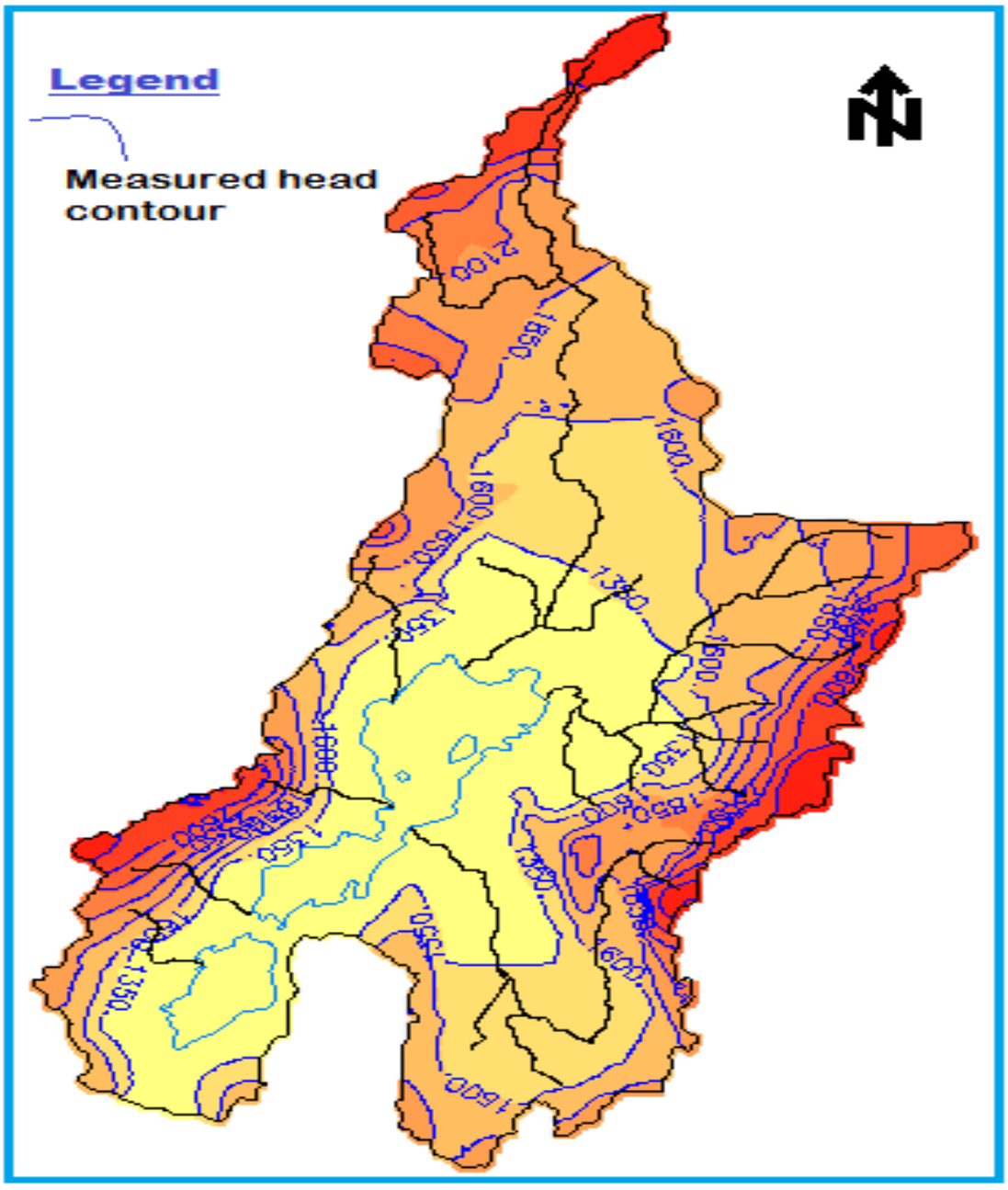

Figure 7.6: (a) 2-dimensional map showing the simulated hydraulic head contour.

The simulated potentiometric contour and hydraulic gradients match the estimated average potentiometric surfaces. As it was discussed in the previous section hydraulic head from the observation wells, groundwater flow generated from the plateau toward the floor into the lakes from both directions with a high gradient in the escarpment. In a similar fashion, the simulated potentiometric surface in two and three dimensions given

in Figure 7.6 (a) and (b), confirms the flow gradient and the flow direction. In another word the simulated steady-state potentiometric contour generally appeared similar to the measured average potentiometric surface.

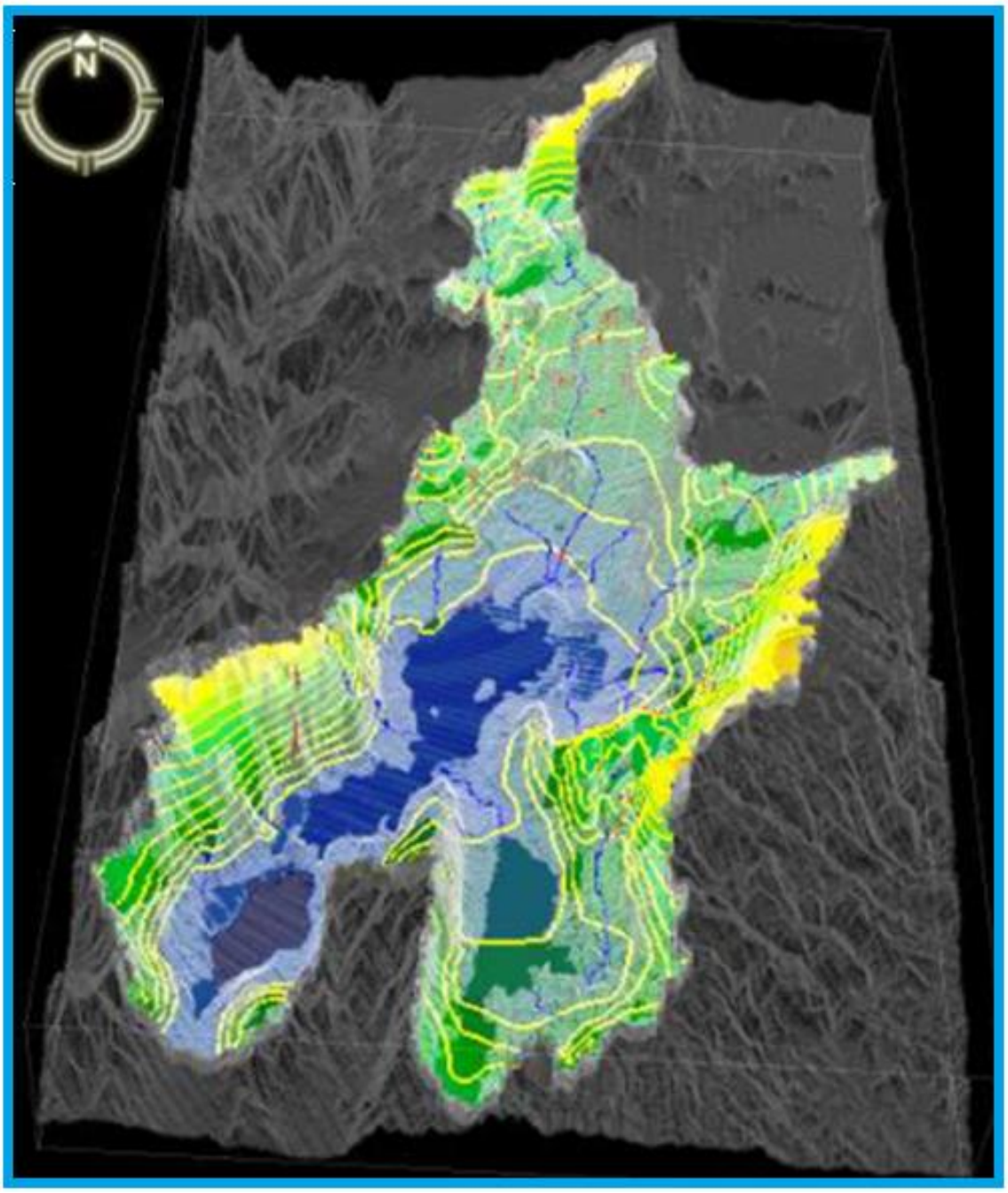

Figure 7.6 : (b) 3-dimensional Contour Map that shows the Comparison of the simulated hydraulic head with topography

The quantitative comparison between the simulated and the measured values of hydraulic heads was done for statistically to assess the calibration match. The overall goodness-of-fit between the simulated and the measured hydraulic heads (Figure 7.7) are determined by the mean error (ME) and the mean absolute error (MAE)

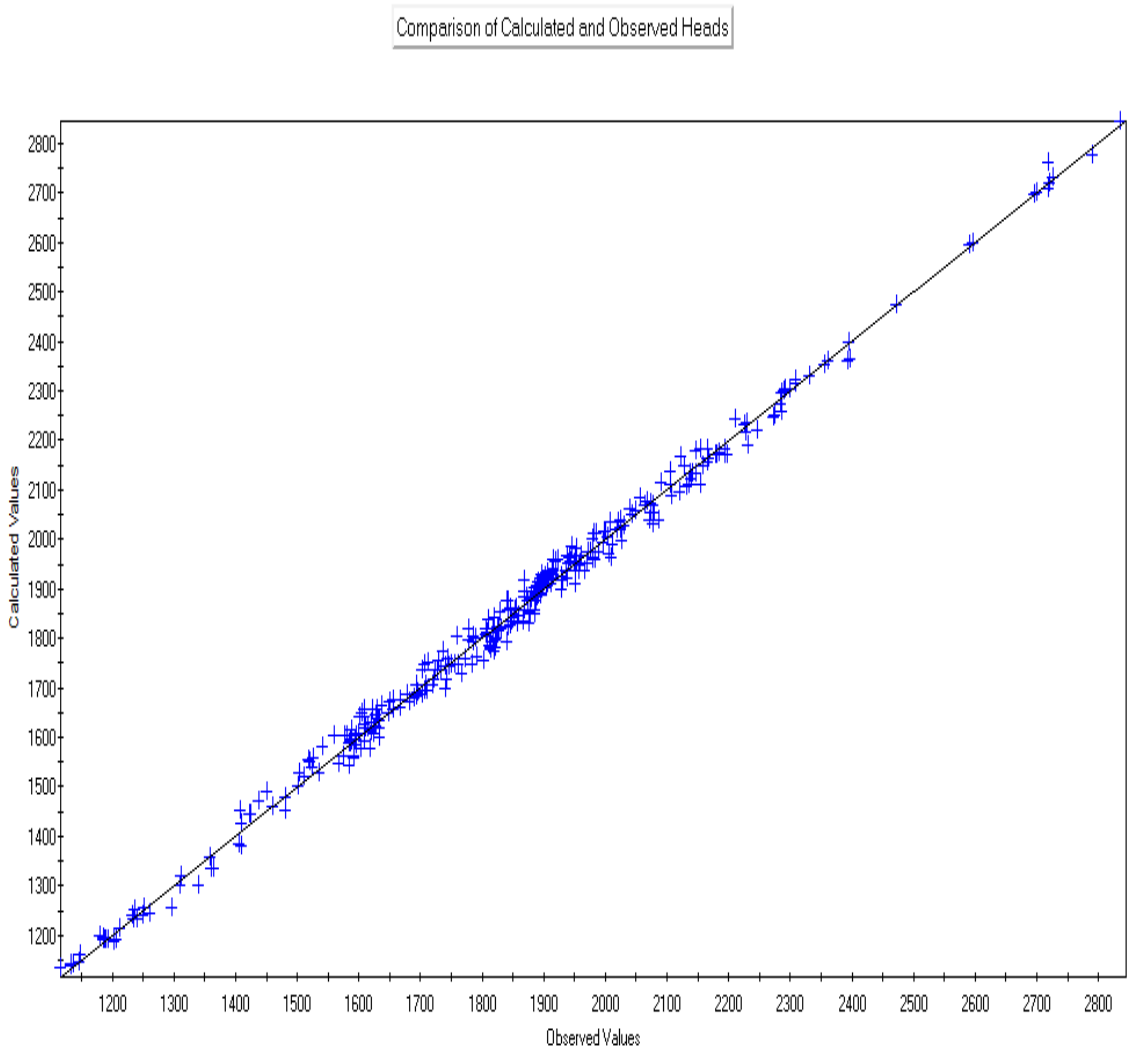

Figure 7.7: A graph that shows the Comparison between Observed and Calculated Heads

The mean error (ME) is the mean difference between measured and simulated heads.

$$ME = \frac{1}{n}\sum_{i=0}^{n}(h_o - h_s)_i \quad \text{..... (7.2)}$$

The mean absolute error (MAE) is the mean of the absolute value of the difference in measured and simulated heads.

$$MAE = \frac{1}{n}\sum_{i=0}^{n} \left| (h_o - h_s)_i \right| \quad \text{..... (7.3)}$$

Where: n = the number of observation points, ho = the observed heads, h_s = the simulated heads (Anderson and Woessner, 1992).

The summary of result statistics after steady state calibration for residual heads between simulated and observed static water values were calculated for 376 well-observations. The computed the mean error (ME) is about -0.8m for all water level measurements for both aquifers. This indicates that there is negative skewness between observed and calculated water levels. The root means average error for all wells is 4.1m. This satisfies 90% of all simulated heads matches with observed hydraulic heads within ±15m.

7.7.2. Sensitivity of hydraulic Conductivity

The basic importance of sensitivity analysis is to quantify the range of uncertainties in the calibrated model caused by uncertain aquifer parameters (Anderson and Woessner, 1992). Of different approach of sensitivity analyses, a common conventional technique works only by adjusting the most important parameters (such as horizontal hydraulic conductivity) based on the selected percentages decrease/increase. This is intended to evaluate the corresponding results in simulated water levels due to changes in the model.

The model is supposed to be sensitive to the parameter when a percent change in parameter value consequently alters the distribution of the simulated hydraulic head. The sensitive input parameter of the model should be accurately represented during the model calibration because small changes in the sensitive parameter value cause a large change in hydraulic head distribution. In another way, if the change of parameter value does not change the simulated hydraulic head, the model is considered insensitive to that parameter.

In our case, the sensitivity of the model to hydraulic conductivity in steady state was determined by systematical increasing and decreasing the model parameter values by 10, 25 and 50 percents. Figure 7.8 shows the sensitivity of horizontal conductivity against hydraulic head which can explain the effects of the adjustments on the conductivity to much up simulated to observed water level distribution in terms of root mean error. The result reveals, the model was sensitive to the horizontal hydraulic conductivity, for

example, a 25% increase or decrease in horizontal hydraulic conductivity in aquifer system increase or decrease the simulated hydraulic head by 11% to 14.5% respectively. Here the sensitivity of the model is amplified for percent decrease in horizontal hydraulic conductivity as compared to the percent increase. The hydraulic head behaves relatively more unstable in the highland than in the rift floor at low altitude of the study area.

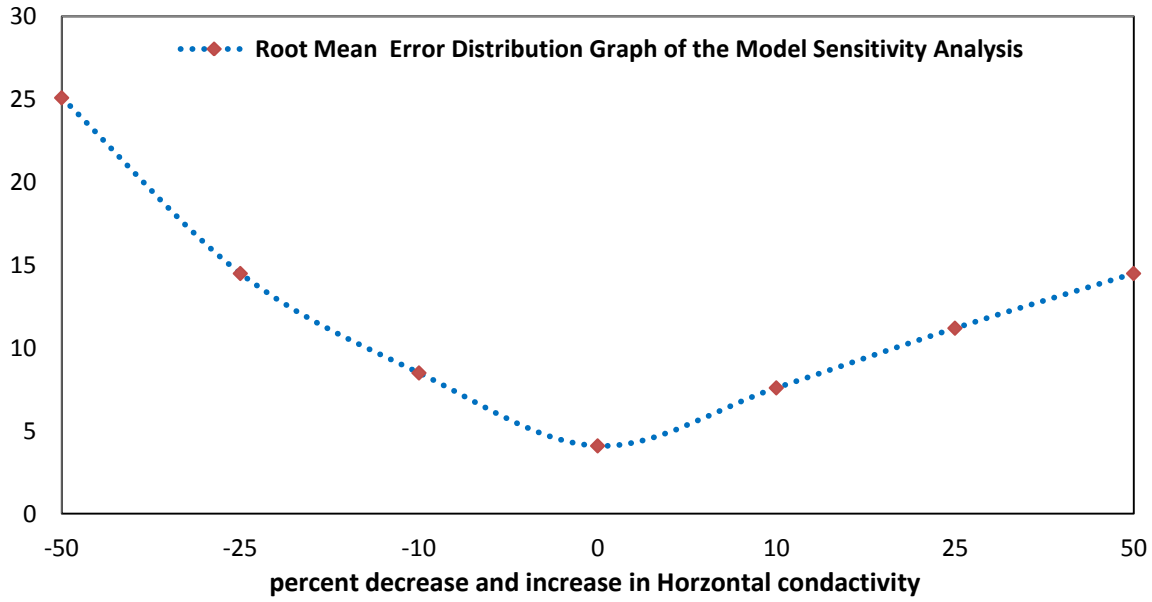

Figure 7.8: Root Mean Error distribution graph of the model sensitivity analysis.

7.8. Groundwater Balance

Water balance is a valuable assessment tool, as it provides a measure of the relative importance of each component to the total budget. Likewise, as discussed in surface water balance in the previous section, the water balance of subsurface is based on the conservation of mass principle for defined boundaries in space and time (Oosterbaan et al 1994). It represents the rate of change in water stored in a system, such as a lakes basin, is balanced by the rate at which water flows into and out of the system and can be written as:

$$\text{Inflow} - \text{Outflow} = \pm\Delta S \quad \text{..... (7.4)}$$

Where, ΔS is the change in water storage, when the change in storage is positive, the water content increases and, when negative (i.e. there is depletion instead of storage), it decreases.

The overall water budget under steady-state simulation is balanced (inflow minus outflow) within a percent discrepancy of 0.00. The comparison of the steady-state water budget for the numerical simulation and estimate for the conceptual model is summarized in Table7.2.

Table 7.2: Simulation result of long-term groundwater balance of the study area (m3/day)

==========	==========	==========	==========
WATER BUDGET OF THE WHOLE MODEL DOMAIN:			
==========	==========	==========	==========
FLOW TERM	**IN**	**OUT**	**IN-OUT**
STORAGE	0.00E+00	0.00E+00	0.00E+00
CONSTANT HEAD	1.97E+04	4.99E+06	-4.97E+06
WELLS	0.00E+00	8.21E+05	-8.21E+05
DRAINS	0.00E+00	0.00E+00	0.00E+00
RECHARGE	5.80E+06	0.00E+00	5.80E+06
ET	0.00E+00	7.34E-01	-7.34E-01
RIVER LEAKAGE	1.05E-00	6.63E+01	-6.53E+01
HEAD DEP BOUNDS	5.20E+02	5.49E+03	-4.67E+03
----------	----------	----------	----------
SUM	5.82E+06	5.82E+06	-6.90E+01
DISCREPANCY [%]	0.00		
==========	==========	==========	==========

7.8.1. Surface and groundwater interaction

As one of the important features of water resource and the hydrologic system is the interaction between surface water (such as a river, lake) and the groundwater table. The leakage flux between the two, comparisons are given in Table7.2. Thus about 66.3m^3/day (0.02MCM/year) groundwater leakage is estimated by the model as a groundwater contribution to river flow from the flow system. While only 1.05m^3/day as a river leakage into the groundwater system. This number indicates about 0.02 million cubic meters (MM^3/year) net water flux is out from the groundwater system through river beds.

Additionally, about 1814.1.MCM net outflow is simulated at constant head boundary (both lakes) annually in the study area. However, the rate of inflow into groundwater system is smaller in comparison with only 7.2MCM/ yr.

7.8.2. Water balance of lake-Abaya and lake-Chamo

In the study area, there are two lakes Abaya and Chamo as described in Section 4.2 as the most important part of the whole hydrologic system where water appears to sink in the center floor from adjoining drainage basins and groundwater system outflow. Thus, Lake inflow/outflow is the main component that plays a major role both as part of groundwater and also as a discharging media to the surrounding flow system.

The water balances of the lakes were treated separately in order to get insight into the interaction of the lakes and adjacent surface flow features in terms of flux contribution as shown in detail in Table 7.3 and 7.4.

Table 7.3: Water budget of Abaya Lake

FLOW TERM	IN	OUT	IN-OUT
STORAGE	0.00E+00	0.00E+00	0.00E+00
CONSTANT HEAD	1.97E+04	4.42E+06	-4.40E+06
HORIZ. EXCHANGE	1.15E+06	1.17E+04	1.14E+06
EXCHANGE (LOWER)	3.27E+06	9.04E+03	3.26E+06
RECHARGE	3.77E+02	0.00E+00	3.77E+02
SUM OF THE LAYER	4.44E+06	4.44E+06	1.00E+00
DISCREPANCY [%]	0		

Table 7.4: Water budget of Chamo Lake

FLOW TERM	IN	OUT	IN-OUT
STORAGE	0.00E+00	0.00E+00	0.00E+00
CONSTANT HEAD	0.00E+00	5.71E+05	-5.71E+05
HORIZ. EXCHANGE	8.60E+04	4.75E+01	8.59E+04
EXCHANGE (LOWER)	4.85E+05	0.00E+00	4.85E+05
RECHARGE	8.71E+01	0.00E+00	8.71E+01
SUM OF THE LAYER	5.71E+05	5.71E+05	0.00E+00
DISCREPANCY [%]	0		

The water balance of the lakes and the entire model domain has been simulated under steady state condition using spatially distributed recharge (by WetSpass surface water balance model) in conjunction with numerical groundwater flow model for estimating groundwater fluxes.

Table 7.3 and 7.4 shows the fluxes of the lakes used to represent groundwater balances of the lakes. The result indicates lake-Abaya receives the largest groundwater influx at the constant head (about 1613.3MCM/yr.) than lake-Chamo (208.4MCM/year). Groundwater flux estimation from the model demonstrates that groundwater controls the inflow of lakes

7.8.3. Groundwater flux's within the model domain

The study area or lakes basin is consisting of different major-river basin as described in the hydrology part in the earlier section (Figure 4.1). Determination of the regional water balances of these compartments of major river basin is also important to step to get insight into the interaction or contributions of river basins to the sink lakes in the middle of the floor, the water flux within the basins themselves and comparative groundwater resource potential for resource management and planning.

Therefore, the overall water balance of Abaya-Chamo lakes basin in the model domain was defined into five subregions as presented in Table 7.4 based on surface water divide in terms of major river basin. Such major river basins are Billate (1), Hamessa-Guracha and Kulfo-Gina (2), Gidabo (3), Galena (4), and Sife-Chamo (5) river basin are assigned as region 1, 2, 3, 4, and 5 respectively.

The corresponding subregions water balances of the groundwater domain are given in Appendix 10-15 shows that the overall water balances of subbasins, water flux among each other and lakes are given in the Table7.5 and also between layers as well.

For the total water influx to the lake-Abaya, groundwater of Gelana (3.81E+05) and Gidabo (2.95E+05) sub-basins contribute much greater than Kulfo-Gina and Hamessa-Guracha; while Bilate contributes the least (1.06E+05). Whereas, Chamo-Sife sub-basin contribute the largest in Lake Chamo as compared to Kulfo-Gina groundwater flow.

Table 7.5: Presents the groundwater flux among major-river basins and lakes in the study area

FLOW MATRIX	Lake-Abaya	Lake-Chamo	Billate	Hamessa-Guracha & Kulfo-Gina	Gidabo	Galena	Sife-Chamo
Lake_Abaya	0.00	0.00	2.49E+06	4.46E+05	1.44E+06	9.48E+05	0.00
Lake-Chamo	0.00	0.00	0.00	1.87E+05	0.00	1.13E+05	2.96E+05
Billate	1.06E+05	0.00	0.00	5.07E+05	1.00E+06	0.00	0.00
Hamessa-Guracha & Kulfo-Gina	1.44E+05	6314	5.37E+05	0.00	0.00	5.41E+04	2.80E+04
Gidabo	2.95E+05	0.00	6.53E+05	0.00	0.00	2.63E+05	0.00
Galena	3.81E+05	0.00	0.00	4.58E+04	5.38E+04	0.00	0.00
Sife-Chamo	0.00	1.77E+04	0.00	2.07E+04	0.00	3.41E+04	0.00

7.8.4. Groundwater outflow

The groundwater outflow from the study area domain is simulated using general head boundary to the south and East of Lake-Chamo (localities as yellow shades in Figure 7.2(b)) where an outflow is expected when the static water level gets increased. The model result in Table 7.2 shows annually a 0.19MCM water influx is added into the model area from south of basin boundary. and about 2MCM outwater flux is also taken away from the system annually. Thus here is about -1.7 MCM/yr a net water outflux is estimated as the outflow from the study area at the south boundary to konso and segen basins.

CHAPTER EIGHT

8. FUTURE WATER RESOURCES UNDER CHANGING CLIMATE

8.1. Climate Change

According to the IPCC (2007), Climate change is "any systematic change in the state of the climate that can be identified by changes in the mean and /or the variability of its properties (such as precipitation, temperature, pressure, or winds) that persists for an extended period typically decades or longer (AMS, 2012). As discussed in the IPCC-report, nowadays there is enough observational evidence of these changes which has been recognized across the world. These are manifested by an increase of global mean temperature (Figure8.1), heavy rainfall occurrences, and average sea levels rise to be mentioned. For instance, the global average warming will be 1.1-6.4^{0}C by 2090-2100 (IPCC 2007).

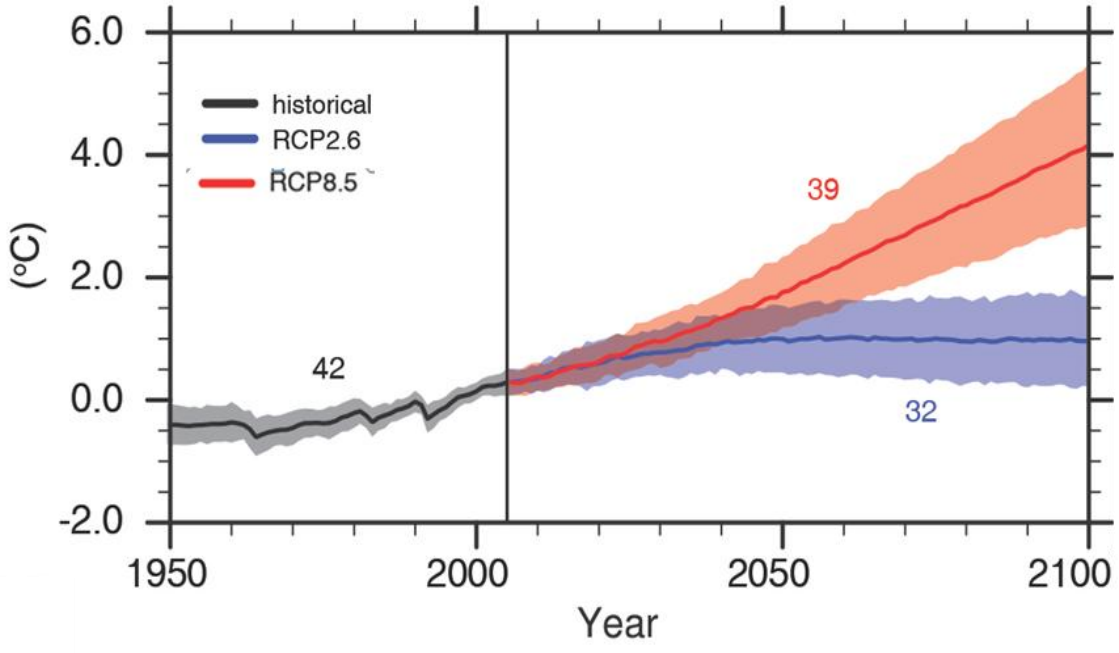

Figure 8.1: The projected Global mean temperature for RCP8.5 and RCP2.6 (IPCC 2007)

The very likely cause of the global temperature changes in the last decade's and that to be expected for the near future is believed to be predominantly driven by greenhouse gas emissions such as CO2, CH4, N2O, O3, HFCS, PFCs SF6 and gases whose emissions are covered on IPPC,(2007).

The emissions are largely associated with burning fossil fuels, assumptions about how much carbon (emissions) is being added to the carbon cycle. They affect through absorption, scattering, and emission of radiation with the atmosphere and at the earth's surface. The resulting consequence in energy balance due to these factors is expressed as radiative forcing, which is used to compare global climate in terms of warming or cooling with respect to the most significant greenhouse gases like carbon dioxide and water vapor (Heger et al., 2007).

The degree of impact depends on the adaptive capacity to the change and in this regard, the developing countries like Africa are one of the most vulnerable continents to climate change and climate variability and related risks; the situation is aggravated by socio-economic factors at various levels (Boko et al., 2007).

According to Kovats, R.S et.al (2014), projected changes in precipitation and temperature in globe varies both in spatial and temporal scales. For appropriate evaluation of climate change impacts on water resources availability, one needs to have a high quality of climate change projections at regional and basin scale.

A few studies of such kind have been carried out in Ethiopia for river basins, most of which are particularly concentrated on the Blue Nile river and upper Awash-river basins. Those few river basin scale studies still have mainly focusing on the assessment of potential climate impacts on runoff using different approaches, and most of which used a selected small number of fourth STRESS emission or an earlier version of IPCC scenarios with one or selected few global circulation model output.

Additionally, the hydrological simulations were done in most cases using a simple water balance method instead of applying the spatially complicated hydrological model.

Therefore, comparison of findings from such fragmented studies is difficult due to their difference in historical and future reference periods, emission scenarios, climate models used and uncertainties in the results as well.

In this study, we have tried to put our effort in improving some of the deficiencies of previous studies as a general approach and applied all available recent climate multi-model output (CMIP5) for two representative concentration pathways (RCP).

8.2. Representative concentration pathways (RCP)

The General Atmospheric and Ocean Circulation Climate Models simulation outputs (GCM) of the fifth assessment report (AR5) of the IPCC are available (Taylor et al 2012). Comparing to the IPCC AR4, the GCMs in AR5 include a more diverse set of model types (i.e., climate/Earth system models with more interactive components such as atmospheric chemistry, aerosols, dynamic vegetation, ice sheets and carbon cycle). A number of improvements in the physics, numerical algorithms and configurations are implemented in the IPCC AR5 models with a new set of scenarios called representative concentration pathways (RCPs) (Liu et al 2013).

Climate change scenarios are not the prediction or forecast of the future but rather they are a plausible future option and each of potential options represents a way in which the future might unfold (IPCC, 2000).

Scenarios of future conditions relevant to analyzing different aspects of the climate change issue have always been an important component of the work of the Intergovernmental Panel on Climate Change (IPCC) because of their utility for representing uncertainties associated with anthropogenic climate change. (IPCC, 2007a)

Emission Scenarios are based on an extensive assessment of driving forces and possible future evolving emissions, assuming a wide range of main demographic, economic, and technological driving forces of GHG and sulfur emissions (Nakicenovic et al., 2000). Previous sets of IPCC scenarios were formulated in this fashion and published in 1990, 1992 and 2000 and also widely used by the research and policy communities in the evaluation of possible climate change, its impacts, and options for adaptation and

mitigation, not only feeding into the IPCC process, but also in the context of other national and international programs and activities.

The earliest third (2001) and fourth (2007) IPCC assessment reports used a set of scenarios known as SRES (Special Report on Emissions Scenarios). The SRES scenarios start with socio-economic 'storylines from which emissions trajectories and climate changes were projected. Because the storyline comes first in SRES scenarios, the socio-economic circumstances are essentially locked in - an SRES scenario cannot be used to test the impacts of policy changes.

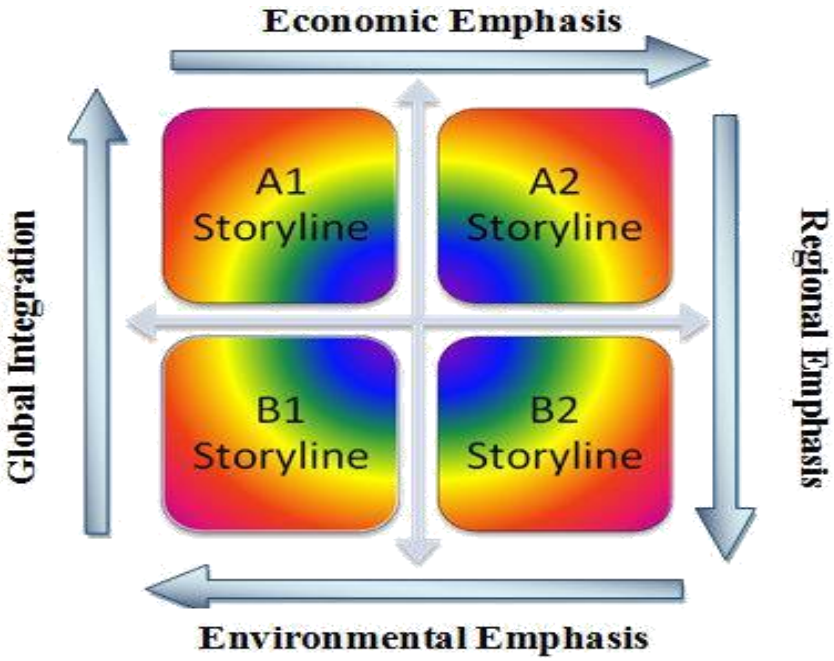

Figure 8.2: Emission scenario storyline (IPCC, 2007)

For instance, the fourth IPCC Special Report on Emissions Scenarios (SRES) was driven by analog and equilibrium scenarios for an impact assessment that included business and policy as well usual scenarios. Almost forty SRES scenarios represented different assumptions on emissions based on economic growth, land use change, and other driving forces of climate change. These futures possible options were then refined to six families for application in risk assessments with the descriptors A1FI, A1B, A1T, A2, B1, and B2 (IPCC, 2000). These refined groups of latter represented into four scenario families or

storylines as described by IPCC, (2007) that explore alternative development pathways as shown in Figure 8.2). A detailed description of the SRES can be found on the IPCC-homepage (http://www.ipcc.ch/).

Currently, the earliest SRES scenarios were replaced with Representative Concentration Pathways (RCP) (Van Vuuren, 2011a). RCPs replaced the SRES storylines with a more scientifically improved approach to GCM scenario input.

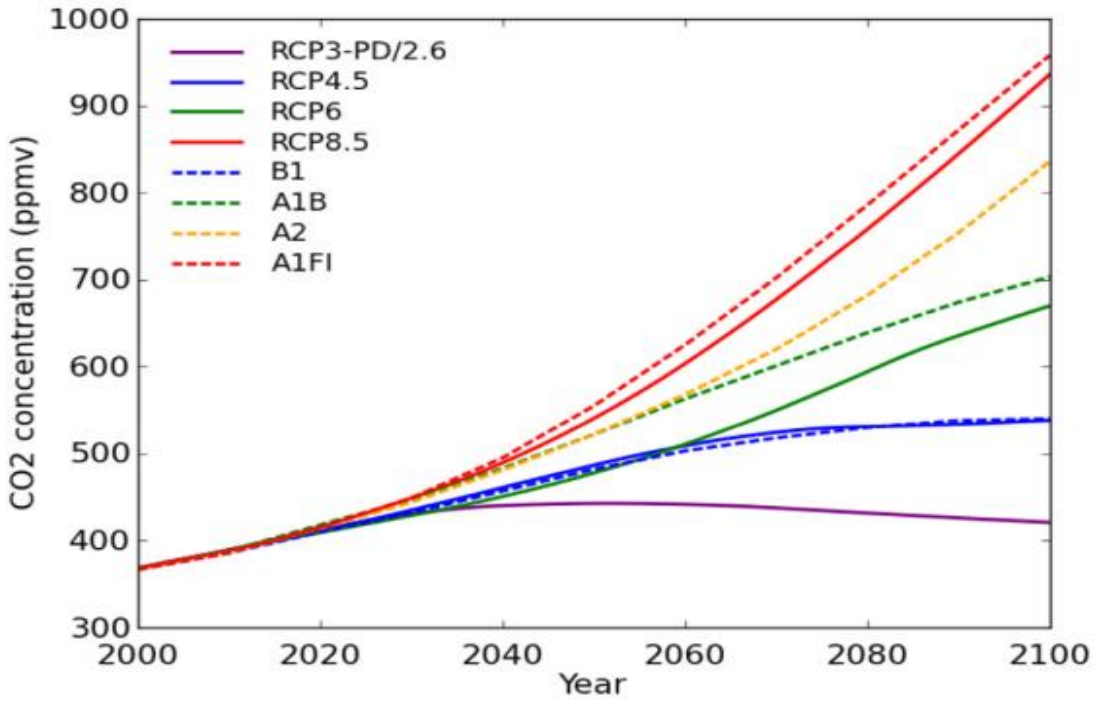

Figure 8.3: Comparison of CO2 concentrations for the 21st century from the RCPs and SRES scenarios. (Source: Meinshausen et al 2011)

RCP now include scenarios that explore approaches to climate change mitigation in addition to traditional "no climate policy" scenarios. A comparison of carbon dioxide concentrations for the 21st century from the RCPs and SRES scenarios is given in Figure 8.3 and Table 8.1 on which RCP8.5 is closest to A1FI, RCP6 is closest to A1B, RCP4.5 is similar to B1, and RCP2.6 is lower than any of the standard SRES scenarios

As a transition approach by IPCC due to its advantage, RCPs fix the emissions trajectory and resultant radiative forcing rather than the socio-economic circumstances. The RCPs

can then be used to test policy decisions on mitigation and adaptation, for example, to see which combinations produce the most cost-effective response and the timeliest return on investment.

Representative Concentration Pathways (RCPs) are concentration pathways used in the latest IPCC (2007) AR5 report. These are prearranged pathways for greenhouse gas and aerosol concentrations, together with land use change, that are consistent with a set of broad climate outcomes used by the climate modeling working groups.

These pathways are characterized by the radiative forcing produced by the end of the 21st century. Radiative forcing is the extra heat the lower atmosphere will retain as a result of additional greenhouse gases, measured in Watts per square meter (W/m^2). The complexity of humanity's possible future emissions has been reduced to just four representative pathways as presented in the following Table 8.1.

Table 8.1: Presents an overview of RCPs, compares emission scenarios from AR4 and AR5, RCP Co2 equivalent concentration and Citations

	Description	SRES Equivalent	Co2 Equivalent	Publication IA Model
RCP8.5	Rising radiative forcing pathway leading to 8.5 W/m2 in 2100.	A1F1	1370	Riahi et al. (2007
RCP6.5	Stabilization without overshoot pathway to 6 W/m2 at stabilization after 2100	B2	850	Fujino et al. (2006)
RCP4.5	Stabilization without overshoot pathway to 4.5 W/m2 at stabilization after 2100	B1	650	Wise et al. (2009)
RCP2.6	Peak in radiative forcing at ~3 W/m2 before 2100 and decline	None	490	van Vuuren et al. (2007)

RCP 2.6: emission pathway is representative scenarios to very low GHG concentration levels as low "peak" scenario: represents a strong mitigation scenario and is extended by assuming constant emissions after 2100 (including net negative CO2 emissions), leading to CO2 concentrations returning to 360 ppm by 2300 (van Vuuren et al. 2007).

RCP 4.5: It is a stabilization scenario where total radiative forcing is stabilized before 2100 by the employment of a range of technologies and strategies for reducing greenhouse gas emissions (Wise et al. 2009).

RCP 6.0: It is a stabilization scenario where total radiative forcing is stabilized after 2100 without overshoot by the employment of a range of technologies and strategies for reducing greenhouse gas emissions (Fujino et al. 2006).

RCP 8.5: It is characterized by increasing greenhouse gas emissions over time representative for scenarios in the literature leading to high GHG concentration levels. The underlying scenario drivers and resulting development path are based on the A2r scenario detailed in Riahi et al. (2007).

8.3. General Circulation Models (GCM)

Climate Change Scenarios projected by GCMs are fundamentally basis for studies related to the potential impact of global warming on the hydrological cycles and water resources in the future (Chen et al., 2006).

GCMs, refer to computer-driven mathematical models that use quantitative methods to simulate the interactions and dynamics among the atmosphere, oceans and land surface that together create our global climate. These models represent the natural processes (physical, chemical, and biological) of the atmosphere, ocean, cryosphere, and land surface and are the most sophisticated available for simulating effects of increased GHG concentrations on the global climate system. Over time there has also been an expansion in modeled variables, including both the marine and atmospheric environment (Wilby et al., 2009).

These numerical solutions of a (set of) partial differential equation(s) set up as an initial value problem. Generally, every GCM is formulated with some fundamental conservation laws, namely: the first law of thermodynamics (describing the movement of energy), Newton's second law of motion (it's about momentum of a particle), three continuity equations (the conservation of mass) and the ideal gas law (for the water vapor) (McGuffie and Sellers, 2005; Wilby et al., 2009). Although GCMs are the only

available tool for a variety of purposes ranging from the study of dynamics of the weather and climate system to the projections of future climate (Houghton et al., 2001), representation of actual complex hydrological parameters are highly simplified (Xu, 1999) and have been a substantial part of the assessment process since 1990 the modeling of future climate change.

Recently during successive IPCC assessments on GCMs, there is markedly increased GCMs development has recognized by the number of climate modeling working groups, from five groups generating their own eight models for the fourth assessment report (FAR) in 1990 to 27 groups producing 61 models for Fifth assessment report (AR5) and most of the AR5 models generate daily and monthly projections of climate elements (such as, maximum, minimum, and mean temperatures and precipitation).

More than 24 GCMs (of the currently available 61) have all the necessary data for post-processing and integration with rainfall event models for risk assessments and the 40 models that can generate spatial scenarios. This data enrichment adds information for tools applied to real-world problems and improves the statistical significance of results. The IPCC advises that an ensemble or combination of models be applied when using GCM data (Stocker et al, 2010). The ensemble approach reduces model-specific bias, thereby providing the best available representation of projected climate change (Knutti et al, 2010).

In this study, over a 24 GCMs outputs obtained from the CMIP5 data archive (http://cmip-pcmdi.llnl.gov/cmip5/index.html) are listed in Table 8.2.

Table 8.2: Available GCM outputs with monthly data including the historical data

GCM	Model	Resolution (km)	Source
1	BCC-CSM 1.1	64 × 128	Beijing Climate Center, China Meteorological Administration, China
2	BCC-CSM1.1(m)	160 × 320	
3	BNU-ESM	64 × 128	Beijing Normal University, China
4	CanESM2	64 × 128	Canadian Centre for Climate Modelling and Analysis, Canada
5	CCSM4	192 × 288	National Center for Atmospheric Research (NCAR), USA
6	CNRM-CM5	128 × 256	National Center for Metrological Research, France

GCM	Model	Resolution (km)	Source
7	CSIRO-Mk3.6.0	96 × 192	Australian Commonwealth Scientific and Industrial Research Organization
8	FGOALS-g2	108 × 128	Institute of Atmospheric Physics, Chinese Academy of Sciences, China
9	FIO-ESM	64 × 128	The First Institute of Oceanography, SOA, China
10	GFDL-CM3	90 × 144	Geophysical Fluid Dynamics Laboratory, USA
11	GFDL-ESM2G	90 × 144	
12	GISS-E2-H	90 × 144	Goddard Institute for Space Studies (NASA), USA
13	GISS-E2-R	90 × 144	
14	HadGEM2-ES	145 × 192	Met Office Hadley Center, UK
15	IPSL-CM5A-LR	96 × 96	Institute Pierre-Simon Laplace, France
16	IPSL-CM5A-MR	143 × 144	
17	MIROC5	128 × 256	Japan Agency for Marine-Earth Science and Technology, Atmosphere and Ocean Research Institute (The University of Tokyo), Japan
18	MIROC-ESM	64 × 128	
19	MIROC-ESM-CHEM	64 × 128	
20	MPI-ESM-LR	96 × 192	Max Planck Institute for Meteorology (MPI-M), Germany
21	MPI-ESM-MR	96 × 192	
22	MRI-CGCM3	160 × 320	Meteorological Research Institute, Japan
23	NorESM1-M	96 × 144	Norwegian Climate Centre, Norway
24	NorESM-ME	96 × 144	

8.4. Sources of uncertainty in future climate projections

Uncertainty in climate system represents the degree to which a value of the future state of the climate is unknown (IPCC, 2007) these can be resulted due to lack of information or from disagreement about what is known or even knowable. This can be explained by a range of quantitative values estimated by multimode's outputs, or through the qualitative description that supposed to cover the judgment of a climate working groups or modeling centers

There have been significant scientific disputes over the selection of the best temporal and spatial resolution for prediction of potential impacts of climate change on hydrology over the particular regime. In many previous studies, several researchers, particularly climatic researchers, believe that the resolution of original GCM should be kept as it is to manage

and understand climate impact issue without any bias correction or alter uncertainties produced by GCMs themselves; however, a coarse resolution of 100 or 200km (or even more) is simply not practical for evaluation of hydrology at smaller basin scale, especially where there is significant topographic and climatic variation over relatively smaller area (Wilby et al., 1998; Tabor and Williams, 2010).

In addition to, topography and climate variability over a small area, the complex interaction of hydrologic components over a given regime in estimating procedures of water resource availability also contributing an uncertainties range with socioeconomic drivers, and making forecasting and assessment models more inaccurate and complicated to calibrate (Hijmans et al., 2005).

Many previous studies (Tabor and Williams, 2010; Fowler et al., 2007; Salathé et al. 2007; Kremen et al., 2008; Jones and Thornton, 2003; Jarvis et al., 2008) has been still describing coarseness of GCM outputs to evaluate assess impacts on hydrology, hydrologic system, water resource availability distribution, planning and management related matters despite the considerable effort done by climate modeling centers, However, uncertainties related to climate projections and spatial disagreement has been improving over time by a number of climate centers around the world which develop climate models to enhance our understanding of climate system and climate change and to support the IPCC activities (IPCC, 2001, 2007) and impact assessments as well.

Moreover, there are noticeable differences among GCMs and their formulations, which are associated with numerical methods, spatial resolutions, and subgrid-scale parameters employed during the development process (IPCC, 2001 and 2007; Govindan et al., 2002). Thus to take advantages of many multimodal's, scientific studies have been making use ranges of available GCMs to assess uncertainties instead of selecting a subset of GCMs.

In this regard, as it was suggested in many of earlier related studies to climate change impact assessment; multi-model ensemble mean is the best approach in order to overcome uncertainties of single model prediction because single models are overconfident (Weigel et al 2008). Multi-model ensembles contain information from all

participating models (Pincus et al 2008) and thus generally believed to be superior to single models (IPCC 2001, Duan and Phillips 2010, Miao et al 2013).

Therefore, in this study, we applied a model averaging technique which is one of commonly used of popular ensemble methods. Model ensemble averaging is the simple straightforward multi-model ensemble technique. Each model has its own contribution and the same weight (w_i = 1/i, where i is the number of models) in the multi-model forecast. When using the model ensemble averaging, any knowledge about a single model performance of the model is neglected rather cumulative average effect is considered (Casanova and Ahrens 2009).

8.5. Downscaling GCM Outputs: The Delta Method

As discussed in the last section GCMs have been the primary information source for construction of climate scenarios and projection in providing ranges of all scales, from local to global as the basis for climate change impacts assessments. The impact studies rarely use GCM outputs directly because errors in GCM simulations relative to historical observations are large (Ramirez-Villegas et al. 2013). The spatial resolution of global scale is generally coarse to satisfy the requirements for small hydrological basin. Hence, it is important to correct bias and downscale the raw climate model outputs.

Due to its requirements in bridging gap related to scaling issue; scientists have developed various downscaling methods. The techniques provide researchers to obtain regional predictions of climatic changes, ranging from smoothing and interpolation of GCM anomalies to regional climate modeling (Tabor and Williams, 2010; Giorgi, 1990).

Of course, downscaling techniques of different types can vary in accuracy, output resolution, computational and time requirements, and climatic science robustness. In this regard, Statistical downscaling provides an easy-to-apply and much more rapid method for developing high-resolution climate change surfaces for high spatiotemporal resolution for local or basin-scale.

The systematic GCMs errors are caused due to imperfect conceptualization, parameterization, discretization and spatial averaging within grid cells. The resulting

output projections often provide bias representations of observed times series. Such a bias accordingly forces the hydrological model through the input data and it could end up in unrealistic simulations of hydrologic components (Bergstro¨m et al. 2001).

In most cases, both precipitation and average air temperature are commonly required as an input to run the hydrological models. In a similar manner for this study, the projected precipitation and average temperature of latest CMIP5 multi-model outputs for both rcp4.5 and rcp8.5 emission scenarios were considered.

In fact, application of bias-correction methods has been commonly used as an approach in previous climate impact studies for hydrology (the forcing parameters such as precipitation and temperature) (Wilby et al. 2000).

1. **Bias-corrected** delta-change approach directly to force the hydrological model with adjustment of the grid for both precipitation and Temperature as presented in Figure 8.4(a) as follows.

This approach corrects the observation of precipitation and temperature for the future period, using the differences (Δ) between the future model output and historical reference data. The correction is done by multiplying and adding the delta factor(Δ) into observation of precipitation and temperature respectively.

Indeed, adjustment of grid includes re-gridding and re-mapping. The re-gridding of all CMIP5 GCM outputs into similar resolution employed remapped in a conservative manner (Bryan et al. 1996) and bilinear interpolation, (ECMWF 2001) for precipitation and temperature respectively.

In a fully coupled climate model, state variables, heat and water fluxes must be transferred between models periodically and such fields must be remapped from one component grid to another. Fluxes, in particular, must be remapped in a conservative manner in order to maintain the energy and water budgets of the coupled climate system. Now a day, many coupled models utilize an area-weighted remapping where the interpolation weights are based on the fractional area-overlap of the source and destination grid cells (Baldwin, 2000; Mesinger 1996; Mesinger et al. 1990).

For temperature, grid transformations may be performed using bilinear interpolation which is operationally used by ECMWF (2001). However, this method may not be desirable for precipitation, because it results in smoothing of the precipitation field, increasing the minima and reducing the maxima. Indeed, the total precipitation forecasted by the model using bilinear interpolation method does not conserved.

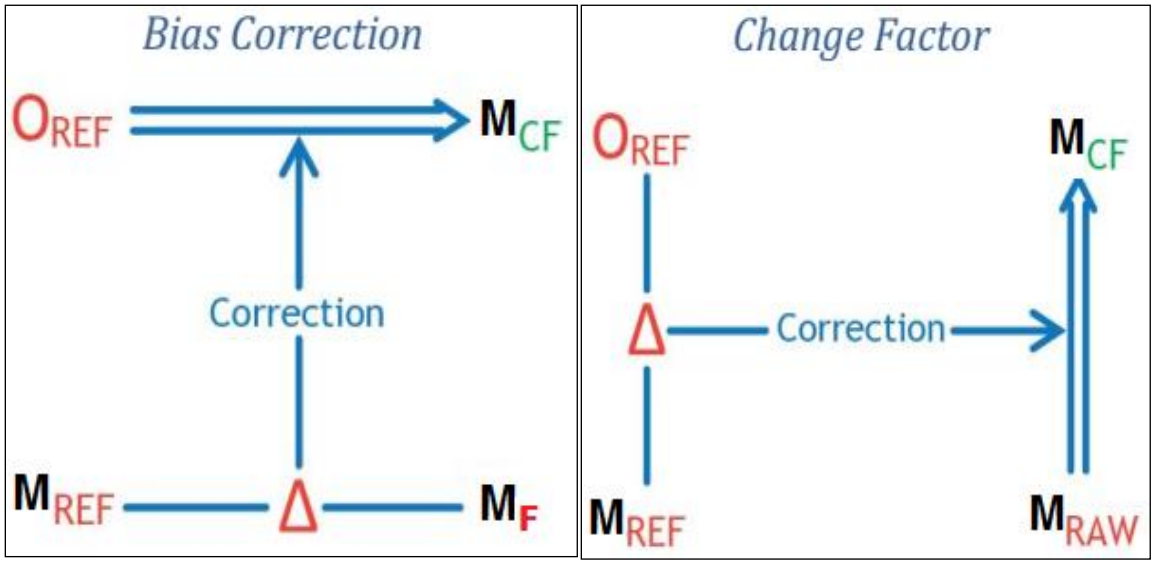

Figure 8.4: shows the bias correction and change factor correction,

Where, OREF: is an observation in the historical reference period M_{CF}: bias-corrected GCM output, M_{REF}: GCM output from the historical reference period, M_F: GCM output for the future period and MRAW: raw GCM output for the future period Source: Hawkins et al., 2013 and (interface in the CCAFS-Climate portal: http://www.ccafs-climate.org)

For comparison purpose, all GCM outputs are re-gridded to the same spatial resolution of ERA-Interim, which is a reanalysis product from the European Centre for Medium-Range Weather Forecasts (ECMWF). The data set is produced at a resolution about 0.75-degree latitude and longitude, with 60 vertical levels. It has a 4-dimensional variation assimilations system (Simmons, Uppala et al. 2006; Uppala, Dee et al. 2008).

2. **Change factor**: as a delta downscaling method relay on high-resolution monthly climate surfaces from WorldClim um of interpolated anomalies to (Hijmans et al., 2005). A global database of climate at a spatial resolution of ~1km at the Equator and the data available at http://www.worldclim.org, this database was

developed from compiled observation at weather stations from a large number of local to global sources. This method provides the delta change of climate as an interpolated smoothed surface in order to make use of this interpolated surface to the reference baseline climate, taking into account the possible bias due to the difference in baselines as given Figure 8.4(b).

This approach assumes that changes in climates are only relevant at coarse scales and that relationships between variables are maintained towards the future. The correction factors based on the difference of reference GCM output and observed values so that GCM simulations matched the long-term monthly averages of the observation. The basic principle here is that biases between the observations and GCM output are identified and then used to correct and scenario runs in order to match observational monthly mean.

The above-mentioned method was applied over 26/24 different GCMs outputs from the IPCC Fifth assessment for both rcp4.5 and rcp8.5 of precipitation and an average temperature that are required as an input component to run the hydrological models.

Besides in order to account for the whole range of uncertainty for 2lth projection quartile 10 (Q_{10}), quartile 50 (Q_{50}) and quartile 90 (Q_{90}) of the model ensemble were considered which is one of effectively used of popular approach. Whereas for spatial scale, model ensemble output means (Q_{50}) using change factor method was employed to evaluate the mean change among periods.

The overall climate change assessment framework in this study is given in Appendix 15, on which the full present day (20C3M) monthly time series were used, Here, we examined 30-year climatologies for four time periods: baseline (1976-2005), near-term (2006-2036), medium-term (2037-2067), and long-term (2068-2099) for each of the GCMs and the 2 variables (precipitation and mean surface temperature) were interest. Then we focus on the GCM output projections under two selected scenarios (i.e., RCP 4.5 and RCP 8.5) for predetermined time steps starting from historical climate to the end of the century. Therefore, the complete time series were reduced to 4 different 31 years

averaged periods, referred in the following section as the base period, 2020s, 2050s and 2080s.

8.6. Assessment of climate change during 21st century

CMIP5 GCMs climate projections of temperature and precipitation constitute 24/26 coupled climate simulations with different resolution under RCP4.5 and RCP8.5 forcing until 2100 were bias-corrected and applied to the calibrated hydrological model. Delta change statistical method was used for bias correction, the period from 1976 to 2005 was considered as the base period. To assess the signal of climate change over the study area, the future period until 2099, to three periods were assigned in an average of 31 years. These are the near future (2006-1936), intermediate future (2037-2067) and far future (2068-2099) are referred as 2020s, 2050s, and 2080s respectively. The simulation results are interpreted in comparison to the base reference period.

Our results revealed an increase in temperature projection and changes in precipitation for upcoming periods of the year until 2099 over the lakes basin.

The relative change or delta in the future projection of temperature and precipitation with respect to the base period is given in Figure 8.5 and Figure 8.6, the bar graph shows the minimum outlier, 10 quartiles (Q_{10}), 50 mean quartile (Q_{50}), 90 quartiles (Q_{90}) and whereas whisker ends represent maximum outlier of the ensemble mean of all CMIP5 model output.

8.6.1. The projected average temperature trend

The projected annual average temperature shows gradual increases for Abaya-Chamo lakes basin until the end of the century. In the basins, air temperature increases more intensively under the high-end RCP8.5 scenarios in comparison to the low-to-intermediate RCP4.5.

The delta change of average annual temperature raises in the basin minimum from $+0.45^0$C to maximum of $+3.6^0$C under the rcp4.5 scenarios and minimum from $+0.55^0$C to maximum of $+5.4^0$C under the rcp8.5 high-end scenarios at the end of the century.

The projected annual average temperature in Figure 8.5 shows gradual increases until the end of the century. the model ensemble projection of average annual temperature rises from the base period by +0.84 ^{0}C, +1.58 ^{0}C, and +1.95 ^{0}C in 2020s, 2050s and 2080s respectively under the rcp4.5 emission scenario whereas under rcp8.5 by +0.94^{0}C, +2.13^{0}C, and +3.57^{0}C respectively.

8.6.2. The projected precipitation trend

Regarding precipitation as given in Figure 8.6, the mean annual precipitation shows also an increasing trend under low- intermediate rcp4.5 and high-end rcp8.5 scenarios in the study area, the projected change in precipitation increases like temperature more intensively under the high-end RCP8.5 scenarios in comparison to the low-to-intermediate rcp4.5.

As minimum outliers, some of few models projected the delta change of annual precipitation decrease by 13.2% and 8.5% in near term (2020s) and at the end of the century (2080s) under rcp4.5 scenarios. Whereas under rcp8.5 the decrease is relatively small in 2020s and 2080s is about 6.9% and 5.1% respectively. However, in both scenarios, the minimum outlier is very aggravated in mid-century (2050s) about more than 50% decline is projected.

In the case of a maximum outlier, as given in Figure 8.6, the precipitation change increases in the basin 64.4%, 125.2% and 151.0% in 2020s, 2050s and 2080s respectively under the rcp4.5 scenarios, and also the number increase by 56%, 137.1% and 218.6 under the rcp8.5 scenarios.

Like average temperature, the increase of projected precipitation is more intensively under the high-end RCP8.5 scenarios in comparison to the low-to-intermediate rcp4.5. The ensemble means of projecting a by 4%, 5.9%, and 8.9% in 2020s, 2050s' and 2080s respectively under the rcp4.5 emission scenario. Whereas the mean precipitation increase more relatively under rcp8.5 by 1%, 9%, and 19.54% in the period 2020s, 2050s and 2080s respectively as compared to the reference period.

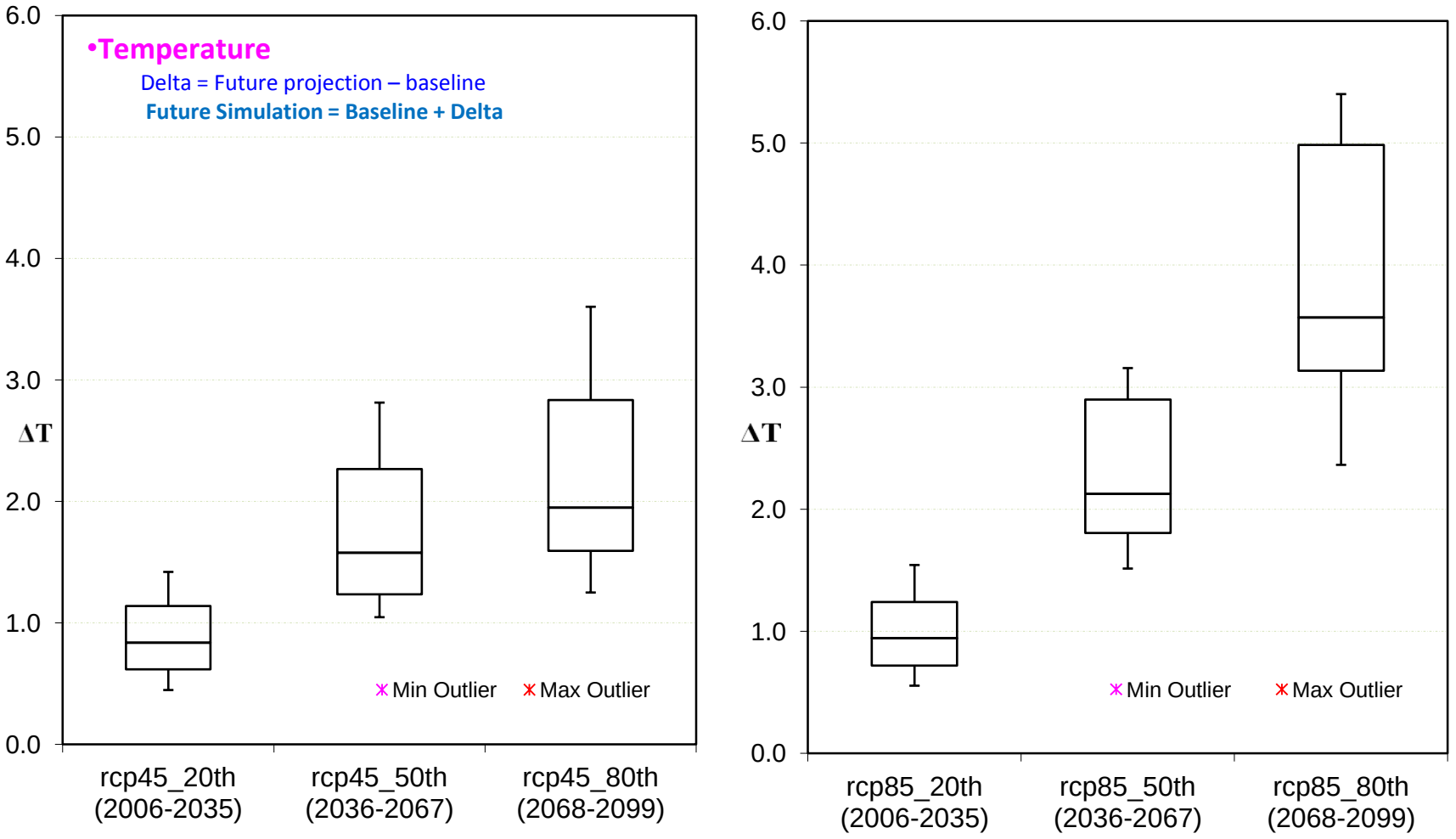

Figure 8.5: Climate change signals for the temperature of three future periods compared to the reference period under two scenarios. (The bar charts in the figure display the inter-quartile range (Q_{50}). The upper end of the whisker represents 90% quartile (Q_{90}) and the lower end represents the 10% quartile (Q_{10}). Minimum or Maximum values that are outside this range are shown as outliers).

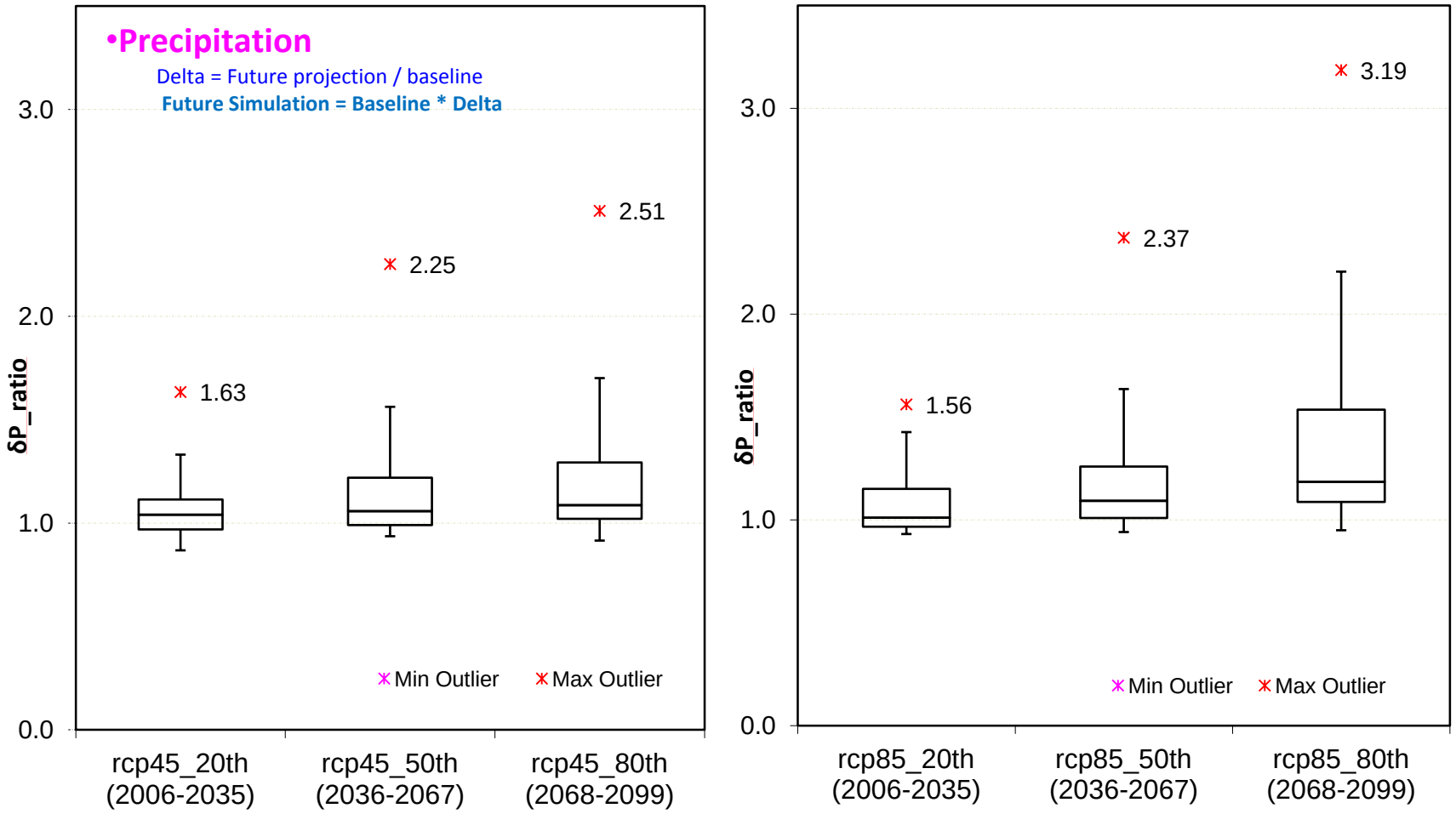

Figure 8.6: Climate change signals for precipitation of three future periods compared to the reference period under two scenarios. (The bar charts in the figure display the inter-quartile range (Q_{50}). The upper end of the whisker represents 90% quartile (Q_{90}) and the lower end represents the 10% quartile (Q_{10}). Minimum or Maximum values that are outside this range are shown as outliers).

Here, the minimum and maximum outliers in the analysis indicate the high uncertainties related to projected precipitation, which means some of the model's future estimation is much far away from the rest of ensemble mean. In another word, use of a single model projection for climate change impact assessment could result in error result

Thus, a comparison or averaging of ensemble model approach is more recommendable as discussed in Section 8.4 in reduces model-specific bias, thereby providing the best available representation of projected climate change (Knutti et al, 2010).

Therefore, as a commonly used approach, Q_{10}, Q_{50}, and Q_{90} (represented in Figure 8.5-Figure 8.6 as lower end, inter-quartile range and upper end of the whisker respectively) of the ensemble mean of CMIP5 output projections were assumed to be the best representation of projected climate change (for both precipitation and temperature) to account the whole range of possible impact on the water resource availability in the study area.

8.6.3. Seasonal change of projected precipitation and temperature

More significant changes occur in the distribution of precipitation during the seasons. The seasonal dynamics of changes show a clear rise more in the dry season (NDJF) than wet seasons (JASO and MAMJ) under both rcp4.5 and rcp8.5 scenarios as presented in Table8.3

Table 8.3: presents projected seasonal precipitation delta change of Q_{10}, Q_{50} and Q_{90} percentage of the ensemble mean for different periods as compared to the base period under RCP4.5 and RCP8.5

Pr(%change)	Season	JASO			MAMJ			NDJF		
Scenarios	period	2020s	2050s	2080s	2020s	2050s	2080s	2020s	2050s	2080s
rcp4.5	Q_{10}	-7	-10	-8	-5	-10	-9	-17	-2	3
	Q_{50}	2	3	2	3	0	3	1	25	43
	Q_{90}	18	23	26	23	26	36	37	59	90
rcp8.5	Q_{10}	-7	-10	-8	-8	-10	-14	-13	-4	24
	Q_{50}	0	4	10	-1	1	4	4	29	81
	Q_{90}	21	23	48	22	35	61	51	81	154

While seasonal ensemble means of quartile ten (Q_{10}) shows considerably decreases only in the wet season (JASO and MAMJ) of in mid future period 2050s, under both low-intermediate and high-end scenarios for the lakes basin.

Under rcp4.5 scenarios, the seasonal precipitation in JASO and MAMJ (rainy season) decreased by 7%, and 9% respectively for Q_{10} of the ensemble projection, while in NDJF (dry) an increase of 3% is projected at the end of the century.

Besides under rcp8.5 scenarios, the seasonal precipitation in JASO and MAMJ (rainy season) decreased by 8%, and 14% respectively for Q_{10} of the ensemble projection, while in NDJF (dry) an increase of 24% is projected at the end of the century.

Generally, the mean seasonal projection of precipitation will rise 20%, 30% and 43% in JASO, MAMJ, and NDJF respectively for low emission scenario at 2099. Similarly, for the high-end scenario, the seasonal precipitation increases in 2099 will be expected about more than 200% relative to present condition.

Table 8.4: presents projected seasonal temperature delta change of Q_{10}, Q_{50} and Q_{90} increment of the ensemble mean for different periods as compared to the base period under RCP4.5 and RCP8.5

T-Delta (^{0}C)	Season	JASO			MAMJ			NDJF		
Scenarios	period	2020s	2050s	2080s	2020s	2050s	2080s	2020s	2050s	2080s
Rcp4.5	Q_{10}	0.6	1.2	1.5	0.6	1.2	1.5	0.5	1.0	1.4
	Q_{50}	0.9	1.6	2.0	0.9	1.6	2.0	0.8	1.5	2.0
	Q_{90}	1.2	2.5	3.1	1.2	2.5	3.1	1.3	2.4	3.2
Rcp8.5	Q_{10}	0.7	1.6	2.8	0.7	1.7	2.9	0.6	1.6	2.7
	Q_{50}	1.0	2.1	3.6	1.0	2.2	3.7	0.9	2.0	3.7
	Q_{90}	1.3	3.0	5.3	1.3	2.8	5.0	1.4	3.1	5.4

In Abaya-Chamo lakes basin as given in the Table 8.4, the variability of projected temperature change by all available CMIP5 multimodel ensemble mean shows

insignificant change in temperature overall wet and dry season from near future to the end of the century under both RCP (4.5 and 8.5) forcing, but these are about nearly 2^0C rise in temperature between rcp4.5 and RCP8.5 for the period of 2050s (2036-2067) and 2080s (2068- 2099).

At the end of the century, the mean seasonal projected rise of average temperature is almost uniform throughout the rainy and dry season under the low-intermediate scenario, which is about 2^0C. Under high-end emission scenario, this projection will increase in the range between 3.6^0C and 3.7^0C.

However, the maximum average temperature projection for the Abaya-Chamo lakes basin based on Q_{90} of all 24 GCMs estimate will be 5.4^0C for the dry season and from 5^0C to 5.3^0C for the rainy season.

8.7. Expected climate change impacts on hydrological components during 21th century

Upon a successful calibration of WETSPASS model, the bias-corrected temporal temperature and precipitation projected time series for each of future periods under rcp4.5 and rcp8.5 were fed into the spatially distributed model to simulate future annual and seasonal surface runoff, actual evapotranspiration and groundwater recharge. The simulation period was split as discussed earlier into four periods (historical and future) in Section 8.5; such as baseline/historical/reference (1976-2005), 2020s (2006-2035), 2050s (2036-2036), and 2080s (2068-2099). The hydrological components of the future periods were compared with the reference baseline period to evaluate the future changes in the lakes basin. Since the observed meteorological data (rainfall and temperature) used to characterize the spatial distribution of the basin start from 1970's to 2005 for WetSpass model for calibration. This simulated absolute observed annual and seasonal from WetSpass simulation can be used to observe the absolute change of hydrologic components in the future.

Thus, with respect to the projected change in precipitation and average temperature in the previous Section 8.6, the Q_{10}, Q_{50}, and Q_{90} weighted absolute values of hydrological components ($\%\Delta = (Xp-Xb)/Xb$, where $\%\Delta$: percent change, Xp: projected absolute value

Xb: annual baseline absolute value) and temporal changes were used as indicators to assess the future changes with respect to the simulated reference baseline under rcp4.5 and rcp8.5 scenarios.

The percent change of projected annual precipitation to the reference period would be within uncertainty range from -5% to 16.9%, -4% to 27.9% and -1% to 35.9% for 2020s, 2050s and 2080s periods respectively which represent Q_{10} to Q_{90} under rcp4.5as given in the Figure8.7(a)-(b): in the Abaya-Chamo lakes basin. Whereas these relative changes with respect the reference base period show a slightly increasing trend to the future respective periods in precipitation under rcp85 which is in the range between -5% to 21.9; -1% to 35.9% and 7% to 35.9%.

8.7.1. Future changes in annual Surface Runoff

Consequently, the projected changes in both average temperature and precipitation would potentially impact the hydrological regime in the lakes basin. In the annual base, the mean annual surface runoff is increased by 4%, 6% and 9% for corresponding future periods with a mean increase of 6.3% representing Q_{50} over the entire lakes basin. Generally, the change in surface runoff is almost consistent with precipitation variation.

Considering the uncertainty of the projections in surface runoff in the study area shows relatively the smaller uncertainty range than groundwater recharge. But the high-end scenarios yield has the highest the range of uncertainty in comparison to the low-end and intermediate scenarios. For instance as given in Figure 8.7(a)-(b), under rcp4.5, the Q_{10} ensemble mean models projection impact on surface runoff estimated a decrease by -5% -4.9%, and -1.9% in near, medium and long-term periods respectively. Whereas under rcp8.5 the decrease is relatively small this is about -5%, -1% and 7% respectively.

In the case of a Q_{90} ensemble as maximum impact, the surface runoff change increases in the basin 17%, 28% and 36.1% in 2020s, 2050s and 2080s respectively under the rcp4.5 scenarios, and also the number increase by 22%, 36.1% and 72.2% under the rcp8.5 scenarios (Appendix 19).

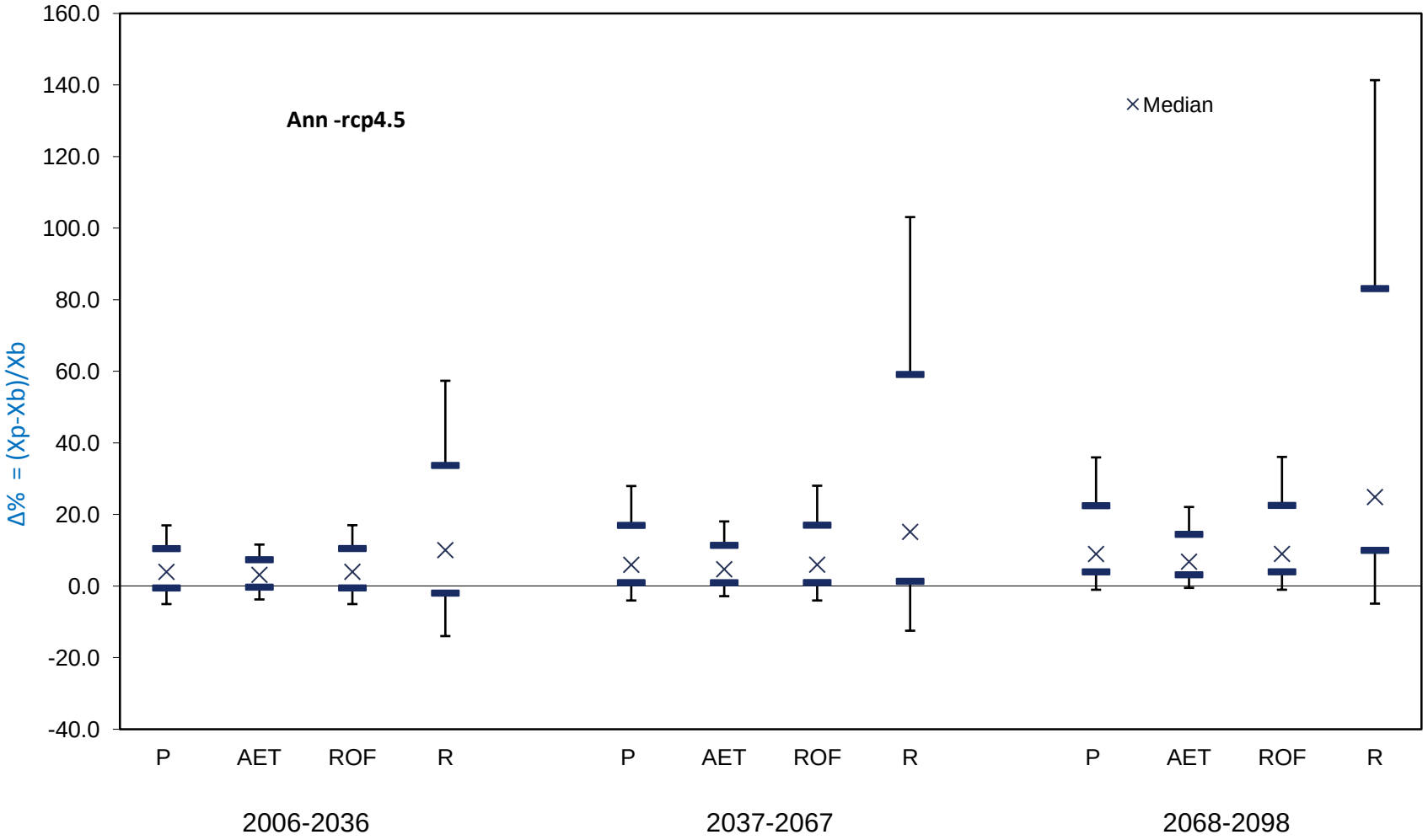

Figure 8.7: (a) The long-term percent delta changes of annual precipitation, actual evaporation, surface runoff and groundwater recharge in three periods under the rcp4.5 scenario (the horizontal markers are used to represent Q_{10} and Q_{90}).

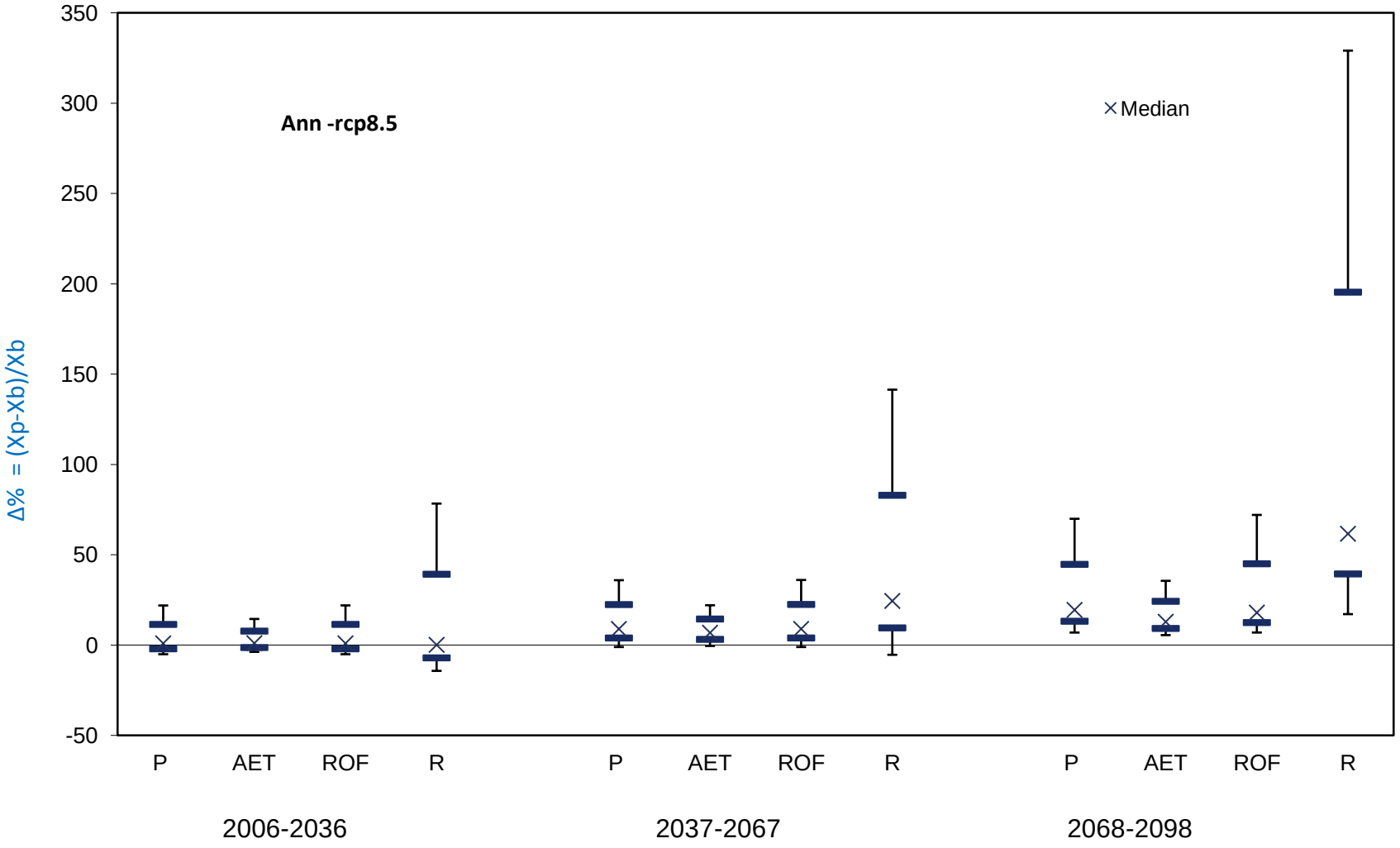

Figure 8.7(b): The long-term percent delta changes of annual precipitation, actual evaporation, surface runoff and groundwater recharge in three periods under the rcp8.5 scenario (the horizontal markers are used to represent Q_{10} and Q_{90}).

8.7.2. Future changes in annual Groundwater Recharge

These change under rcp4.5 in the mean state of climatic parameters would have relatively the largest significant impact is expected annual groundwater recharge which has an important implication on the future groundwater resource availability of the regime. The annual mean groundwater recharge will increase up to about 10%, 15% and 25% for Q50 of 2020s, 2050s' and 2080s respectively as compared to the base period.

The mean rise in groundwater recharge in the study area is about 24.8% to 61.7% with respect to present day annually at the end of the century (2067-2099) as a most pronounced finding. This higher level of groundwater in this lakes basin can be explained by the larger influence precipitation amount under climate change. The tendency of the rise in precipitation has more impact over temperature increase and appeared to be the most important parameter that governs the hydrology of the area, which means a small change in the mean precipitation has a potential in the distribution of hydrologic components in space and time.

Considering the uncertainty of the projections in groundwater recharge under the study, it should be mentioned that in the high-end scenarios yield has the highest the range of uncertainty in comparison to the low-end and intermediate scenarios, which increase from near to far future period.

For instance under rcp4.5, Q_{10} ensemble mean models projection impact on recharge estimated decrease by -13.9%, -12.5% and -4.9% in near, medium and long-term periods respectively. Whereas under rcp8.5 the decrease is relatively small this is about 14.2%, -5.4% and 17.2% respectively.

In the case of a Q_{90} ensemble as maximum impact, as given in Figure 8.7(a)-(b), the groundwater recharge change increases in the basin 57.3%, 103.1% and 141.30% in 2020s, 2050s and 2080s respectively under the rcp4.5 scenarios, and also the number increase by 78.4%, 140.4% and 339.1% under the rcp8.5 scenarios.

8.7.3. Future changes in annual Actual Evapotranspiration

Similarly, actual evapotranspiration is projected to rise for all future period till 2099 under both scenarios and the increase of 3.1%, 4.7%, and 6.8%, in 2020s, 2050s' and 2080s respectively. The mean annual increase is about 6.8% to 12.9% with small range uncertainties of present actual value under rcp4.5 and rcp8.5 respectively at the end of the century (2068-2099).

As given in Figure 8.7(a)-(b), the uncertainty range for projection impact on actual evapotranspiration under rcp4.5, the Q_{10} ensemble mean models estimated decrease by -3.7%, -2.8% and -0.5% in near, medium and long-term periods respectively. Whereas under rcp8.5 the decrease is relatively small this is about -3.7%, -0.5% and 35.6% respectively.

In the case of a Q_{90} ensemble as maximum impact, actual evapotranspiration change increases in the basin 11.6%, 18% and 22.1% in 2020s, 2050s and 2080s respectively under the rcp4.5 scenarios, and also the number increase by 14.5%, 22.2% and 35.6% under the rcp8.5 scenarios.

8.7.4. Seasonal future changes in Hydrological components

Seasonal changes of hydrological components due to climate were analyzed according to the two wet rainy and one dry average month as identified and discussed in the previous sections.

In the basin, as given in Table 8.3 for both wet season, the projected seasonal mean precipitation have a small steady rise during both wet seasons (MAMJ and JASO) less than 4% expect for 2080s JASO (about 10% mean increase) with respect to the historical base period with the lower ranges of uncertainty (for Q_{10}– Q_{90} percentiles). The mean change is characterized by small climate change signals between scenarios and periods, especially for near future (2020s) to mid future (2050s).

But, still the range of seasonal uncertainty in projected precipitation for the wet season is significant. Generally as shown in the Figure 8.8 (a)-(b), and Figure 8.9 (a)-(b), the seasonal precipitation increases during the wet season. For example, The percent change

of projected MAMJ seasonal precipitation to the reference period would be within uncertainty range from -5% to 23%, -10% to 26% and -9% to 36% for 2020s, 2050s and 2080s periods respectively which represent Q_{10} to Q_{90} under rcp4.5 as given in the Figure 8.8(a)-(b), and Figure 8.9(a)-(b). Whereas these relative changes show a slightly increasing trend to the future respective periods in precipitation under rcp85 which is in the range between -8% to 22%; -10% to 35% and -14% to 61.9%. The uncertainty range for JASO is also given in Table 8.3.

Similarly as given in Table 8.4, the wet seasonal temperature increase is about nearly 0.6^0C to 2.8^0C for 2020s and 2050s future periods under both the low-intermediate (rcp4.5) and high-end scenarios (rcp8.5).

During the end period (2080s), an increase of seasonal temperature especially under the high-end scenarios would rise up to 5.3^0C with smaller uncertainty in the range of values between $Q_{10} - Q_{90}$ percentiles. But the projected seasonal temperature shows slightly greater for JJAS than in MAMJ relative to the reference period.

These some small sporadic increase in precipitation and temperature of wet months in the intermediate and far future under all scenarios compared to the reference period has a significant impact on the hydrology of the lakes basin.

For the wet season scenarios, an increase in the average runoff, groundwater recharge, and actual evapotranspiration is observed for all seasons and annual totals, except for the 2050s JASO_rcp4.5 and 2020s MAMJ_rcp8.5. Although the percentage decrease in runoff is shown in the intermediate period under high-end scenario for MAMJ season and an increase of groundwater recharge in present gets higher than for the other water-balance components.

The 2080s, far future period shows a higher increase of surface runoff discharge about 30-50% and groundwater recharge from 50% to double the amount during all wet seasons under both rcp4.5 and rcp8.5 scenarios, with the higher ranges of uncertainty (for 10^{th} – 90^{th} percentiles).

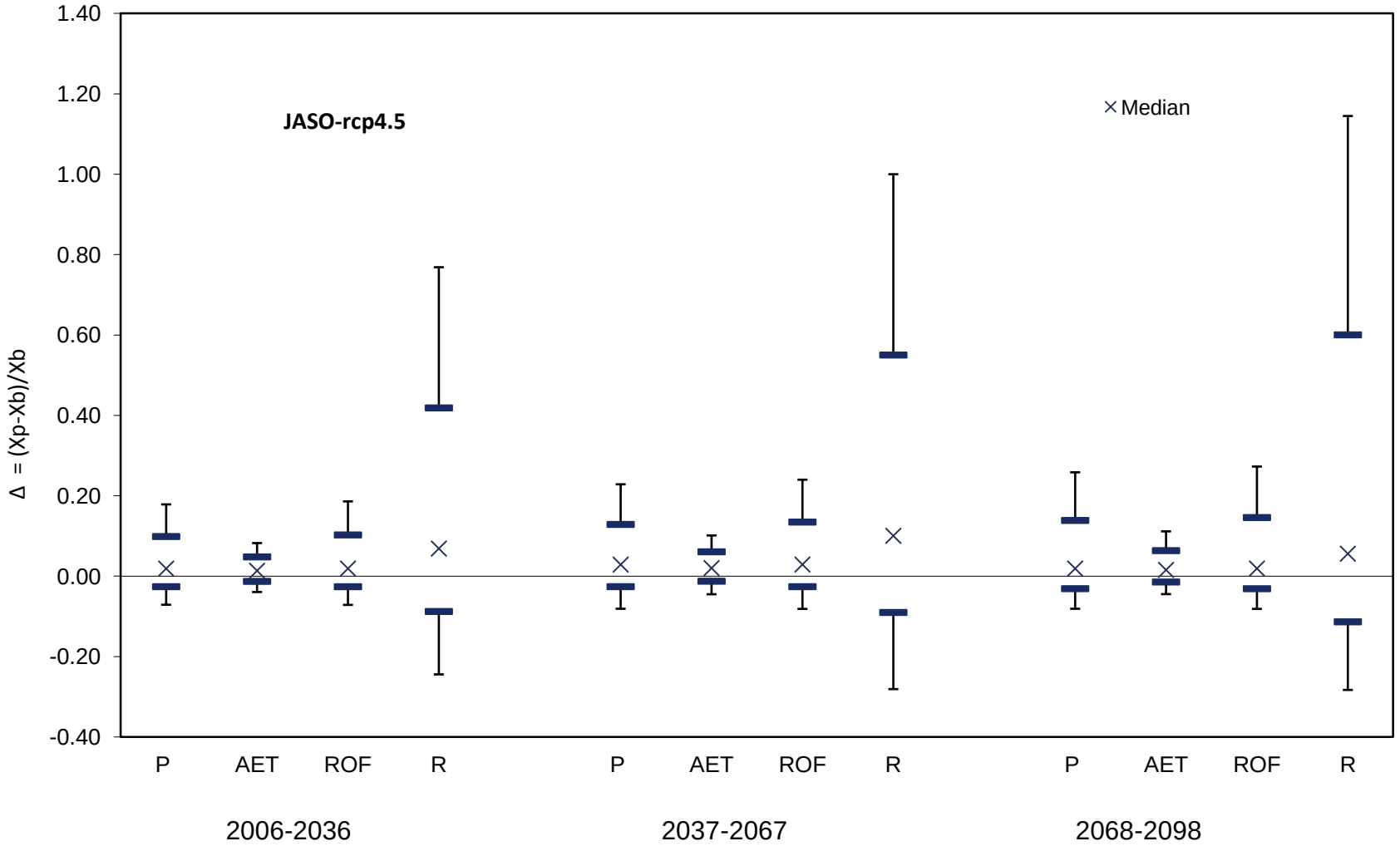

Figure 8.8: (a) Delta of JASO wet seasonal mean (Precipitation, actual evapotranspiration, surface runoff and groundwater recharge weighted by reference mean in three periods under in the rcp4.5 scenarios (the horizontal markers are used to represent Q_{10} and Q_{90}).

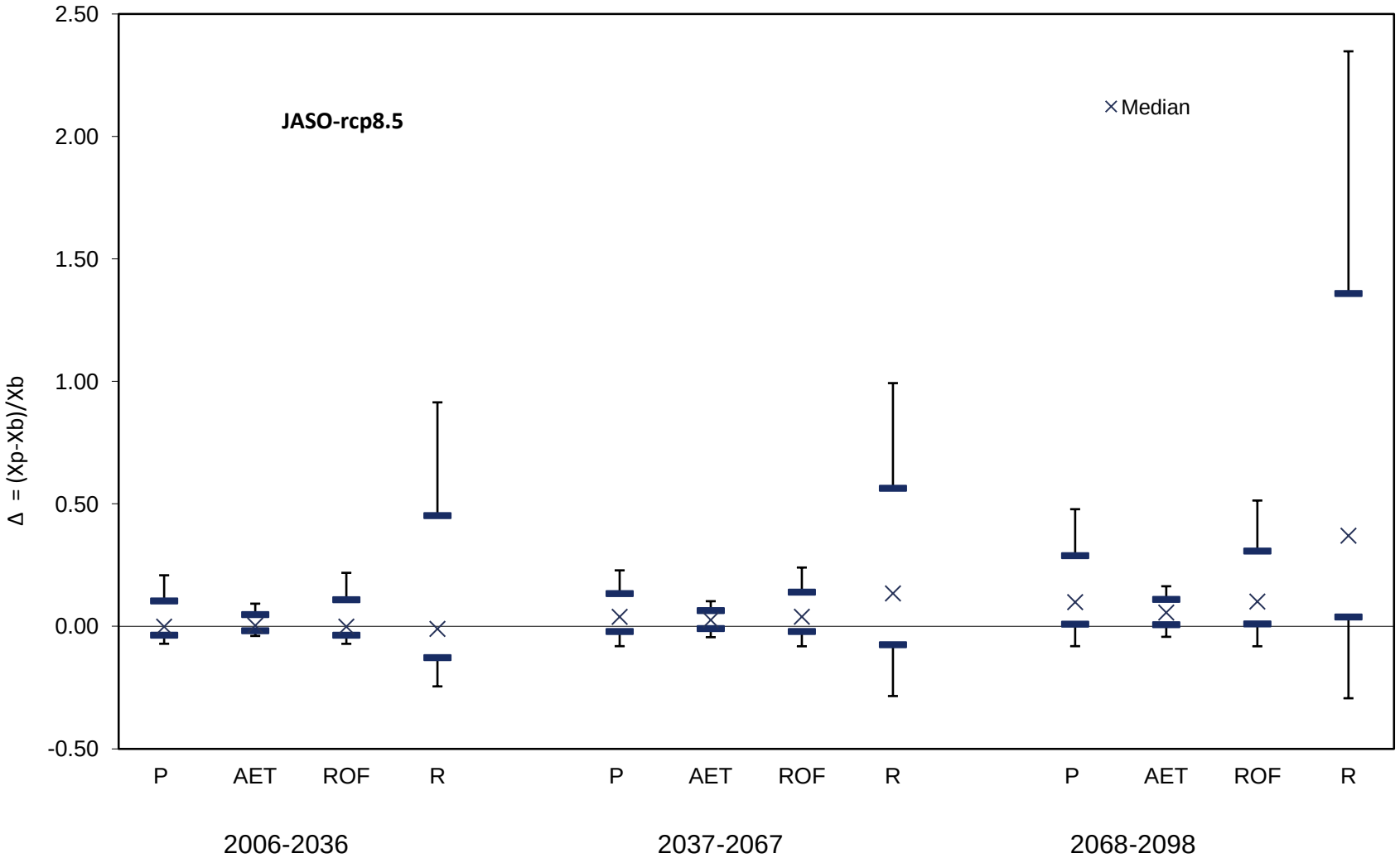

Figure 8.8: (b) Delta of JASO wet seasonal mean precipitation, actual evapotranspiration, surface runoff and groundwater recharge weighted by reference mean in three periods under in the rcp8.5 scenarios (horizontal markers are used to represent Q_{10} and Q_{90}).

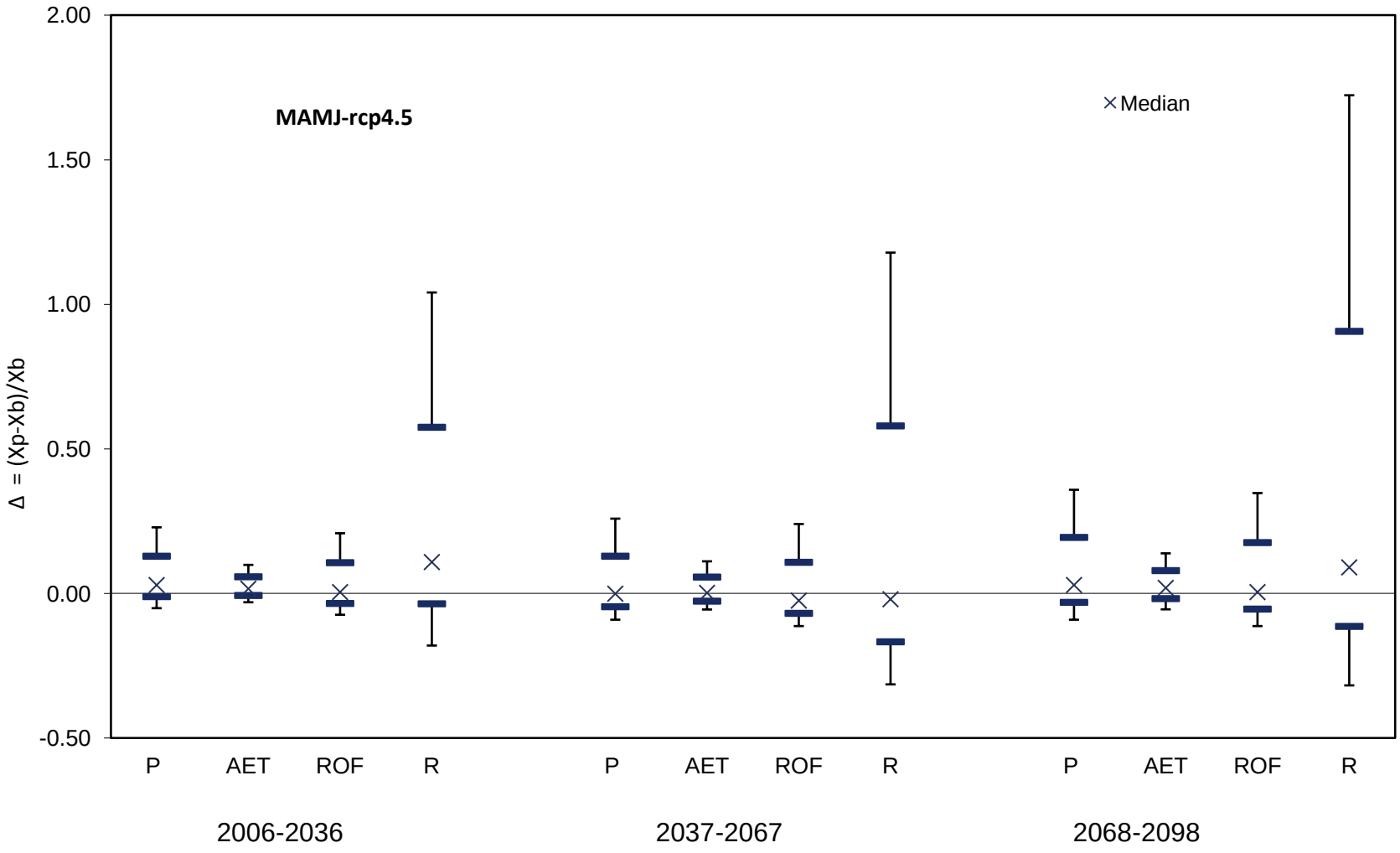

Figure 8.9: (a) Delta of MAMJ wet seasonal mean precipitation, actual evapotranspiration, surface runoff and groundwater recharge weighted by reference mean in three periods under in the rcp4.5 scenario (horizontal markers are used to represent Q_{10} and Q_{90})

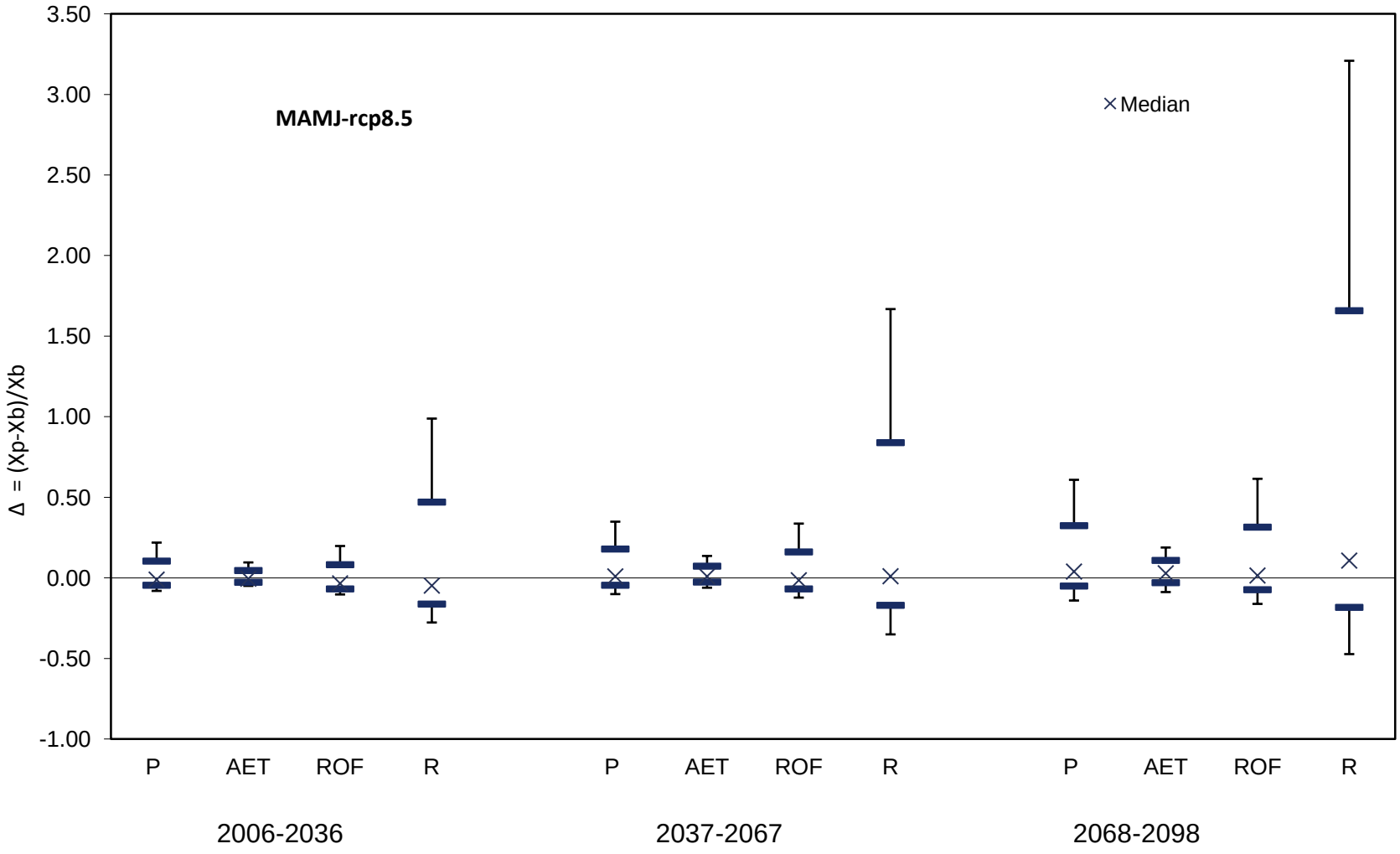

Figure 8.9: (b) Delta of MAMJ wet seasonal mean precipitation, actual evapotranspiration, surface runoff and groundwater recharge weighted by reference mean in three periods under in the rcp8.5 scenarios (horizontal markers are used to represent Q_{10} and Q_{90}).

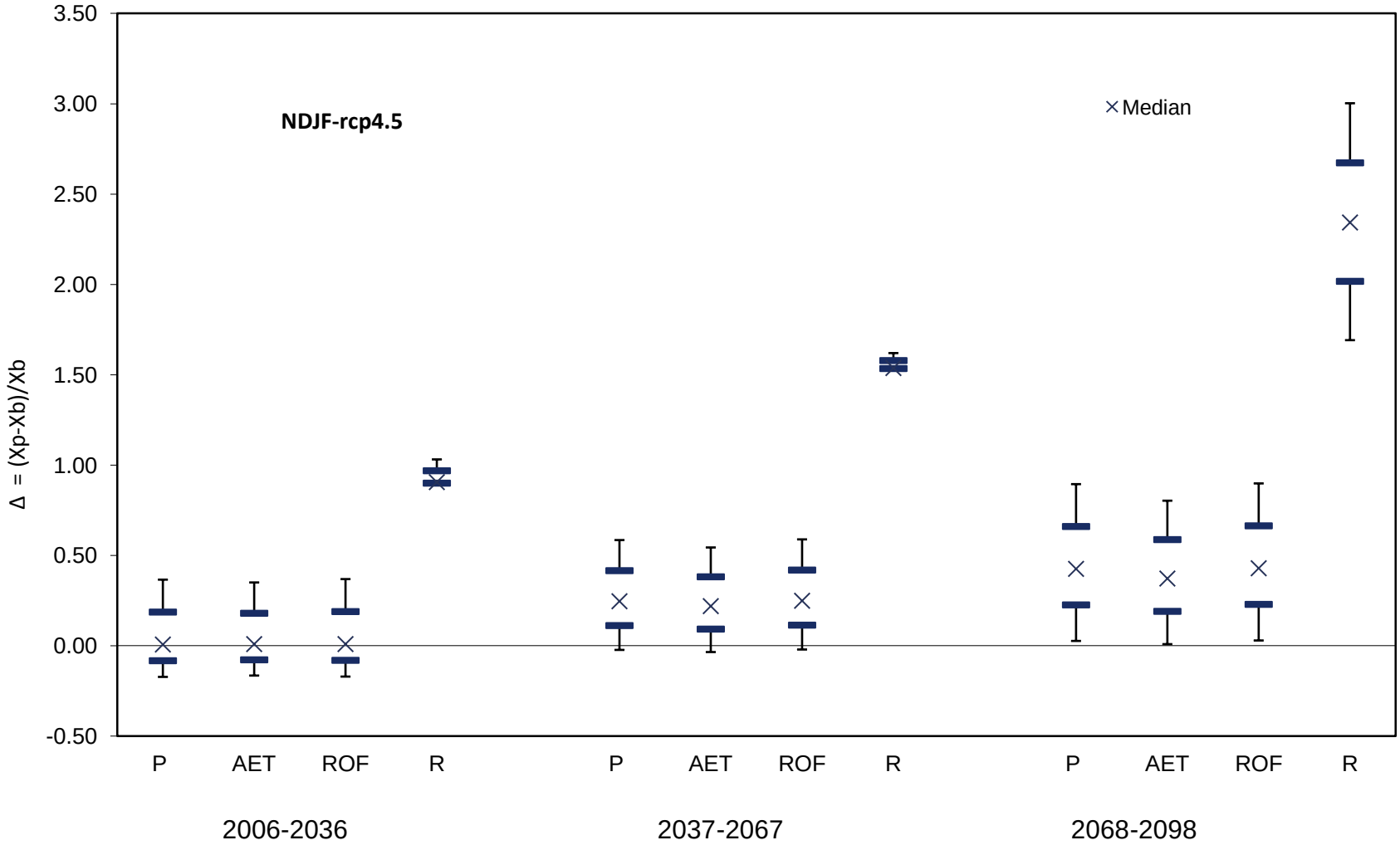

Figure 8.10: (a) Delta of NDJF dry seasonal mean precipitation, actual evapotranspiration, surface runoff and groundwater recharge weighted by reference mean in three periods under in the rcp4.5 scenario (the horizontal markers are used to represent Q_{10} and Q_{90})

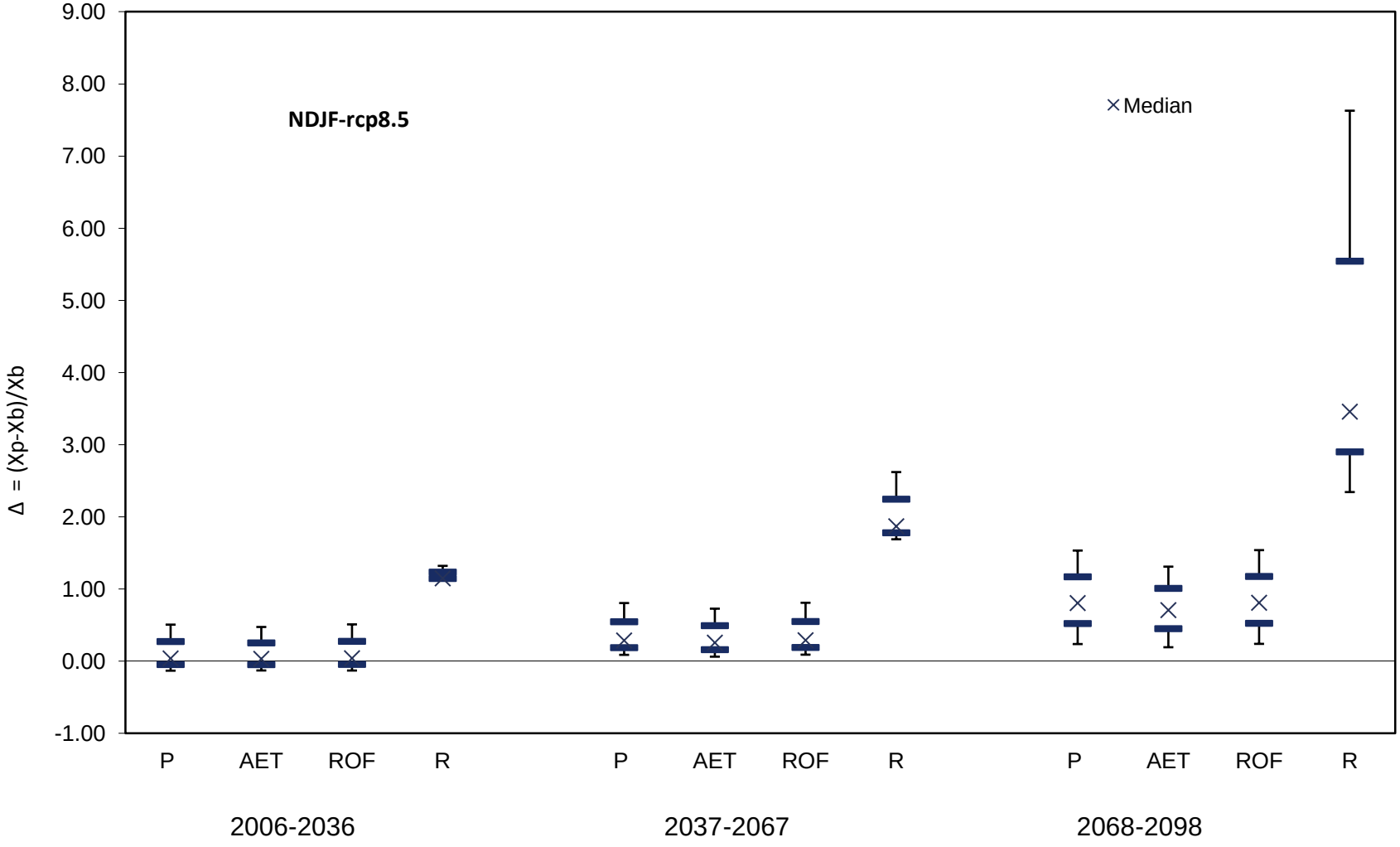

Figure 8.10 (b): delta of NDJF dry seasonal mean precipitation, actual evapotranspiration, surface runoff and groundwater recharge weighted by reference mean in three periods under in the rcp8.5 scenarios (horizontal markers are used to represent Q_{10} and Q_{90}).

The increases in river runoff in MAMJ and JASO months during 2050s, even under precipitation decrease for Q_{10} in these months, could be explained by a delayed runoff due to a high level of groundwater in the earlier period. While the effect on near 2020s to intermediate 2050s future surface runoff and groundwater recharge is small with an exception in actual evapotranspiration, which shows a considerably continuous increase in amount as per precipitation from near future to end of the century.

Likewise, during the dry period (NDJF), there is a remarkable and clear increase in precipitation about 5%, 24.6% and 42.63% for 2020s, 2050s' and 2080s respectively under a low-intermediate rcp4.5 scenarios with lower uncertainties for 90^{th} percentile. This effect plays pronounced role in water availability in the dry season of the basin. So that the actual evapotranspiration and surface runoff are projected to have a steady rise during all periods form near future (2020s) to end of the century (2080s) with some very large sporadic increase in groundwater recharge as compared to wet months in the near and far future. i.e. 243% and 345% increase is projected under both emission scenarios with respect to the reference base period, still, the mean value is small as compared to the mean wet seasonal value.

During this dry season under the high-end scenario, from intermediate to far future period shows a higher rise of all water balance components for Q_{10}, Q_{50}, and Q_{90} percentile, compared to the previous time period, season and low-intermediate rcp4.5 scenarios.

The results obtained for the lakes basin as whole show wide ranges of uncertainty under high-end and intermediate scenarios. The changes in seasonal dynamics of groundwater recharge are quite similar for all three periods. The groundwater recharge increases in virtually all months during two wet seasons (MAMJ and JASO), and the relatively dry months (NDJF) under the high-end scenarios in all future periods. As presented in the Figure 8.10 (a)-(b), the last periods of the Dry season, especially at the end of the century (2080s), shows a quite increase in precipitation and all water balance components including actual evapotranspiration, and somehow an opposite signal under both low-intermediate and high-end scenarios.

8.8. Assessment of expected spatial climate change impacts

In this case, the bias-corrected and downscaled of all 24/26 different GCMs ensemble outputs were used to run the WetSpass model in order to predict the future hydrological components.

The results of the mean future changes of spatially simulated hydrological components in the Abaya-Chamo lakes basin for 2080 are depicted in Figure 8.11(a)-(c) which shows long-term future changes of the main components of the water balance (such as surface runoff, Actual evapotranspiration, and groundwater recharge) under both rcp4.5 and rcp8.5 emission scenario. As precipitation amounts are simulated to increase in the future, all components in hydrologic system keep increasing with different magnitude. For example, in the basin, the areal mean annual actual evapotranspiration increase by 22.1 mm/yr. in between 2020s and 2050s, and also by 16.2 mm/yr. increase in between 2050s and 2080s under rcp4.5 as shown in Figure 8.11(a)-(c) and Appendix 16-18 whereas, under rcp8.5, the increase is about 21.1mm/yr. and 63.2 mm/yr. respectively.

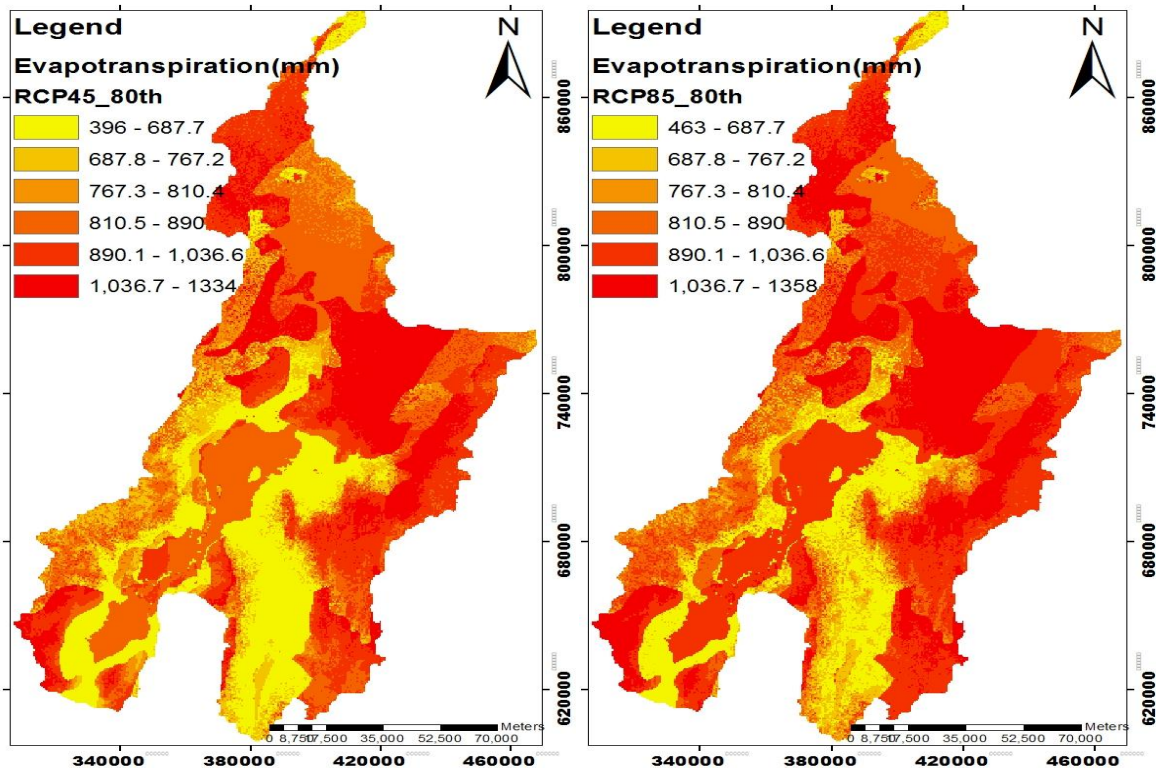

Figure 8.11: (a) simulated mean future actual evapotranspiration for the periods 2080s under both RCP4.5 (left).and RCP8.5 (right)

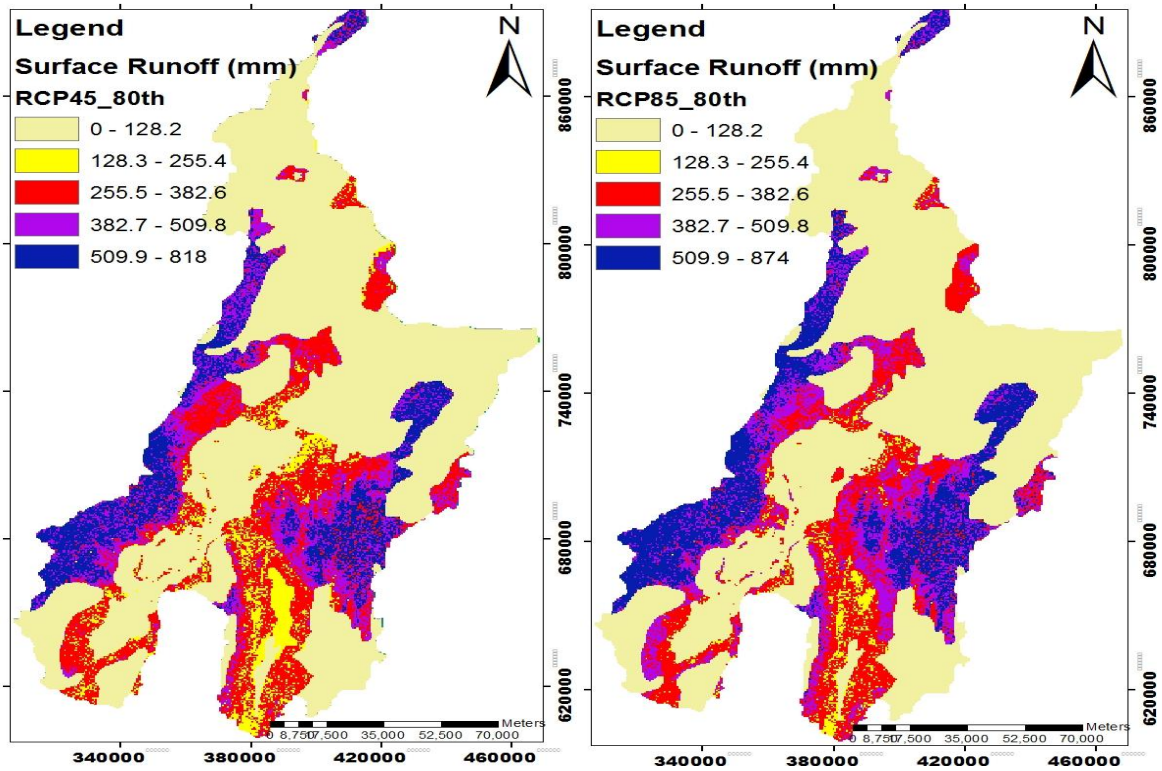

Figure 8.11: (b) simulated mean future surface runoff for the periods 2080s under both RCP4.5(left).and RCP8.5 (right)

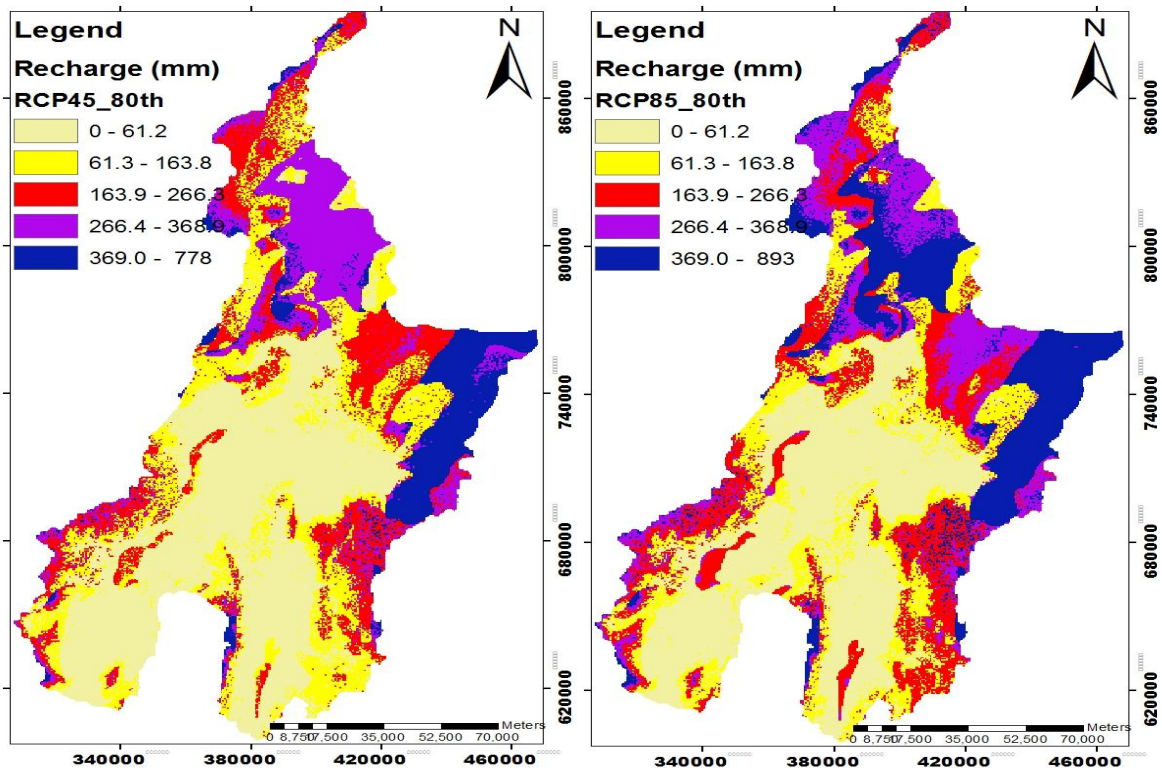

Figure 8.11: (c) simulated mean future groundwater recharge for the periods 2080s under both RCP 4.5(left).and RCP8.5 (right)

Over all, spatially simulated future change of water balance components between periods is summarized in Table 8.5.

Table 8.5: Presents the spatial mean change of hydrologic components between future periods under both RCP4.5 and RCP8.5

Scenarios	Hydrological parameter	Mean change between 2020s and 2050s (mm/yr.)	Mean change between 2050s and 2080s (mm/yr.)
RCP4.5	Actual evapotranspiration	22.1	16.2
	Surface runoff	6.8	5.0
	Groundwater recharge	12.1	9.9
RCP8.5	Actual evapotranspiration	21.1	63.2
	Surface runoff	6.2	21.1
	Groundwater recharge	12.3	45

Annually magnitude of the mean change will greater in between 2020s and 2050s than 2050s and 2080s under RCP4.5, while in the case of RCP8.5 the rate of change will much higher in between 2050s to 2080s which explains the climate change signal will be amplified relatively extra at the end of the century as presented in Table8.5.

8.9. Future water balances due to climate change impact

The simulated future changes of the hydrological components are subjected to relatively largest uncertainties associated with climate model (Samuels et al. 2011). A study by Kay and Davies (2008) pointed the importance of the future estimates of main water balance components due to the projected climate uncertainties with taking into consideration the change/ transferability of the calibrated parameters to the future and computational adequacy of the hydrological models.

A water balance is an accounting of water availability in the storage of water resource system over a particular period of time as the inputs and outputs of water flux. A water balance equation can be used to describe the water flux in and out of a system and can help in managing and planning water resource in a given basin or region. It has also important implication in any socioeconomic developmental activities related to water

resource (Xuand Singh, 1998). Water balance of a water resource system can be assessed periodically in terms of decades or century for many purposes. In this study, the future water balance assessments were used to analyze impacts of climate change on a water resource system.

Climate change impacts on water balance might be reflected through a change in magnitude and fraction percentage of hydrologic components against precipitation (Combalicer et al. 2010). For instance, either the increase/decrease of actual evapotranspiration could result in the decrease/increase in runoff, and the dramatic fluctuations of hydrologic events.

In our lakes basin, the distribution of water balance components due to the projected climate change impact in the future three predetermined periods with respect to the base period under both rcp4.5 and rcp8.5 scenarios is given in Table 8.6 as follows.

Table 8.6: the projected and simulated mean ensemble (Q_{50}) percentage proportion of water balance components compared with base period for selected future periods under both rcp4.5 and rcp8.5

Mean CMIP5 (Q_{50})		Precipitation			Actual Evaporation			Surface runoff		
Scenario	period	mm/yr	%	%Δ	mm/yr	%	%Δ	mm/yr	%	%Δ
	Base (20th C)	1169.6	100	0	873.2	74.7	0	183.4	15.7	0
rcp45	Near	1215.9	100	4.0	900.5	74.1	3.1	190.7	15.7	4.0
	Intermediate	1239	100	5.9	914.2	73.8	4.7	194.4	15.7	6.0
	Far	1274.3	100	9.0	932.6	73.2	6.8	199.9	15.7	9.0
rcp85	Near	1180.8	100	1.0	882.5	74.7	1.1	185.2	15.7	1.0
	Intermediate	1274.3	100	9.0	933	73.2	6.8	199.9	15.7	9.0
	Far	1397.5	100	19.5	986.1	70.6	12.9	216.4	15.5	18.0

Mean ensemble (Q_{50})			Interception			Groundwater recharge		
	Scenario	Period	mm/yr	%	%Δ	mm/yr	%	%Δ
		Base(20th C)	3.1	0.3	0	113.7	9.7	0
	Rcp45	Near	3.2	0.3	4	125.1	10.3	10
		Intermediate	3.3	0.3	6	130.9	10.6	15.1
		Far	3.4	0.3	9	142.0	11.1	24.9
	rcp85	Near	3.1	0.3	1	113.9	9.6	0.1
		Intermediate	3.4	0.3	9	141.5	11.1	24.4
		Far	3.7	0.3	18	183.8	13.2	61.7

Where, **mm/yr** - the long term annual amount
% - percent fraction of precipitation in the respective period
%Δ – percent change as compared to the base period

The magnitude of the water balance components increases in the amount due to increase in the amount of precipitation as a whole for all from near future to the end of the century, under both selected representative pathways as given Table 8.6. But there is a considerable change in the mean percentage change among the components. For example, the long term actual evapotranspiration is about 74.7% of precipitation in the base period, while at the end of the century, the fractional percentage will decline to 73.2% and 70.6% for rcp4.5 and rcp8.5 respectively with respect to corresponding period, however, it increase in amount as compared to the base period by 6.8% and 12.9% .

Conversely, the fractional part of groundwater recharge will increase to 10.3%, 10.6% and 11.1% for 2020s, 2050s and 2080s respectively for rcp4.5, whereas slightly more increase will be expected under rcp8.5 scenarios up to about 13.2% shift in proportions as compared to the precipitation proportions in the corresponding period in the far future (2080s). Also the mean change will increase about 24.9% and 61.7% in 2080^{s} under rcp4.5 and rcp8.5 respectively as compared to present condition. The mean addition of groundwater recharge of 11.4 to 28.3mm/yr under rcp4.5 and 0.2 to 69.6mm/yr under rcp8.5 will be expected until 2099.

As shown up in Table 8.6, the precipitation fractional percentage of surface runoff and interception is similar in the corresponding all respective future period but the mean change will expected to increase linearly to the increase precipitation rate as compared to the base period under both scenarios. On which the mean surface runoff will change about 9% to 18% in 2080s.

The simulated uncertainty ranges of all water balance components based on the projected climate of Q_{10} and Q_{90} is given Appendix 19. For instance: under rcp4.5, the Q_{90} of ensemble projected the water balance at 2080 as 67.1% of Actual Evapotranspiration, 15.7 of surface runoff and the remaining 17.3% as groundwater recharge with 1589.9mm/yr projected precipitation. Whereas under rcp8.5, the precipitation will be 1987.5mm/year and the percent fractions will shift to 59.6 % (AET), 15.9 %(ROF) and 24.5% (R). This range of uncertainty indicates about 35.6% (AET), 72.1 %(ROF) and

329.1% (R) change will expected as compared to the current situation in 2080s as high climate impact on the study are.

8.10. Expected climate change impact on groundwater level

In global climate change studies, the impact of climate change on groundwater resource and the interaction with especially the top unconfined aquifers determine the groundwater levels. It is expected that the projected climate changes in precipitation and temperature will change the groundwater recharge to the aquifer which in turn affect the distribution of hydraulic head as a response.

In this study, the impact of climate change on groundwater was estimated on the basis of two scenarios' (rcp4.5 and rcp8.5) for the periods 2020s, 2050s and 2080s. The simulated groundwater recharge upon projected precipitation and temperature were provided using WetSpass model. The future prediction of groundwater fluctuation were then done using calibrated numerical groundwater flow model based on future simulation of groundwater recharge in the model area.

The simulated WetSpass results in Table 8.7, presents the projected seasonal groundwater recharge values with corresponding precipitation for the respective future periods under rcp4.5 and rcp8.5.

Table 8.7: Presents the simulated seasonal mean precipitation and recharge for the future period based on projected climate change

		RCP4.5			RCP8.5		
	Season	**2020s**	**2050s**	**2080s**	**2020s**	**2050s**	**2080s**
Precipitation (mm)	**JASO**	491.3	496.1	491.3	481.6	500.8	529.8
	NDJF	162.3	200.9	229.8	167.1	207.3	290.9
	MAMJ	541.4	525.7	541.4	520.4	530.9	546.7
Recharge (mm)	**JASO**	61.2	63.1	60.6	56.8	65.0	78.5
	NDJF	-0.4	2.2	4.8	0.5	2.4	8.6
	MAMJ	66.4	58.7	65.4	57.1	60.5	66.3

The MODFLOW simulation results in Figure 8.12(a)-(b) presents mean seasonal future changes of groundwater head against precipitation and groundwater recharge, relative to the present situation under selected scenarios (rcp4.5 and rcp8.5).

Generally, the main source of the groundwater resources and cause of its changes is related to recharge into shallow groundwater, therefore the highest change as impact on resources is expected in the shallow unconfined aquifer.

The simulation result shows the groundwater level rise linearly with precipitation and recharge. Under both climate change scenarios, the mean dynamic groundwater resources in all season will predict to increase, except for wet seasons particularly in JASO_rcp8.5 (2020s) and MAMJ_rcp4.5 (2020s to 2050s). Figure 8.14 (a)-(b) shows the increase of JASO mean groundwater depth is about 0.8% and 0.3% in 2050s and 2080s respectively under rcp4.5 relative to the present.

In the rcp8.5 case, the highest groundwater level is expected in 2080s particularly in a second wet season (JASO). At that time generally, the mean seasonal groundwater recharge will increase from 65mm/year to 78.5mm/year adding a mean of 13.5mm/year. Similar increment of resources is anticipated in rcp8.5 about 8.8% increases in water level as compared to present condition.

Under dry condition (NDJF-rcp4.5/rcp8.5), as given in Figure 8.14 (a)-(b) the situation is more dramatic and the changes in hydrological parameters are more pronounced. The overall increase in projected seasonal precipitation and recharge leads to an increase in the mean groundwater level of the basin ranges from 0.1 to 0.5% and 0.1 to 1.6% for rcp4.5 and rcp8.5 respectively

At the end of the century (1968-2099), the highest increase of mean annual shallow groundwater recharge is predicted about 24.8% and 61.7% relative to present under rcp4.5 and rcp8.5 respectively; consequently the corresponding average annual groundwater level could rise by 0.4% and 3.7%. Therefore in annual base for all future periods, there will no danger of groundwater resources decrease rather an increase might affect the ecosystem especially low lying discharge areas

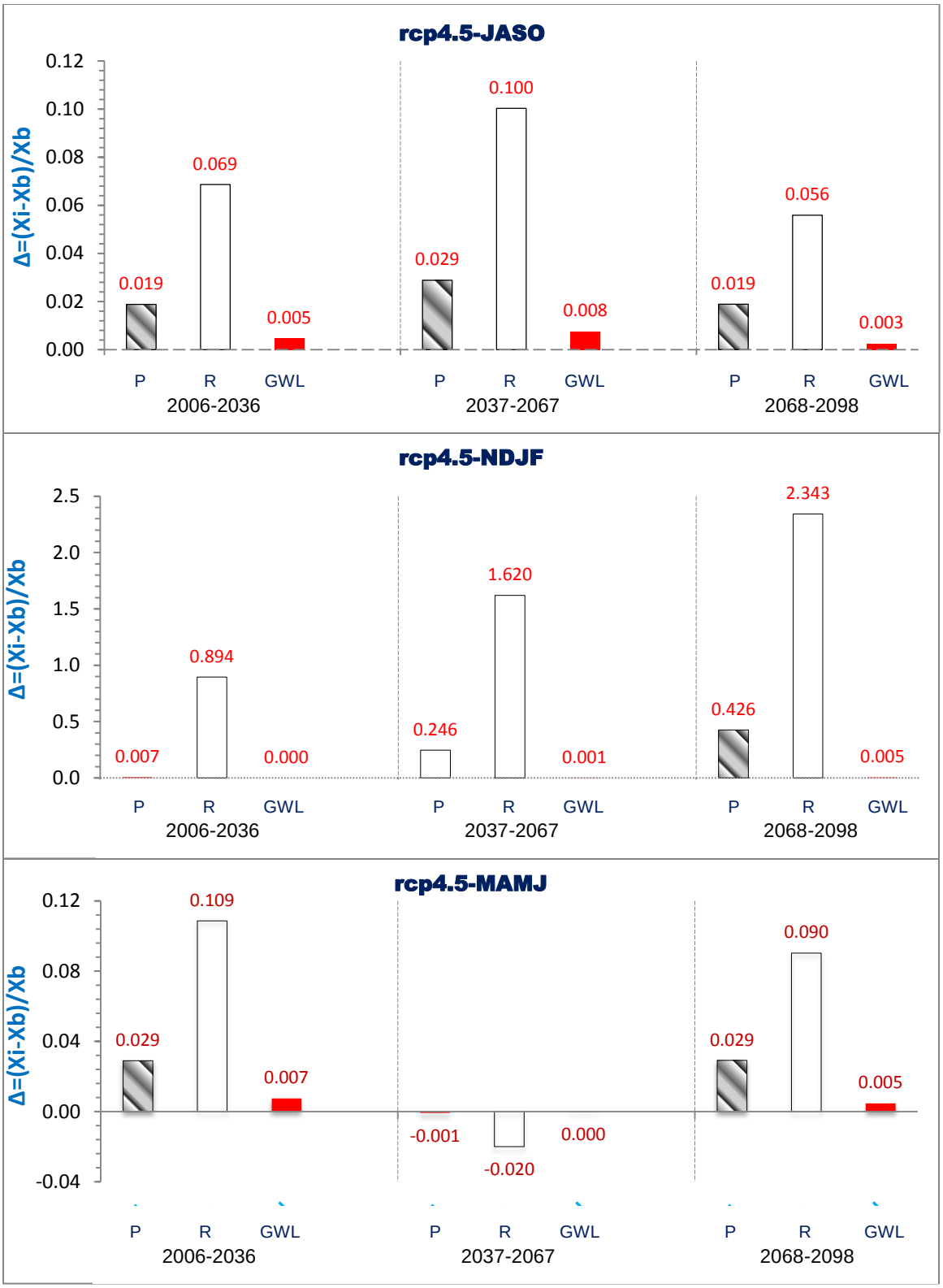

Figure 8.12: (a) shows the delta change of seasonal (JASO, NDJF, and MAMJ) precipitation, groundwater recharge and groundwater level with respect to reference base period under rcp4.5.

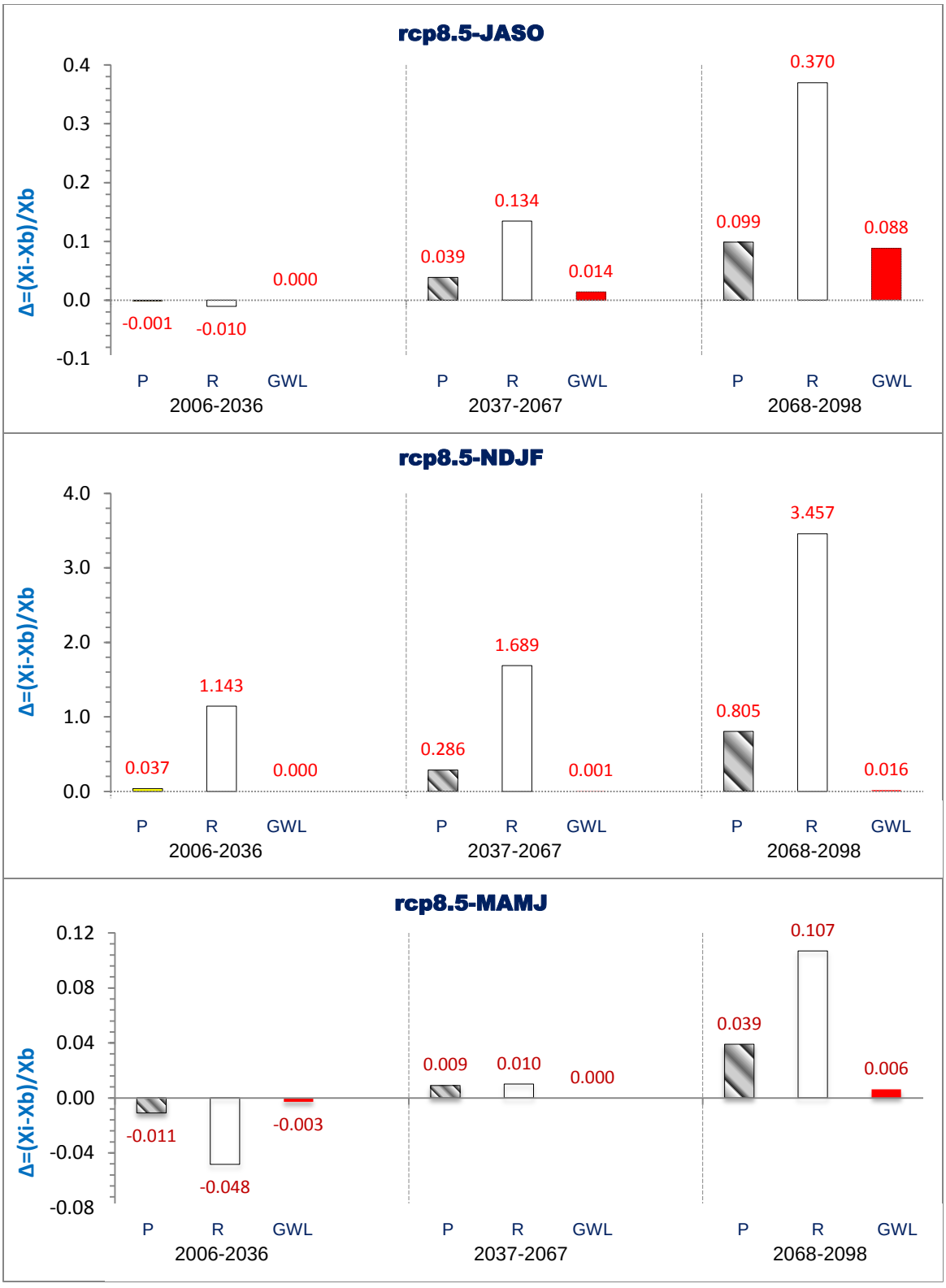

Figure 8.12: (b) shows the delta change of seasonal (JASO, NDJF, and MAMJ) precipitation, groundwater recharge and groundwater level with respect to reference base period under rcp8.5.

CHAPTER NINE

9. CONCLUSION AND RECOMMENDATION

9.1. Conclusions

Fragmented scientific studies, poor resource management practice in the existing knowledge and traditional way of future water resource estimation needs modern scientific prospects and approaches to support the overwhelming rapid growth of population and satisfying increasing water demand.

A comprehensive and integrated evaluation of expected changes is fundamental for a whole range of scales of water resource management and planning under projected global changes. This research is believed to provide a sound foundation for modern scientific direction in water resource evaluation as decision support tool by establishing integrated surface and groundwater model under changing the climate for sustainable water resources management and is only viable by considering the complete water cycle in the lake basin.

Thus, the projected changes were evaluated by using the latest CMIP5 GCM model for future periods (2020s, 2050s and 2080s) under rcp4.5 and rcp8.5. These changes were then used to force independently modeled spatially distributed WetSpass model and ModFlow under steady state condition to represent the surface and sub-surface hydrologic system. A parameter integration of surface and groundwater model has an important advantage in the inclusion of verity of cases in an integrated manner since the lakes basin is characterized as a complex rift margin zone due to its diverse variation in topography, hydro-climate feature, and geology and associated geologic structure. Being the first integration work (CMIP5-WetSpass-MODFLOW) for the lake basin, a lot of challenges and constraints were encountered particularly in the groundwater flow modeling of the whole area as one unified system.

Hydro-meteorological and hydrogeological data are generally very limited and unevenly distributed; mostly concentrated around northeast and west of Lake Abaya. An effort has been made to apply various regionalization techniques and harmonize datasets to the maximum possible reliability of the study in representing the actual situation. This includes characterization of the hydrologic system using baseflow index indirectly based on different spatially varying basin features (geomorphometric, hydro-Climatic, land cover and aquifer variables).

The analysis and results overall elucidated the high range spatial variation and complexity of basin hydrology in terms of hydrodynamics and hydrologic system as part of rift margin zone. This last summery section point out the most significant study implications of the whole thesis work.

Estimation of groundwater recharge is the most challenging parameter in hydrogeology. Base flow separation techniques indicate a significant spatial distribution of the recharge for the study area. The estimated average annual base flow of major sub-river basins based on sixteen gauged rivers are varied between (0.21 to 3.37)m^3/s, (0.25 to 3.61)m^3/s, (0.30 to 2.94)m^3/s using three base flow separation algorithms (such as RAP, K, and TP respectively) with estimating 44% total discharge accounts for groundwater contribution. The estimate of the BF were compared with spatially distributed simulation groundwater recharge (WetSpass model) and the model proves about 38.3% of the total flow as a groundwater recharge with around 5.7% overestimation by RAP and TP baseflow separation.

Look up tebles of the WetSpass model are adjusted or contextualized to the lakes basin prevailing conditions and validated by total mean river discharge and estimated base flow. The overall areal water balance is presented under long-term average annual conditions, the balance structure becomes dominated by Actual evapotranspiration (74.6%); surface runoff is approximately 15.7% and the rest part as a groundwater recharge (9.7). Only a small fraction of the annual precipitation remains to interception (0.3%). In another word, the water resource availability of the lakes basin as a whole has about a total of 22.1 billion lit/year rainfall potential, out of which around 16.5billion

lit/yr. account for the actual evapotranspiration as the largest part and the rest are a surface runoff and groundwater recharge are 3.5 billion lit/yr. and 2.1 billion lit/yr. respectively. Therefore, the lakes basin has a total of nearly 5.6 billion lit/yr available potential for both surface and groundwater resources. Future water demands of both the potential irrigation and another development strategy can be supported according to the respective potential by both the surface and groundwater resources in the lakes basin.

The multivariate analysis is used in characterizing the basin hydrologic system based on the baseflow index. Following these, the physical interpretations about the interaction in the hydrologic system among variables show relatively similar result with spatially distributed water balance model.

In terms of hydrologic system interaction, land use and soil class combination effect from the model output revealed that the largest actual evapotranspiration found on forest cover with sandy clay loam and sandy loam soils textural class. Whereas, the highest surface runoff occurs on clay soils with agricultural land, swamp/marsh or wood/bush-land land use. A small change in soil texture can influence more surface runoff than land use type. The highest spatial variation of recharge is found by the soil textural classes which have small standard deviation than land use type. Besides, recharge increases distinctly with coarse soil texture regardless of the land cover classes.

Moreover, Multivariate analysis (using geomorphometric, hydrogeological, land cover and hydro-climatic attribute) in controlling basin hydrology suggests, morphometric variables such as slope, Elevation, hypsometric integral with associated climate (rainfall and Potential evaporation) appear to be a dominant factor than land cover and lithological factor in Abaya-Chamo lakes basin this explain the evolution of geomorphological features have been in charge of controlling the hydrological system. Additionally, the peak baseflow yield is found at highest elevation/physiographic region in the plateau. This highest physiographic region in the study area is characterized with high hypsometric integral and low drainage density as compared with the escarpment and the rift floor.

The calibrated steady-state groundwater flow modeling simulation of Abaya-Chamo lakes basin also confirmed through flow system in terms of groundwater gradient and flow direction, on which groundwater flow happens from the plateau toward the floor into the lakes from both directions with high gradient exist in the escarpment.

Upon the range of used CMIP5 multi-model GCMs, the projected future climate especially precipitation showed relatively high uncertainty for selected scenarios in the study area.

The performed simulations using CMIP5 model output show steadily rising temperatures in the entire lakes basin. For the periods 2037–2067 and 2070–99, annual-mean temperatures are expected to increase with an area average of 1.8^0C and 2.8^0C, both compared to the 1976–2005 mean. At the same time, precipitation amounts are expected to increase annually in the entire Abaya-Chamo lakes basin.

The projected precipitation trends are insignificant until the middle of the century about 2% (till 2037), although an increase is pronounced a nearly between 7.5 and 14.2% in the intermediate and end of the century with relatively higher uncertainties which can be related to the variability of annual rainfall in the region. These mean change precipitation consequently affects the mean AET, ROF and R vary from (5.8 to 9.9%), (7.5 to 13.5%) and (19.8 to 43.3%) respectively.

Making use of multimodal and quartile approach was facilitated in reducing the range of uncertainty by either some a few models together or single model projections. For the end of the century (2080s), the maximum increase in rainfall is projected in the ranging between 35.9% and 69.9%. Correspondingly, the expected maximum impact as a change on AET, ROF and R would vary from (22.1to 35.6%), (36.1 to 72.1%) and (141.4 to 329.1%) respectively for high emission scenario.

While under low emission scenario, the long term projection of precipitation in 2080s will be in the ranging between (-1 to 7%) and the corresponding expected minimum impact as a change on AET, ROF and R would vary from (-0.5 to 5.5%), (-1 to 7%) and (-4.9 to 17.2%) respectively.

For all months, groundwater recharge was the most sensitive component showing the highest percent increase with respect to present days under both scenarios. The increase of groundwater recharge, in turn, affects groundwater level. Surface runoff and actual evapotranspiration are also linearly increase with projected seasonal precipitation but in the intermediate period (2037-2067) slight decrease in a surface runoff will be anticipated only in wet season. These combined with the increase in wet season groundwater level and groundwater discharge over low laying areas, might pose more risk of flooding especially in the 2080s (2068-2099). On the other hand, the increase in seasonal amount in groundwater recharge and groundwater depth in dry period from near to far future result in a small difference between dry months and wet months of the year, which implies smaller seasonal fluctuation of the groundwater levels, may influence the hydrodynamics, the distribution surface-groundwater fluxes and the ecosystem.

Generally, there is a significant change is observed in the percentage fraction of future water balance as compared to the base period in all water balance components. But with regard to the projected precipitation, the corresponding fraction between water balance components particularly actual evaporation and recharge changes. For instance the simulated mean water balance under rcp4.5 in 2080 projected as 73.2% (AET), 15.7% (ROF) and 11.1% (R) with 1274.3mm/yr projected precipitation. Whereas under rcp8.5, the precipitation will be1397.5mm/year and the percent fractions will shift to 70.6 % (AET), 15.5 % (ROF) and 13.2% (R). Thus, water balance fraction percentage of Actual evapotranspiration will decline by -1.5% and -4.1% under rcp4.5 and rcp8.5 respectably at the end of century as compared to present water balance while, the fractional percentage will rise for groundwater recharge about 1.4% and 3.5%.

This study has both practical and scientific importance. It provides the outline of climate, surface water and groundwater systems highlighting hydrological and hydrogeological characteristics of the Abaya-Chamo lakes basin, On the other hand, is the first integrated CMIP5- WetSpass-MODFLOW model through parameter for the lake basin as a single unit in steady state condition, concepts, methods, and synthesis embedded in this study can be useful reference for future analogous research that will be conducted in similar modeling environments. Furthermore, data, maps, and illustrations provided in this study

can be used for sustainable water resource evaluation, managements and planning .Such study is becoming more important in the developing world including many basins in Ethiopia.

9.2. Recommendations

The established relationship between multivariate factors a major river basin of study can be extrapolated as a base for estimating the base flows in the ungauged section of the basin with great care and can be used easily with reasonable accuracy. This is pointing the advantage of regional base flow separation for characterization of the hydrologic system.

The spatially distributed WetSpass model is also verified for its applicability in the assessment of regional long-term water resources quantification purposes in contemporary practice. Thus, the model can be appreciated in other similar basins, especially in developing regions with limited high-resolution time series and spatial data.

Despite, the ranges of uncertainties of GCM models in projecting future scenario in the study area, the analysis is strongly recommended making use of more than one single GCM model for impact assessment in order to provide the best available representation of projected climate change and used to reduce overconfidence due to model-specific bias.

Further studies pertaining to climate change impacts for the study region should still focus mainly on these scenarios (RCP4.5 and RCP8.8). However, the appropriate adaptation management, planning, and mitigation strategies will depend on the potential impact climate change. Also, the upcoming continuous observations in the area may reveal which scenario is more likely to take place.

In this study, steady-state groundwater flow model was used partly to simulate long-term groundwater balance and the sensitivity/seasonal variation of groundwater system to the future projected climate in the study area. However further extreme event studies should be conducted based on time-varying, more rigorous and data-intensive transient flow modeling approach.

Also, the calibrated groundwater flow model for the study area will still further be calibrated for plenty of additional investigations of hydro-stratigraphic, aquifer properties, stress parameters and evenly distributed observation wells in order to enhance the predictive capability.

The current water demands for irrigation and another development strategy should be supported to the respective surface and groundwater resources potential in the lake basin. Besides, climate change is expected to bring significant changes to the hydro climate of the region.

The escarpment and highland of west of lake-Abaya is significantly potential area for flash flooding, land degradation and sediment transport into the lakes. Additionally the west highland is appeared as recharge zone for Arba Minch-spring. While, the eastern plateaus identified as dominant recharge zones and groundwater influx to lakes. Therefore, as per the role of water resource availability in socio-economic development and owing potential future changes in both hydrologic components and regimes with respect to findings. It is so necessary to develop sustainable adaptive measures especially on the annual and seasonal regime for effective water use and development purposes over the sub-catchments with focusing on regulation of land and water resource through integrated manner.

REFERENCE

Abebe T, Manetti P, Bonini M, Corti G, Innocenti F, and Mazzarini M (2005). Geological map of the N. MER. The Geological Society of America, Boulder, CO

Abebe, A., Foerch, G., (2006). Catchment characteristics as predictors of base flow index(BFI) in Wabi-Shebele-river basin, East Africa. In: Conference on International Agricultural Research for Development, Tropentag, The University of Bonn, pp. 1–5.

Abrahams AD. (1984). Channel networks: A geomorphological perspective. Water Resources Research20 (2): 161– 168.

Abu-Saleem A, Al-Zubi Y, Rimawi O, Al-Zubi J and Alouran N (2010). Estimation of water balance components in the Hasa basin with GIS-based WetSpass model. Journal of Agronomy 9(3): 119-125

Al Kuisi M. and El-Naqa A. (2013). GIS-based spatial groundwater recharge estimation in the Jafr basin, Jordan-Application of WetSpass models for arid regions. Revista Mexicana de Ciencias Geologicas 30(1):96-109

Alemayehu T, Legesse D, Ayenew T et al. (2005) Hydrogeology, water quality and degree of groundwater vulnerability to pollution in Addis Ababa, UNEP-UNESCO report, Nairobi

AMS (2012). Glossary of Meteorology. American Meteorological Society, Boston, Mass. http://glossary.ametsoc. org/wiki/Climate change (accessed January 2014).

Anderson MP, and Woessner WW, (1992). Applied groundwater modeling. Academic Press, Inc. San Diego, California: 381 pp

Armbruster V and Leibundgut C (2001) Determination of spatially and temporally highly detailed groundwater recharge in porous aquifers by an SVAT model. Physics and Chemistry of the Earth, Part B: Hydrology, Oceans, and Atmosphere, 26(7):607-611.

Arnold JG, Muttiah RS, Srinivasan R and Allen PM (2000) Regional estimation of base-flow and groundwater recharge in the Upper Mississippi-river basin. Journal of Hydrology, 227(1):21-40

Arnold, J.G., Allen, P.M., (1999). Validation of automated methods for estimating baseflow and groundwater recharge from streamflow records. Journal of the American Water Resources Association 35, 411–424

Arnold, J.G., Allen, P.M., Muttiah, R., Bernhardt, G., (1995). Automated base flow separation and recession analysis techniques. Ground Water 33, 1010–

1018.
Astatike, Kiflu; Sima, Jiri (2012): Hydrogeological and hydro-chemical maps of Asela NB 37-3. Explanatory notes. AQUATEST a.s., Prague. Czech Rep.
Awulachew S. B. (2001).Investigation of water resources aimed at multi-objective development with respect to limited data situation: The case of the Abaya-Chamo basin, Ethiopia. Ph.D. Thesis, Technische Universität, Dresden, Germany.
Awulachew S. B. (2006).Characteristics Investigation of physical and bathymetric characteristics of Lakes Abaya and Chamo, Ethiopia, and their management implications
Ayenew, T., (2002). Recent changes in the level of Lake Abiyata, central main Ethiopian Rift. Hydrological Sciences Journal. 47(3): 493-503.
Ayenew, T., (2009). Natural Lakes of Ethiopia. Addis Ababa University Press. Addis Ababa, Ethiopia
Ayenew.T, (2007). Comparative study of the hydrology and hydrogeology of selected Ethio-Kenyan- rift lakes. Catchment and Lake Research, LARS 2007
Baldwin, M. E., cited (2000): QPF verification system documentation. [Available online at http://sgi62.wwb.noaa.gov:8080/testmb/ verfsp.doc.html.]
Batelaan O, De Smedt F and Triest L (2003) Regional groundwater discharge: phreatophyte mapping, groundwater modeling and impact analysis of land-use change. Journal of Hydrology, 275(1-2):86-108
Batelaan O., (2006). Phreatology. Characterizing groundwater recharge and discharge using remote sensing, GIS, ecology, hydrochemistry and groundwater modeling. Department of Hydrology and Hydraulic Engineering Faculty of Engineering Vrije Universiteit Brussels.
Batelaan, O., De Smedt, F., (2007). GIS-based recharge estimation by coupling surface-subsurface water balances. J. Hydrol. 337 (3–4), 337–355.
BCEOM – French Engineering Consultants, in association with ISL, BRGM (1999). Abbay-river Basin Integrated Development Master Plan Project, phase 2 Volume I Main report.
Bekele, S., (2001). Investigation of water resources aimed at multi-objective development with respect to limited data situation: The case of Abaya-Chamo basin, Ethiopia. –Institut für Wasserbau und Technische Hydromechanik, Wasserbauliche Mitteilungen, 19. Dresden.
Belete, A (2009). Climate Change Impact on Lake Abaya Water Level. Unpublished MSc. Thesis, Addis Ababa University, Addis Ababa.
Beltrando G., P. Camberlin (1993). Interannual variability of rainfall in the Eastern Horn of Africa and indicators of atmospheric circulation, International

Journal of Climatology 13, 533-546
Bergstrom S, Carlsson B, Gardelin M, Lindstrom G, Pettersson A, Rummukainen M. (2001). Climate change impacts on run-off in Sweden—assessments by global climate models, dynamical downscaling and hydrological modeling. Climate Research 16: 101–112
Block P., Balaji Rajagopalan (2007). Interannual Variability and Ensemble Forecast of Upper Blue Nile Basin Kiremt Season Precipitation, Journal of Hydrometeorology. Vol.8, 10.1175.
Bloomfield JP, Allen DJ, and Griffiths KJ (2009) Examining geological controls on the baseflow index (BFI) using regression analysis: An illustration from the Thames Basin, UK. Journal of Hydrology373 (1–2): 164–176.
Bloomfield JP, Bricker SH, and Newell AJ (2011): Some relationships between lithology, basin form, and hydrology: a case study from the Thames basin, UK. Hydrol. Process.25, 2518– 2530.
Bonan G., (2002). Ecological Climatology. Cambridge, U.K.: CUP. Boorman D., Sefton.M., 1997.Recognising the Uncertainty in the Quantification of the Effects of Climate Change on Hydrological Response. Climatic Change 35 (4): 415-434.
Camberlin, P. (2009). Nile Basin Climates. In "The Nile: Origin, Environments, Limnology and Human Use", Dumont, Henri J. (Ed.), Monographiae Biologicae, Springer, 307-333.
Carlston CW. (1963). Drainage density and streamflow, USGS Geological Survey Professional Paper, 422-C.
Casanova S, Ahrens B (2009) on the weighting of multi-model ensembles in seasonal and short-range weather forecasting. Mon Weather Rev 137(11):3811–3822. doi:10.1175/2009MWR2893.1
Chapman, T. (1999) A comparison of algorithms for streamflow recession and baseflow separation. Hydrol. Processes 13(5), 701–714.
Chapman, T., (1999). A comparison of algorithms for streamflow recession and baseflow separation. Hydrological Processes 13,701–714.
Chapman, T., Maxwell, A., (1996). Baseflow separation – comparison of numerical methods with tracer experiments. In: Hydrology and Water Resources Symposium, Institution of Engineers Australia, Hobart, pp. 539–545.
Chen (2006). Downscaling of daily precipitation with a stochastic weather generator for the subtropical region in South China, Hydrol. Earth Syst. Sci. Discuss., 3, 1145–1183.
Cherkauer, D.S., Ansari, S.A., (2005). Estimating groundwater recharge from topography, hydrogeology, and land cover. Ground Water 43 (1), 102–112.

Chorowicz, J., Collet, B., Bonavia, F., and Korme, T., (1999), Left-lateral strike-slip tectonic and gravity induced individualization of wide continental blocks in the western Afar margin: Eclogae Geologicae Helvetiae, v. 92, p. 149–158

Combalicer, E.A., R.V.O. Cruz, S. Lee, and S. lm, (2010): Assessing climate change impacts on water balance in the Mount Makiling forest, Philippines. Journal of Earth System Science

Coulié E, Quideleur X, Gillot PY, Courtillot V, Lefevre JC, Chiesa S (2003) Comparative K–Ar and Ar/Ar dating of Ethiopian and Yemenite Oligocene volcanism: implications for timing and duration of the Ethiopian traps. Earth Planet Sci Lett 206:477–492

Cubasch U, Meehl GA, Boer GJ, Stouffer RJ, Dix M, Noda A, Senior CA, Raper S, Yap KS (2001) Projections of future climate change. In: Houghton JT, Ding Y, Griggs DJ, Noguer M, van der Linden PJ, Dai X, Maskell K, Johnson CA (eds) Climate Change 2001: the scientific basis. The contribution of Working Group I to the Third Assessment Report of the IPCC Cambridge: University Press, pp 525–582

Dąbrowski S., Kapuściński J., Nowicki K., Przybyłek J., Szczepański A., (2011). Mathematical modeling methodology in hydrogeological research and calculations. Poradnik metodyczny. Bogucki Wyd. Naukowe, Poznań.

Davidson (1983): The Omo-river Project, Reconnaissance Geology and Geochemistry of Parts of Ilubabor, Kefa, Gemu Kefa and Sidams, Ethiopia, EIGs.

De Vries, J.J., Simmers, I., (2002). Groundwater recharge: an overview of processes and challenges. Hydrogeology Journal 10 (1), 5–17.

De Wit, M., and Stankiewicz, J (2006). Changes in surface water supply across Africa with predicted climate change, Science, 311, 1917– 21.

Delin, G.N., Healy, R.W., Lorenz, D.., Nimmo, J.R., (2007). Comparison of local to regional scale estimates of groundwater recharge in Minnesota, USA. Journal of Hydrology 334, 231–249.

Demis, Alemirew (2009): Detailed Hydrogeological and Hydro Geophysical Study of Ketar Basin, Central Ethiopian Rift (Lakes Region).

DEMUTH, S. (1993): Investigation of low water in Western Europe). Freiburger Schriften zur Hydrologie 1. Freiburg im Breisgau.

Diro G, Black E, Grimes D (2008) Seasonal forecasting of Ethiopian spring rains. Meteorol Appl 15:73–83

Duan Q Y and Phillips T J (2010) Bayesian estimation of local signal and noise in multimodel simulations of climate change J.

Eckhardt, K., (2005). How to construct recursive digital filters for baseflow

separation. Hydrol. Proc. 19 (2), 507–515.
ECMWF cited (2001): Gridpoint to grid point interpolation. [Available online at http://www.ecmwf.int/publications/manuals/libraries/interpolation/gridToGridFIS.html.]
Endalew, Gebru Jember (2007). Changes in the frequency and intensity of extremes over Northeast Africa, KNMI scientific report, WR 2007-02, De Bilt, The Netherlands
FAO, (1998). Land and water digital media series – the soil and terrain database for northeastern Africa. FAO, Land and Water Digital Media Series no. 2, FAO, Rome.
Fazal, M.A., Imaizumi, M., Ishida, S., Kawachi, T., Tsuchihara, T., (2005). Estimating groundwater recharge using the SMAR conceptual model calibrated by genetic algorithm. Journal of Hydrology 303 (1–4), 56–78.
Fiedler F.R., Ramirez J.A., (2000). A numerical method for simulating discontinuous shallow flow over an infiltrating surface. International Journal of Numerical Methods in Fluids32 (2): 219–240.
Flint, A.L., Flint, L.E., Kwicklis, E.M., Fabryka-Martin, J.T., Bodvarsson, G.S., (2002). Estimating recharge at Yucca Mountain, Nevada, USA: comparison of methods. Hydrogeology Journal 10 (1), 180–204.
Fowler, H. J., S. Blenkinsop, C. Tebaldi (2007). Review Linking climate change modeling to impacts studies: Recent advances in downscaling techniques for hydrological modeling, Int.J. Climatol.27, 1547-1578
Fujino, J.; Nair, R.; Kainuma, M.; Masui, T.; & Matsuoka, Y., (2006). Multigas Mitigation Analysis on Stabilization Scenarios Using Aim Global Model. The Energy Journal, Special Issue 3:343.
Gadgil, S., M. Rajeevan, et al. (2007). Monsoon variability: Links to major oscillations over the equatorial Pacific and Indian oceans. Current Science 93(2): 182–194.
Gebert, W.A., Mandy, J., Ellen, J., Kennedy, J.L., (2007). Use of streamflow data to estimate base flow/ ground-water recharge for Wisconsin. J. Am. Water Resour. Assoc. 43, 220–236
Gebreyohannes T, De Smedt F, Walraevens K, Gebresilassie S, Hussien A, Hagos M and Gebrehiwot K (2013). Application of a spatially distributed water balance model for assessing surface water and groundwater resources in the Geba basin, Tigray, Ethiopia. Journal of Hydrology, 499:110-123
Gilboy, C.F. (1970): The geology of the Gariboro Region of Southern Ethiopia, Ph.D. Thesis, Leeds University, England 176 pp.
Giorgi, F. (1990): Simulation of regional climate using a limited area model nested in a general circulation model, J. Climate, 3, 941–963.

Gissila T., E. Black, D. I. F. Grimes and J. M. Slingo (2004). Seasonal forecasting of the Ethiopian summer rains, International Journal of Climatology 24, 1345-1358.

Gizaw, B., (2002). Hydro-chemical and environmental investigation of the Addis Ababa region, Ethiopia. Ph.D. Thesis, Faculty of Earth and Environmental Sciences, Ludwig-Maximilians-University of Munich, p. 157.

Goerner A, Jolie E and Gloaguen R (2009). The non-climatic growth of the saline Lake Beseka, Main Ethiopian Rift, J. Arid Environ. 3: 287-295

Govindan, R.B., Vyushin, D., Bunde, A., Brenner, S., Havlin, S. and H.J. Schellnhuber (2002) Global climate models violate scaling of the observed atmospheric variability. Physical Review Letters 89, 028501

Haile T. (1990). Drought in Ethiopia, In 3rd WMO Symposium on Meteorological aspects of Tropical Droughts, Niamey, 30 April- 4 May 1990, WMO TMRP Series 36, 273-278.

Halcrow (2008): Rift Valley Lakes Basin Integrated Resources Development Master Plan Study Project, Draft Phase 2 Report Part II Prefeasibility Studies, Halcrow Group Limited, and Generation Integrated Rural Development (GIRD) consultants. Unpublished report. AA.

Harbaugh, A.W., Banta, E.R., Hill, M.C., and McDonald, M.G., 2000, MODFLOW-2000, the U.S Geological Survey Modular Ground-Water Model—User guide to modularization concepts and the ground-water flow process: U.S. Geological Survey Open-File Report 00-92, 121 p.

Harbaugh, A.W., (2005), MODFLOW-2005, the U.S. Geological Survey modular ground-water model—The ground-water flow process: U.S. Geological Survey Techniques and Methods 6–A16, variously paged.

Harr RD, Levno A, and Mersereau R (1982) Streamflow changes after logging 130-year-old douglas fir in two small watersheds. Water Resources Research18 (3): 644–647.

Hawkins, E., Osborne, T. M., Ho, C. K., & Challinor, A. J. (2013). Calibration and bias correction of climate projections for crop modeling: An idealized case study over Europe. Agricultural and Forest Meteorology, 170(0), 19–31.

Hayl, E., M. P. Clark, R. L. Wilby, W. J. Gutowski, JR.G. H. Leavesley, Z. Pan, R. W. Arritt, E. S. Takle (2002). Use of Regional Climate Model Output for Hydrologic Simulations, Journal of hydrometeorology-vol.3.

Healy, R.W., Cook, P.G., (2002). Using groundwater levels to estimate recharge. Hydrogeology Journal 10 (1), 91–109.

Hegerl, G.C., F. W. Zwiers, P. Braconnot, N.P. Gillett, Y. Luo, J.A. Marengo Orsini, N. Nicholls, J.E. Penner, P.A. Stott (2007). Understanding and Attributing Climate Change, Climate Change 2007: Cambridge University Press,

Cambridge, United Kingdom and New York, NY, USA.
Hicks, B. J., R. L. Beschta, and R. D. Harr (1991), Long-term changes in streamflow following logging in western Oregon and associated fisheries implications, Water Res. Bull 27(2), 217-226.
Hijmans, R.J., Cameron, S.E., Parra, J.L., Jones, P.G., and A. Jarvis (2005) Very high resolution interpolated climate surfaces for global land areas. International Journal of Climatology, 25:1965-1978
Horton, C.R. E., (1945). "Erosional development of streams and their drainage basins: a Hydrophysical approach to quantitative morphology". Bull. Geol. Soc. Am. 56, 275-370
Houghton, J.T., Ding Y, Griggs DJ, Noguer M, van der Linden PJ, Xiaosu D (2001) The Scientific Basis. The contribution of Working Group I to the Third Assessment Report of the Governmental Panel on Climate Change, Cambridge University Press
Institute of Hydrology, (1980). Low Flow Studies Report. Wallingford, UK Lacey, G.C.,
IPCC (2000). Special Report Emissions Scenarios, Summary for Policymakers, IPCC, Geneva.
IPCC (2001). Third Assessment Report: Climate Change 2001, IPCC, Geneva.
IPCC (2007). Fourth Assessment Report: Climate Change 2007, IPCC, Geneva.
IPCC, (1990): The IPCC Scientific Assessment. The First Assessment Report (ARl). The World Meteorological Organization I the United Nations Environment Programme. ISBN: 0-521-40720-6
IPCC, (1992): Climate Change 1992. The Supplementary Report to The PCC Scientific Assessment. The World Meteorological Organization I the United Nations Environment Programme. ISBN: 0-521-43829-2.
Jackson, T.J., (2002). Remote sensing of soil moisture: implications for groundwater recharge. Hydrogeology Journal 10 (1), 40–51.
Jarvis, A., Lane, A., and R.J. Hijmans (2008) The effect of climate change on crop wild relatives. Agriculture, Ecosystems & Environment 126:13-23
JICA (2012): The Study on Groundwater Resources Assessment in the Rift Valley Lakes Basin in Ethiopia, JICA, Kokusai Kogyo Co., Ltd., MoWE), Ethiopia. Final Report (Main Report).
Jochen H. Schenk and Robert B. Jackson: Rooting depths, lateral root spreads and below-ground above-ground allometries of plants in water-limited ecosystems: Journal of Ecology (2002) 90, 480 – 494
Johnson, R. (1998). The forest cycle and low river flow: a review of UK and international studies. Forest Ecology and Management 109: 1-7.
Jones, P.G. and P.K. Thornton (2003) the potential impacts of climate change on

maize production in Africa and Latin America in 2055. Global Environmental Change 13:51–59

Kay, A. L., and Davies, H. N. (2008): Calculating potential evaporation from climate model data: A source of uncertainty for hydrological climate change impacts, J. Hydrol., 358, 221–239.

Kazmin, V. (1973): Geological Map of Ethiopia. Geological Survey of Ethiopia: Addis Ababa, Ethiopia.

Kazmin, V.; Berhe, S.M. (1978): Geological map of Nazareth Sheet, Scale 1: 250,000, Geological Survey of Ethiopia, Addis Ababa.

Kazmin, V.; Berhe, S.M.; Nicoletti, M.; Petrucciani, C. (1980): Evolution of the northern part of the Ethiopian Rift. Accad. Naz. Lincei, Rome 47, 275-291. Italy.

Kebede, S., 2013. Groundwater in Ethiopia: Features, Numbers, and Opportunities. Springer Verlag Berlin Heidelberg, pp 283. http://dx.doi.org/10.1007/978-3-642-30391-3.

Kefale T., Jiri S.; (2013): Hydrogeological and hydrochemical maps of Hossaina NB 37-2. Explanatory notes. AQUATEST a.s., Geologicka 4, 152 00 Prague 5, Czech Rep.

Keir D, Ebinger CJ, Stuart GW, Daly E, and Ayele A (2006) Strain accommodation by magmatism and faulting as rifting proceeds to breakup: Seismicity of the northern Ethiopian rift. Journal of Geophys. Res., 111, B05314, doi: 10.1029/2005JB003748

Kelson KI, Wells SG. (1989). Geologic influences on fluvial hydrology and bedload transport in small mountainous watersheds, NW New Mexico, USA. Earth Surface Processes and Landforms 14:671– 690

Keppeler ET and Ziemer RR (1990) Logging effects and streamflow: Water yield and summer low flows at Caspar Creek in NW California. Water Resources Research26 (7): 1669–1679.

Knutti, R.; Abramowitz, G.; Collins, M.; Eyring, V.; Gleckler, P.J.; Hewitson, B.; & Mearns, L., (2010). Good Practice Guidance Paper on Assessing and Combining Multi Model Climate Projections. National Center for Atmospheric Research, Boulder, Colo.

Korecha D., A. G. Barnston (2007). Predictability of June–September Rainfall in Ethiopia, Monthly Weather Review 135, 628–650.

Kovats S, Valentini R, Bouwer LM et al. (2014) IPCC AR5 Chapter 23, Europe, an online resource available at http://ipcc-wg2.gov/AR5/images/uploads/WGIIAR5-Chap23_FGDall.pdf, Accessed 29/7/2014

Kremen, C., et al. (2008) Aligning conservation priorities across taxa in Madagascar

with high resolution planning tools. Science 320: 222-226
Lacey, C.G., Grayson, R.B., (1998). Relating baseflow to catchment properties in south-eastern Australia. Journal of Hydrology 204,231–250.
Ladekarl, U.L., Rasmussen, K.R., Christensen, S., Jensen, K.H., Hansen, B., (2005). Groundwater recharge and evapotranspiration for two natural ecosystems covered with oak and heather. Journal of Hydrology 300 (1–4), 76–99.
Le Turdu C, Tiercelin JJ, Gibert E, Travi Y, Lezzar K, Richert J, Massault M, Gasse F, Bonnefille R, Decobert M, Gensous B, Jeudy V, Tamrat E, Mohamed MU, Martens K, Balemwal A, Chernet T, Williamson D, TaiebM (1999). The Ziway-Shala lakes basin system, main Ethiopian rift: influence of volcanism, tectonics, and climatic forcing on human formation and sedimentation. Palaeogeogr Palaeoclimatol Palaeoecol 150:135–177
Lim, K.J., Engel, B.A., Tang, Z., Choi, J., Kim, K., Muthukrishnan, S., Tripathy, D., (2005). Automated web GIS based hydrograph analysis tool, what1. JAWRA J. Am.WaterResour. Assoc. 41 (6), 1407–1416.
Liu JP, Song M R, Horton R M and Hu Y (2013). Reducing spread in climate model projections of a September ice-free arctic P. Natl. Acad. Sci. USA 110 12571–6
Longobardi A and Villani P (2008). Baseflow index regionalization analysis in a Mediterranean area and data scarcity context: Role of the catchment permeability index. Journal of Hydrology355: 63–75.
Losjo K, Johansson B, Bringfelt B, Oleskog I and Bergstroem S (1999) Groundwater recharge-climatic and vegetation induced variations. Simulations in the Emaan and Aespoe areas in southern Sweden. Swedish Nuclear Fuel and Waste Management Co., Stockholm (Sweden), Technical Report TR-99-01, 38 pp
Lyne, V.D., Hollick, M., 1979. Stochastic Time-Variable Rainfall-Runoff Modeling. Hydro. Water Resour. Symp. The institution of Engineers Australia, Perth, Australia, pp. 89–92.
Mackenzi GD, Thybo H, and Maguire PKH (2005) Crustal velocity structure across the Main Ethiopian Rift: Results from 2-dimensional wide-angle seismic modeling. Geophysical Journal International, 162, pp.994–1006
Maguire PKH, Keller GR, Klemperer SL, Mackenzie GD, Keranen K, Harder S, O'Reilly B, Thybo H, Asfaw L, Khan MA, and Amha M (2006) Crustal Structure of the Northern Main Ethiopian Rift from the EAGLE controlled – source survey, a snapshot lithospheric Breakup. Geological Society, London, Special Publications, v.259; pp. 269 -292
Manfreda S, Fiorentino M, and Iacobellis V (2005) DREAM: a distributed model for

runoff, evapotranspiration, and antecedent soil moisture simulation. Advances in Geosciences, (2): 31-39

Marani M, Eltahir E, Rinaldo A. (2001). Geomorphic controls on regional baseflow, Water Resources Research37 (10): 2691– 2630.

Marsh, N.A., Stewardson, M.J. and Kennard, M.J. (2003). River analysis package, a cooperative research center for catchment hydrology. Monash University Melbourne, Australia

Mazvimavi, D., Maijerink, A.M.J., Savenije, H.H.G., Stein, A., (2005). Prediction of flow characteristics using multiple regression and neural networks: a case study in Zimbabwe. Physics and Chemistry of the Earth 30, 639–647.

McGuffie, K., A. Henderson-Sellers (2005). A Climate Modeling Primer-Book, Third Edition. ©2005 John Wiley & Sons, Ltd ISBN: 0-470-85750-1 (HB); 0-470-85751-X (PB)

Meinshausen, M., Smith, S. J., Calvin, K., Daniel, J. S., Kainuma, M. L. T., Lamarque, J.-F., Matsumoto, K., Montzka, S. A., Raper, S. C. B., Riahi, K., Thomson, A., Velders, G. J. M., and van Vuuren, D. P. P.: The RCP greenhouse gas concentrations and their extensions from 1765 to 2300, Clim. Change, 109, 213– 241, doi:10.1007/s10584-011-0156-z, 2011.

Memon, B.A., (1995). Quantitative-analysis of springs. Environ. Geol. 26 (2), 111–120.

Mengesha Tefera et at, (1996), Geological map of Ethiopia,

Mengesha, T.; Tadiwos, C.; Workneh, H. (1996): The geological map of Ethiopia, 1: 2,000,000 scale, (2nd edition), EIGS, Addis Ababa.

Merla, G.; Abbate, E.; Canuti, P.; Sagri, M.; Tacconi, P. (1973): Geological map of Ethiopia and Somalia, 1: 2,000,000. Consiglio Nazionale delle Ricerche Italy, Stabilimento Poligrafico Fiorentino, Firenze

Mesinger, T. L. Black, D. W. Plummer, and J. H. Ward, (1990): Eta model precipitation forecasts for a period including Tropical Storm Al- lison. Wea. Forecasting, 5, 483–493.

Miao C Y, Duan Q Y, Sun Q H and Li J D (2013). Evaluation and application of Bayesian multi-model estimation in temperature simulations Prog. Phys. Geog. 37 727–44

Milly, P. C.D., J. Betancourt, M. Falkenmark, R.M.Hirsch, Z.W. Kundzewicz, D. P. Lettenmaier, and R. J. Stouffer (2008), Stationarity is dead: Whither water management?, Science, 319(5863), 573–574

Moglen and R.L. Bras, (1995). "The effect of spatial heterogeneities on geomorphic expression in a model of basin evolution" Water Resources Research 31, pp. 2613–2623.

Mohr (1968): The Ethiopian Rift System. Bulletin of the Geophysical Observatory,

vol.71, p1–65, Addis Ababa.
Mwakalila S, Feyen J, and Wyesure G (2002) the influence of physical catchment properties on baseflow in semi-arid environments. Journal of Arid Environments 52: 245–258.
Nag, S.K., (1998). Morphometric analysis using remote sensing techniques in the Chaka sub-basin Purulia district, West Bengal". J.Indian Soc. Remote Sens. 26, 6976 ".
Nakicenovic, R. (2000). IPCC Special Report on Emission Scenarios, Cambridge University, Press, UK
Nathan, R.J., Austin, K., Crawford, D., Jayasuriya, N., (1996). The estimation of monthly yield in ungauged catchments using a lumped conceptual model. Australian Journal of Water Resources 1 (2), 65–75.
Nathan, R.J., McMahon, T.A., (1990a). Evaluation of automated techniques for baseflow and recession analysis. Water Resources Research 26 (7), 1465–1473.
Nagano, K; Tsujimura, M; O,, Yuichi; Iwagami, Sho; Sakakibara, Koichi; Sato, Yutaro, (2017), Seasonal change of residence time in spring water and groundwater at a mountainous headwater catchment, 19th EGU General Assembly, EGU2017, proceedings from the conference held 23-28 April, 2017 in Vienna, Austria., p.3857
Otterbach L. (1995); Water resources quality and potential assessment for irrigation agriculture in the Abaya-Chamo Basin, south Ethiopia. The University of Siegen. Germany
Oyebande, L., (2001). Water problems in Africa—how can sciences help? Hydrological Sciences Journal 46 (6), 947–961.
Pincus R, Batstone CP, Hofmann R J P, Taylor K E and Glecker P J (2008) Evaluating the present-day simulation of clouds, precipitation, and radiation in climate models J. Geophys. Res. 13 D14209
Ponce M.V., Shetty A.V., (1995). A conceptual model of catchment water balance: formulation and calibration. Journal Hydrology173: 27–40.
Price, K., (2011). Effects of watershed topography, soils, land use, and climate on baseflow hydrology in humid regions: a review. Progr. Phys. Geogr. 35 (4), 465–492.
Rasool Q.A, Singh, V.K &, Singh, U.C.,(2011) "The evaluation of morphometric characteristics of Upper Subarnarekha Watershed drainage basin using Geo-informatics as a tool, Ranchi, Jharkhand". Int. J. Envir. Sci. 1(7), 1921-1927.
Riahi, K.; Grübler, A.; & Nakicenovic, N., (2007). Scenarios of Long-term Socio-economic and Environmental Development Under Climate Stabilization.

Technological Forecasting and Social Change, 74:7:887.
Roberts J., (1983) "Forest Transpiration: A Conservative Hydrological Process?" J. Hydrol., 66, pp. 133–141.
Salathé, P.Jr., Mote, P.W., and M.W. Wiley (2007) Review of scenario selection and downscaling methods for the assessment of CC impacts on hydrology in the United States Pacific Northwest. International Journal of Climatology, 27:1611-1621.
Samuels, Givati, R. and P. Alpert, (2011): Using ensemble of climate models to evaluate future water and solutes budgets in Lake Kinneret, Israel. J. Hydrol., 410, 248–259, doi:10.1016/ j. hydro.2011.09.025.
Santhi C, Allen PM, Muttiah RS, Arnold JG, and Tuppad P (2008) Regional estimation of base flow for the conterminous United States by hydrologic landscape regions. Journal of Hydrology351 (1–2): 139–153.;
Scanlon, B.R., Healy, R.W., Cook, P.G., (2002). Choosing appropriate techniques for quantifying groundwater recharge. Hydrogeology Journal 10 (1), 18–39. Scanlon, B.R., Healy, R.W., Cook, P.G., 2002. Choosing appropriate techniques for quantifying groundwater recharge. Hydrogeology Journal 10 (1), 18–39.
Schütt, B., Förch, G., Bekele, S., Thiemann, S. (2002): Modern water level and Sediment accumulation changes of Lake Abaya, southern Ethiopia-A case study from the northern lake area. Water Resources and Environment Research, 2: 418–422.
Segele Z. T., P. J. Lamb (2005). Characterization and variability of Kiremt rainy season over Ethiopia, Meteorology and Atmospheric Physics 89, 153-180.
Seleshi Y., U. Zanke (2004). Recent changes in rainfall and rainy days in Ethiopia, International Journal of Climatology 24, 973-983.
Servat, E., Hughes, D., Fritsch, J.-M. and Hume, M. (Eds), (1998). Water Resources Variability in Africa during the XXth Century. (Proc. Abidjan Conf., November 1998). IAHS Publ. no. 252.103
Shelton, M.L. (2009). Hydro-climatology Perspective, and Applications; Cambridge University Press: Cambridge, UK, p. 436.
Shirmohammadi, A., Chaubey, I., Harmel, R.D., Bosch, D.D., Muñoz-Carpena, R., Dharmasri, C., Sexton, A., Arabi, M., Wolfe, M.L., Frankenberger, J., Graff, C., Sohrabi, T.M., (2006). Uncertainty in TMDL models. Trans. ASABE 49 (4), 1033–1049.
Sima, Jiri et al. (2004): Explanatory notes to the hydrogeological and hydro-chemical maps of the Adi Ramets Area (ND 37-5 Adi Ramets and ND 37-9 Gulch sheets).
Simmers, I., (1988). Estimation of Natural Groundwater Recharge. D.Reidel,

Dordrecht, Holland
Simmons, A. J., S. M. Uppala, et al. (2006). ERA-Interim: New ECMWF reanalysis products from 1989 onwards. ECMWF Newsletter (110): 25–35
Sivapalan, M., S. E. Thompson, C. J. Harman, N. B. Basu, and P. Kumar (2011), Water cycle dynamics in a changing environment: Improving predictability through synthesis, Water Resour. Res., 47 , W00J01, doi:10.1029/2011WR011377
SMEC (2007) Hydrological study of the Tana-Beles Sub Basins, Technical report (Ministry of Water Resources, Addis Ababa
Smith, S.J. & Wigley, T.M.L., (2006). Multi-gas Forcing Stabilization with Minicam. The Energy Journal, Special Issue 3:373.
Soczyńska U., (1989), The hydrological catchment system and modeling of water circulation systems in Soczyńska U., (ed.). Process hydrologic zone. Fizycznogeograficzne podstawy modelowania, PWN, Warszawa: 9–19.
Sophocleous, M.A., (1992). Groundwater recharges estimation and regionalization: The Great Bend Prairie of central Kansas and its recharge statistics. Journal of Hydrology 137 (1–4), 113–140.
Sophocleous, M.A., (2000). From safe yield to sustainable development of water resources – the Kansas experience. J. Hydrol. 235, 27–43
Soulsby C, Neal C, Laudon H, Burns DA, Merot P, Bonell M, Dunn SM, Tetzlaff D. (2008). Catchment data for process conceptualization: simply not enough. Hydrological Processes22: 2057– 2061.
Stocker, T.; Qin, D.; Plattner, G.-K.M.; & Midgley, P., (2010). Good Practice Guidance Paper on Assessing and Combining Multi Model Climate Projections. IPCC Expert Meeting on Assessing and Combining Multi Model Climate Projections, Boulder, Colo.
Strahler, A.N, (1957) "Quantitative analysis of watershed geomorphology", Trans. Am. Geophys. UN. 38, 913-920.
Stuckey, M.H. (2006) Low-flow, Base-Flow, and Mean-Flow Regression Equations for Pennsylvania Streams; U.S. Geological Survey Scientific Investigations Report 2006-5130; U.S. Geological Survey: Denver, CO, USA,
Tabor, K and J.W. Williams (2010) Globally downscaled climate projections for assessing the conservation impacts of climate change, Ecological Applications, 20(2): 554-565.
Tandon SK. (1974). Litho-control of some geomorphic properties: an illustration from Kumaun Himalaya, India. Zeitschrift fur Geomorphologie18 (4): 460– 471.
Taylor, K. E., R. J. Stouffer, and G. A. Meehl, (2012): An overview of CMIP5 and the experiment design. Bull. Amer. Meteor. Soc., 93, 485–498,

doi:10.1175/BAMS-D-11-00094.1
Thomas A; Tegist R. and Jiri S. (2015): Hydrogeological and hydro-chemical maps of Dila NB 37-6. Explanatory notes. AQUATEST a.s., Geologicka 4, 152 00 Prague 5, Czech Republic.
Uppala, S. M., D. Dee, et al. (2008). Towards a climate data assimilation system: status update of ERA-Interim. ECMWF Newsletter. Reading, ECMWF: 12–18.
van Vuuren, D.P.; den Elzen, M.G.J.; Lucas, P.L.; Eickhout, B.; Strangers, B.J.; van Ruijven, B.; Wonink, S.; & van Houdt, R., (2007). Stabilizing Greenhouse Gas Concentrations at Low Levels: An Assessment of Reduction Strategies and Costs. Climate Change, 81:2:11. http://dx. doi.org/10.1007/s10584-006-9172-9.
van Vuuren, D.P.; Edmonds, J.A.; Kainuma, M.; Riahi, K.; Weyant, J., (2011a). A Special Issue on the RCPs. Climatic Change, 109:1-2:1. http://dx.doi.org/10.1007/ s10584-011-0157-y.
Vivoni ER, Di Benedetto F, Grimaldi S, Eltahir EAB. (2008). Hypsometric control on the surface and subsurface runoff. Water Resources Research44: W12502, DOI: 10.1029/2008WR006931.
WABCO (1990): Water Resources Development Master Plan for Ethiopia.
Wang QJ, Pagano TC, Zhou SL, Hapuarachchi HAP, Zhang L and Robertson DE (2011) Monthly versus daily water balance models in simulating a monthly runoff. Journal of Hydrology 404(3): 166-175
Wang D. and Wu L, (2013): Similarity of climate control on base flow and perennial stream density in the Budyko framework. Hydrol. Earth Syst. Sci., 17, 315-324, 2013.
Wang ZM, Batelaan O, and De Smedt F (1996) A distributed model for water and energy transfer between soil, plants, and atmosphere (WetSpa). Physics and Chemistry of the Earth 21(3):189-193
Warburton, M.L., Schulze, R.E., (2005). Chapter 15: Detection of Climate Change: A Review of Literature on Changes in Temperature, Rainfall, and Streamflow, on Detection Methods and Data Problems, pp257 274. [In Schulze, R.E., (ed) Climate Change and Water Resources in southern Africa: Studies on Scenarios, Impacts, Vulnerabilities, and Adaptation. Water Research Commission, Pretoria, RSA, WRC Report 1430/1/05].
Wigley, T. (2003). Eighteenth sessions of the subsidiary bodies 4-13 June 2003, Bonn, Germany.
Wigley, T., NCAR, Boulder (2008). MAGICC /SCENGEN5.3 user's manual.
Wilby, R. L., J. Troni, Y. Biot, L. Tedd, B. C. Hewitson, D. M. Smith, R. T. Sutton (2009). Review of climate risk information for adaptation and development

planning, Int. J. Climatol.29, 1193–1215.
Wilby, R. L., T. M. Wigley (2000). Precipitation Predictors for Downscaling: Observed and Generated Circulation Model Relationships, Int. J. Climatol. 20, 641–661.
Willgoose and Hancock, (1998); Drainage density, Length ratios, and lithology in the glaciated area of southern Connecticut. Geological Society of America Bulletin 82: 2955– 2956.
Winkler A, Krabaugh J, Fleage J, Glanz M, Gordon A, Jacobs B, Maga M, Muldoon K, Pan A, Pyne L, Richmond B, Ryan T, Selffert ER, Sen S, Todd L, Wlemann MC, (2003) Oligocene mammals from Ethiopia and faunal exchange between Afro-Arabia and Eurasia. Nature 426:549–552
Woldegebriel, G., Aronson, J.L., Walter, R.C., (1990). Geology, geochronology, and rift basin development in the central sector of the Main Ethiopian Rift. Geol. Soc. Am. Bull. 102, 439 –458. [B34.022].
Xu CY and Singh VP (1998) a review of monthly water balance models for water resources investigations. Water Resources Management 12(1): 20-50
Xu, C.Y. and V.P. Singh, (1998): "A Review of Monthly Water Balance Models for Water Resources Investigations". Water Resources Management 12 (1): 31- 50
Xu, Chong-yu (1999). From GCMs to river flow: a review of downscaling methods and hydrologic modeling approaches, Progress in Physical Geography, 23, 229
Zecharias, Y.B., Brntsaert, W., 1988. The influence of basin morphology on groundwater outflow, Water Resour. Res., 24 (10), 1645-1650.
Zenawi, Tessema; Tadesse, Dessie (2003): Hydrology and Engineering Geology of Awassa Lake Catchment, Geological survey of Ethiopia

Appendices

Appendix 1: shows the analysis result of important climatological values of annual rainfall and years for maximum and minimum recodes

No	Station Name	Duration		Mean	Minimum	Year	Maximum	year
1	Aje	1984	2014	861.3	329.8	1990	1089.1	1982
2	Alaba K	1984	2014	1030.9	752.3	2012	2017.6	2013
3	Aleta Wondo	1984	2014	1595.9	1153.2	2012	2050.3	2007
4	Amaro Kelle	1984	2014	994.2	654.6	1993	1450.1	1988
5	Angacha	1987	2014	1493.2	913.7	1994	2407.6	2001
6	Apo/yekatit 25	1984	2014	1150.9	658	1999	1773.8	1987
7	Arba minch	1987	2014	908.5	581.5	1976	1253.9	1997
8	Bedessa	1987	2014	1113.4	711.5	1997	1382.7	1997
9	Belela	1996	2014	973.1	559	2009	1612	2010
10	Bera	1997	2014	1292	845.3	2005	1906.5	2001
11	Billate	1985	2014	766.5	492.7	1999	1617.2	1986
12	Billate Tena	1984	2014	891.9	435.8	1984	1343.9	1996
13	Bodity	1984	2014	1305.7	951.7	2000	2441.1	1989
14	Buele	2003	2014	1528.3	1249.5	2008	1940.4	2010
15	Burji	1956	2014	893.7	628	1999	1267	1972
16	Butajra	1952	2014	1023.6	513	2009	1783	2005
17	Chelelektu	1984	2014	1217.2	765.2	1984	1661.5	2001
18	Chencha	1987	2014	1248.1	739.2	2004	2176.9	1997
19	Derara	1990	2014	1225.4	855.3	2000	2525.5	1992
20	Dilla	1987	2014	1443	1043.8	1980	3408.4	2008
21	Dorze	2001	2014	1545.1	437.6	2003	2981.6	2007
22	Durame	1984	2014	1146.9	812.8	1994	1580.8	1989
23	Fisha Gent	1984	2014	1372.7	1084	2004	2335.3	1992
24	Fonko	1987	2014	1236.5	891.9	1994	1664.9	1997
25	Gato	1973	2014	1045.6	479.7	1975	1708.8	1982
26	Gedeb	1984	2014	1445.3	795.8	2003	2690.4	1995
27	Geresse	1987	2014	2160.3	1244.5	2002	4023.2	1993
28	Gidole	1986	2014	1190.6	302.8	1987	1256.6	2008
29	Gumaide	1984	2014	910.5	518.4	2000	1674.4	1989
30	H/mariam	1980	2014	955.1	567.4	1998	1466.5	1987
31	H/selam	1980	2014	1304	913.3	1981	2028.3	1982
32	Hossina	1980	2014	1178.9	850.3	1981	1626.8	1982
33	Humbo	1987	2014	1136.1	680	1991	1853.6	1996
34	Kebado	1991	2014	1404.3	1027.7	1991	1762.6	1996
35	Konso	1984	2014	777.9	452	2000	1006	2001
36	Leku	2002	2014	1092	894.3	2009	1280.4	2013
37	MIDRE GENET	1978	2014	1305.9	393.9	1992	1349	2010
38	M/Abaya	1987	2014	757.4	393.9	1992	2165.5	1988
39	Shone	1984	2014	1437	931.2	2003	2447.3	1997
40	Telemokentise	1991	2014	1338.4	869.2	1999	1861.4	2006

No	Station Name	Duration		Mean	Minimum	Year	Maximum	year
41	W/sodo	1987	2014	1239.3	19.2	1987	1752.5	2005
42	Wajifo	1984	2014	1054.6	589.6	1955	1970.4	2006
43	Wulbareg	1984	2014	1262.8	672	1981	2196	1979
44	Yirga chelte	1984	2014	1373	853.5	2011	2080.3	1996
45	Yirgalem	1981	2014	1230.2	832.8	2004	1658.8	1998
46	Ymbadubanch	1984	2014	1079.2	763.3	2009	1574.6	1987

Appendix 2: shows the numbers of annual total rainfall for each station that represent the areal rainfall depth.

Rep_Station	Long_X	Lat_Y	Mean rain (mm/yr)	Area (km^2)	Fraction of total area (%)	Mean vol. Rainfall ($10^6 m^3/yr$)
Aje	428683	806427	861.3	206.4	1.09	177760.7
Alaba K	399984	808110	1030.9	910.6	4.82	938693.3
Aleta Wondo	435663	729916	1595.9	324.2	1.71	517452.3
Amaro Kelle	377975	645265	994.2	1090	5.77	1083652.6
Angacha	374299	812007	1493.2	376.4	1.99	562010.6
Apst/yekatit 25	430617	744523	1150.9	278.5	1.47	320471.5
Arba minch	340804	670223	908.5	1117.8	5.91	1015533.9
Bedessa	382685	759469	1113.4	334.5	1.77	372431.9
Belela	435787	767294	973.1	104.5	0.55	101690.2
Bera	435585	741509	1292	162.6	0.86	210116.1
Billate	399204	754132	766.5	683.7	3.62	524020.2
Billate Tena	403434	766257	891.9	516.6	2.73	460749
Bodity	373901	768994	1305.7	227.6	1.20	297119.2
Buele	434305	696849	1528.3	311.3	1.65	475827.3
Burji	374596	606280	893.7	461	2.44	411973
Chelelektu	406393	663831	1217.2	583.9	3.09	710749.6
Chencha	348391	688893	1248.1	358.2	1.89	447039.3
Derara	422798	757163	1225.4	360.3	1.91	441489.2
Dilla	423349	705247	1443	415.9	2.20	600177.4
Dorze	349414	685347	1545.1	354.8	1.88	548233.2
Durame	377700	800000	1146.9	134	0.71	153696.8
Fisha Gent	411262	671676	1372.7	191.7	1.01	263168.3
Fonko	386297	845480	1236.5	551.6	2.92	682026.8
Gato	324403	614371	1045.6	73.5	0.39	76810.4
Gedeb	416292	653210	1445.3	346.2	1.83	500327.3
Gidole	318278	624579	1190.6	364.6	1.93	434044.2
Gumaide	339137	617631	910.5	475.8	2.52	433171.9
H/mariam	415094	622671	955.1	558.2	2.95	533156.8

Rep_Station	Long_X	Lat_Y	Mean rain (mm/yr)	Area (km^2)	Fraction of total area (%)	Mean vol. Rainfall ($10^6 m^3$/yr)
H/selam	447354	716973	1304	179.7	0.95	234367.2
Hossina	373808	836608	1178.9	272.6	1.44	321324.1
Humbo	363569	741036	1136.1	564.1	2.98	640859.8
Kebado	427614	711106	1404.3	183.2	0.97	257249.2
Leku	442494	759893	1092	277.9	1.47	303517.5
M/abaya	364002	695383	757.4	1008.1	5.33	763537.2
Moroch	434627	759466	1305.9	108.4	0.57	141563.6
Shone	384545	788590	1437	433.1	2.29	622389.5
Telemokentise	420299	718326	1338.4	833.3	4.41	1115300.3
W/sodo	361754	754133	1239.3	129.3	0.68	160222.7
Wajifo	360848	713703	1054.6	869.6	4.60	917094.1
Wulbareg	403265	855389	1262.8	382.9	2.03	483573.6
Yirga chelfe	412300	679766	1373	722.8	3.82	992373.9
Yirgalem	442703	751521	1230.2	315.2	1.67	387741.2
Ymbadubanch	392752	765842	1079.2	234.9	1.24	253554.8
Geresse	312134	654714	2160.3	515.4	2.73	1113414.7
Sum				18904.9	100	22001676.4
			Areal basin mean rainfall (mm/year)			**1163.8**

Appendix 3: Monthly rainfall total of the meteorological station in the Abaya- Chamo lakes basin

Station	Jan	Feb	Mar	Apr	May	Jun	Jul	Aug	Sep	Oct	Nov	Dec
Aje	20.7	30.7	80.5	88.9	133.0	83.8	115.0	112.0	117.0	57.3	9.6	12.8
Alaba K	27.5	43.0	89.4	136.4	123.2	94.0	116.5	140.0	107.3	75.6	55.6	22.4
Aleta Wondo	36.7	46.0	112.7	206.7	239.3	141.8	155.3	157.5	219.0	181.3	68.6	31.0
Amaro Kelle	19.5	32.9	76.6	200.6	151.4	55.9	49.1	65.2	95.8	145.5	75.3	26.4
Angacha	39.6	63.2	109.4	185.0	172.4	156.4	194.1	209.5	182.3	101.1	48.9	31.3
Aposto/yekatit	25.3	43.3	91.1	172.1	134.9	120.1	110.4	100.0	156.8	131.2	37.2	28.5
Arba minch	31.7	35.1	58.3	160.5	147.4	65.0	41.5	49.6	89.9	125.2	67.5	36.8
Bedessa	38.3	38.3	87.4	160.9	157.9	118.4	120.5	120.5	90.4	106.2	46.6	28.0
Belela	2.0	16.1	59.8	167.9	131.1	31.4	153.1	99.1	155.9	105.8	27.6	23.3
Bera	30.0	23.4	107.7	154.5	198.4	118.4	108.8	133.6	186.4	165.3	40.9	24.6
Billate	27.0	30.3	58.3	112.5	106.2	74.9	61.9	75.0	68.3	80.5	46.4	25.2
Billate Tena	29.7	30.7	77.9	128.1	110.4	83.5	93.0	93.5	93.1	92.8	33.4	25.8
Bodity	29.0	54.4	100.0	171.9	182.2	137.3	162.0	166.6	135.3	89.4	40.6	37.0
Buele	42.7	59.7	76.7	191.1	211.8	165.2	121.6	163.7	176.1	179.3	93.3	47.1
Burji	29.4	27.9	88.4	161.0	142.9	40.0	34.2	38.4	73.2	147.9	80.7	29.7
Butagira	32.2	67.8	107	91.3	130	92.7	158	163	113	41.3	17.3	10
Chelelektu	18.9	35.9	109.6	209.2	195.6	100.7	47.7	65.6	128.1	196.1	80.1	29.7
Chencha	45.8	51.9	118.6	174.3	158.6	87.6	115.2	104.8	100.8	157.2	79.4	53.9
Derara	36.8	53.3	109.1	173.5	161.8	101.8	103.9	109.8	149.0	145.8	49.2	31.4

Station	Jan	Feb	Mar	Apr	May	Jun	Jul	Aug	Sep	Oct	Nov	Dec
Dilla	37.3	66.3	129.2	190.5	194.5	129.3	101.5	129.4	173.4	192.2	68.5	30.9
Dorze	40.0	33.4	123.2	199.0	213.1	132.0	101.6	150.5	180.2	187.8	131.3	53.0
Durame	26.0	51.5	92.8	154.5	145.0	100.7	134.0	156.7	135.8	97.3	26.2	26.4
Fisha Gent	28.9	43.9	87.8	198.9	232.9	93.5	78.2	99.4	160.3	206.3	86.3	56.3
Fonko	27.1	47.8	121.0	148.8	143.4	126.0	167.7	178.6	149.5	86.7	17.7	22.2
Gato	29.5	51.5	116	174	169	48.2	43.3	61.8	117	89.3	127	19
Gedeb	34.4	37.4	105.3	231.7	256.6	112.6	88.8	99.5	127.0	235.1	90.9	26.0
Geresse	45.9	47.9	173.1	370.7	383.8	170.6	193.4	176.9	199.6	226.4	110.5	61.5
Gidole	28.7	71.6	115	173	123	77.2	73.7	110	95	198	69.4	56
Gumaide	40.3	31.6	84.2	178.9	137.7	46.0	36.4	32.9	81.1	107.8	89.2	44.4
H/mariam	12.5	22.6	75.8	195.8	227.2	65.1	37.3	41.6	66.6	111.9	80.8	17.9
H/selam	50.3	51.2	88.8	167.9	152.7	128.7	119.4	150.4	145.5	152.5	53.6	43.0
Hossina	27.5	49.5	105.9	143.8	142.9	121.0	156.2	174.4	147.2	71.0	20.7	18.8
Humbo	35.1	34.1	66.2	140.0	147.0	128.0	155.0	154.0	92.0	99.0	42.1	43.6
Kebado	36.1	48.1	110.3	204.4	222.0	112.1	92.0	123.1	182.2	178.7	55.7	39.6
Konso	26	35.2	86.4	178	111	35.7	21.2	34.2	58.9	94.8	55.5	41
Leku	33.3	39.3	88.5	146.0	131.5	90.0	110.9	122.7	153.7	91.0	57.7	27.4
M/abaya	21.4	27.0	53.6	112.4	116.3	74.8	59.1	54.6	56.3	79.2	69.8	32.9
Moroch	36.2	59.8	122.2	170.0	166.1	101.3	123.2	122.5	188.1	139.5	49.8	27.2
Shone	39.0	52.9	113.1	191.9	176.4	135.5	174.5	190.2	181.0	99.4	44.3	38.8
Telemokentise	31.7	48.7	121.9	186.0	178.1	112.8	135.0	139.6	179.1	137.9	40.6	27.0
W/sodo	28.5	38.0	70.5	151.6	168.6	127.8	177.9	178.5	107.5	95.1	57.4	37.9
Wajifo	20.7	16.3	67.3	140.4	149.7	99.1	127.1	166.0	75.3	100.8	56.6	35.3
Wulbareg	30.5	53.2	96.8	121.0	143.0	148.0	211.0	196.0	165.0	69.5	17.7	11.1
Yirga chelte	22.0	37.2	88.3	226.9	251.7	98.5	87.5	99.4	154.8	197.2	77.1	32.4
Yirgalem	35.5	24.1	90.7	162.7	168.7	102.8	112.1	134.1	155.3	178.3	40.3	25.6
Ymbadubanch	27.6	48.5	96.9	151.4	155.6	93.4	91.0	113.2	147.4	95.5	32.5	26.2

Appendix 4: monthly average temperature of all available station over the basin

Station	Jan	Feb	Mar	Apr	May	Jun	Jul	Aug	Sep	Oct	Nov	Dec	Avg. Temp
Aje	19.1	19.7	20.5	20.6	20.6	20.2	19.6	18.4	19.3	19.3	19.8	19.3	**20**
Alaba K	20.7	21.4	21.2	20.8	20.3	19.3	18.4	18.8	19.3	19.3	19.5	20.0	**20**
Amaro K.	22.3	23.7	23.1	21.6	20.6	20.1	19.4	19.8	20.4	20.2	20.7	21.9	**21**
Angacha	19.7	19.6	19.3	19.2	19.3	18.7	18.8	18.8	18.7	19.2	19.8	19.6	**19**
Arba minch	24.2	25.2	25.9	24.7	23.6	23.1	22.9	23.4	24.0	23.7	23.3	23.7	**24**
Belela	21.8	22.0	22.0	21.9	21.4	21.5	21.3	21.7	21.8	21.4	21.7	22.0	**22**
Billate	24.2	24.7	24.5	23.8	22.9	22.1	21.5	21.9	22.4	22.3	22.5	23.2	**23**
Bodity	19.2	20.1	20.2	19.4	18.7	17.5	16.5	16.8	17.8	18.3	18.6	18.7	**18**
Burji	20.7	21.4	21.1	20.8	20.1	19.2	19.0	19.2	19.7	19.7	19.8	19.9	**20**
Butajra	18.4	19.0	19.7	19.8	19.6	19.0	18.3	18.1	18.8	18.6	18.1	18.0	**19**

Station	Jan	Feb	Mar	Apr	May	Jun	Jul	Aug	Sep	Oct	Nov	Dec	Avg. Temp
Dilla	10.8	11.2	12.7	13.9	13.8	13.7	14.4	14.2	13.8	13.7	11.8	10.6	**13**
Fisha Gent	18.1	18.8	18.8	17.7	17.0	16.2	15.9	16.2	16.8	16.7	17.1	17.5	**17**
Gato	25.0	25.6	25.4	24.4	23.9	23.3	22.8	23.4	24.1	23.9	23.8	24.4	**24**
Gidole	22.6	24.4	24.3	23.4	22.8	21.1	20.5	20.8	21.0	20.6	22.5	22.7	**22**
H/mariam	18.7	19.6	20.0	19.3	18.3	17.8	17.3	17.0	18.0	17.4	17.2	17.2	**18**
H/selam	12.9	13.5	13.8	13.5	13.4	12.4	11.6	12.1	11.9	12.0	12.3	12.4	**13**
Hossina	17.1	17.8	18.4	18.1	17.5	16.0	15.4	15.5	16.2	16.2	16.3	16.3	**17**
M/abaya	24.0	24.6	25.0	24.3	23.7	23.0	22.6	23.0	23.3	23.2	23.1	23.3	**24**
W/sodo	20.4	21.4	21.5	20.7	19.5	18.6	17.7	18.1	18.8	19.4	20.4	20.4	**20**
Wulbareg	18.3	18.6	19.0	18.9	18.8	18.5	18.3	18.4	18.4	18.1	18.1	18.3	**18**
Y/ Chefe	18.0	18.6	19.1	18.6	18.4	18.0	17.7	17.8	17.9	17.8	17.7	17.6	**18**
Yirgalem	19.5	19.9	20.4	19.8	19.2	18.8	18.3	18.4	18.4	18.5	18.8	18.7	**19**
Geresse	17.6	17.7	17.1	16.2	15.8	15.5	15.7	15.6	16.0	16.0	16.5	17.0	**16**

Appendix 5: Monthly Evapotranspiration for 7 Stations (Source: Halcrow 2008)

Station	Jan	Feb	Mar	Apr	May	Jun	July	Aug	Sep	Oct	Nov	Dec	Total
Jinka	121	119	132	111	105	90	96	100	107	111	108	112	1311
Konso	152	158	171	138	131	119	110	133	144	138	137	141	1671
M/Abaya	140	138	158	144	141	133	122	128	139	135	129	134	1642
Hossiana	117	117	133	118	116	94	84	87	98	118	117	121	1320
A/Minch	150	148	159	124	111	95	93	108	127	119	128	143	1504
Dilla	113	114	128	113	110	94	86	99	97	103	107	109	1272
W/ Sodo	149	147	152	130	117	98	88	98	108	126	149	152	1514

Appendix 6 shows the correlation between the different sets of BFI values

	T_ROF	Sp.ROF	BFI_RAP	BFI_KILLE	BFI_TP	BFI_RK_{av}	BFI_KT_{av}	BFI_RT_{av}	BFI_Avg
T_ROF	1.00								
Sp.ROF	0.31	1.00							
BFI_RAP	0.40	0.46	1.00						
BFI_KILLE	-0.04	0.21	0.81	1.00					
BFI_TP	0.41	0.37	0.97	0.76	1.00				
BFI_RKav	0.15	0.33	0.93	0.97	0.89	1.00			
BFI_KTav	0.14	0.29	0.93	0.96	0.91	0.99	1.00		
BFI_RTav	0.41	0.42	0.99	0.80	0.99	0.92	0.93	1.00	
BFI_Avg	0.23	0.35	0.97	0.93	0.94	0.99	0.99	0.96	1.00

Appendix 7 : shows the Graphical method (Kille) result of Base flow

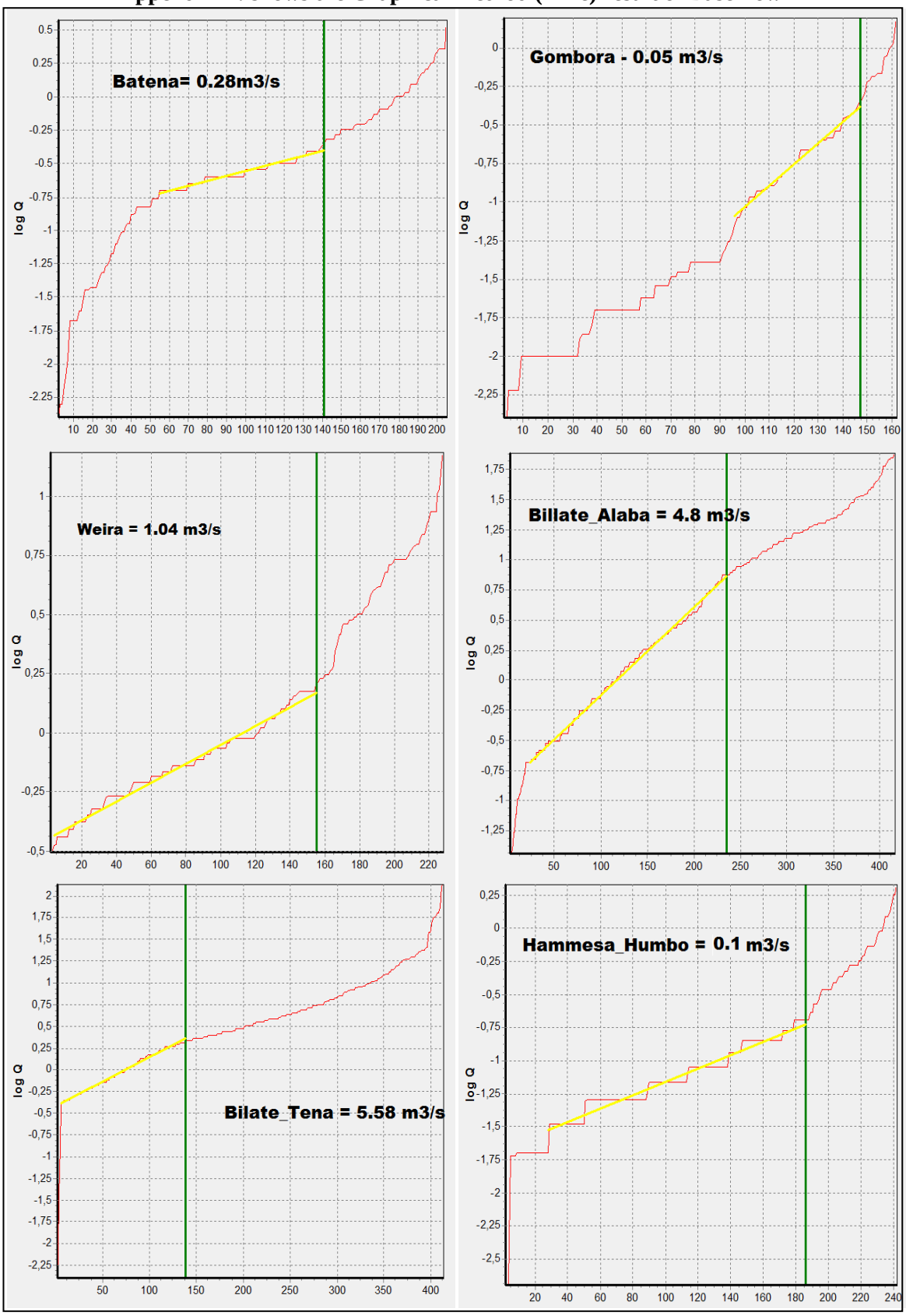

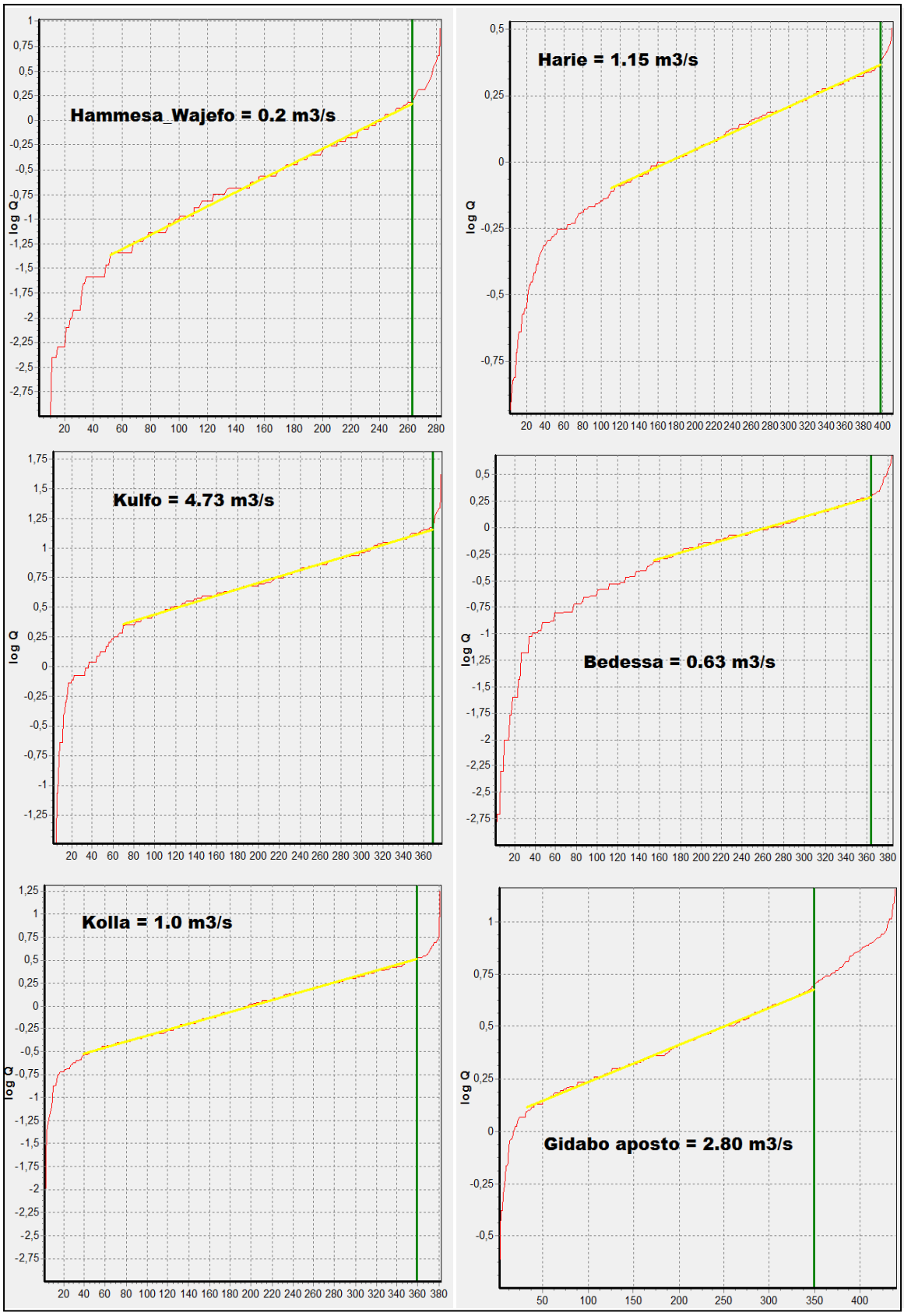
Hammesa_Wajefo = 0.2 m3/s
Harie = 1.15 m3/s
Kulfo = 4.73 m3/s
Bedessa = 0.63 m3/s
Kolla = 1.0 m3/s
Gidabo aposto = 2.80 m3/s
log Q

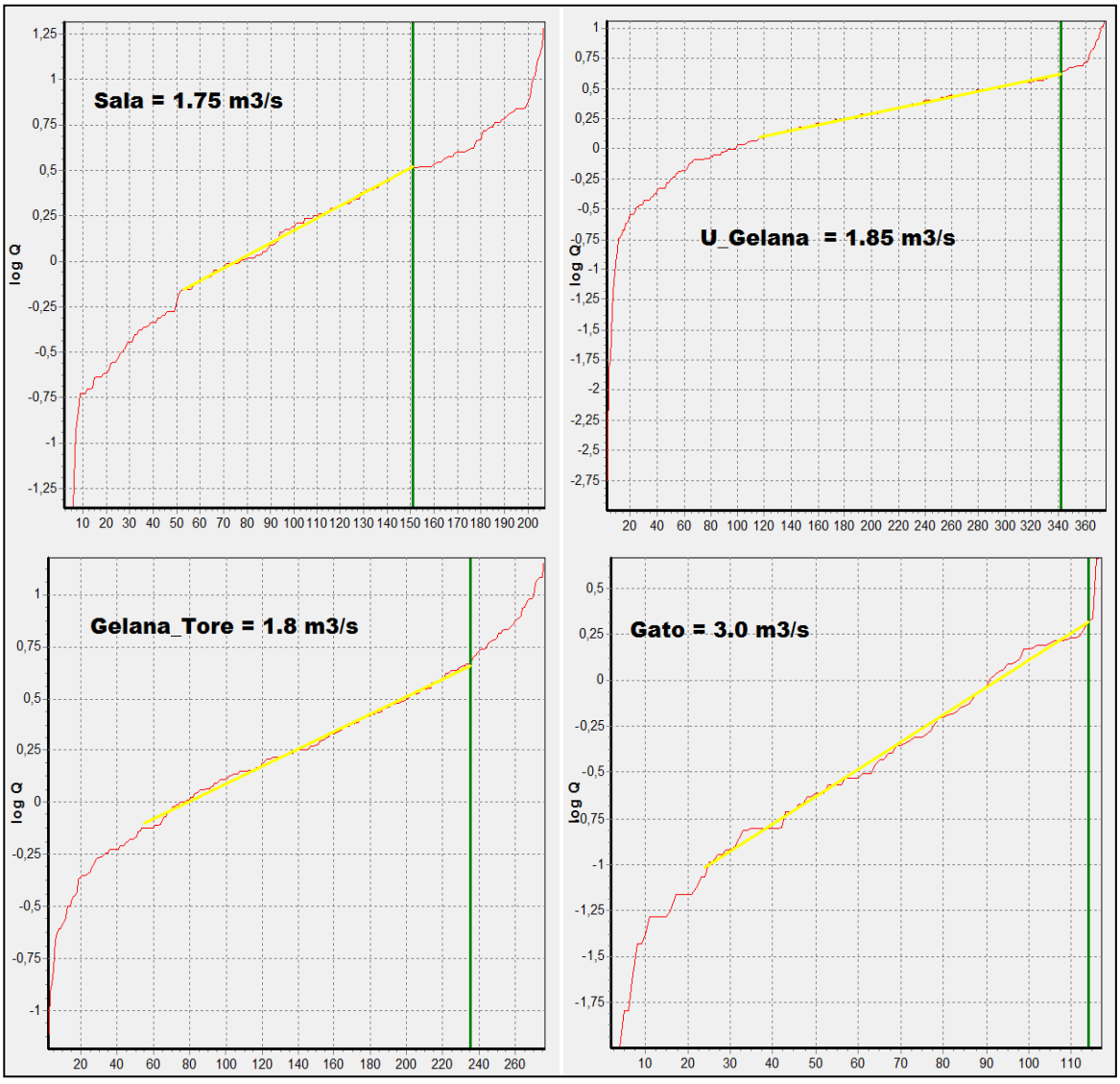
Sala = 1.75 m3/s
log Q
U_Gelana = 1.85 m3/s
log Q
Gelana_Tore = 1.8 m3/s
log Q
Gato = 3.0 m3/s
log Q

Appendix 8: Major river basin characteristics: Geomorphological, Hydro-Climatic and Aquifer Properties used as independent variables for baseflow regression analysis

Major River Basins	BFI	Sp.RoF	Sp.BF	BF	RoF	T_RoF	RF	PET	CI	Cat_A	Slop	Elv	HI	DD	Floor	Escarp	Plat	Cult	For	Grass	WBS	Age	T	q
Billate	0.38	9.6	3.34	3.09	4.2	7.3	1257	1428	0.88	100.0	2.5	1897	0.34	0.17	9.6	33.4	56.9	28.8	5.3	36.6	27.3	2.1	275.5	20.7
Gidabo	0.42	25.4	11.3	1.83	2.2	4.0	1288	1455	0.88	24.8	3.6	1875	0.36	0.21	19.8	32.4	47.8	55.0	8.6	8.5	24.8	5.4	355.1	22.5
Gelana	0.52	28.3	14.4	2.31	2.1	4.4	1160	1539	0.75	12.2	4.6	1702	0.26	0.19	26.1	41.7	32.1	25.1	16.0	0.0	58.6	191.8	126.5	3.0
Amssa_Guracha	0.29	4.6	1.2	0.36	1.1	1.5	1158	1560	0.74	56.8	3.7	1577	0.23	0.25	35.9	45.0	19.0	66.0	0.0	17.9	16.1	10.8	115.0	10.7
Kulifo_Gina	0.62	18.3	10.8	3.49	2.5	6.0	1314	1732	0.76	44.8	8.0	1945	0.35	0.26	31.9	17.1	50.9	81.7	2.5	0.0	15.3	11.5	162.9	3.9
Chamo_Sife	0.42	3.8	1.6	0.24	0.4	0.6	1244	1670	0.74	10.7	5.7	1539	0.20	0.25	45.2	36.8	18.0	38.0	0.0	0.0	61.1	11.4	162.9	6.5

Appendix 9: Correlation matrix for multivariate used in baseflow regression analysis

	BFI	Sp.RoF	Sp.BF	BF	RoF	T_RoF	RF	PET	CI	Cat_A	Slop	Elv	HI	DD	Floor	Escarp	Plat	Cult	For	Grass	WBS	Age	T	q
BFI	1.00																							
Sp.RoF	0.58	1.00																						
Sp.BF	0.72	0.98	1.00																					
BF	0.60	0.43	0.48	1.00																				
RoF	0.18	0.23	0.20	0.89	1.00																			
T_RoF	0.40	0.34	0.34	0.97	0.97	1.00																		
RF	0.48	0.12	0.16	0.48	0.32	0.41	1.00																	
PET	0.51	-0.21	-0.03	-0.18	-0.54	-0.37	0.20	1.00																
CI	-0.14	0.25	0.12	0.50	0.72	0.62	0.48	-0.76	1.00															
Cat_A	-0.28	-0.38	-0.41	0.52	0.76	0.66	0.13	-0.41	0.48	1.00														
Slop	0.75	0.09	0.27	0.07	-0.36	-0.15	0.39	0.94	-0.58	-0.43	1.00													
Elv	0.54	0.51	0.52	0.89	0.78	0.86	0.71	-0.21	0.66	0.42	0.09	1.00												
HI	0.41	0.52	0.50	0.80	0.74	0.79	0.70	-0.32	0.75	0.40	-0.02	0.98	1.00											
DD	0.09	-0.38	-0.27	-0.50	-0.72	-0.62	0.14	0.84	-0.66	-0.35	0.71	-0.34	-0.35	1.00										
Floor	-0.01	-0.41	-0.32	-0.74	-0.92	-0.85	-0.21	0.79	-0.86	-0.60	0.59	-0.72	-0.75	0.85	1.00									
Escarp	-0.74	-0.22	-0.33	-0.63	-0.34	-0.50	-0.89	-0.44	-0.21	-0.13	-0.65	-0.76	-0.69	-0.25	0.13	1.00								
Plat	0.44	0.43	0.43	0.92	0.88	0.92	0.67	-0.34	0.76	0.52	-0.06	0.98	0.96	-0.49	-0.82	-0.68	1.00							
Cult	0.19	-0.08	0.00	-0.03	-0.23	-0.12	0.39	0.52	-0.21	0.03	0.55	0.24	0.27	0.76	0.32	-0.53	0.07	1.00						
For	0.34	0.87	0.81	0.36	0.30	0.33	-0.24	-0.45	0.23	-0.29	-0.23	0.26	0.25	-0.69	-0.50	0.17	0.27	-0.52	1.00					
Grass	-0.56	-0.38	-0.48	0.31	0.69	0.52	-0.05	-0.69	0.61	0.91	-0.75	0.23	0.27	-0.55	-0.66	0.19	0.38	-0.24	-0.16	1.00				
WBS	0.10	0.08	0.09	-0.31	-0.35	-0.35	-0.35	0.09	-0.32	-0.61	0.03	-0.53	-0.59	-0.20	0.31	0.40	-0.46	-0.74	0.37	-0.42	1.00			
Age	0.34	0.60	0.62	0.07	-0.06	0.00	-0.59	-0.06	-0.34	-0.45	0.02	-0.18	-0.24	-0.37	-0.03	0.36	-0.19	-0.50	0.82	-0.39	0.59	1.00		
T	-0.10	0.28	0.16	0.33	0.49	0.42	0.60	-0.62	0.95	0.23	-0.44	0.60	0.71	-0.47	-0.67	-0.27	0.66	-0.10	0.16	0.37	-0.26	-0.41	1.00	
q	-0.50	-0.02	-0.18	0.17	0.50	0.34	0.30	-0.80	0.92	0.50	-0.74	0.39	0.52	-0.50	-0.69	0.04	0.49	-0.13	-0.01	0.70	-0.40	-0.51	0.88	1.00

Appendix 10: Groundwater budget of Billate-river basin

REGION: 1			
	IN	OUT	IN-OUT
STORAGE	0.00E+00	0.00E+00	0.00E+00
CONSTANT HEAD	0.00E+00	0.00E+00	0.00E+00
HORIZ. EXCHANGE	1.61E+06	3.68E+06	-2.07E+06
EXCHANGE (UPPER)	0.00E+00	0.00E+00	0.00E+00
EXCHANGE (LOWER)	0.00E+00	0.00E+00	0.00E+00
WELLS	0.00E+00	3.43E+05	-3.43E+05
DRAINS	0.00E+00	0.00E+00	0.00E+00
RECHARGE	2.41E+06	0.00E+00	2.41E+06
ET	0.00E+00	0.00E+00	0.00E+00
RIVER LEAKAGE	4.61E-01	1.70E+01	-1.66E+01
HEAD DEP BOUNDS	0.00E+00	0.00E+00	0.00E+00
SUM OF THE REGION	4.03E+06	4.03E+06	-1.67E+01
DISCREPANCY [%]	0.00		

Appendix 11: Groundwater budget of Amessa_ Guracha & Kulfo-Gina-river basin

REGION: 2			
	IN	OUT	IN-OUT
STORAGE	0.00E+00	0.00E+00	0.00E+00
CONSTANT HEAD	0.00E+00	0.00E+00	0.00E+00
HORIZ. EXCHANGE	7.69E+05	1.21E+06	-4.37E+05
EXCHANGE (UPPER)	0.00E+00	0.00E+00	0.00E+00
EXCHANGE (LOWER)	0.00E+00	0.00E+00	0.00E+00
WELLS	0.00E+00	2.93E+04	-2.93E+04
DRAINS	0.00E+00	0.00E+00	0.00E+00
RECHARGE	4.66E+05	0.00E+00	4.66E+05
ET	0.00E+00	0.00E+00	0.00E+00
RIVER LEAKAGE	2.52E-02	3.02E+00	-2.99E+00
HEAD DEP BOUNDS	0.00E+00	0.00E+00	0.00E+00
SUM OF THE REGION	1.24E+06	1.24E+06	-3.05E+00
DISCREPANCY [%]	0.00		

Appendix 12: **Groundwater budget of Gidabo-river basin**

REGION: 3			
	IN	OUT	IN-OUT
STORAGE	0.00E+00	0.00E+00	0.00E+00
CONSTANT HEAD	0.00E+00	0.00E+00	0.00E+00
HORIZ. EXCHANGE	1.21E+06	2.49E+06	-1.28E+06
EXCHANGE (UPPER)	0.00E+00	0.00E+00	0.00E+00
EXCHANGE (LOWER)	0.00E+00	0.00E+00	0.00E+00
WELLS	0.00E+00	3.71E+05	-3.71E+05
DRAINS	0.00E+00	0.00E+00	0.00E+00
RECHARGE	1.66E+06	0.00E+00	1.66E+06
ET	0.00E+00	7.34E-01	-7.34E-01
RIVER LEAKAGE	3.41E-01	2.16E+01	-2.13E+01
HEAD DEP BOUNDS	0.00E+00	0.00E+00	0.00E+00
SUM OF THE REGION	2.87E+06	2.87E+06	-2.32E+01
DISCREPANCY [%]	0.00		

Appendix 13: Groundwater budget of Gelana-river basin

REGION: 4			
	IN	OUT	IN-OUT
STORAGE	0.00E+00	0.00E+00	0.00E+00
CONSTANT HEAD	0.00E+00	0.00E+00	0.00E+00
HORIZ. EXCHANGE	4.81E+05	1.41E+06	-9.32E+05
EXCHANGE (UPPER)	0.00E+00	0.00E+00	0.00E+00
EXCHANGE (LOWER)	0.00E+00	0.00E+00	0.00E+00
WELLS	0.00E+00	7.76E+04	-7.76E+04
DRAINS	0.00E+00	0.00E+00	0.00E+00
RECHARGE	1.02E+06	0.00E+00	1.02E+06
ET	0.00E+00	0.00E+00	0.00E+00
RIVER LEAKAGE	2.20E-01	2.45E+01	-2.42E+01
HEAD DEP BOUNDS	0.00E+00	5.49E+03	-5.49E+03
SUM OF THE REGION	1.50E+06	1.50E+06	-2.47E+01
DISCREPANCY [%]	0.00		

Appendix 14: Groundwater budget of Sife_Chamo-river basin

REGION: 5			
	IN	OUT	IN-OUT
STORAGE	0.00E+00	0.00E+00	0.00E+00
CONSTANT HEAD	0.00E+00	0.00E+00	0.00E+00
HORIZ. EXCHANGE	7.26E+04	3.24E+05	-2.51E+05
EXCHANGE (UPPER)	0.00E+00	0.00E+00	0.00E+00
EXCHANGE (LOWER)	0.00E+00	0.00E+00	0.00E+00
WELLS	0.00E+00	6.00E+00	-6.00E+00
DRAINS	0.00E+00	0.00E+00	0.00E+00
RECHARGE	2.51E+05	0.00E+00	2.51E+05
ET	0.00E+00	0.00E+00	0.00E+00
RIVER LEAKAGE	2.23E-03	2.65E-01	-2.63E-01
HEAD DEP BOUNDS	5.20E+02	0.00E+00	5.20E+02
SUM OF THE REGION	3.24E+05	3.24E+05	-3.01E-01
DISCREPANCY [%]	0.00		

Appendix 15: climate change assessment framework

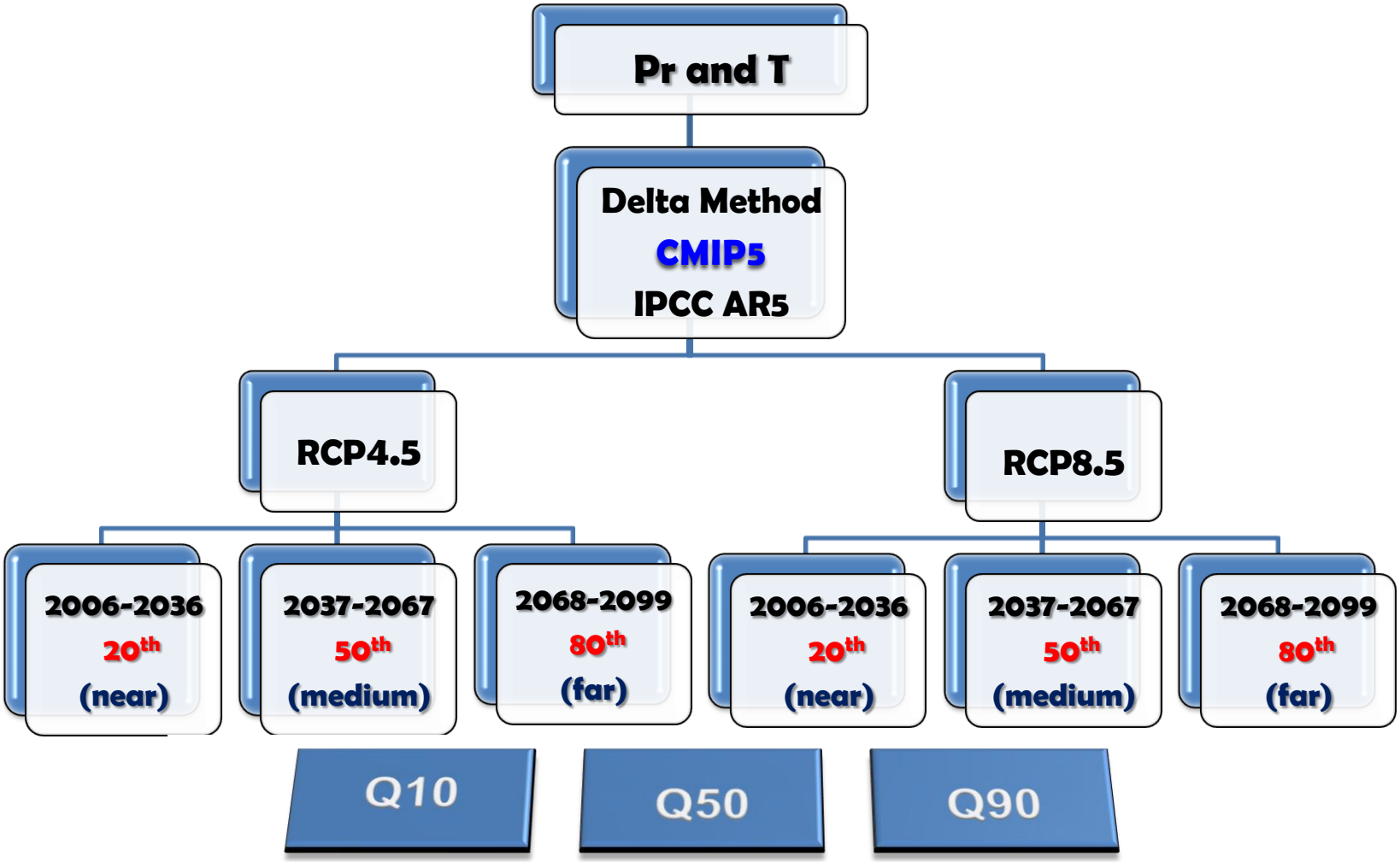

Appendix 16: simulated mean future actual evapotranspiration for the periods 2020s and 2050s under both RCP 4.5(upper).and RCP8. (lower)

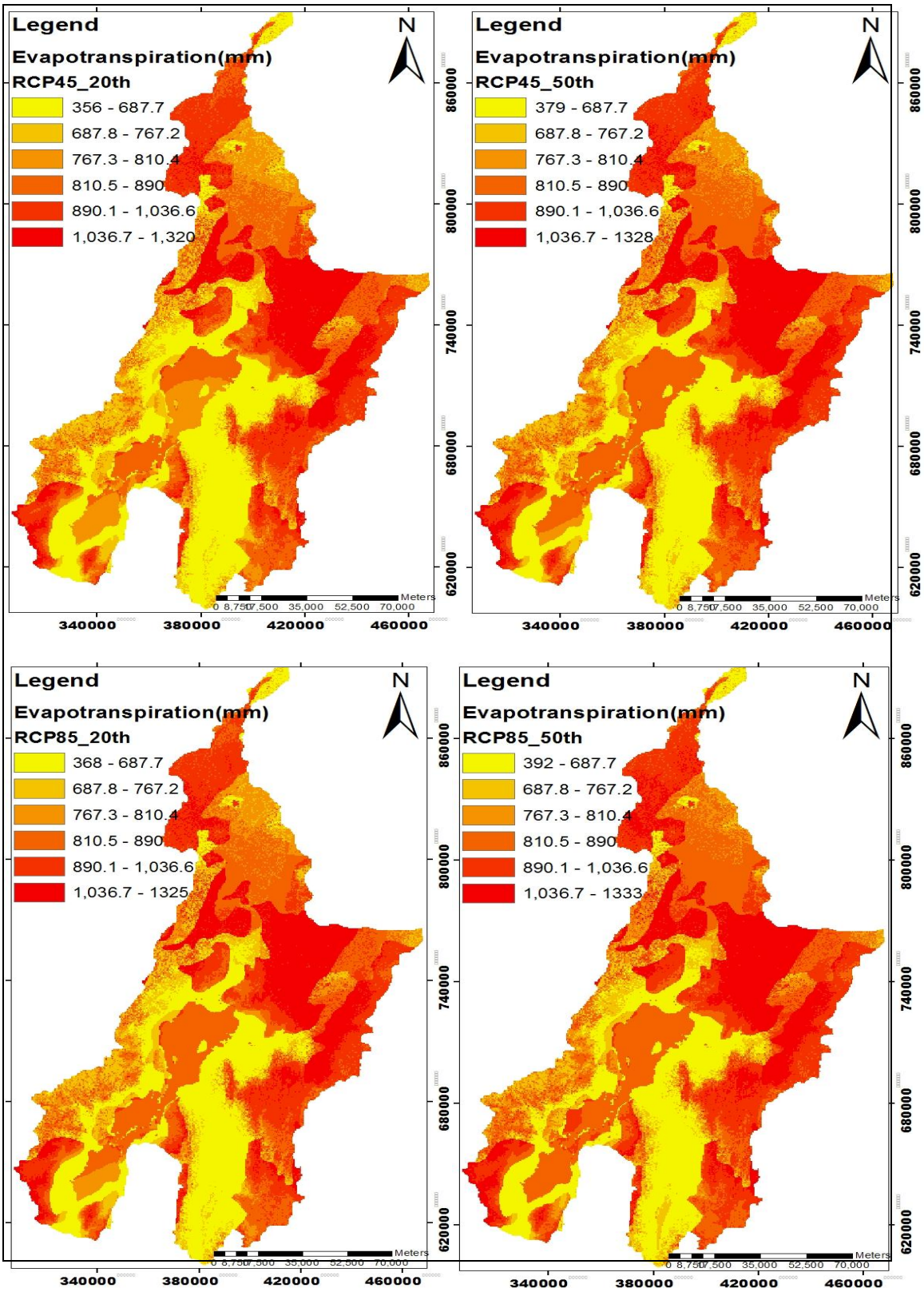

Appendix 17: simulated mean future surface runoff for the periods 2020s and 2050s under both RCP 4.5(upper).and RCP8.5 (lower)

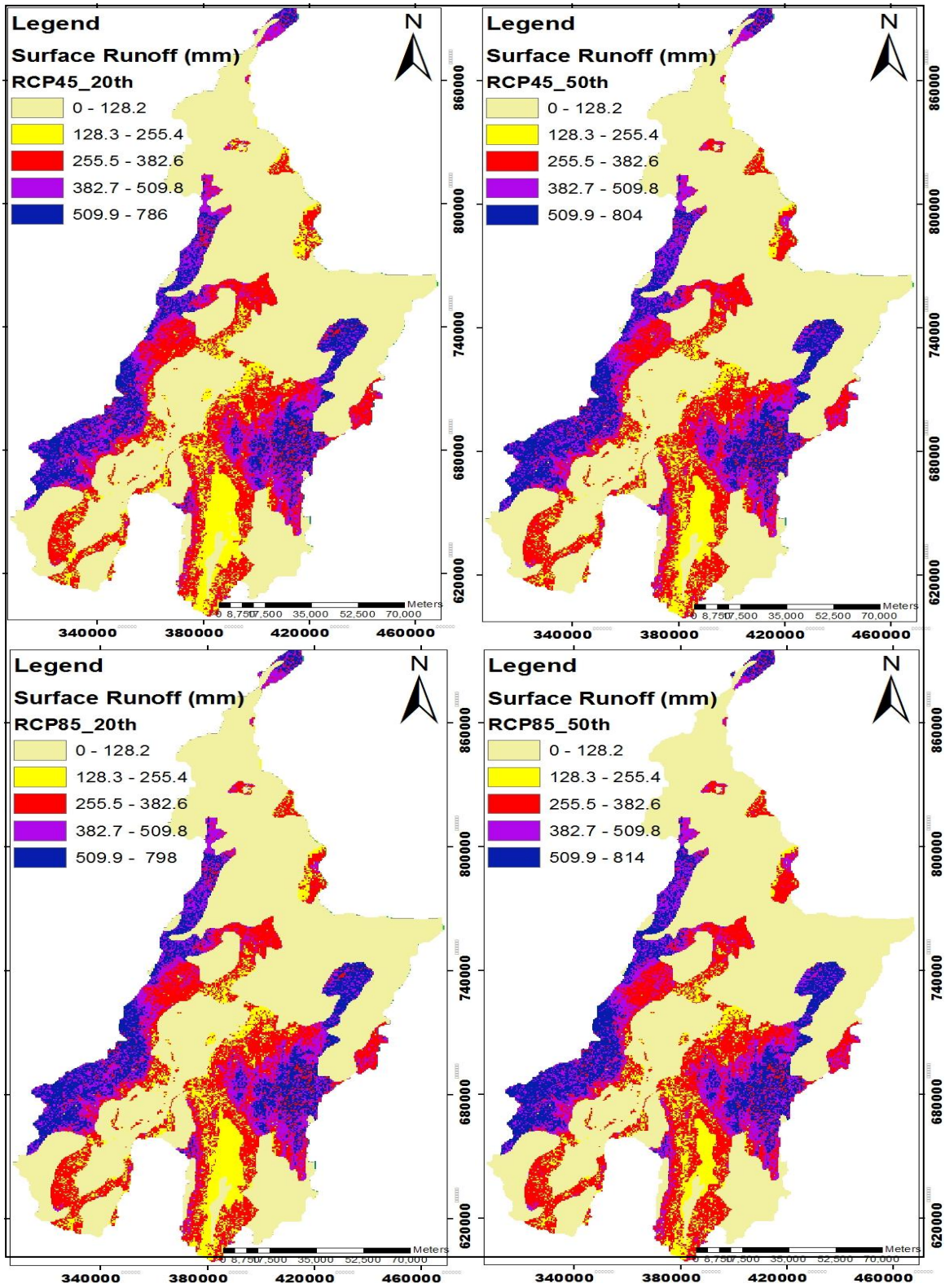

Appendix 18: simulated mean future groundwater recharge for the periods 2020s and 2050s under both RCP 4.5(upper).and RCP8.5 (lower)

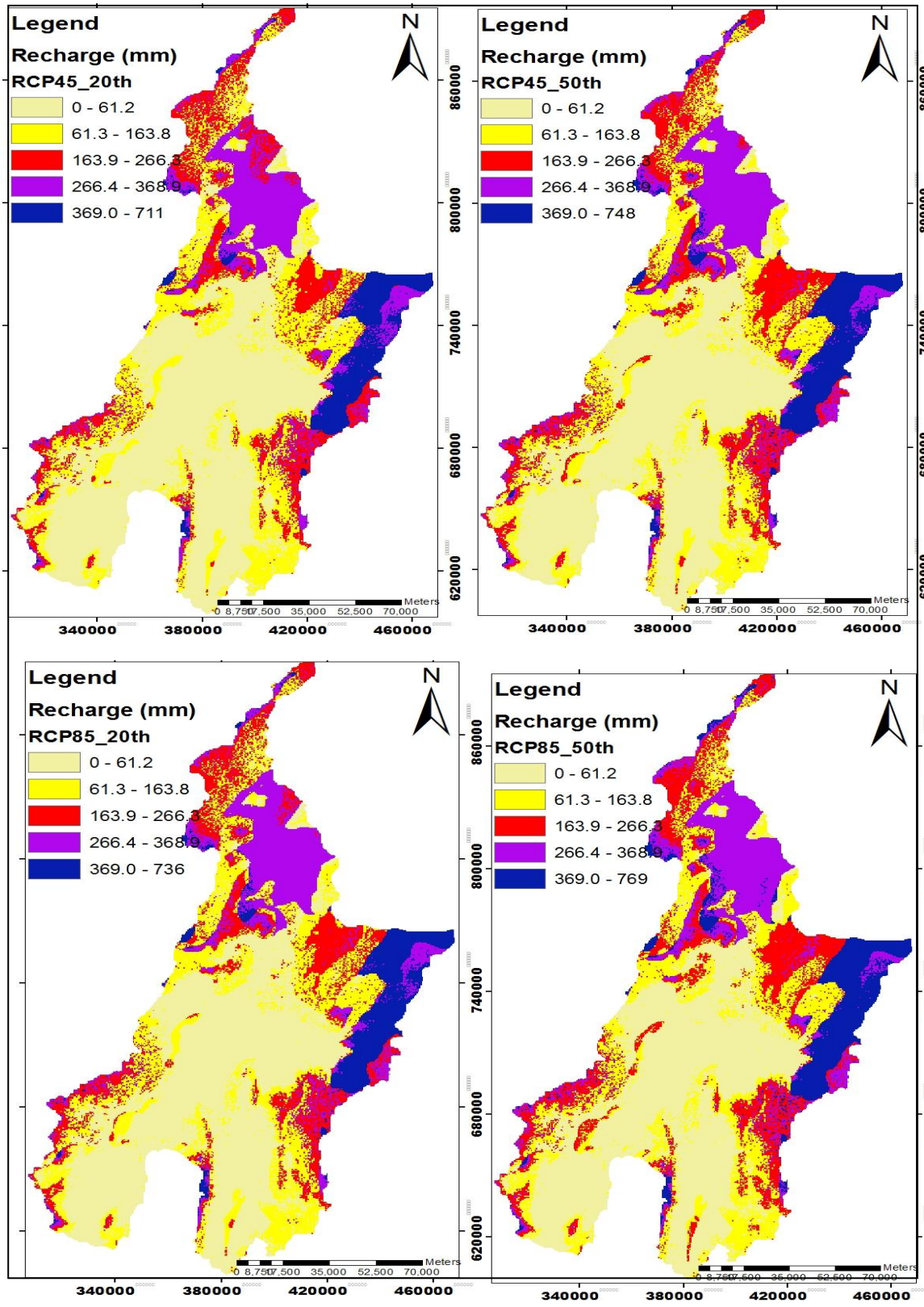

Appendix 19: the projected and simulated ensemble of Q_{10} and Q_{90} percentage proportion of water balance components compared with base period for selected future periods under both rcp4.5 and rcp8.5

CMIP5 (Q_{10} and Q_{90})			Precipitation			Actual Evaporation			Surface runoff			Interception			Groundwater recharge		
Scenarios	period	Uncertainty ranges	mm/yr	%	%Δ	mm/yr	%	%Δ	mm/yr	%	%Δ	mm/yr	%	%Δ	mm/yr	%	%Δ
20th C	Base (1976-2005)		1169.6	100	0	873.2	74.7	0	183.4	15.7	0	3.1	0.3	0	113.7	9.7	0
RCP4.5	Near (2006-2036)	Q_{10}	1110.6	100	-5	840.5	75.7	-3.7	174.2	15.7	-5	2.9	0.3	-5	97.8	8.8	-14
		Q_{90}	1367.8	100	16.9	974.4	71.2	11.6	214.6	15.7	17	3.6	0.3	17	178.9	13.1	57.3
	Intermediate (2037-2067)	Q_{10}	1122.3	100	-4	848.4	75.6	-2.8	176	15.7	-4	3	0.3	-4	99.5	8.9	-12.5
		Q_{90}	1496.4	100	27.9	1030.8	68.9	18	234.8	15.7	28	4	0.3	27.9	230.9	15.4	103.1
	Far (2068-2099)	Q_{10}	1157.4	100	-1	868.8	75.1	-0.5	181.5	15.7	-1	3.1	0.3	-1	108.1	9.3	-4.9
		Q_{90}	1589.9	100	35.9	1066.1	67.1	22.1	249.6	15.7	36.1	4.2	0.3	35.9	274.4	17.3	141.3
RCP8.5	Near (2006-2036)	Q_{10}	1110.6	100	-5	840.8	75.7	-3.7	174.2	15.7	-5	2.9	0.3	-5	97.5	8.8	-14.2
		Q_{90}	1426.3	100	21.9	999.7	70.1	14.5	223.8	15.7	22	3.8	0.3	22	202.8	14.2	78.4
	Intermediate (2037-2067)	Q_{10}	1157.4	100	-1	869.3	75.1	-0.5	181.5	15.7	-1	3.1	0.3	-1	107.6	9.3	-5.4
		Q_{90}	1589.9	100	35.9	1066	67.0	22.1	249.6	15.7	36.1	4.2	0.3	35.9	274.5	17.3	141.4
	Far (2068-2099)	Q_{10}	1250.9	100	7	921.7	73.7	5.5	196.2	15.7	7	3.3	0.3	7	133.2	10.6	17.2
		Q_{90}	1987.5	100	69.9	1184	59.6	35.6	315.7	15.9	72.1	5.3	0.3	69.9	487.9	24.5	329.1